Additively manufactured suspension components for an F1 car

Design, Simulation, Manufacturing and Testing

Nicolò Zamariola

Technische Universiteit Delft

TU Delft Delft University of Technology

Challenge the future

ADDITIVELY MANUFACTURED SUSPENSION COMPONENTS FOR AN F1 CAR

DESIGN, SIMULATION, MANUFACTURING AND TESTING

by

Nicolò Zamariola

in partial fulfillment of the requirements for the

Master of Science
in Mechanical Engineering - Materials Engineering and Applications

at the Delft University of Technology,
in collaboration with Scuderia Ferrari
to be presented publicly on January 12, 2018 at 10:00 AM.

Supervisor:	Prof. dr. ir. J. Sietsma	
Company Supervisor:	Ir. M. Civinelli	
Thesis committee:	Prof. dr. ir. J. Sietsma,	TU Delft
	Dr. ir. M. J. M. Hermans,	TU Delft
	Dr. ir. D. de Klerk,	TU Delft
	Ir. M. Civinelli,	Scuderia Ferrari

This thesis is confidential and cannot be made public until January, 2023.

TU Delft Delft University of Technology

ACKNOWLEDGMENTS

The present report represents the final summary of a shared project between TU Delft and Scuderia Ferrari F1 team. As such, the collaboration of many people is involved and it would need much better reward than the brief acknowledgments hereby presented.

Among the numerous personalities involved I would like to thank in the first place Prof. Sietsma for its full support, during the year spent in Maranello, and fruitful availability as well for the critical discussion on the scientific aspects of the project. From the Scuderia Ferrari team I am honored to thank my supervisor Marco Civinelli for the never ending patience and numerous chances given to me to learn and to be part of a wonderful team. As involved parts, a general thanks is due to the others departments among which I would like to cite the structural stress team, the quality department and the mechanical manufacturing team. Their collaboration in setting high standards for the project has been one of the main reasons for the successful results obtained and furthermore has been the chance of discovering new friends.

Moreover I would like to thank all my friends, old and new, for their continuous support and the numerous chances of relieving the accumulated fatigue together. Without your fruitful help and presence I would not be the person I am now.

Finally, this project represents the final achievement of an educational period of my life that would have never been the same without the support of my family. From my siblings to my parents and relatives, the continuous presence and respectful criticism as well as their constant counseling in the choice-making process throughout this journey made possible to accomplish personal satisfaction with high level of synergy with them.

ABSTRACT

The recent possibilities given by additive manufacturing in free shape design have been seen as a potential breakthrough in the design and production of structural components of a racecar and more generally their influences on the future lightweight strategies in the automotive industry is expected to influence the next generation of products. Among the emerging techniques for the production of metal products, *Direct Metal Laser Sintering* (DMLS) and *Selective Laser Melting* (SLM) technologies are becoming technically ahead of the competition: the possibility of direct production of aluminum and titanium alloys components with good surface finishing and net shape from CAD geometry is nowadays a concrete option for the mechanical designer.

The purpose of the present study is to demonstrate the feasibility of the mentioned AM techniques and to exploit their potential weight saving opportunities in the design of highly structurally optimized racing components while determining the current *state-of-art* of AM for metallic components. The present project reports the design and production of two car components redesigned in the perspective of the novel manufacturing techniques.

The first component is the rear top wishbone bracket of the rear suspension. The production has been developed following the best practices for the design of additively manufactured structures such as complete topology optimization and a reconstruction with special focus on the design for manufacturing assessment. The bracket has been developed for DMLS manufacturing in titanium alloy Ti6Al4V. On the contrary, the second component has been developed in a novel aluminum alloy: the Scalmalloy, commercial name of a high strength aluminum alloy specifically developed for high strength to weight critical applications. For this novel material a characterization campaign has been set up comprehending tensile testing, micro-graphical analysis, tomography inspection and an X-ray analysis. Both component underwent a full scale fatigue testing.

Both components proved an achievement in terms of weight saving between 7% and 10% with the same functionality and performance level of the machine counterparts. The material characterization campaign revealed the concrete maturity of the DMLS process for Ti6Al4V while the process of SLM production of Scalmalloy requires some final tuning. The tensile strength levels achieved are compliant for both materials' specifications but the presence of localized lack of fusion in the Scalmalloy specimens reduced the final ductility of the material considerably.

The obtained results are an encouraging step towards the application of the analyzed technology in structural components for the motorsport industry and possibly, in the near future, for the wider automotive industry. The limited standardization in the quality processes is addressed as well with a concrete proposal for establishing a controlled level of defects in additively manufactured components.

Nicolò Zamariola

Maranello, December 2017

NOMENCLATURE

α	alpha can indicate a microstructural phase
δ	Penetration depth
μ	micro
AM	Additive manufacturing
AMC	Aluminum metal matrix
$AMed$	Additively manufactured
AMS	Aerospace material specification
$ASTM$	American society for testing and materials
$BAAM$	Big area additive manufacturing
CAD	Computer aided design
CAE	Computer aided engineering
$CFRP$	Carbon fiber reinforced polymer
CNC	Computer numerical control
CTE	Linear coefficient of thermal expansion
$CTScan$	Computed tomography scan
DED	Direct energy deposition
$DMLS$	Direct metal laser sintering
DPI	Dye penetrant inspection
DTM	Deterministic turing machine
$E-4D$	Elongation at brake measured from an initial length equals to 4 times the diameter dimension
EBM	Electon beam melting
$F1$	Formula One
FAI	First Article Inspection

FEM	Finite element method
GA	Gas atomization
HdH	Hydride-Dehydride
HIP	Hot isostatic pressing - *hipping*
ISF	Isotropic superfinishing process
LC	Laser cusing
LENS	Laser engineered net shaping
LOM	Light optical microscope
LOM	Low optical magnification
LPI	Liquid penetrant inspection
MMC	Metal matrix composite
NDT	Non destructive testing
OEM	Original equipment manufacturer
PA	Plasma atomization
PBF	Powder bed fusion
PREP	Plasma rotating electrode process
RA	Rotary atomization
RB	Rocker beam
RTWB	Rear top wishbone
SAE	Society of automotive engineers
SLM	Selective laser melting
SLPS	Supersolidus liquid phase sintering
SLS	Selective laser sintering
UNS	Unified numbering system
WAAM	Wire and arc additive manufacturing
YM	Young modulus
YS	Yield strength

LIST OF FIGURES

LIST OF TABLES

CONTENTS

1

INTRODUCTION

The first part of the present thesis presents the literature research that has been the foundation of the work. It is structured around the main topics that are the focus of project from the consequences additive manufacturing has on the novel design processes to the analysis of micro-structural changes and peculiarities related to specific processing techniques. The criterion of choice for each topic, hereby presented, has been, not only the strict relevance to the performed work, but also the chance to give to the study a broader view and general sense of the application in a highly demanding environment of such revolutionary manufacturing techniques.

Additive manufacturing (from here onwards referred to with the abbreviation AM) [1] has been indicated by many experts and *mass-media* [2, 30] as one of the technologies able to ignite a third industrial revolution characterized by the so far unknown easiness of production for geometrically complex and functional parts, with no need for expensive casting dies or machining processes and very limited post processing needed. Since 2009 with the publication of the *"Roadmap for Additive Manufacturing"* [31] the development of the technology with its natural market has been growing consistently [15, 32].

The chance to shorten the path between design and the final industrialized part has been seen as a potentially innovating factor able to cut down costs and lead time while granting extreme flexibility in design changes and *in-the-loop* updates.

Among a diversity of processing techniques a few are emerging as market leaders from different points of view. The choice of the current project to proceed with DMLS (Direct Metal Laser Sintering) has been dictated by availability of the selected materials and as well by the processed quality that is

[1] In this thesis report the use of the terms additive manufacturing, rapid prototyping, rapid manufacturing and near net shape manufacturing is interchangeable and refers to every manufacturing methods that does not involve any material subtraction but processes the part with a *layer-by-layer* approach and when a specific meaning is address to any of this terms has been clearly specified. Furthermore the indication of *AMed* would indicate any processed part in additive manufacturing and has to be read *"Additively Manufactur-ed"*

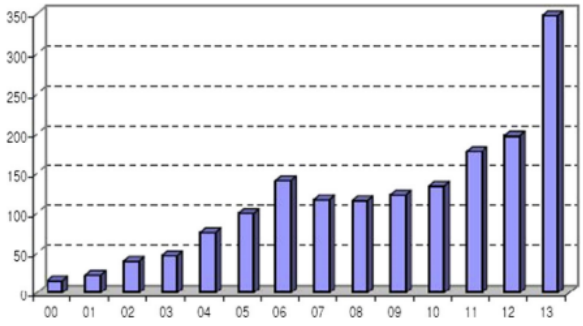

(a) Number of machines sold for metal additive manufacturing from the year 2000 (00) [32]

.

(b) A door hinge in DMLS produced titanium of a turbine installed on an Airbus A380 [33]. The component dimensions are such to grant a weight saving of 10 kg on the whole aircraft.

Figure 1.1: Market request for AM production machines and an example of a topology optimized component printed in titanium alloy showing the gain complexity given by the freedom of shape generation

ensured by the process. Materials of interest for the project are all alloys with high specific stiffness and strength and titanium alloys and aluminum alloys were selected for a deeper review for their relatively higher advantage over heavier metals by the chance of minimizing weight in geometrically fixed regions where the density overcomes the importance of specific properties as we will see in depth in the following chapters.

1.1. THESIS PURPOSE AND STRUCTURE

The present project aims to show what is the present *state-of-art* of additive manufacturing for the motorsport industries and what possibilities the implementation on a larger scale of the mentioned technology would have on the current design process for structural components in the suspension systems of an F1 car.

At present, all car manufacturers and motorsport companies are trying to implement additive manufacturing to exploit design opportunities and reduced lead times which are constrained with the respective traditionally machined or cast counterparts. To show real life benefits of the aforementioned process and in order to understand its current maturity the present project has been started with a collaboration between Scuderia Ferrari and the Delft University of Technology as the two sponsors of the project. The whole project for reasons of ownership and confidentiality has been carried at the Scuderia Ferrari's facilities in Maranello, Italy.

The present thesis work is structured into two main sections: the literature review, presented in Chapter 2, and the constitutive work. After a brief description of the thesis purpose the literature review is presented in two principal sections: the first section focuses on the new possibilities promoted by the use of additive manufacturing in automotive and more specifically motorsport industries; the second half of this chapter analyzes in depth the process of additive manufacturing for metallic materials. At the end of this chapter the main topics are summarized as the basis of the explanation of the constitutive work of the present thesis.

The constitutive work section follows the engineering process that lead to the successful conclusion of the present project. Each subdivision is divided into two parts, each one regarding one of the two components developed in the framework of the thesis: the rear top wishbone bracket and the rocker beam. The first is a component that connects the upper side of the upright to the kinematic joint of the suspension while the second is mounted in the gearbox case and provides support for the inboard components of the rear suspension as it will be explained further.

In Chapter 3 the design of the components is presented. Each of the two items designed and produced has its own set of requirements and the implementation of those within the boundary conditions imposed by all aspects of an engineering task will be reviewed. The topology optimization strategy will be explained and the final geometry reconstruction shown. Afterwards, in Chapter 4, the final assessment of calculation on the definitive geometries is presented. The iterative process of solving stress issues and by optimizing the figure of merit of the two structures is presented in parallel. In Chapter 5 the manufacturing process of the two components is presented highlighting the peculiarities of AM processing techniques as well as the dissimilarities from conventional subtractive manufacturing practices. In Chapter 6 the results of fatigue testing are presented alongside the results from the quality assessment for the two products. Particular emphasis is put in the qualitative analysis of a novel material- *the Scalmalloy aluminum alloy*-. In Chapter 7 the presented results are discussed benchmarking the additive manufacturing techniques with the conventional counterparts and presenting the materials behavior and peculiarities. In Chapter 8 the conclusions of the present project are presented giving a final judgment on the actual situation of additive manufacturing for motorsport applications and analyzing briefly the chain of knowledge, the know how for the current *state-of-art* and finally propose how the investigations should be carried out in the industrial practice to successfully apply this technology for replacing traditionally machined parts with better components.

I

LITERATURE REVIEW

2

ADDITIVE MANUFACTURING - CHALLENGES AND OPPORTUNITIES

In the first part of the literature review the implications that novel technologies for additive manufacturing will have in the near future for automotive and especially in the motorsport industries are presented. After a brief introduction about the main driving factors for the implementation of such processing techniques into specific environments (F1), the changes induced by such technologies are reviewed. The differences that will be highlighted will range from the discrepancies in the design process to the new integration of calculation tools in the *design-in-the-loop* procedure. Since its appearance on the manufacturing technological world the presence of additive manufacturing has given the chance to design and produce components with almost no limitation in shape and geometrical complexity with small to none added costs [1]. In the figure presented earlier (see Fig.1.1b) the concept of complexity can be better understood and the benefit of Rapid Manufacturing is evident.

2.1. OVERVIEW - FORMULA 1 AND MOTORSPORT INDUSTRY

Formula 1 is an annual motorsport competition for land vehicles with four nonaligned wheels, two of which are used to steering and at least two for propulsion [34]. The competition has been known during the years as the clearest example of engineering challenge and nowadays is a good showcase for tomorrow's automotive technologies. Since the competition takes place on a number of different tracks the vehicle should be able to cope in the most efficient way across all of them. Since the very early years motorsport and specifically Formula 1 has been pushing the limits of lightweight design and the breakthrough offered by novel technologies has been in the last 50 years welcomed as they could provide competitive advantages if implemented (cfr. Fig.2.1 and Fig.2.2)[1].

[1] Within each set of rules during the years the chance of racing on a lighter car has numerous benefits: from the obvious lower inertia to deceleration and accelerations in the propelling direction to lower yaw inertia in the negotiation of a series of corners, to the lower impact on the tyre consumption and the possibilities given by the higher level of ballasts to achieve the lower weight limit

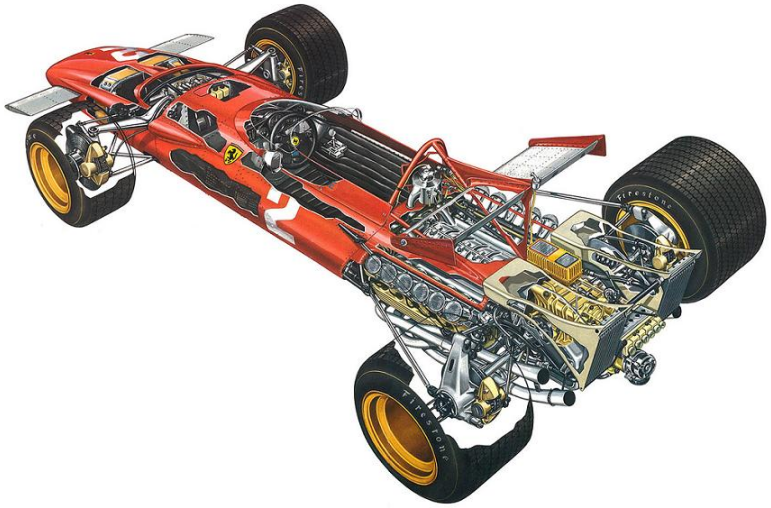

Figure 2.1: The famous Ferrari F312B known for the use of the engine as a fully stressed member, a choice dictated by the desperate quest for lightness

As of today the strict regulatory bodies of the sport are limiting the choice of exotic metallic materials and impose selected materials among certain components [34]. This is limiting the wealthier teams in terms of material choice but forces every competitor to outsmart the others through the implementation of an higher level of design refinement and novel manufacturing technologies able to overrun with complex geometries that would cope the less performing materials.

More specifically, materials with specific stiffness, expressed as the ratio between the Young modulus of the material and the specific weight (or density), higher than 40 MN/(mm*kg) are forbidden, and other materials must be listed in the regulation. This limitation prevents the use of mostly any aluminum matrix composite that is not specifically designed to meet this rule. Among them it is worth to mention the most common legal materials that can be explicitly used:

1. Aluminum alloys
2. Steel Alloys
3. Titanium Alloys *(not for fasteners with male thread smaller in diameter <15mm)*
4. Magnesium Alloys
5. Copper Alloys *(with less than 2.5% wt. of Be)*
6. Cobalt alloys
7. Silicon Carbide particulate reinforced aluminum matrix composites (AMC)
8. Nickel based alloys *(with Ni content 50%wt to 69 wt. %)*

Furthermore materials should not be provided under exclusive basis and special commercial terms as stated in article 5.16.3 [34]. Specifically, for the suspension components which are of interest in this work a few extra rules have to be met.

Figure 2.2: Renault F1 car uprights in which the presence of heavy machined zones is a clear indication of the research for lightweight and functional components. The dimension of the components can be understood by the distance between the studs brake caliper attachments which is usually between 20 and 25 cm.

Among them the more restrictive are:

- 10.5.1 which states *'The suspension uprights may only be made from UNS A92014, UNS A92618, UNS A97075 or EN/AA 7022 aluminum alloys.'*
- 10.5.2 which states *'The loads from the suspension members and wheel bearings must individually and entirely be carried by the suspension upright. Exceptionally up to three suspension members may be connected together by titanium, aluminum alloy or steel components before their load is passed into the upright.'*

In the design process of the components, which constitutes the main topic of this thesis, we will come back to these rules to specifically analyze their influence on the made design choices. As stated before, the continuous search for lightweight component design asks designers to be able to use the lowest quantity of material able to fully comply with the expected load cases and be able to functionally bring performance to the all engineering systems in terms of stiffness, finishing and fatigue life.

Since F1 racing teams are usually not encouraged to publish too much about their research and development projects there are few examples from literature of real case scenarios in which this process has been used for suspension components and still several issues need to be properly addressed to demonstrate its full reliability (*designers have been skeptical with respect to repeatability and mechanical soundness of structural components produced by AM* as described in [1]). Among the few documents and available reports a first interesting application of AM has been documented in [1] even though it does not cover the topic of structural components.

In the aforementioned article Cooper demonstrates how the implementation of DMLS - AM of titanium alloys for hydraulic manifolds can represent a game changer technology in the quest for lighter and more efficient components. Typically hydraulic manifolds are produced by conventional milling and CNC-processes of high grade aluminum alloy billets (Al7075 from the aerospace quality of Al2099 with lithium), including also spark erosion and drilling operations [1]. The evolution of this alloy as well as his eighth series counterpart (Al8090) was developed exactly for lightweight application by Alcoa and other aluminum producers to establish new standards in the material properties. Their density can be up to 10% lower in respect of conventional aluminum alloys with some percent gains

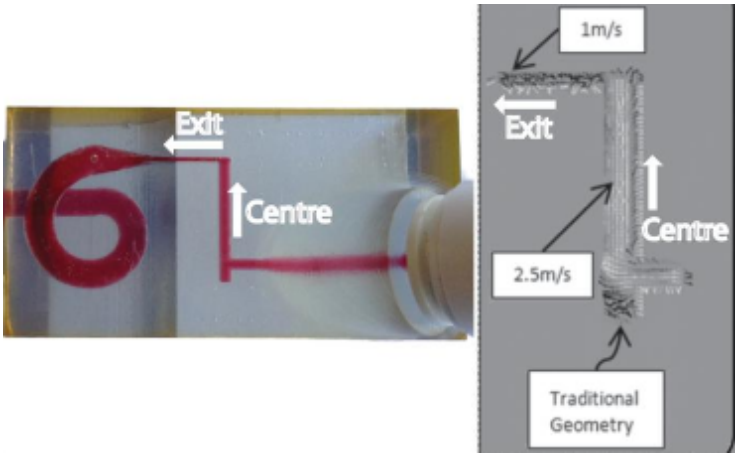

Figure 2.3: Traditionally machined hydraulic channel for fluid operation as it can be found in [1]. The characteristic dimension of the channel is of 0.5 mm (diameter).

on the modulus as well (up to 10% between 2024 and 8090) due to the presence of lithium. Lithium in solid solution (concentration lower than the solubility of 4.2% wt) being the lightest metal available with a bulk solid density of 0.5 g/cm^3 reduces the alloy's specific weight while contributing in stiffening the material.

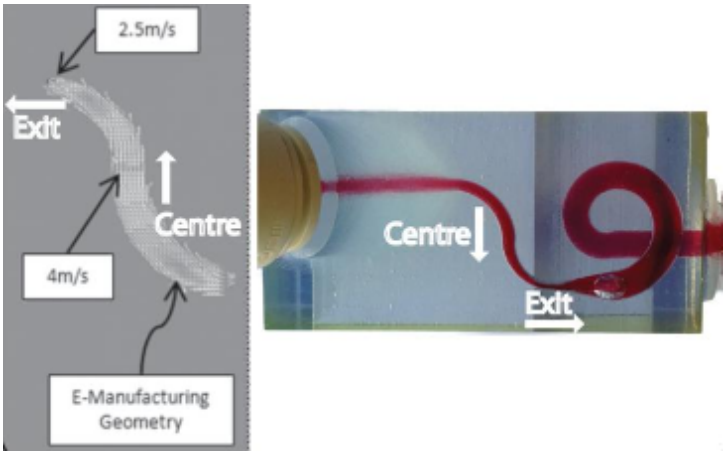

Figure 2.4: The AM components made possible an alternative geometry for the channeling with a smoother pass that should enhance the flow properties as reported in [1]

Due to the need of complex channels design the machinability of such components is essential and quite a portion of the design is uniquely related to this aspect and provides no additional performance to the component apart from the possibility of being produced. The possibilities given by AM in this context are quite unique since very little machining would be necessary and the added material for this purpose can be eliminated with considerable weight gain. Flow characteristics can also be improved if channel paths are improved through the absence of sharp corners which are usually the standard for machined counterparts. From an operational point of view, the absence of machining lines reduces the need for post-working application which is usually need for sealing. Examples of the different paths can be seen in Fig.2.3 and Fig.2.4. The end result reports increased velocities up to 250% and validation for operating channels produced in DMLS Titanium as low as 0.5 mm. In Fig.2.5 a section of the aforementioned tube is presented and the superficial finishing can be seen. The areal

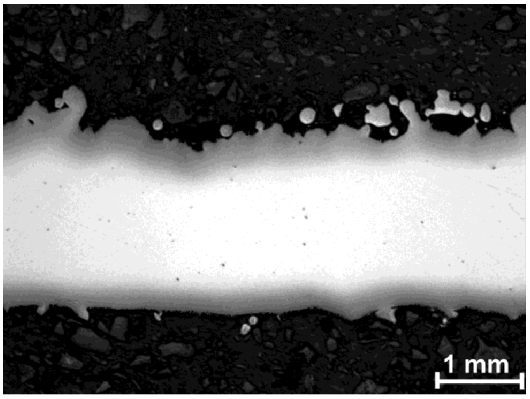

Figure 2.5: Section of an thin hydraulic manifold produced by DMLS in Titanium Ti6Al4V [1] with a diameter of 0.5 mm. The rough surface might have been improved with the implementation of surface finishing technologies such as AFM.

density is reported to be in line with manufacturers descriptions. It is interesting to note how the poor finishing[2] did not influence the flow velocities as much as the geometry change making the rough surface acceptable with possibly no post processing needed. Furthermore, it is possible to treat inner tubes and surfaces through the implementation of AFM (Abrasive Fluid Machining) that has proven to be able to reduce surface roughness and eliminate the trace of layering [35].

Since the literature about AM technology within the F1 environment is limited as a good reference point, some examples from Formula SAE[3] teams are hereby presented. Among the numerous examples of successfully designed and tested parts it is interesting to note how all referenced articles report similar design flow to maximize the output benefits. The design process of parts that are going to be produced through AM follows an optimization step before any modeling and starts therefore with the designation of geometric constraints and applied loads to better understand the most efficient way to distribute material in the design region (through the application of topology optimization strategies as will be discussed in following sections).

An early attempt to employ titanium in AM in a Formula SAE application for a structural component through Laser Powder Deposition has been made at South Dakota School of Mines and Technology [37] in 2004. The components that have been taken for this particular application were the front and rear uprights[4]. The design criterion, chosen for leading the optimization routine, was the deflection of the two components in particular load cases: the front was designed with a cornering steering angle deflection limit while the rear one was limited by the camber[5] stiffness. Both designed components feature an hollow structure that could not be processed by conventional machining. The

[2] The poor finishing was evident by the reported surface roughness: *Ra* values ranging from Ra4 to Ra28 depending on the orientation with respect to the printing direction - while for machining counterparts is usually requested to remain below Ra0.4

[3] Formula SAE/Formula Student is an annual competition among universities that takes place with several events around the globe. The main focus of the project is to realize a racing car propelled either by combustion or electrical engines and to compete in various challenges representing the tasks of any motorsport business in a reduced and *ad hoc* environment. For additional information see [36]

[4] The upright is the component which fixes the wheel assembly to the suspension system. All rotating parts of the wheel assembly (rim, tire, spacers and brake disc) are connected to the upright through the wheel hub. The upright connects those rotating components to the fixed part of the suspension links, and therefore provide housing for the braking system as well. The hub and the upright are connected by a set of angular bearings to allow relative rotation and load transmission. Front uprights do provide attachment points for the steering link while rear upright, in racing cars, has the implementation of the traction shaft (half-shafts).

[5] Camber angle and the relative parameter reported as camber stiffness is presented extensively at the beginning of Chapter 3.

alternatives for producing the parts were either casting (which was judged too costly) or welding of titanium sheets. The choice for AM was preferred over welding for the lack of expertise in titanium welding and the possibility to develop a background knowledge in a novel technological sector. The component in the previous car iterations was made in Al2124 and titanium (Ti6Al4V) proved to be a better choice for the component (see [37] *Table 3* [6]). Despite a missing note on the final weight of the part a successful application of additive manufacturing on structural components for a racecar application can be dated as early as in 2004.

A second example, reported in [2], shows again the optimization of a pair of uprights. The challenge has been taken as an optimization of the existing design with no reconsideration on the total design area. The present sentence on the design space can be checked in Fig.2.6 and a possible comparison could be made on the actual work performed on components that have been redesigned during the present thesis work. The recurrent choice of optimization of uprights geometries can be explained with the central importance that this components has for each car corner. All loads from the contact patches to the suspension have to travel through those parts which are conventionally machined or cast. The weight of the part itself is a considerable share of the car unsprung mass which has a high weight on the car performances.

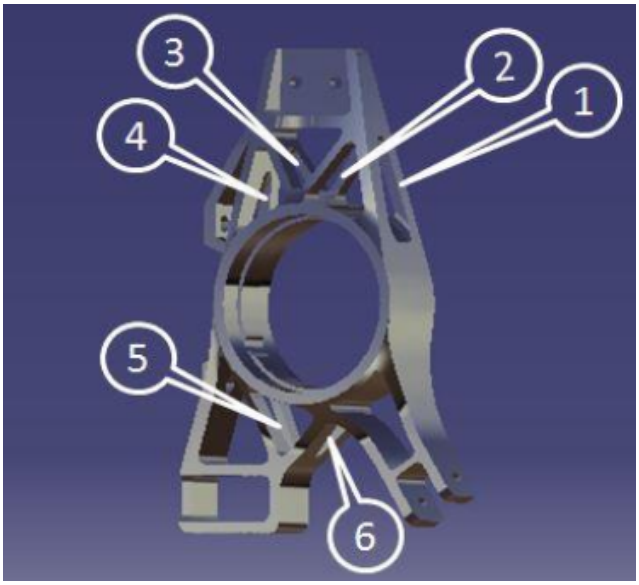

Figure 2.6: Internal cavities modeled on the upright after the topology optimization: the lack of having used a larger design space has reduced the possibilities of better using the material that is connecting the bearings to the suspensions [2]. The component dimension is not reported by the indicated reference but the total volume is reported to be of 138.64 x10^{-6}m^3.

A third example in the field, which could be considered as well as a reference point for designing on structural components with AM technologies, is presented in [3]. In the mentioned article the focus on the technology is the possibility to substitute suspension mounting brackets from parts produced with conventional manufacturing to parts in SLM (Selective Laser Melting - an AM technique that will be analyzed in the second section of this review). The weight reduction amplified by proper enhanced

[6] In the material properties comparison the specific stiffness is missing which would have granted a better understanding of the material choice between aluminum and titanium

geometrical complexity was a key player for this redesign exercise. Furthermore, during the project also suspension bearing bolts have been redesigned and the material change from Al7075 to steel 316L provided components with the same weight but better stiffness [7]. At the end of the article an interesting Ishikawa diagram is presented of the different fields that would be needed to cooperate for successful industrial application of AM in highly technological areas.

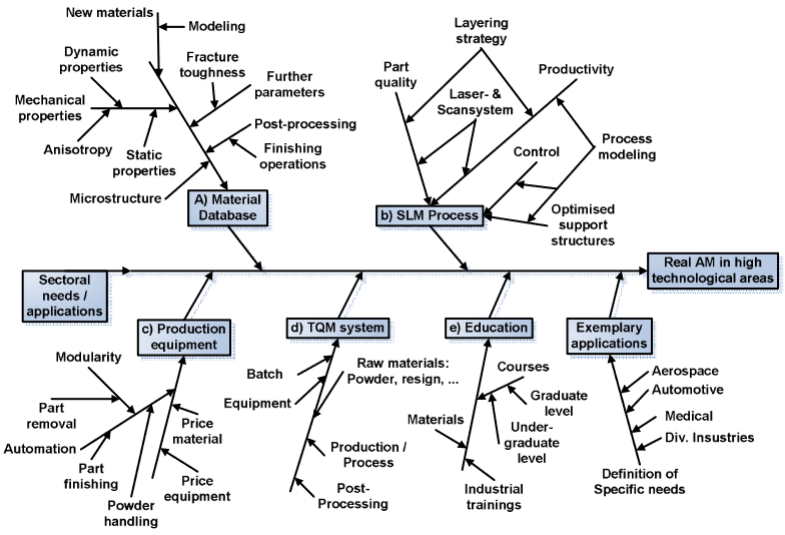

Figure 2.7: Ishikawa Diagram which represents the various contributions that are needed to a future establishment of AM as a competitive processing techniques[3]

From the time of the study, some of the needs have been successfully filled and achieved, within the author's perspective and experience, while others are still a concern. The biggest improvements are in the field on the machine side and on the process itself (being it SLM - Selective Laser Melting or DMLS) and on the quality of the raw materials that has been given industrial standards for additive manufacturing. On the contrary some of the highlighted issues are still problematic nowadays: materials database is missing due to the number of processing techniques and materials on today's market, education is moving the steps towards the integration of graduate courses on AM and powder metallurgy but still proper finishing processes for surface quality have not been developed specifically to reduce layering and others peculiar AM produced components defects. The diagram is presented in Fig.2.7.

A further example of the implementation of a proper design process for additive manufacturing components is presented in [38] in which a brake caliper has been optimized and produced in DMLS. In the definition of a proper design space a correct evaluation of the geometrical constraints and interfaces with other components has been performed and the result can be see in Fig.2.8a. The material chosen for the application is AlSi10Mg which, as we will further discuss in the following sections, is considered the baseline material for lightweight components. The design constraints in term of thermal dissipation made the choice for an aluminum alloy evident. Through different iterations the authors provide a clear example on the correct approach to achieve the optimal results with AM processing techniques. The final component can be seen in Fig.2.8b

So far the needs and some examples of applied racing industry in additive manufacturing have

[7] The limited space for a bearing bolt is the clear example of a geometrical limitation that prevents the specific properties of a material to overrun the pure properties.

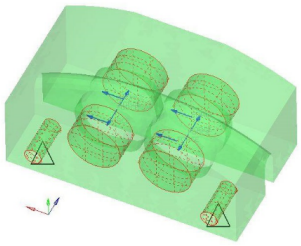

(a) Design Space prepared for topology optimization of the brake caliper [38]

(b) Final shape of an optimized brake caliper as presented in [38]

Figure 2.8: Design Space and final geometry of the optimized part. As in can be easily seen the freedom given by the additive process in combination with a topology optimized structure made possible the creation of specific reinforcements limiting the brake caliper axial displacement.

been presented, in the following section the greater automotive scenario will be analyzed.

2.2. OVERVIEW - AUTOMOTIVE INDUSTRY

As we have seen a brief overview of the F1 and motorsport industry situation regarding the possibilities given by additive manufacturing, here a similar analysis will be carried out on the broader automotive industry. For standard automotive OEMs[8] two big advantages can be easily found in the introduction of AM techniques in their production and design process as recognized in [39]. AM can be seen in the automotive industry:

- **As a source of product innovation:** the design can be carried out and produced with less geometrical constraints, this would revolutionize the design of assemblies that might be substituted by single components with a high influence on the cost break down of engineering systems. Several examples are available from the aeronautical industry which faces similar challenges as the automotive sector and is usually regarded as a reference to introduce new technologies in the more cost constrained automobile industries *(e.g. introduction of aluminum chassis on a large production scale or high strength materials and composites).*

- **As a driver of supply chain transformation:** cutting down the time for tooling production every manufacturer can provide parts with considerably shorter lead times which gives the opportunity to achieve better customization and dramatic reduction of scrap materials. Furthermore, the mass scale production reduces the need of big manufacturing sites but could be the starting point to a new supply chain of medium sized and delocalized part producers.

Four scenarios are explained by [39] as the path from the current situation to an evolution o the business model. In each model the technology plays a different role from being a key for design and rapid prototyping during the early stages of product development (in the current industry) to enable the chance of having mass production customization and supply chain disintermediation in the long time perspective.

One of the driving factors for automotive brands innovative design is the compliance with environmental regulations. Being introduced in the early 1990s (1993) from the European Commission

[8] Original Equipment Manufacturer

the regulatory laws for emission reduction have been evolving up to the present regulation as stricter and stricter framework to which all OEMs have to adapt. Similar standards have been promulgated worldwide by competent regulatory bodies. Whereas a range of strategies can be applied to become compliant to the current set of regulations for what concerns most pollutants there has always been a limit in the reduction of a natural product of the combustion which is CO_2. Despite it cannot be considered strictly as a pollutant the regulation strives for a reduction due to the interaction of this gas with the climate change. As the only viable way to reduce this component is consuming less carbon-fossil-fuels the trend of engine downsizing and lighter vehicle designs goes in this direction and since lighter design can be implemented usually through more complex parts and assemblies the potential unexploited by the introduction of AM processes is seen as strategical advantage.

Among the several examples of how complex redesign and material choices can effectively synchronize to achieve the quest for lighter vehicles two are especially renown and self-explanatory:

- **The redesign of the Ford F-150 (my2015)[9]:** the complete aluminum body has helped in cut down the weight of around 320 kg with media acclaim and the ability to set new standards for US truck market in term of fuel consumption. The body which contributed in the biggest share of the weight reduction can be seen in Fig.2.9a

(a) F150 full aluminum body as the example reported by [39, 40]

(b) The body of the Range Rover my2014 commonly reported as an example of how complex design and implication of newer materials is the factor to drastically remove mass from an automobile [41]

Figure 2.9: Two examples of the need to move the automotive market towards the implementation of new design materials and to improve the ability of integrating complex geometries replacing assemblies of substructures: in Fig.2.9b the Range Rover Vogue my 2014 is presented with its an aluminum chassis while in Fig.2.9a reports the *body-in-white* of the Ford F150 my2015.

- **The redesign of the Range Rover (my2014):** similarly the introduction of aluminum in the all body-chassis implemented a weight reduction of more than 400 kg on its predecessor. As well the new model has received media acclaim and raised the bar against the previous model both in terms of performance and fuel consumption. The chassis body can be seen in Fig:2.9b.

Having the chance to exploit the potential of complex geometries, lattice structures and topology optimized components regardless of the increased cost that a conventionally machined product might

[9] my2015 stands for model year 2015 and is considered to be the usual standard nomenclature for the designation of car model within different years.

bring and combining it with materials with high specific strength and stiffness is surely the next step most manufacturers are going to take in the described technological direction [42] [43].

When it comes to reorder the potential driving factors to employ this new technology today rather than in the recent past there is common agreement on a series of reasons:

- **More materials are available for AM including high performance alloys:** It has been always a technical drawback to rely solely on few materials, in the design perspective, when AM has been introduced and most of them were not specifically designed for the application but where rather the best choice of commercially available product (in case of aluminum derived from casting materials (AlSi10 would be a clear example)). Nowadays, the trend of specifically designed materials and alloys has made the growth of peculiar combination of processing and powders available for OEMs and suppliers possible. Furthermore, now the research is deeply involved in the tuning of advanced materials like aluminum matrix composites with *in situ* production of reinforcement phase. As well the possibility to print carbon reinforced thermoplastic is soon to be available and could be rivaling the metal deposition and sintering processes in certain specific applications.

- **Increasing quality of AM product is reducing the need of post processing** Though same post-processing is needed for high precision component as we will have the chance to demonstrate in the course of this thesis, the quality of near net shape directly manufactured product has been increasing dramatically with the last generation of machines introduced. As well techniques like EBM promise to achieve apart from high fidelity of the 3D model also surface finishing of level superior to what is available through conventional casting and sandblasting and similar to machined components. Still a certain degree of operation work would have to be performed on AM-produced parts and the trend would be a sort of *mixed* production process in which the basic complex shape will be implemented through AM and conventional machining would be used as a finishing tool to prepare the component for assembling operations and compliant to dimensional tolerances, or alternatively AM used in special application to be able to apply coating layers on machined products where conventional processes would not be able to be effective [43].

Although the series of reasons which have been earlier mentioned, ahead of the AM challenging introduction in the mass production automotive sector there are several challenges to be correctly addressed. Among the most recurrent we can cite in accordance with [39]:

- **Economical breakthrough of AM limited to low-volume production**
  As is widely reported [39], automotive industries make their profit on market volume. The profit for each car is usually small, especially on lower range models, and therefore the need of break-down costs is fundamental to sustain the whole process. Since the significantly lower production speed of additive processes compared to conventional production techniques their success would be initially devoted to small batch production in which customization and complexity would play a major role since it is still unclear if the capability to scale up the production rate would change significantly any time soon [44].

- **Possibility to print large parts (engine and bodywork components) - BAAM (Big Area Additive Manufacturing)**
  The chance that recently has been given to manufacturer to directly produce products of large dimensions with little need to assemble them thanks to AM has questioned researchers in the direction of investigating current limitations in this field. In a recent work Curran et. al. at Oak Ridge Laboratory, TN [4] have taken up the challenge of printing several Shelby Cobra's subframe structures and bodywork parts in order to bridge the gap between engine testing on the bench and full vehicle testing. The objective of the study is to provide indications about the compliance of the final version of the machine with EPA standard cycles. The advantage given in terms of reduced lead time and cost was substantial and gave consequently the possibility to make vehicle prototyping before having industrialized the chassis production processes with no need to rely on expensive technologies and several operations of assemblies and post processing. The material chosen was a peculiar carbon fiber reinforced ABS able to guarantee good stiffness performances and adequate strength for limited vehicle testing time. The parts produced in the experiment are presented in Fig. 2.10.

Figure 2.10: The Shelby Cobra with the ABS printed chassis before the final assembly of the whole car [4]

Even tough the testing has demonstrated how, with pragmatic scientific approach, BAAM might be ready for prototyping the challenge to bring such technologies into the medium and high volume production has to face several inconveniences such as the possibility to customize part and design to guarantee an increased cost coverage for a process likely to be slower at least at the beginning compared to the mass production counterparts (it is worth to note that still BAAM is considered to be from 100 to 1000 times faster than conventionally AM). In this specific case the focus was the development of an electric powertrain system able to cope with the old-fashioned Cobra body design. Even though the experiment was successful in the conclusions the authors explain their skeptical opinions regarding the actual effectiveness of carbon fiber reinforced ABS as the target material for BAAM since it cannot be used properly to recreate subframe structures as its stiffness could not pare a steel counterpart (*in facts a steel torsion bar has been implemented to achieve successful testing*). The process has a second downside which was the need for a filler for the ABS structure to make it able to better withstand the loads and to achieve proper bonding between the different components: the fill up process with a closer look on the finishing of the front subframe can be seen in Fig. 2.11.

Similarly a mammoth stereolithography process has been developed by *Materialise* [45] that

Figure 2.11: The filling and bonding of the huge ABS 3d-printed front subframe [4]

has been used to produce plastic panels for a Formula Group T race car. Still the limitation of these technologies to plastic and carbon reinforced plastic materials constitutes a considerable obstacle to the introduction of BAAM in any phase of the prototyping process of a motor car.

Having proposed a brief overview of the interested industries on which the project is more related the branches in the design process that the introduction of AM would cause in those industries is going to be briefly presented.

2.3. DESIGN PROCESS FOR ADDITIVE MANUFACTURING

As already explained in the earlier part of this literature review the opportunities given by the introduction of a new manufacturing process like rapid prototyping into established industries departments has brought with it an evolution of the design process in order to optimize the whole process from the designer *idea* to the finished product. The main changes in the design processes are integration of novel calculation techniques such as topology optimization and some new strategies for geometry reconstruction. A brief description of those innovative approaches will be briefly introduced in the next section.

2.3.1. DESIGN PRACTICES INTRODUCED BY ADDITIVE MANUFACTURING

Innovative processing techniques have always been the turning point for the application of properly tuned engineering tools to exploit the maximum performances of the technology introduced. When it comes to AM several approaches have been tried and still nowadays there is debate on how designer should revolutionize their way of proceeding in the definition of new component geometries. Since the freedom of shape has been implemented, even though introducing more subtle limitations, the design process must be rethought in order to take advantage of the novel producing environment. Even more since the design work has different and minimal limitation in the geometrical reconstruction new methods have to be established in order to provide a robust and reliable process in which the capabilities of the new manufacturing technique can be exploited completely. Among the most diverse approaches here we would like to make a brief description of what, within the author experience,

are two methods to correctly proceed while engaging a project that involves additive manufacturing and optimizations routines.

TOPOLOGY OPTIMIZATION - CAE INTERFACE

Topology optimization is a process established in the years based on the material distribution approach presented through the implementation of the **homogenization theory** (see [6, 46]) . The history of topology optimization is relatively recent basing its first studies on previous structural optimization practices. The main steps to the approach of the last established techniques can be seen in Fig. 2.12. The first step has been the optimization of truss structures [46]. The optimization in a truss-structure design involves only the cross section of the members and the length of each truss (Fig. 2.12 *a)*). The second historical step was the problem of optimum shape. Here the problem is the optimization of a fixed topology but with features able to change in size and aspect ratios. Eventually structural engineers and researchers in the field of *finite element analysis* introduced the possibility of optimizing the topology itself. This was considered a big step forwards since it allows engineers to reinvent their structure basic geometry in order to face different needs driving the optimization routines out of the conventional boundaries of best design practices. The basic solution and the most common for structural application is the compliance minimization solution approach which is itself a minimization problem. The objective of the optimization is to find the optimal combination of a given structural parameter -stiffness for instance - among the feasible geometries that fit a design space and complain with the imposed boundary conditions.

The process is a distribution problem in which the material of the design space [10] has to be ranked in such a way that the final shape is the optimum of a certain optimization function. The process, as described in the aforementioned theory can be resumed in five principal steps, from an algorithmic point of view[6]:

1. Choose a proper reference domain: definition of design space, boundaries and exclusion zones
2. Choose a composite structure that would define the density of each mesh element (*holes in a solid for instance* as originally proposed by Bendsoe in [6])
3. Compute the effective material properties of the composite through homogenization theory to establish a relation between the properties and the density of the material
4. Compute the optimal distribution of this composite material through the definition of a density function (the final density of the elements represents their figure of merit and is usually scaled from 0 to 1), this is a sizing problem in which the density is the sizing variable
5. Interpret the optimal distribution as a final shape of the element with the highest density

The steps introduced in [6] established the new trend for this application over the composite theory that was proposed in the same years of defining the structure as a composite of two materials and defining the different elements as part of the soft or the hard material. The ideal design optimization is the *so-called* black and white design in which after the optimization the only elements that are present are the one with an high ranking for which regards the structural behavior of the component.

[10] Defined as the space available for the creation of a component that would resolve the prescribed functions.

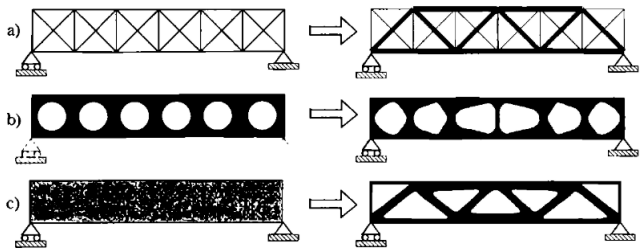

Figure 2.12: Evolution of the computational methods for structural optimization as described in [5, 6]: a) the initial truss structure and the standard structural optimization (*section and length of each component, number of components*), b) the shape optimization method of a fixed topology, c) the topology optimized structure.

A chapter of the constitutive work presents the optimization work that has been performed on the components that are the main focus of this project.

FREE SURFACE RECONSTRUCTION - CAD INTERFACE

The method that provides the designer the possibility to reconstruct surfaces based on a mesh STL file are present in today's CAD market place under different names and description (CATIA V6 Reverse Engineering, Vger Reverse Engineering) are all examples of this new techniques. Alternatively, most of the CAE interfaces (*Abaqus with CATIA V6 and ANSYS with SpaceClaim*) provide tools to reconstruct meshed parts into solids that could be integrated in the CAD process to reach the geometrical soundness to be successfully produced.

The concept behind those is the development of an interface that mixes the parametric solid design as it has been known by engineers since the 1970s in which the definition of parameters and their combinations was the logical process to finalize the 3D mathematics of a part, with the intuition of following the shapes of the optimized geometries.

The process, mathematically, is carried out in different ways but a great example is the free design of surfaces which is usually the best method to approach such a problem of reconstruction. Instead of being parametrically defined through surfaces, intersections, coordinates, split operations and so on, the shape is the result of an interaction between the user and the 3d mesh through the application of **controlling points** (points that lay onto the mesh surface - *we shall better say onto the mesh nodes*) that using rectangular portion of the space create surfaces that are continuous curvature *(C2)*. The surfaces are created in such a way that their distance from the mesh nodes is the smallest possible in order to satisfy different criteria.

The possibilities open by such integration, and subsequent integration of CAE interfaces into CAD software, would make possible the iteration about different design options with no need to interface different offices and involve the time schedule of different resources optimizing the whole designing process either through the possibility of doing more iteration in the same amount of time that would result in a better finished product or alternatively in reduced design time. An example of the end result of the integration of such technologies is presented in Fig. 2.14. The possibility of shaping the material with no geometrical constraint others than the AM limits and boundary interfaces gives rise to a structure with a uniform stress distribution in which no low stressed zone are present. The progress of stress distribution, and especially of strain energy, on a topology optimized component can be seen as a qualitative assessment for a design case as it will be analyzed more deeply in the constitutive work section.

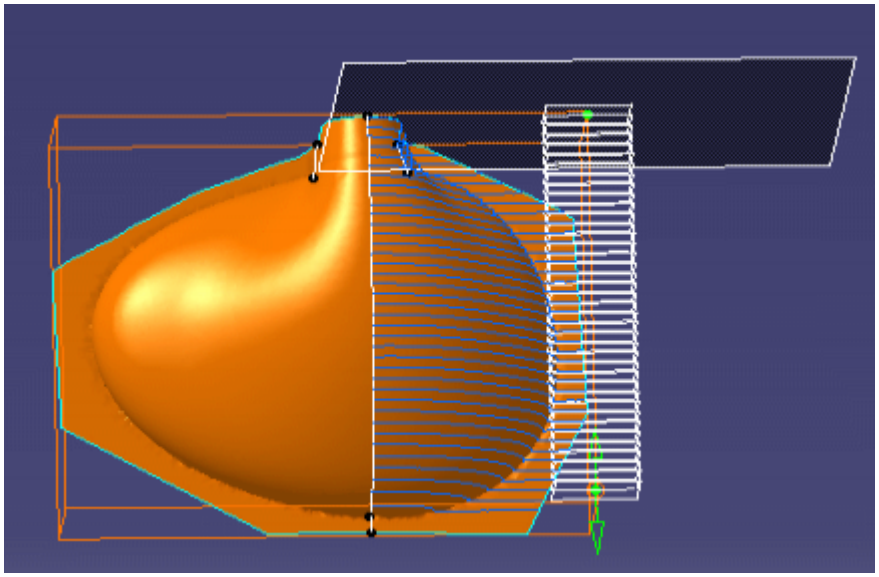

(a) Traditional QSR tools for the parametric reconstruction of surfaces as present in CATIA V5 User Guide[47]

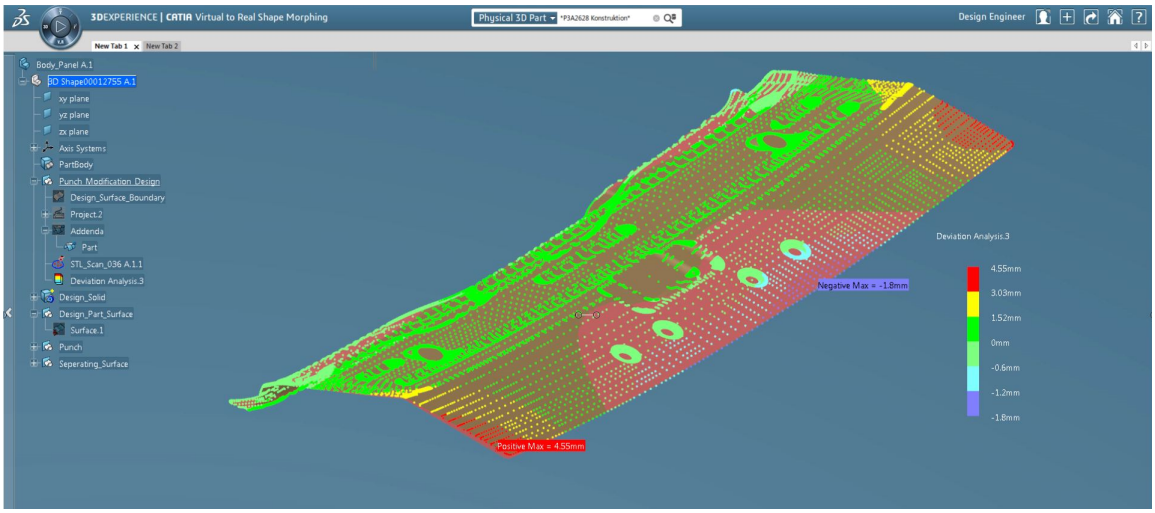

(b) Point driven reconstruction on STL mesh [8]

Figure 2.13: Comparison of graphical interface between traditional QSR (Quick Surface Reconstruction) tools and innovative Reverse Engineering shape interactive interface as present in different edition of CATIA (V5 and V6) CAD interface[7]

2.4. ADDITIVE MANUFACTURING: METAL DEPOSITION METHODS

As the main purpose of this project is to achieve and present the *state-of-art* of AM applied in highly challenging and demanding technological environment, the main part of this chapter presents the current most renown and fundamental techniques for direct metal deposition. The following section will address the topic of processing powders material into solid work-piece by the addition of localized energy flow that would cause the powder to melt (*or partially melt*) and stick together on subsequent layers.

Direct metal deposition process with a *layer-by-layer* technique can be dated back in 1971 with the deposition of Ciraud patent [48]. Soon afterwards a series a institutes take on the proposed challenge and develop a series of methods to implement the technology on different materials. Among all attempts is worth to mention University of Texas in Austin's DTM (*deterministic turing machine*)

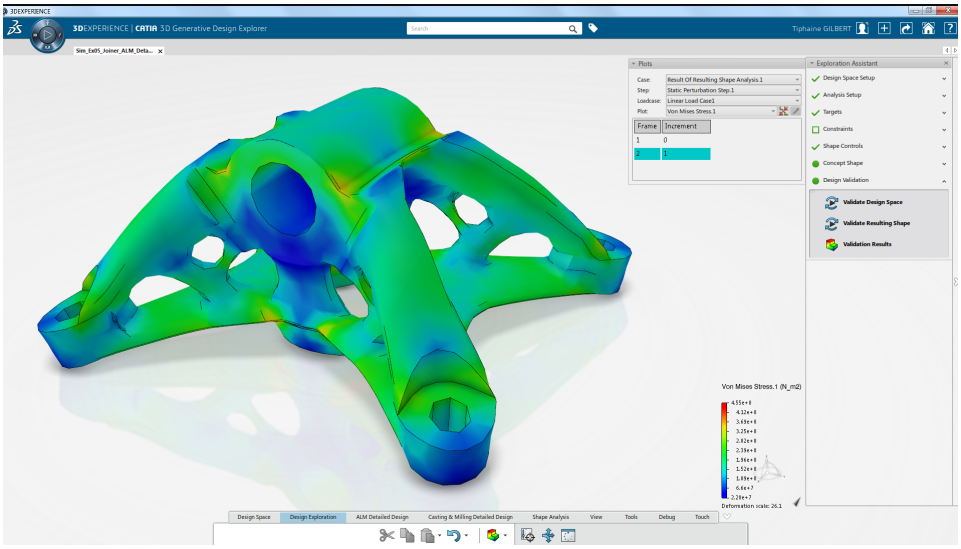

Figure 2.14: End stress evaluation of a topology optimized bracket reconstructed with integrated CAD and CAE interface [8]

technique (1992) which evolved in SLS (*Selective Laser Sintering*)-concept that entered the market few years later. On the other side of the Atlantic ocean, the first European based institution to hit the market with machines for additive manufacturing has been EOS GmbH Electro Optical Systems with early machine for plastic additive manufacturing followed soon after by, through the acquisition of DTM rights, machines for metal deposition and sintering of which evolution still are market best sellers. Meanwhile in Aachen, Germany, at Fraunhoffer Institute the SLM(*Selective Laser Melting*) process was being developed [49].

This original fragmentation of processing techniques, which brings a rich variety of possibilities while approaching the field of direct metal deposition, gives researcher the issue of properly categorize the process them-self. Following the current literature trend [49, 50], the current work would consider AM processes divided in two categories based on the method in which the layer is created if either from a bed fusion process (PBF - *Powder Bed Fusion*) or through a directed energy deposition (DED). The main difference among the two processes is the addition of material to the layer: in the case of PBF the energy comes from a external source such a laser beam and requires the bed thickness to be replaced after each deposition while on the contrary the addition of material in DED processes is included in the beam energy source.

Among DED techniques we can cite following the classification presented in [16]:

- **DMD - *Direct Metal Deposition***: This process employs a closed loop control process through which using laser and metal powder the component is produced. The commercialization has been done by *DM3D Technology LLC.*
- **LENS - *Laser Engineered Net Shaping***: A laser based process developed by *Optomec Inc.* which uses metal powder to produce metallic components
- **WAAM - *Wire and Arc Additive Manufacturing***: Developed by both aerospace and naval industries in order to provide alternative manufacturing processes for a series of components actually limited in lead time and repairability by manufacturing techniques. An example of such components are naval propellers developed in Aluminum-bronze.

On the other hand we can mention among PBF processes:

- **SLS - *Selective Laser Sintering***: Is a process close to DMLS and involves the same technological content. The term refers sometime to technologies used for the production of plastic composite materials. The company that sells machines for SLS processing is *3D Systems Corp.*
- **DMLS - *Direct Metal Laser Sintering***: A sector leading technology that uses sintering through a laser beam of prealloyed metal powders. The system is owned by *EOS GmbH* which serves the market with different machines with available materials scanning from titanium alloys to Inconel and high temperature materials as well as steel and high strength aluminum alloys.
- **SLM - *Selective Laser Melting***: Similarly to SLS this methods differs by the fact that the material undergoes complete melting during the solidification process. The process is property of *SLS Solutions* and is specular to what *Renishaw* provides under the commercial name of Laser Melting (LM) and *Concept Laser*[11] offers with the denomination of Laser Cusing.
- **EBM - *Electronic Beam Melting***: This methods differs from the others since the energy source is not a laser beam produced in different ways but an electron beam that provides the energy needed for a complete fusion of the material. The system is commercialized by *Arcam AB* company.

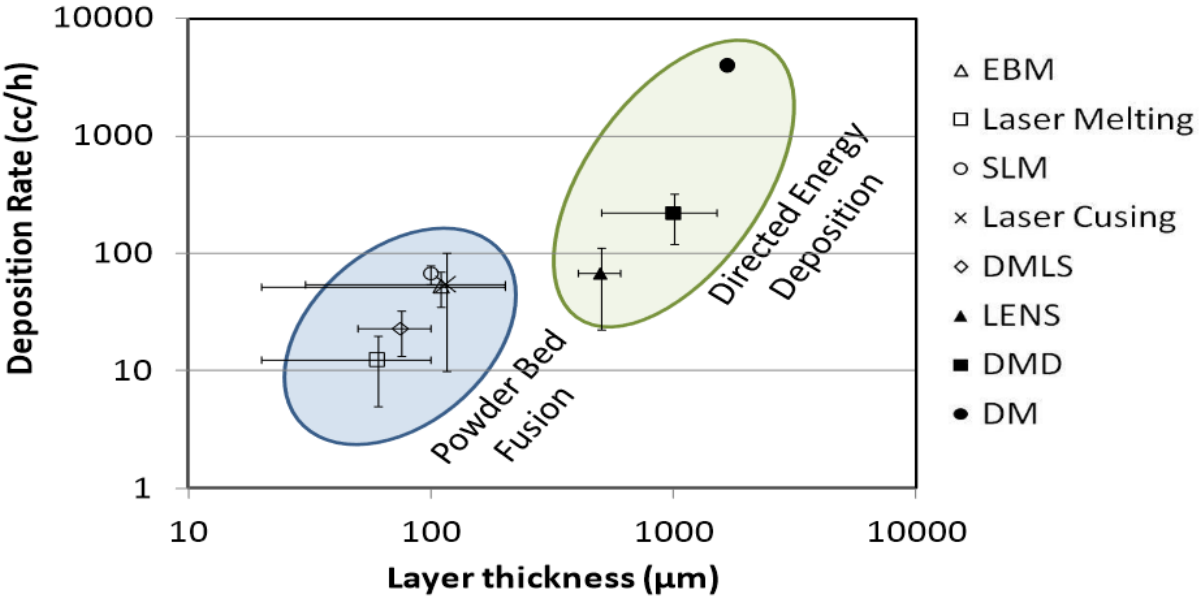

Figure 2.15: Comparison of multiple AM processes in which is highlighted the production rate in respect of its relationship with the layer thickness [9]. As it will be further investigated the better accuracy of PBF methods is related to their lower deposition rate which is mainly due to thinner thicknesses of deposition layer. Furthermore, the focus dimension of PBF methods is smaller that the relative parameter of DED processes.

A quick overview of the main characteristics of the two different classes of techniques for AM presented in the previous list can be seen in Fig.2.16.

[11] A General Electrics spin off.

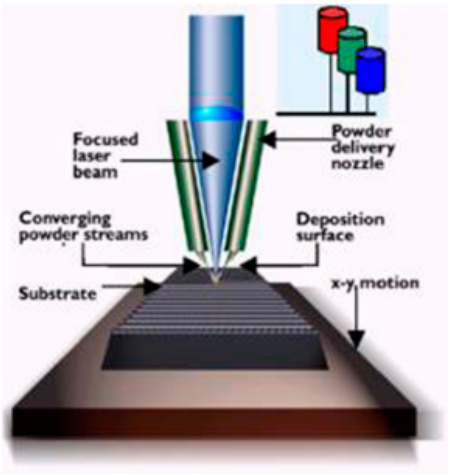

(a) Lens DED processing method

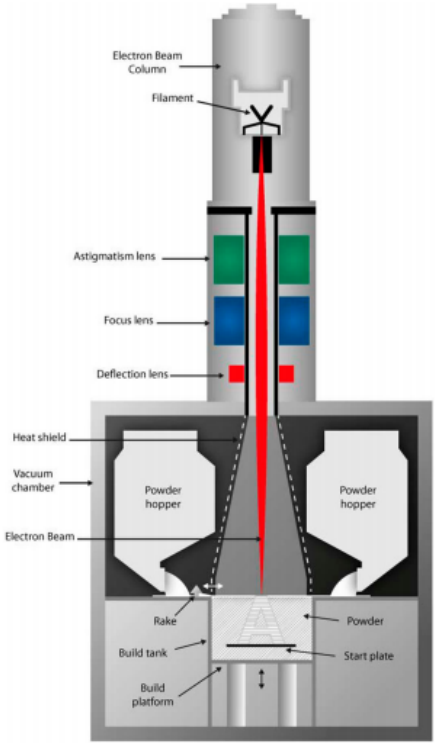

(b) EBM functioning scheme

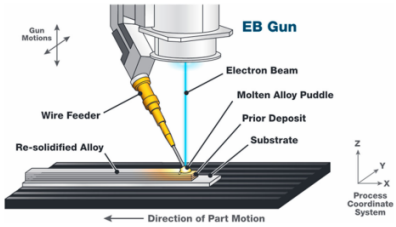

(c) Electron Beam DED functioning scheme

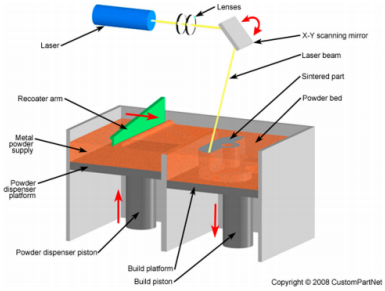

(d) SLM functioning scheme

Figure 2.16: Different Processing schemes for PBF and DED methods as presented in [10]. Their different descriptions are reported to highlight the advantages and disadvantages of each technique. Generally PBF methods are more time consuming (lower deposition rate) but they feature better accuracy and superior mechanical properties.

Since the core topic of the present project is DMLS components the main review would be on the Powder Bed Fusion processing techniques.

A further classification, more specifically related on the metallurgical and physical processes taking place during the production, can be introduced as suggested by Gu in [49] dividing the laser technologies in two categories: *laser melting technologies* and *laser sintering technologies*.The difference in the metallurgical state of the powder is the synthesis of this classification: in sintering processes the metal is partially molten and technologically this is achieved through the use of multi-components pure metals or by the mean of a prealloyed powder material.

Solid state sintering is a process through which solid components are created from powder materials through the application of temperature and pressure with ideally no fusion of the material. Since solid state sintering could not be achieved in the limited time span of a 3D laser scan the energy

supplied must be enough to provoke partial melting of the powder supplied and granting the solidification of the processed part. In powder technologies the chance of partial melting can be achieved in two ways as already mentioned:

- **Multi-component powder of pure metals and prealloyed powder**

  Solidification occurs in the case of a multi-component thanks to the fact that one metal has a lower melting point than the other metal present in the powder. This low-melting point metal (or alloy) is considered the *binding component* while particles of high-melting point pure metal can be considered as the *strengthening component*. An example on a microstructure based on the aforementioned process with a Cu-SCuP powder can be seen in Fig.2.17 in which the lighter and lower melting point alloy can be clearly distinguished in a gray color while the Cu particles are in black.

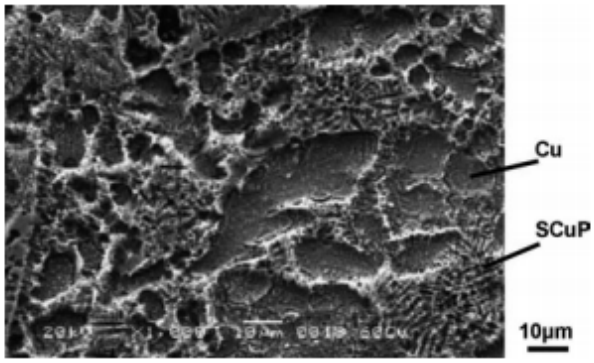

Figure 2.17: Laser Sintered Cu-SCuP multi-component powder

  Usually, part of the composition carries small fraction of fluxing agent and deoxidizers as well to improve the sintering process.

  Acting as a viscous interaction between solid particles and completely melted binding component, the solidification takes place with the presence of capillary forces driven by the small gaps between the unmelted particles. Therefore the liquid solid wetting properties influence greatly the chances of success of laser sintering processes with multi-component powder materials. As well the mechanical characteristic are influenced by the size of original particles and on the success of the solidification process. An example of multi-component system that has been successfully processed is a combination of Cu and Cu-10Sn (pre-alloyed powder) Cu-8.4P (prealloyed powder).Other examples are Fe-based multi-component powder system including but not limited to Fe-Cu and Fe-C-Cu-P [51].

  A clear advantage of implementing a prealloyed powder to the laser sintering of multi-component powders for additive manufacturing for metal components is the heterogeneous melting temperature that opens the temperature windows at which the sintering can take place thanks to the presence of a bi-phase region under the *liquidus* and *solidus* curves on the phase diagram (cfr. Fig.2.18). A good example of taking advantage of a quasi-eutectic composition would be analyzed during the description of Aluminum alloys sintering.

- **Prealloyed powder**:

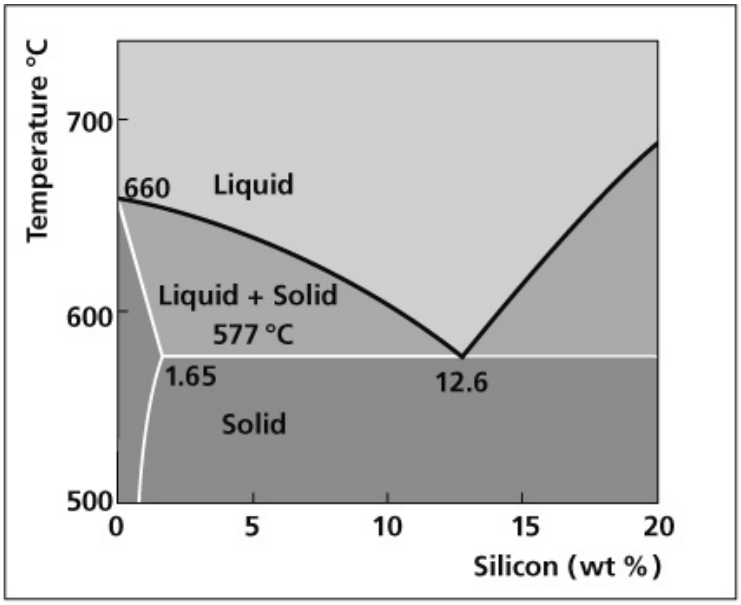

Figure 2.18: The binary system of Aluminum and Silicum: the composition usually implemented for AM sintering is near the eutectic point (AlSi10Mg) to provide better performances in terms of density of the end product. The low melting point is responsible for the poor properties of the alloy in temperature as it will further explained in the course of Chapter 3.

As already mentioned the presence of a *mushy* zone affects greatly the behavior of prealloyed powders while compared to pure metals. The presence of an heterogeneous melting point would cause the powder to start behaving viscously once a sufficient part of the particles under the laser beam effect have reached the mushy zone. The presence of such a phenomenon affects also the local composition of the novel microstructure and the process is sometimes referred to as SLPS (Supersolidus Liquid Phase Sintering). The liquid phase starts developing at grain boundaries and apex since the energy available in those location is usually higher than what is available in the grains. There are two recognized methods that cooperates in the solidification of this semi-solid state of the material and is the wetting of solid particles as well as a solution re-precipitation. There has been scientific proof of the mentioned methods such as reported by Niu [11]. A good explanation of SLPS process can be resumed through the illustration presented in Fig. 2.19 [49], the liquefaction of the *mushy* zone exposes grains to the pores and through the viscous motion of those solid particles the densification process can start. Differently from what has been mentioned about Fig. 2.17 it is not possible to show clearly where the liquid molten pool was but still the trace of it at grain boundaries can be identified as reported in Fig.2.20

Among the mentioned technologies some of them seem to be clearly in advance regarding compatibility with market's demand, dimensional accuracy, available materials and material properties after printing. Of these technologies a deeper review is presented in the following sections. The DMLS process is going to be presented first as they were the actual manufacturing processes implemented in this thesis project. An overview of EBM will be presented as well as a possible competitive technologies and advantages and disadvantages of the two technologies will be highlighted.

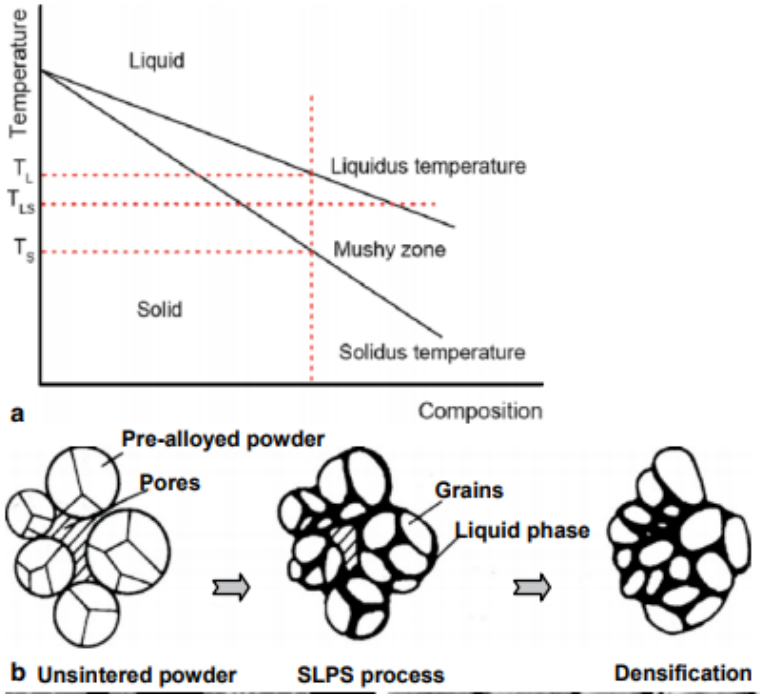

Figure 2.19: SLPS Process and relative temperature on a binary phase diagram: the process features three different phases. From left to right it can be noted the change from the unsintered powder to the dense product at the end of the sintering.

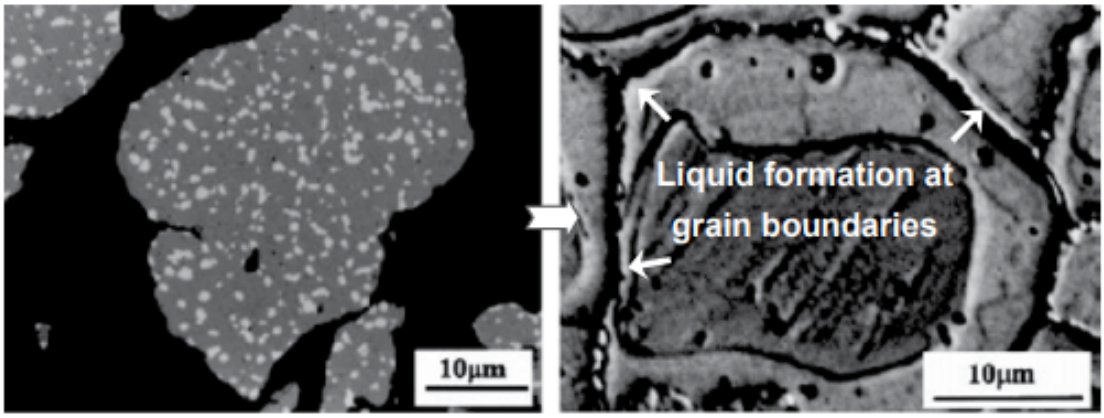

Figure 2.20: *a* Pre-alloyed metal powder, *b* DMLS processed part (high speed steel see[11]). The liquid formation at grain boundaries is evident at the right side of the picture while the center of the grain remains untouched.

2.4.1. DMLS - DIRECT METAL LASER SINTERING

As presented in the previous section DMLS is a Powder Bed Fusion process address to as Direct Metal Laser Sintering and is a laser sintering method in which the component (or components) that undergoes full liquefaction is part of the overall powder material. The system is patented by EOS (Electro Optical Systems), Germany, that during the years has developed partnerships and acquired other patents on processing techniques from DTM and 3D Systems. The laser beam is produced through CO2 methods or in recent machine by a fiber laser, that with a vector scanning method provides the energy for the powder to sinter. The layer deposition occurs through a mechanism that involves a vibrating channel as reported in [12].

The DMLS processing technique evolves from the early concepts of Ciraud and the Hull method

for 3D printed fabrication starting from powder materials [52]. The project is co-eve with similar processes developed by EOS market competitors already mentioned in the previous section such as 3D Systems and DTM. The first machine ready for commercialization has been presented in 1994 and at the time was the only option to the previous DTM machine (Sinterstation 2000). Those machines were able to successfully print polymeric material such as wax, polystyrene and a nylon mixture but no metal sintering was ready to hit the market until the summer of 1995 even tough a year earlier at the Fraunhofer Institute in Germany and in the Belgian Katholieke Universiteit Leaven successful attempt of printing stainless steel (316L) and Fe-Cu mixtures respectively were reported [12]. The Sinterstation 2000 can be seen in Fig.2.21.

Figure 2.21: The first laser sintering machine available for the first time in December 1992: the **Sinterstation 2000** by DTM

The first machine able to produce sintered metals was therefore the EOSINT M250 featuring a 0.1mm layer thickness and a CO2 laser beam with a maximum output power rated at 100W. The material chosen for the first machine was a mixture of bronze and nickel powder developed by Nyrhila for pressure-less sintering [53]. The material development followed consequently with the commercial success of the machine. The initial concept of a material that would grant low shrinkage during melting and remelting was a key contribution to the technology success and directly derives from the very first material used in DMLS [53].

The first full dense steel available for DMLS machines was the DirectSteel20 (in which the 20 represent the thickness of each deposited layer in μm). Then the natural evolution of this process was the developing of a tool high strength steel (DirectSteel H20) which featured a Rm in excess of 1100 MPa. As more performer materials began to show undisclosed potential for DMLS technique the machines have evolved consequently. The end result was a change in the laser source from CO2 to Nd:YAG to end up with fiber laser able to provide narrower beam focus able to project (with a power that reached the 200W in the EOS M270) a specific output of 25kW/mm2. The higher surface energy made possible the sintering of material that were not absorbing enough energy due to their reflection index and thermal conductivity. As well a shorter wavelength promoted by the use of fiber laser provides more effective power since the frequency is considerably close to the maximum absorption that metals exhibit. The increased efficiency of the laser beam and the higher absorbed energy have unlocked the chance to proceed with higher processing speeds, beneficial for the customer use.

In the first decade of development the process was ready to step up the production standards and evolve from a "Rapid tooling" manufacturing process, in which the main interest was the production of molds or similar objects for plastic injection avoiding the high cost of casting molds, to a full "Rapid prototyping" techniques. This involved the need of full dense part that could exhibit 100% of the mechanical properties, good surface finishing and accurate dimensioning directly from the first printing to avoid costly re-machining operations. In Fig. 2.22 an tooling cross-through section is presented, the part is printed by an EOSINT M250 machine in DirectSteel H20 and three different layers can be noted:

1. The surface (outer skin) present a full dense structure with a density close to 100%. The component underwent a shot peening process in order to ensure a better surface finishing

2. The inner skin is somewhat less dense and some lack of fusion or voids can be clearly seen, the reported density is around 97% and the volume rate at which this zone has been manufactured is 6 times the outer surface

3. Finally the core of this tooling component can be seen at the bottom of the picture: the density is definitely lower than the higher layers (94%) but the material adding rate is slightly superior(4 mm3/s instead of 3 for the inner skin)

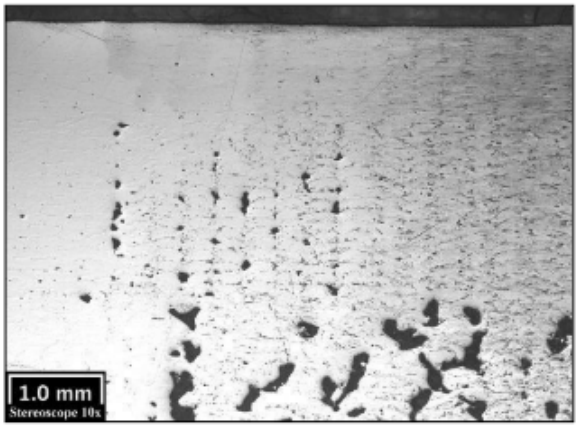

Figure 2.22: An EOSINT M250 processed section at different deposition rate as presented in [12]

As already mentioned the need to step up the process involved the creation of better laser sources able to cope with the increased need of full dense component to implement a real "Rapid prototyping" process. The variable density that was used for optimizing the tooling is no longer acceptable for real components during the product development phase. The natural evolution of the processing techniques has involved a series of materials available nowadays for DMLS processing that vary. A partial overview on those can mention (partly but not only from [54]):

- **Steel Alloys:** Maraging Steel (commercially named MS1), Tool Steel (17-4PH) and various stainless steel (17-4 - known as X5CrNiCuNb16-4)

- **Aluminum Alloys:** AlSi10Mg, Scalmalloy (Scandium modified aluminum alloy)

- **Titanium Alloys:** Ti6Al4V and the low interstitial version of the same alloy (Ti6Al4V-ELI), TiCP (grade 2) commercially pure titanium
- **Superalloys:** Nickel based and Cobalt based (among which: IN625, IN718)

Furthermore, specific alloys such as bronze and silver have been developed in order to satisfy peculiar request but since their use as structural materials provide no interest, due to their poor specific properties, we will no longer mention them in this project.

2.4.2. EBM

Electron Beam Melting as already mentioned is a processing technique developed by Arcam in Sweden [15]. The patent for EBM dates back to 2000 by Larsonn [55]. Being a Powder Bed Fusion method it does not differ significantly from DLMS schematics but the acting mechanism for the solidification and the energy source is different and this brings consequences also on the final properties of the material produced with such techniques. In 2011 60 systems for EBM were reported to be installed [56]. The basic scheme of an EBM machine with its main components is presented in Fig. 2.16b [56]. Achieving complete fusion of the metal powder the process is quite similar to processes like SLM. As the two processes are compared in [57] is reported their capability to reach density levels close to 100%.

As the technology is relatively new, only a few materials are available, mainly titanium alloys and cobalt chrome.

Usually parts processed by EBM show a better density lever rather than DMLS processed counterparts but as a side effect the resolution does not reach the level of DMLS due to the different dimension of the minimum laser focus [16]. An interesting study conducted on the differences of residual stresses and proceedings of the two manufacturing techniques[13]. A first glimpse of the main differences can be understood in Fig.2.23a and Fig.2.23b in which the comparison were evaluated on IN718 parts[12]. The end result of the study is the evidence that due to some processing parameters (such as layer thickness and scanning speed) the DMLS process can produce a pore-free material with the drawback of some residual stresses. On the contrary due to higher pre-heating level in the EBM machine the residual stress levels were substantially lower. It is worth to note the different level of homogenization of the two microstructures. Since the cooling rate is enormously slower on the EBM processed part there is clearly evident how the DMLS part presents a more layered structure with less amalgamation between the scan passes.

A second microstructure presented is a section of Ti6Al4V in Fig.2.24: the alloy is presented in four different states: from the print to the final heat treat. In Fig.2.24*b)* the microstructure after printing presents an extremely fine grain structure that reflects how the cooling rate, even if considerably lower than in the DMLS process, are still considerably high. Such dispersion of precipitates and phases in small grains is what grants AMed parts good tensile properties and the possibility to have consistent elongations and therefore ductility despite the presence of geometrical incoherences and numerous defects. The part has been heat treated with a HIP process and eventually with a full heat treatment. The evolution of the microstructure is evident: as the relatively equiaxed structure after EBM undergoes crystal growth and full re-crystallization during the HIP process and afterwards a lamellar du-

[12] IN718 is the abbreviation for a nickel based superalloys. A typical specification for DMLS product can be found at[58]

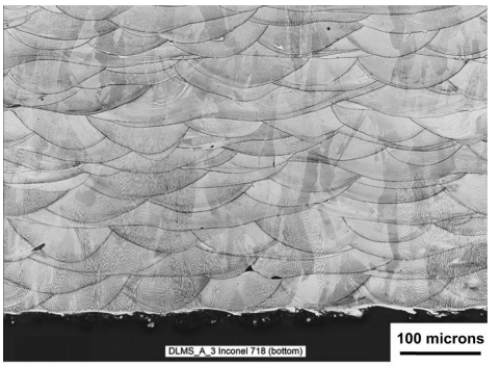

(a) Bottom section in LOM of a DMLS produced workpiece in IN718

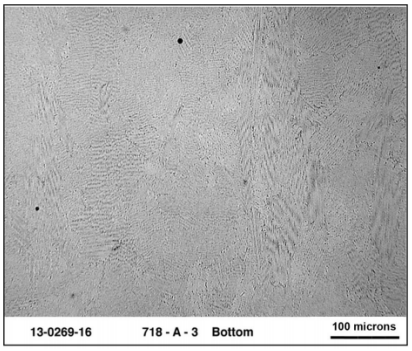

(b) Bottom section of a IN718 alloy workpiece produced by EBM

Figure 2.23: Comparison between the different processing techniques for the production of IN718 parts as reported in [13]. The section oriented alongside the Z direction (Fig.2.23a) shows clearly the effect of layering and subsequent fusion passes on the DMLS produced micrography.

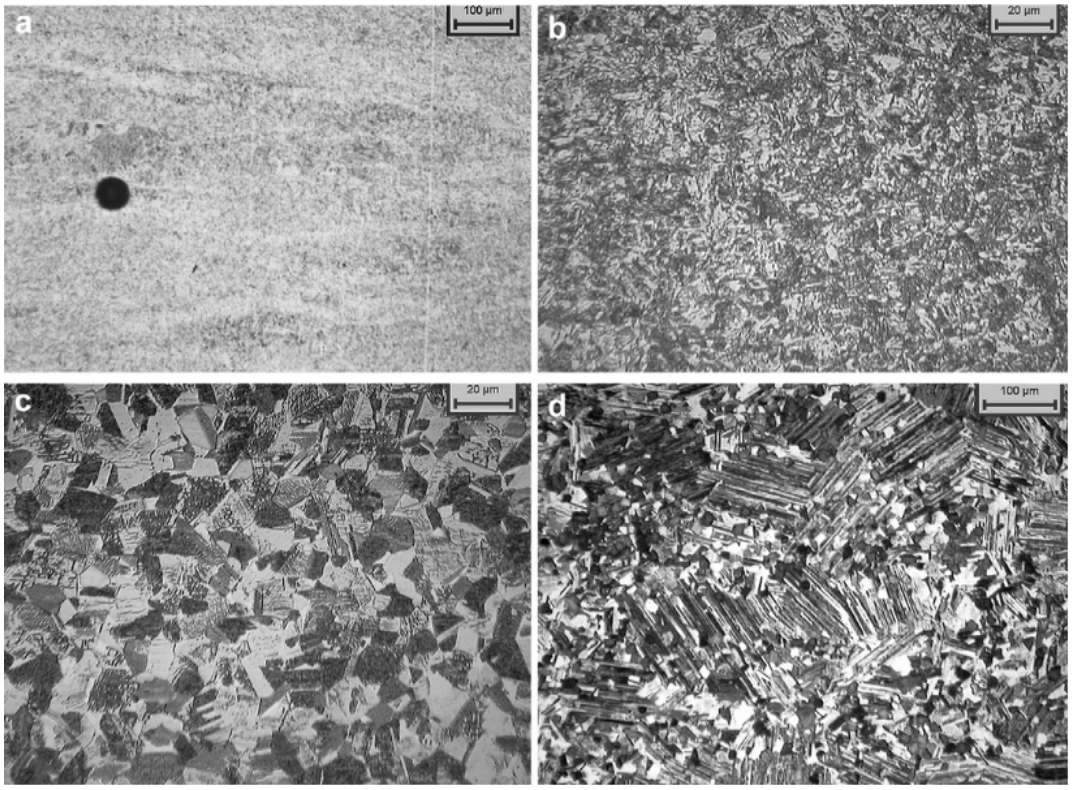

Figure 2.24: Microstructures of processed γ-TiAl: typical spherical gas induced porosity (a); after printing by EBM (b); after HIP *(Hot Isostatic Pressing)* (c); after thermal treatment (d). Printing sample is showing a small equiaxed microstructure while HIP processed sample shows bigger grains and a more uniform equiaxed structure. Finally, the heat treatment performed gave rise to a lamellar structure which is originated by the low cooling rate from the annealing temperature.

plex microstructure is obtained featuring small (averagely sized around 15-20 μm) equiaxed grains (around 60%) with a remaining bigger lamellar phase grains (*circa* 100 μm).

2.5. MATERIAL CONSIDERATIONS - MICROSTRUCTURES, PROCESSING AND TREATMENTS

Having reviewed the main processing techniques from a broader point of view, in the last section of this literature review the peculiar material properties and microstructural and physical events that take place during the process of AM will be presented. Firstly the powder materials are shown and typical defects from AM reported as in the current literature trend. The subsequent section will deal with the thermal history of AMed parts and how this is related to the mechanical properties through the presence of peculiar microstructures. Before a brief presentation on specific materials, which have been investigated for the application of the current project, the current *state-of-art* of the post processing techniques is presented covering both mechanical post processing and post printing heat treatment.

2.5.1. POWDER MATERIALS AND AM TYPICAL DEFECTS

The raw materials for all PBF-AM techniques is a powder. The powder quality represents the first quality assessment of a DMLS process or any other relevant near net shape direct manufacturing process [10]. Since the variety of processing methods for powder production can have a significant impact on the overall quality of the print a brief explanation of those is presented and strictly linked to the possible phenomena that are cause of defects.

POWDER MATERIALS

Among different processing techniques there are five of them that are seen as emerging for the production of metallic powder of prealloyed materials:

- **Rotary Atomization (RA) [16]** This process involves the mechanical energy due to centrifugal forces acting on the melt of an alloy. Due to the proper interaction with the rotating equipment the metal is fragmented is small particles that would solidifies singularly making possible the solidification of a powder material. Since the process is driven by the mechanical interaction of the melt with the equipment the end result is usually a powder of low quality.

- **Gas Atomization (GA) [10, 16]** The process involves a gas nozzle that sprays the molten metal in a series of small droplets. Thanks to the specific inert atmosphere that is provided during this process the droplets are able to solidify without incorporating any gas particle. The present method is usually carried out in synchronization with a vacuum induction melting process and a subsequent degasification that is the step ahead the atomization.

- **Hydride-Dehydride (HdH) [16]** The HdH process is a method of creating titanium powders from ingots material or also a mean by which scrap can be recycled, involving the properties of Ti hydrate[59]. Since those compound are exceptionally brittle once the baseline materials is treated to make hydrates it is possible to brake it very small particles by mechanical processing. Due to the fact that the method is basically relying on the brittle fracture of Ti-hydrates particles the shape cannot be easily controlled.

- **Plasma Atomization (PA)** This process sometimes is called Plasma Spheroidization can be used

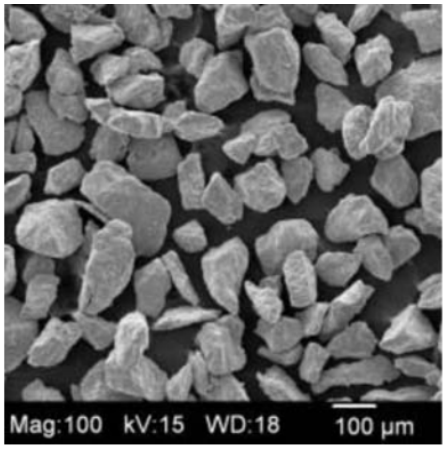

(a) Irregular shaped Ti6Al4V powder hydride-dehydride

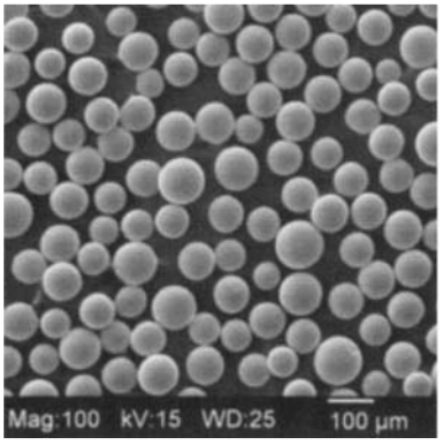

(b) Spherical prealloyed Ti6Al4V powder produced by Tekna techniques (produced by processing angular HDH) [16]

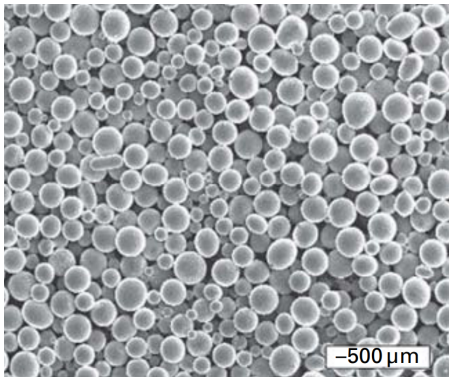

(c) Spherical prealloyed Ti6Al4V powder

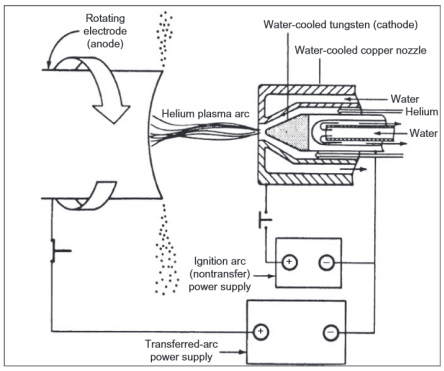

(d) PREP processing techniques for powder production scheme

Figure 2.25: Different Ti powder aspects from SEM images and the scheme in Fig.2.25d of *Plasma Rotating Electrode Process*. As it can be seen by the different typical sizes and aspect ratios the powder production method has a huge influence on the quality of the raw material that is the base on which the AM process will build the finished component.

to reduce the shape errors in HdH processed powders. The quality of the latter is usually not high enough to provide a useful material for processes such as DMLS and EBM.

- **Plasma Rotating Electrode Process (PREP)** The latter technique is the one which provides the highest quality material among the selected technologies. The particles are highly smooth and the ratio between the highest and smalls diameter on the particle (a parameter which relates directly to the high spherical shape) is the closest to one. Still this process involves the uses of high cost machines and therefore attempt to avoid atomization through PREP have been tried being the starting point for alternatives processing powder production methods.

As the present list presents the most common ways for powder production, it can be easily noted that there are two main categories: melt processes and non-melt processes. Non-melt processes cannot produce regularly shaped particles since they base the production on the mechanical fracture of wrought products or chemical decomposition of their derived products. There have been attempt to use HdH powders in to EBM machines but the porosity level (which is one of the benefits of this specific processing technique) has never reached decent standard [10]. HIP (Hot Isostatic Pressing) and

a custom *double melt* process have been tried but as of now none of the conducted studies claims successful implementation of HdH or mixed powders onto EBM processing.

Following the already cited work of Somes at Oak Ridge Laboratories, as a general guidance, we can distinguish powder with small amount of satellites (GA) and others with smoother and spherical aspect (PA and PREP). Gas Atomized powders carries as well the issue of intrinsic porosity due to the entrapped gases during the production step.

The main characteristics of a powder material that reflect its quality are the flow-ability and the apparent density (as a measure of how well the powder can be packed) [10]. Furthermore, other important aspects[16] of a powder material are: size and size distribution (as already discussed) which determines the lowest possible thickness of the additive process, the presence of satellites which nullifies the printability and flow characteristic, the powder morphology *(angular or spheroidal, needle shaped, nodular, platelet or plates)* and the chemical composition[13]. Eventually, in the quality assessment of a powder material other aspects should be considered as they represent potential starting points for defects formation. Among the most common sources of problems there are issues related to the humidity content which is a tunneling through which oxygen can reach the solidification chamber and the powder handling and contamination.

AM TYPICAL DEFECTS

Defects represent a critical aspect for any additive manufacturing technique. Due to the fact that material is added throughout the structure internal defects such as lack of fusion, inclusion, balling or excessive porosity cannot be neglected since the health of the structure would be highly damaged. Furthermore the implementation of complex and optimized geometries usually leads to stressed structures in which the presence of a defect could make critical any reduction of the Reserve Factor (RF) of the component itself[14].

Typical defects for additive manufacturing of metal component are: inclusions, lack of fusion, gas incorporation, cracking and delamination as well as swelling. Other aspects of 3D printed metal parts that cannot be regarded as defects (since they are intrinsically related to the *layer-by layer* processing) but still from a mechanical point of view can be considered as degradation of the structure. Among those we can cite the porosity level, which is directly responsible for the mechanical properties, and the *layering effect* that influences the level of surface finishing.

In the images reported various examples of typical defects are presented (Fig. 2.26).

One more effect which is related not only to structural defects but also with the thermal history of the processed material is presence of residual stresses. Since the thermal history of each layer experiences temperature gradients throughout the printing process the interaction between the hot zones and the low temperature points gives rise to high thermal residual stresses.

An analytical analysis of each defect would go beyond the scope of this review but still some clarification on specific defects might be worth mentioning since their presence on AMed components is

[13] As reported by Dutta and Froes [16] there is current no chemical evaluation of the powder their self but all references from the ASTM committee is done to the end product. typical is the addition of Al in Ti6Al4V in EBM processes to compensate for the aluminum losses (see [56]) during the process itself.

[14] The Reserve Factor, sometimes referred to as Safety Factor, represents the ratio between the allowable stress in a structure and the yield stress of the material. In structural components the definition of a proper target RF is critical for the design. Furthermore, despite the use of RF is considered to be a conservative approach since represents the confident level of the designer on the most stressed point of an object the presence of highly optimized structures might lead to component design in which the areas involved in the definition of the RF would not be constituted by singularities.

(a) Delamination between layer as the combined effect of residual stresses and poor *inter-layer* melting

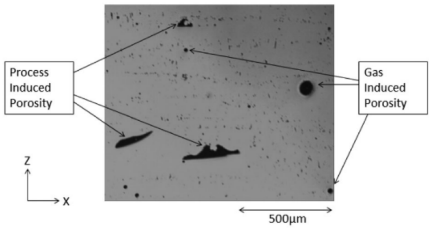

(b) Lack of fusion and porosity deriving either from processing (left) or from powder defects

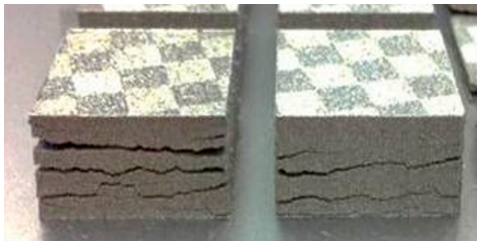

(c) *Inter-Layer* Cracking in tool steel

(d) Metal Balling Formation on Stainless Steel

Figure 2.26: Different typical defects typically encountered in the manufacturing of AM parts as reported by [10]. The difference of defects origin influences the methods for correcting the AM defect level. Defect level can be described for surface and volume defects and their characteristic dimensions for DMLS and SLM processes is usually in the order of tenths of millimeter.

relatively frequent. Starting from what has been presented in Fig. 2.26, we can see how porosity is the most common defect or characteristic of AMed components.

Porosity has different sources as already mentioned: it can be due to high porosity already present in the powder material *(powder -induced)* or it can be created during the sintering process *(process-induced)* as it can be clearly seen in Fig. 2.26b. The *process-induced* porosity presents typically a stretched geometries in the direction of the print since the lack of fusion which might be the cause of the porosity tends to follow the melting pool of the laser scan. While the causes for *powder-induced* porosity can be found in the low quality of the powder itself or in the presence of moisture in the raw material, the *process-induced* porosity is usually due to insufficient energy from the scanning laser or because of *spatter ejection*[15] [10].

The second most common defect of any near net shaping direct manufacturing method is the possibility to encounter the presence of the so-called *Balling Effect*. An example of such defect is reported in Fig. 2.26d. The presence of high surface tension is responsible for the activation of this event. It has been report a direct link to a physical explanation for metal balling and its related to the molten pool aspect ratio[61]. In facts, when the length of the pool is bigger than twice the diameter balling effect is likely to be present since the force that is keeping the molten pool in the form of a bead would be lower than the reduction of energy possible for the minimization of the exposed surface

[15]Spatter Ejection is a phenomenon which involves the interactions between the fusion bed and the beam. Due to the fact that sometimes the energy locally is increased in some zones the might be the sufficient temperature to provoke boiling of the alloy. The convective motion that causes the droplet to escape the melt pool is usually referred to as 'Spatter Ejection'. To happen the energy of the vapor has to overrun the tension surface forces of the molten pool. The process is similar to what happens in welding [60]

which tends to create molten pool that are spherically shaped. Metal balling is less likely to appear on sintered parts (DMLS) since the portion of material that undergoes melting is not as much as it is during melting processes (SLM or EBM).

2.5.2. THERMAL HISTORY, MICROSTRUCTURE AND MECHANICAL PROPERTIES

As the central point of the processing the thermal history of any 3D printed component represents the moment in which the sintering process takes place. Even though some peculiar aspects are present for any processing techniques all of the PBF processes share some elemental physics that is worth to analyze.

Due to the intrinsic repetitive nature of an additive manufacturing process which through the deposition of consecutive layers produces a solid part, each layer of the component experiences a series of decreasing temperature peak in a very limited time span. In order to focus the attention of the project to the relevant subject of the constitutive work the discussion will be limited to the case of mainly prealloyed powder sintering but with some cross references to other processes when those would be useful to achieve a broader comprehension of the thermal phenomena going on at a microstructural level.

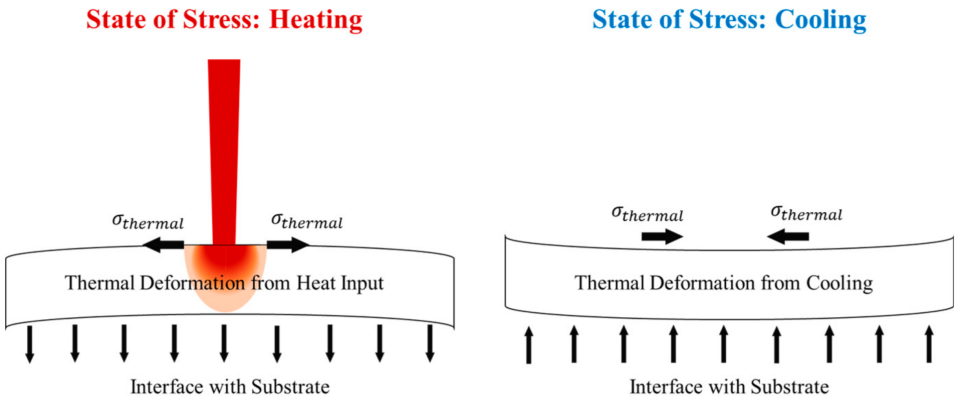

Figure 2.27: Basic scheme of traction and compression residual stresses created by localized heating of a material substrate. The thermal gradient in the component during the printing process is the phenomenon that leads to the formation of residual stresses. The main material properties involved in the determination of residual stresses are the CTE, the heat conductivity and the shrinkage upon solidification (especially for SLM technique) [14].

The first phenomenon that needs to be analyzed is the repetitive heating to zone up to the mushy zone between the *solidus* and the *liquidus* curves on the typical binary phase diagram. In Fig.2.3 a qualitative profile of temperature is presented: in this specific case the temperature peak would take the powder into the molten liquid state. During the following passes the material above is screening part of the energy by partial melting and by the resistance to conduction of heat and the peak temperature reduces. The higher the absorbed energy the higher the penetration depth of the radiation. Usually the penetration depth (δ) of an incident beam is defined as the length from the surface at which the energy is equal to $1\backslash e$ (around 37%). Since the process of powder absorption is different from the bulk material behavior different approaches have been taken to address this issue.

The first process taking place during the sintering process is the interaction between the powder bed and the laser or electronic beam, generally the energy source. The phenomenon of interest is the absorption of energy by the material and the subsequent physical phenomena that are started by the

heating process. The property that indicates how well a material is able to absorb energy coming from an electromagnetic wave is the *absorptance*: the higher is the ratio between the absorbed radiation and the total incident radiation the higher is the absorptance[49].

To better understand the thermal history of additively produced components after the presence of localized melting there is the need to clarify the heat transfer modes that take place during the cooling process. Depending on the processing technique the cooling process can act differently: if in SLM and DMLS the presence of an ambient gas can stimulate heat losses though convection transfer this is not possible for EBM which is carried out in a vacuum atmosphere. If in sintering and laser melting processes the substrate is usually heathen up to prevent excessive deformation and residual stresses[16] the process for EBM takes place at higher temperature and this is responsible for usually lower tensile properties for materials printed with this technology which exhibit a more ductile behavior. The EBM titanium due to the slow cooling process granted by the technology that provides an high temperature throughout the manufacturing can be considered to be in the naturally aged condition when in *'as built'* conditions[62].

The solidification process though is guided by the melt pool characteristic. As already mentioned the melting pool geometry influences the overall defect formation as is usually a compromise between scan speed and beam power. As seen in previous section during the development of DMLS the laser beam became a limiting factor due to its low initial power[17]. As the cooling and heating rates changes their influence on residual stresses is increased or diminished the basic stress state induced by local heating are graphically represented in Fig.2.27.

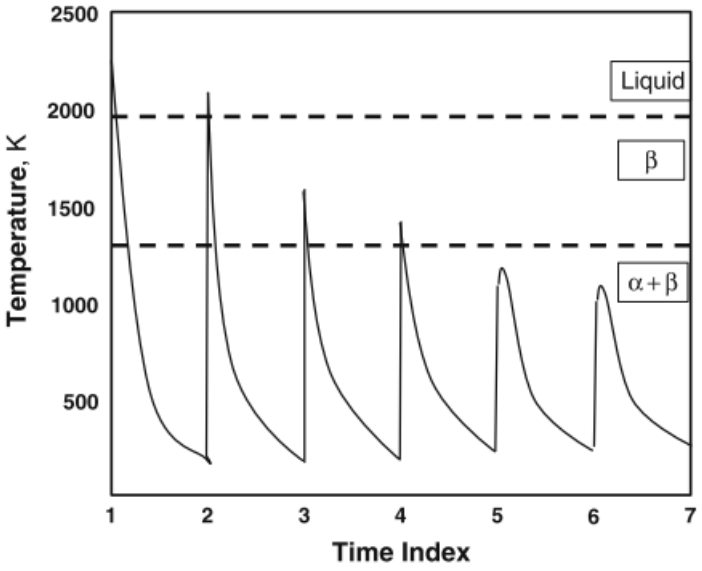

Figure 2.28: Typical temperature profile that a (Ti6Al4V) layer experience during the production of an AMed component [15]. As it can be noted the first pass induces complete melting and also in the second pass some melting might be present; subsequently the material undergoes a series of rapid cycles of heating and cooling determined by processing parameters (scan input energy), material properties (heat conductivity) and environment variables (chamber temperature).

2.5.3. POST PROCESSING TECHNIQUES

[16] Usually around 100-200°C [10]

[17] CO_2 laser with a nominal power of 100W then increased to 200W with the introduction of the fiber laser

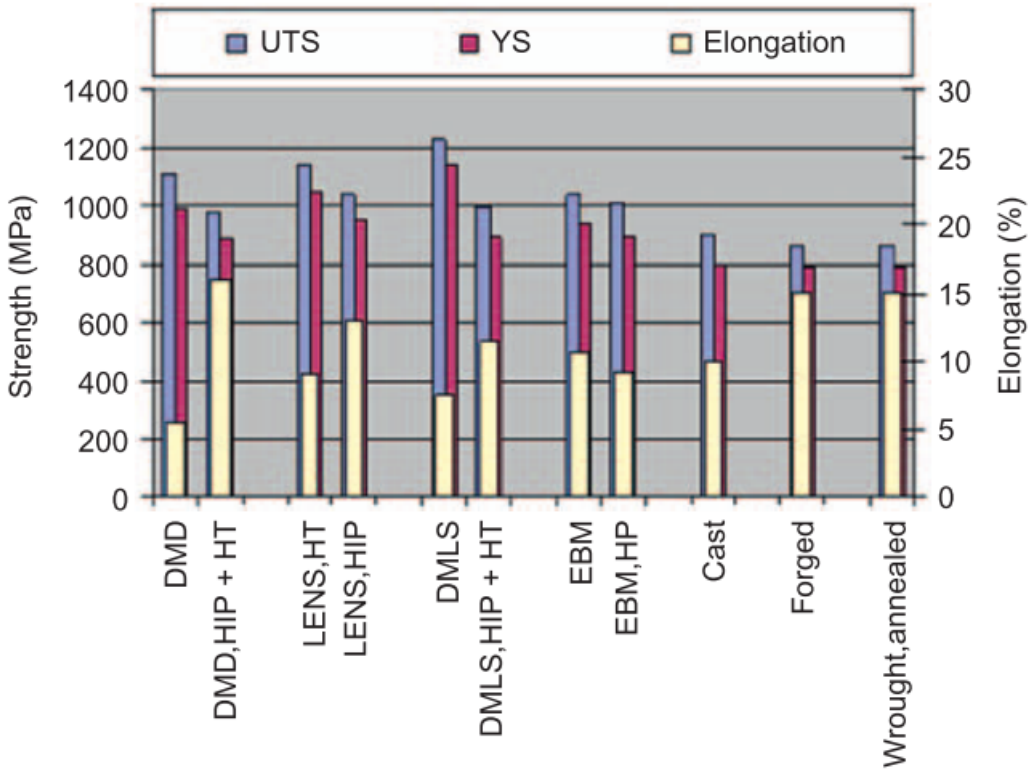

Figure 2.29: Properties of Ti6Al4V with various processing techniques and different post processing heat treatments [16]: the influence of the processing technique is evident since it is responsible of the microstructure granting either sufficient strength without loosing the ductility of the alloy. DMLS processing for titanium shows among the best strength levels: the elongation values is slightly less than annealed wrought products. The implementation of hipping restores the lost ductility without compromising the strength levels.

HEAT TREATMENTS

Different heat treatments are available for different purposes in DMLS and more generally in AM. Most of them have the object of reducing the internal residual stresses due to the thermal processing during production. Other treatments are customized to increase the density in applications that would not allow any porosity in the material especially at a surface layer (as in hydraulics manifold [1]). Among the most common heat treatments it is useful to get description for three of them:

- **SR - Stress Relief**

  The most common post processing heat treatment for AMed parts, as already mentioned previously, is a distention process. The objective of such treatment is to resolve the internal residual stresses that rise up during the *layer-by-layer* production process. The typical temperature strongly depends on the alloy. Since residual stresses indicate the presence of a certain level of dislocation movement a certain recrystallization is needed to restore the original ductility. The temperature level is usually over half of the Tm[18] which is considered to be the conventional recrystallization temperature[19]. This specific process has been applied in the current process to recover the serious residual stresses present in the titanium component as it will be seen in

[18] Melting point expressed in K.
[19] Temperature at which 50% of the recrystallization takes place in 1 hr.

following section of the constitutive work.

- **HIP - Hot Isostatic Pressing**
  HIP is a process developed originally for casted powders and for castings that found application in AMed components especially at the beginning as it is a viable method to increase the density level of a component. The process involves the application of both temperature and pressure levels in order to force the compaction of the material while being held over the recrystallization temperature and therefore without inducing any local plastic flow [63]. The use of a non reacting medium is usually a wise choice especially for Ti alloys and the use of argon is a clear implementation of the concept. The fatigue properties are usually enhanced which are critical for application where titanium is used. The current standard for HIP processing of titanium alloys through furnace heating at 900°C for 2 hr. Similar processes exist for steel and aluminum alloys. The better ductility is followed usually by a reduction of tensile admissible stress (see [64]).

- **PH - Precipitation Hardening**
  PH is not a commonly used process in AM manufacturing[20] but since it has a relevance to one of the design components of the present project in the author's view the description is seen as strictly relevant to this literature review. With the definition of precipitation hardening it is intended a process in which a material with a *frozen*[21] microstructure coming from a solubilization treatment is heated to provoke the growth and coalescence of precipitates that would strive to reach the equilibrium composition and substitute the monophasic supersaturated solution with a biphasic microstructure[65]. Since the high cooling rates of additive manufacturing aluminum alloys might finish the production process with a supersaturated solution which is not optimal in the case of precipitation hardened aluminum alloys as the Cu-aluminum alloys. As it can be easily understood the complicated thermal history of an AMed part leads to an intrinsic heat treatment (see Fig.2.30). The homogenization that is needed to provide constant properties to such a complex microstructure is achieved through a custom age hardening process that depends closely on each different material composition. The mechanisms of precipitation and of undesirable precipitates will be discussed for the case of Scalmalloy in the following sections.

SURFACE FINISHING

Surface finishing is a fundamental constituent of the 3D printing process. Since the surface roughness is considerably higher than conventionally machined components there is the need to reduce any sign from the manufacturing processing such as layering. Since the rise of AM it has been clear that for structural components the surface finishing was not able make competitive component for fatigue application. Since fatigue is usually initiated at a surface level the presence of natural indentation such as the already mentioned layering effect would play the role of stress raisers. In order to accomplish higher fatigue life expectancy a proper surface treatment might be used if the properties of the material do not cope with the intended application.

[20] With the exception of aluminum alloys that need precipitation hardening to reach their best mechanical properties. A further exception are maraging steels which are specifically intended for age hardening.
[21] Quenched.

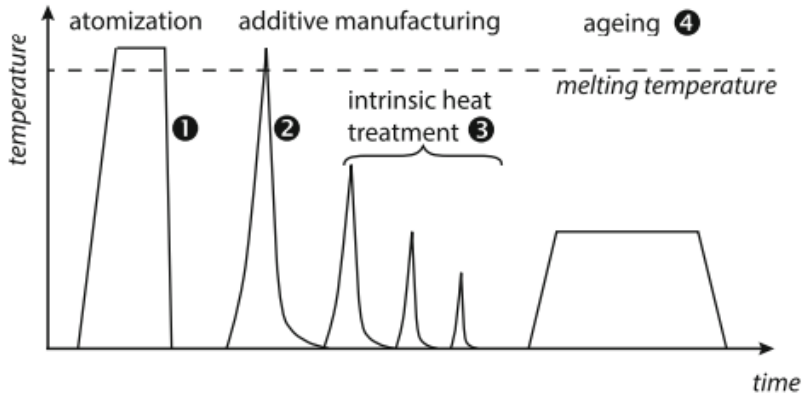

Figure 2.30: Thermal history of the material from melting powder production to artificial aging [17]. The complex interactions between the processes and the material properties will determine the rise of different microstructures. The ageing process can be done at a temperature level around the recrystallization temperature in order to reduce the internal residual stress by the nucleation of new grains in regions with high density of dislocations.

As a reference point to address the problem correctly we can rely on the fatigue data for a titanium alloy. Since one of the component which have been redesigned during the project has been made in Ti6Al4V, as it will be described properly in the following chapters, is possible to draw a comparison between the tensile properties of a bar (wrought) alloy against its respective AM material. A standard alloy from bar at the annealed state has a reference[66] ultimate tensile strength (UTS) of 1035 MPa and yield strength (YS) at 965 Mpa with a minimum elongation of 8% the fatigue strength is ranked at 700 MPa at 10 million cycles with a smooth[22] specimen. For comparison the typical material for DMLS printing is rated[64] to have in printed conditions[23] to have a UTS of 1290 MPa for specimen in the print plane *(XoY)* and of 1240MPa[24]along the layering axis. The reported YS levels are correspondingly 1140 and 1120 MPa. The elongation ranges from 7 to 10%. As it can be easily understood the tensile properties are equal or superior rather than the bar material[25]. The fatigue limit for DMLS or generally AMed titanium is not reported. An internal campaign of testing has been conducted in Scuderia Ferrari[26] to address the specific limit of the material in both conditions of machined and printed specimens. For a machined specimen the fatigue limit at 10 million cycles is 470 MPa while for an as built part the value is decreased at 250 MPa which a value close to a level reachable by the highest aluminum qualities. The comparison makes clear the evidence that if the bar material retains 67.6% *circa* of its UTS in fatigue application this value lowers to 36.4 - 19.4 % (respectively for machined and 'as built' specimens).

The different surface finishing processes that have been developed for treating AMed products are mainly the processed developed for processing castings or other machining operations with low surface quality. Among them we could list for pertinence and importance in automotive and motorsport applications:

[22] machined.
[23] Many times the as *in printed condition* will be addressed to as it is common in literature as *as built*.
[24] Total uncertainty levels are considered as +/-50 Mpa.
[25] It is also worth to note that the comparison of the bar material is not completely fair since higher tensile properties can be achieved with a solubilization and aging heat treatment.
[26] The fatigue cycling stress ration in those tested were set to -1 which represents a full inverse cycle of fatigue in which the part would be likely to experience localized fatigue twice per cycle. There is no reference for the stress ratio for the bar material presented.

- **Sand blasting**

  Sand blasting is considered the elemental finishing technique since the apparatus to be performed require no complex items. Through the action of a compress air flow sand particles impact on the surface of the workpiece in order to smoothen its external surface. As any process based on the impact of abrasive particles care has to be taken for shadow effects in respect of the blasting direction. The layout scheme of a sand blasting process can be found in Fig.2.32b.

- **Shot peening**

  Shot peening as sandblasting is a finishing process with involves projectiles design to hit the target component. Through the optimization of the speed and certain mechanical and geometrical properties of the particles (usually spheroidal) characteristic in order to achieve two different objectives: elimination of any surface defect such as small inclusions or unpolished remaining from machining operations and induce a localized compression region on the surface of the component in order to maximize the fatigue properties of a certain manufactured product [67, 68].

  The material characteristics are crucial to determine the correct peening process for each chosen material: a softer material would need softer spheres to prevent damage and the intensity of the peening as to be reduce consequently. It has to be mentioned that shot peening high quality surfaces involves a degradation of the surface roughness while the same process can positively influence the surface finishing.

  The final plastic deformation obtainable is the result of localized dimples and indentation as found in Fig.2.31. The induced work hardening provides a stronger material at the surface that would better resist crack initiation. Since the material below is still ductile the benefit in fatigue life granted by phenomena like crack tip blunting are not penalized by shot peening processes[69].

- **Laser Peening**

  Laser Peening is an emerging technology that has shown promising increase of fretting corrosion and fatigue properties for additively manufactured components. The basic concept of laser peening is the application of sacrificial coating in the metal component that is then removed by a short laser pulse under a water blanket. The shock-wave produces is responsible for interacting with the material below the surface and induces a stress state of compression. One of the advantages of laser peening is that it does not reduces the surface quality in case of machined parts. The absence of a reduced surface quality can further increase the benefits on fatigue life. The possibility to operate on components with reduced sections and high surface quality makes LP advantageous over traditional shot peening processes for titanium alloys carrying comparable results in fatigue life extension similar to deep rolling processes[70][27].

- **Superfinishing - Isotropic Tribological Finishing**

  With the definition of superfinishing a vast variety of surface treatment are considered by literature and industrial practice. The common feature for all those processes is the high quality of

[27] Deep Rolling is a technology that involves the passage of the component under a roller drum to induce surface compression. See again [70]

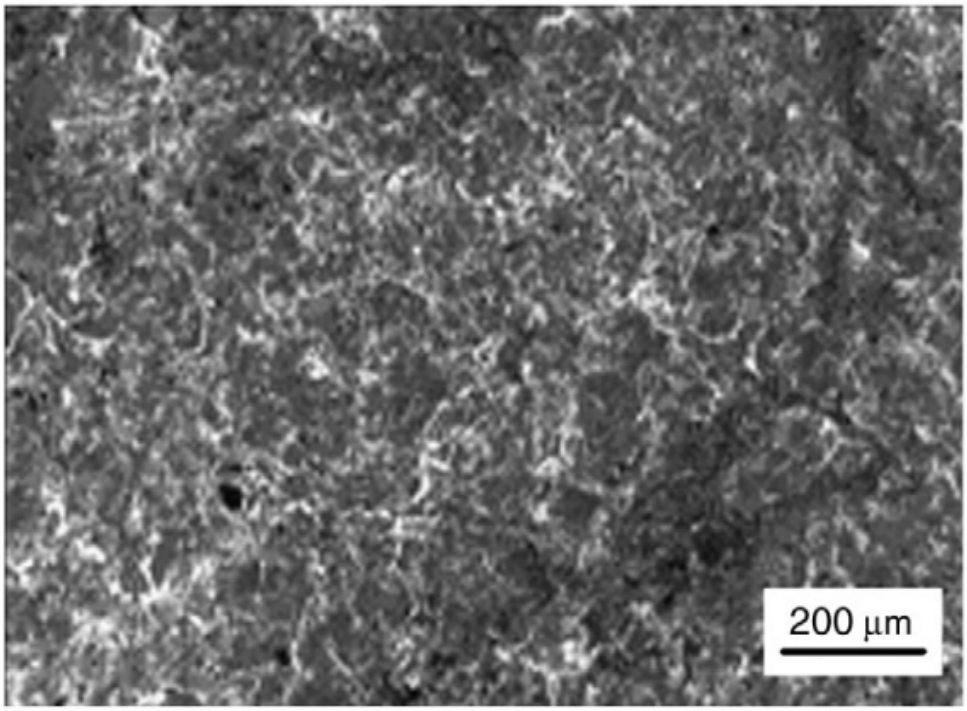

Figure 2.31: SEM image of peening surface dimples on 316L steel after 15 minutes of treatment[18]. At this magnification level the presence of dimples is evident: there is steel some debate around the effectiveness of shot peening for mechanical components subject to fatigue loads: the presence of small indentation and highly localized stresses does not grant the biggest advantage of increased fatigue life strength permitted by the induced negative stress on the component surface.

the ending surface that can go below Ra0.8.

- **Abrasive Flow Machining**
  As already described earlier[28] this process consist in forcing a flow into the inner channel of a geometry. Especially if the channels cannot be reached by machining operation easily as in hydraulic manifolds there is no option to guarantee surface quality without a finishing process. The basic concept of the process can be seen in Fig 2.32a.

2.5.4. ALUMINUM ALLOYS

Among available alloys aluminum is reported to be a common choice for additive manufacturing [15]. Since aluminum features an high reflective [29]nature the implementation of a laser melting process has not been as fast as for other materials. High oxidation rate is an other factor that played a role in the development of high strength aluminum alloys readily usable on AM machines. On the process side as well there have been difficulties: aluminum powder are relatively light and feature very low flowability. The poor flowability makes hard to produce a thin layer of material with a low density of defects. The typical development for AM powders start with consideration about the castability and weldability of the alloy and many AM aluminum alloys have composition which is close to the cast counterparts.

The main alloys for rapid prototyping with additive technologies are AlSi10Mg, 6061 and 200X. A

[28] During the analysis of the work performed by Cooper et al. in [1]
[29] Reflectivity for aluminum alloys is reported to be around 91%. See [49].

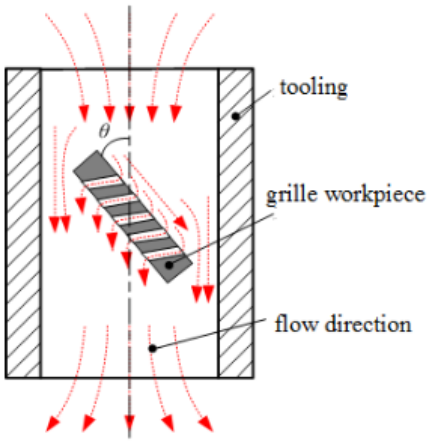

(a) Tooling and flow direction in the process of AFM [35]

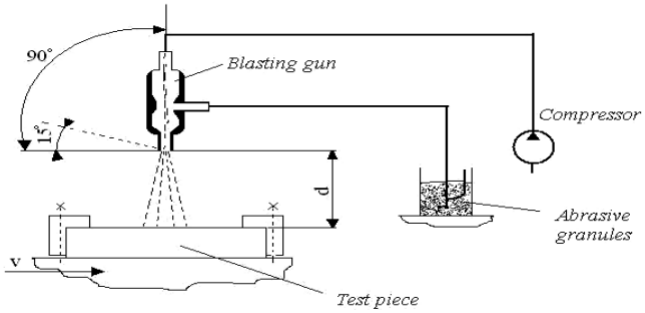

(b) Basic layout of the sand blasting process as described in [71]

Figure 2.32: In the present picture two schemes are reported: in Fig.2.32a the AFM is presented with the workpiece surrounded by the particle flow; in Fig.2.32b the layout of the sandblasting is reported: the compressor blasts small sand particles to hit the workpiece and by removing small imperfections is supposed to uniform the surface roughness.

Table 2.1: AlSi10Mg composition as reported by [28]

Element	%wt.
Ti	0.15 MAX
Si	9.0-11
Fe	0.55 MAX
Cu	0.05 MAX
Mg	0.2-0.45
Ni	0.05 MAX
Al	balance

few option for higher performance alloys are today available among which we mention the Scalmalloy [30].

In the following sections each material will be briefly presented from both the metallurgical, processing and properties point of view.

ALSI10MG

As already mentioned in the introduction to the present section AlSi10Mg is the baseline material for automotive and racing applications regarding aluminum alloys. The material has been successfully produced with very low distortion[31] by the Fraunhofer Institute [73]. The composition of the alloy is reported in Table 2.1.

The base alloy has been used for casting dies and it is known to reach a quasi-eutectic composition [74]. The phase diagram of a binary mixture of Al and Si has been reported in 2.18. The eutectic composition is rated at 12.6%wt. but in order to keep the best mechanical properties the industrial standards stop the composition at 10%wt. The needs for a low melting point has to be searched in the primary use of the alloy: complex cavities would be easily reached during the solidification process with an alloy that retains the liquid structure at low temperature. The role of Mg in the alloy is

[30] Scalmalloy is a registered material by APWorks which developed it in collaboration with Airbus [72]
[31] This characteristic is referred alternatively as *net shaping* or *near net shaping*

the possibility to strengthen the material with an age hardening process[32]. The possibility of small precipitates able to lock dislocation movement is the principle that the hardening processes put in place. As we already seen the rapid and various heating steps during the layer process is responsible for an intrinsic heat treatment in direct laser sintered parts [28]. With successful heat treatments different level of tensile properties can be achieved and as well the increment that can be obtained on the fatigue properties thanks to treatment like HIP are consistent.

SCALMALLOY

Scalmalloy is a novel alloy developed by Airbus company APWorks which is specialized in providing metal powders [72]. The composition of the Scalmalloy is registered and is reported to be as presented in Table2.2. The starting material to develop this alloy is the Al5083. The Al5083 is a castable alloy with a composition that features Si and Mg as the strengthening elements. It is part of the 5XXX series of aluminum alloys which are not heat treatable and are not recommended for use above temperature of 65°C. The performances under corrosive environment and welding did make the fortune of this alloy as today it is used in the marine sector. In facts, apart the excellent corrosion resistance in extreme environment[33], the ability of retaining high admissible strength after welding are fundamental for the implementation where assembly operation through welding are required. The original alloy is rated for a UTS value of 345 MPa according to BS EN 485[75]. From the original composition the addition of a fraction of Sc and Zr made possible the strengthening effect of the coherency of the precipitate Al3ScZr stable at high temperature. This effect has been demonstrated for a mixture of Al and Sc and the result has been extended by the creation of Scalmalloy from the Al5083 [76]. The end result of those microstructural changes shows a ultra fine microstructure after the deposition and the possibility to precipitate the excess of Sc and Zr in the mixture is responsible for an UTS reported to be [72] 520 MPa with an increase of more than 50%. As well due to the presence of a refined microstructure the elongation values are relatively high for an high strength aluminum alloy exceeding 13% [34].

A section of specimen in the deposition direction is presented in 2.33. From the section is evident the presence of a relevant circular porosity. As well the subsequent layer of deposition are visible progressing from left to right. Smaller porosity are present as well throughout the section as an indication of a not properly tuned process. From this section the microstructure is not easily readable. The composition of the structure is reported to be made up of two main constituents: a portion of equiaxed "cast" grains surrounded by columnar grains.

The final properties evaluated for the application on the present project are presented in the following chapters within the description of the heat treatment that have been necessary to post-process the components.

2.5.5. TITANIUM ALLOYS

Titanium alloys show great level of ductility in as built state if compared to other AMed materials. The possibility to match the high elongation with strength level comparable to the best steel alloys available for additive manufacturing processes and the low specific weight makes it a logical choice for safety application in which the specific strength is a figure of merit [19]. Due to the high cost of the

[32] This is usually implemented with an artificial aging treatment as the T6 [28]
[33] *E.g.:* seawater.
[34] Always from [72].

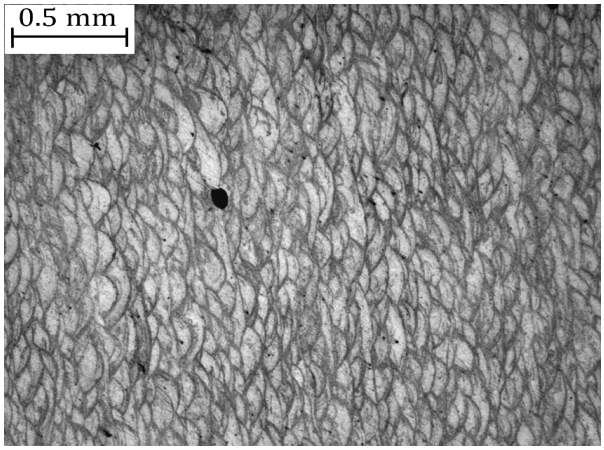

Figure 2.33: OM image of a specimen of Scalmalloy printed with DMLS machine within the context of an internal characterization campaign.

Table 2.2: Scalmalloy composition as reported by [29]

Element	%wt.
Sc	0.66
Zr	0.37
Mg	0.2-0.45
Si	0.17
Al	balance

raw material [77], vast scale production of titanium component is not yet present in the manufacturing industry. The less strict cost constraints would allow its wide presence in the motorsport industry. Still the possibility of reducing machining costs Actually the choice for titanium alloys for AM is rather limited depending on the specific application. Among titanium alloys the market benchmark is considered to be the Ti6Al4V, commercially referred to as Titanium Grade 5 [16]. A modified version with Extremely Low Interstitial is used for special application in which the fracture toughness and the ductility are fundamental[35]. Apart from its alloys titanium is available as a pure element (*commercially pure*): the level of corrosion resistance and ductility is usually higher than its alloys but the level of strength is considerably lower[36]. In this section the material treated will be only the alloy that has been used during the project which is the Ti6Al4V.

TIAL6V4

Titanium Grade 5 is the commercial standard alloy for titanium components in the racing industry and generally is largely considered as the base material for components to be processed with titanium alloys [16]. The typical microstructure for wrought product is a biphasic structure in which there is the coexistence of α and β phases. Due to the different thermal history of a AM-produced product the microstructure of rapid prototyping Ti6Al4V are process depending [16].

Starting from the composition of the alloy is possible to draw a first analysis on its strengthening methods and on how the metallurgy is likely to develop. From the mentioned AMS4999A the composition is reported in Table 2.3.

[35] *E.g.*:Aerospace application, cryogenic components, offshore equipment due to the high level of resistance in presence of Stress Corrosion Cracking (SCC) [62].

[36] As reported by the ASTM in the ASTM F67 (Unalloyed Titanium for Surgical Implant Applications) the strength level required is 345 MPa (UTS) compared to the 855 MPa prescribed in the already mentioned AMS4999A specification [78].

Table 2.3: Ti6Al4V composition as reported by AMS4999A

Element	%wt.
Al	5.50-6.75
V	3.50-4.50
Fe	0.30 MAX
O	0.20 MAX
C	0.10 MAX
N	500 ppm
Ti	Balance

The typical CCT[37] diagram for the cooling solid phase transformation is reported in 2.34 [79]. The different phase formation for different cooling rates are presented from left to right. A fast cool down of the alloys does not allow a reorganization at crystalline level and the formation of the α equilibrium phase is not possible. Instead there is the formation of martensite and β. Further cooling time allow the formation of martensite and some α+ β. If the cooling process is slow enough the composition of the microstructure is equivalent to the one presented by the equilibrium phase diagram.

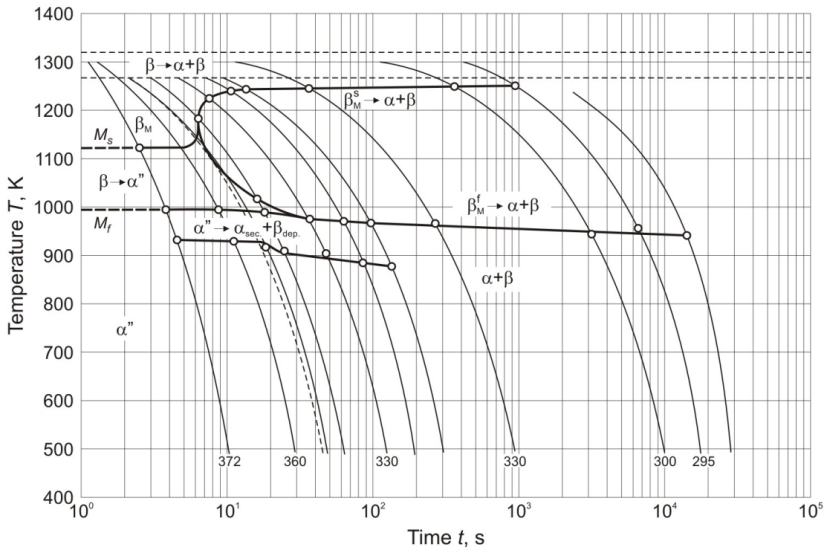

Figure 2.34: CCT curves for Ti6Al4V titanium alloy. The transformation are driven by the cooling rate that the material experiences: since the complex cooling profile that has been seen happening in DMLS and more generally in AM the microstructure presents a portion of martensite. Upon stress relief procedures this fraction is partly removed since the energy for the transformation is provided in the form of heat energy.

From the picture is clear that the rate of cooling is the fundamental parameter to distinguish the different processes. As it has been already mentioned in the section regarding DMLS and EBM, the main difference in the microstructures is the absence of a formed β-phase in the DMLS processed specimen. This is due to the fact that the cooling rate is higher than the critical and there is the formation of a fraction of martensite. On the contrary the high temperature in the EBM process and the relative slower cooling process gives rise to full biphasic structure (α + β).

As some developing of microstructure have been presented in earlier section for titanium alloys (about an alloy of Ti and Al reported as a γ Titanium) a description of the differences between microstructures for wrought products and AM products is shown. As visually described in Fig.2.35c the

[37] Continous Cooling Transformation

differences are related to the different cooling rates that the three Ti64[38] experienced. The cast product shows a lamellar structure with the β phase forming elongated grains in the α matrix. Since the repetition between the two different phases is at constant interaxial distance this can be considered to be a lamellar microstructure. Contrary to this there is no clear formation of α in the SLM produced specimen and there is an high fraction of martensite with some elongated β grains that interrupt the other phase. As a third version of the alloy the wrought product in Fig.2.35c the grain are equiaxed. The β phase is constrained to the grain boundaries of the α matrix.

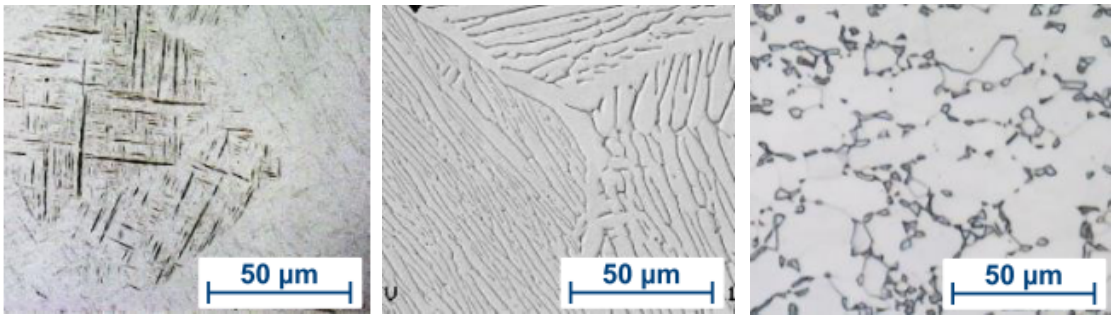

(a) SLM produced Ti64. (b) Cast product. (c) Wrought product.

Figure 2.35: Different microstructures coming from the three different manufacturing methods for producing components with Ti6Al4V: SLM (representing AM), Cast and a Wrought product from ingot metallurgy as reported by [19, 20]. The AM produced sample shows a martensitic structure while the cast sample is representative of a dentritic structure. The wrought product shows a biphasic structure with both phases present.

Since the SLM processed microstructure (which can be compared to what could be achieved by DMLS) represents on the CCT diagram the most extreme case of cooling rate it is possible to heat treat the alloy to change the microstructure from a relieving heat treatment in which the martensite get converted in α phase to achieve complete annealing and recrystallization. Similarly to what presented in 2.24 variable condition of Ti64 are presented in Fig.2.36.

The transformation of the martensite from Fig.2.36a to Fig.2.36b is clear and the structure becomes more or less lamellar. The study reports a diminished tensile strength with a significant increase in elongation that represents the removal of high dislocation density present in the original martensitic structure. The elongation in facts jumps from 5% up to 13-15% with strength decreasing from 1100 MPa to *circa* 950-900 MPa for the two different temperature levels.

The trade off between those possibilities will be analyzed during the assessment of the material properties in the design section of the project.

[38]The indication for convenience of Ti64 refers to Ti6Al4V as commonly done in literature and in the industry practise.

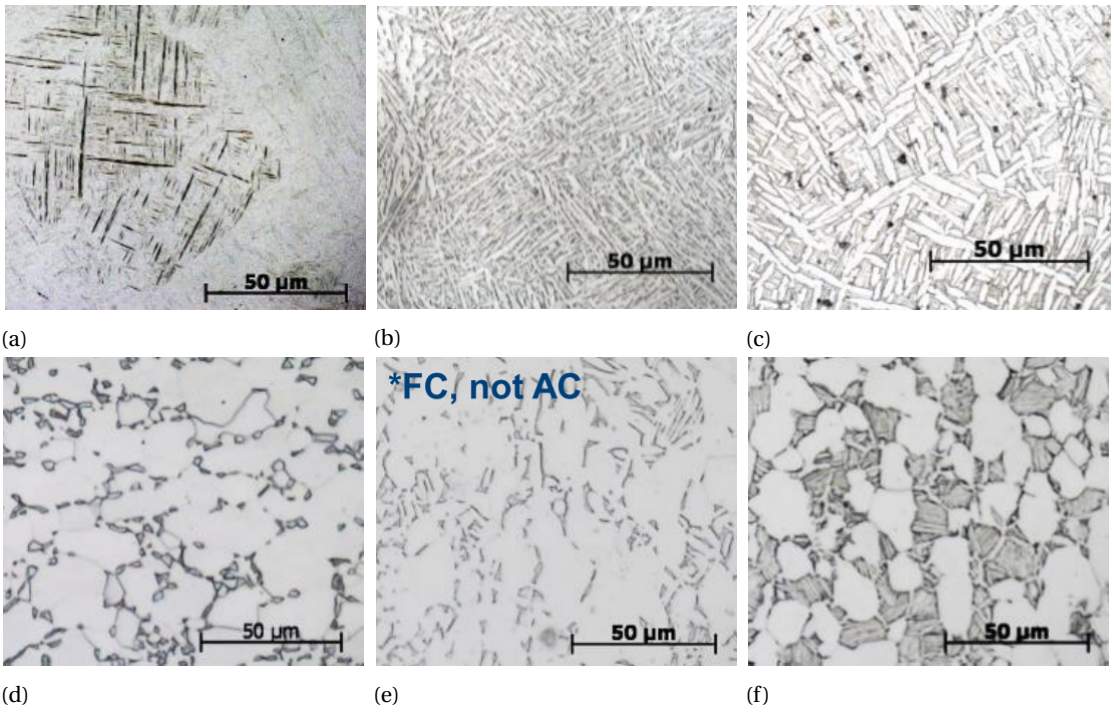

Figure 2.36: Comparison of microstructural changes given by three different heat treatment temperatures (ambient, 850°C and 950°C) of two Ti64 alloys: AM produced product (a, b, c) and Wrought product (d, e, f) as presented by [19]. The complex martensitic structure presented in Fig.2.36a is relieved after annealing and the grain dimension depends on the stress relief process temperature. On the contrary, the biphasic structure in Fig.2.36d evolves towards a lamellar structures with vast region of α phase alternated by lamellar zones of alternated α and β *lamellae*.

II

Constitutive Work

3

DESIGN OF SUSPENSION COMPONENTS FOR ADDITIVE MANUFACTURING

As anticipated in the introduction, the present chapter reports the first section of the engineering process that brings a conceptual decision and model into a finished product ready to be installed and raced on the car. The internal structure of the chapter is split in two and presents the different but parallel processes of design of the two components developed in the course of this thesis[1].

The first half, after briefly presenting the project context as anticipated in the literature review [2], reports the performed activities on the rear top wishbone bracket [3]: from the design optimization through the implementation of topology optimization routines to the definition of the design criteria, from the geometry reconstruction to the manufacturing assessment.

Similarly the same topics will be presented in the second half of the present chapter with the focus on the rocker beam that has been designed in Scalmalloy. Since the material choice has been more complex on this component a dedicated section that will properly present all the influencing factors regarding the material choice is present.

3.1. PROJECT CONTEXT: THE SF70H AND ITS SUSPENSION SYSTEM

Officially presented on the Fiorano track, located next to the Scuderia Ferrari's facilities in Maranello, on the 24th of February 2017 the SF70H is the latest racing machine for the F1 season of 2017. The project is a revolution of the previous car that has participated in 2016 F1 competition. Since the set of regulations has undergone a deep revision from previous year the car features new track and wheel base[4] as well a new and revised aerodynamic concept featuring a longer motor hood that ends with a peculiar set of small wings defined as T-wing. The front aerodynamics changed as well now featur-

[1] cfr. with the introductory section in 1.1.
[2] Specifically in section 2.1.
[3] As specified in the nomenclature from now onwards the RTWB bracket.
[4] The track is defined as the minimum distance between the centerline of two tires aligned in the same axle while the wheel base is the minimum distance on from the center of the front and the rear hubs.

ing a wider and arrow-shaped front wing. At rear end, of the sixty-third Maranello F1 single-seater, the revision included a new and wider rear wing closely developed with the new diffuser. Regarding the suspension components which are of interest in the present work, they have followed closely the new regulation set that, prescribing larger tires and a larger track, would have brought the car to feature higher load for all structural components since the cornering speed of the car was expected to be increased by several points percent [5]. More specifically the suspension system features two independent front and rear suspensions. The suspension scheme did not change from the previous year and presents a pushrod double wishbone design at the front end of the car and a full split multi-link pullrod design at the rear end[6].

Following the regulations all suspension links are designed and manufacturing in CFRP[7] with the only exception of the rear pullrod that is in ultra high strength steel.

(a) Front view of the SF70H.

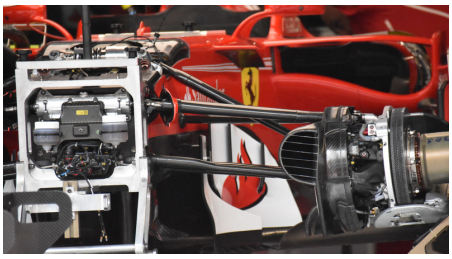

(b) Front detail of the suspension right end: leverages and internal components.

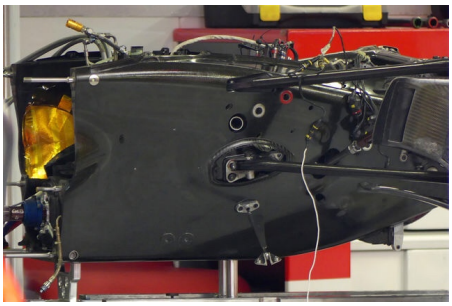

(c) Detail of the connection between the rear subframe and the rear suspension components (outboard).

(d) Frontal view of the right end of the rear suspension outboard components. The rear top wishbone bracket can be seen in the upper left connection between the wheel group and the upper wishbone.

Figure 3.1: Track images of the SF70H: the suspension system features two independent system for the front and rear end of the car: both suspensions are based on the double wishbone layout.

From the wheel groups the load is carried through the hub and upright which are connected to the suspension by a maximum of three metal components [34]. As described in the previous sections, the presence of a specific rule on the metallic components connecting the upright to the suspension members [8]intrinsically limits their design to metal alloys and prevents the use of, for instance, MMC[9]. In the figure presented (Fig.3.1) there are a few views of the suspension layout.

The components designed during the course of this thesis project are, as already mentioned, the

[5] cfr. [80] in which is stated that only in the fastest corner (Monza Parabolica for instance - Author's note) the speed would have increased by 20mph.

[6] By pushrod is intended a system that carries bump vertical load with the leading member of the suspension that undergoes a compression load while on the contrary the pullrod scheme has the connection link in tension with a bump load applied at the wheel.

[7] Carbon Fiber Reinforced Plastic.

[8] cfr. Article 10.5.2 of the FIA F1 regulations [34].

[9] Metal Matrix Composites.

RTWB bracket and the rocker beam. Since the second component is placed in the gearbox housing (that represents a sort of rear subframe connected with the stressed engine) its visualization is rather complex in the real operating life of the car. On the contrary the RTWB bracket that connects the top wishbone of the rear suspension to the upright can be see in Fig.3.2.

Figure 3.2: Top view of the rear end of the SF70H: the RTWB bracket is the metallic part which can be seen at the two ends of the triangular shaped wishbone (in black) partially hidden by the rims and tires.

3.2. DESIGN OPTIMIZATION OF THE RTWB BRACKET

The design optimization problem of a structural component requires the iteration of calculation steps in order to assess what is the best geometry to be able to use the material as effectively as possible. The optimization problem regarding the RTWB bracket is based on the structure that has been used during the year in the SF70H. The section will start analyzing the existent component to assess how the current design limitation imposed by conventional machining can be overcome with the added freedom given by additive manufacturing as presented in Section 2.3. Afterwards, the topology optimization set-up will be presented and the interpretation of the simulation result will be showed. Finally the reconstruction of the geometry will be assessed posing the problem of how to best follow the structural suggestion coming from the simulation.

3.2.1. ANALYSIS OF MACHINED COUNTERPART

The current component design has been prepared as the baseline for the suspension set-up of the SF70H. The component has to face a series of loads coming from the wheel that are reacted by the rear top wishbone. As it can be see from the Fig.3.3 the component features a non symmetrical geometry. From top to bottom the shape can be described as a bracket with four lower attachment points sharing a common planar interface with the upright and a top attachment in which a ball joint is placed to enable the relative motion of the upright-bracket monolith and the RTWB. The connection between the two attachment points represents the compromise between a shape that is able to follow

Table 3.1: Main characteristics of the current component that represented the baseline to which the benchmark comparison has been made.

Bracket Standard MK2 (Machined Counterpart)	
Weight	1183 g
Material	Ti6Al4V Annealed
Camber Compliance	33.89°/MN

Table 3.2: Main characteristics of the hypothetic component that represents the first design iteration of the design of this component.

Bracket MK1 (hypothetic component - CAD Design)	
Weight	1689 g
Material	Ti6Al4V Annealed
Camber Compliance	32.1°/MN

the aerodynamics restriction of the rear end of the car[10] and the structural requirements of the component. The internal cavity represents a machining issue since all tooling has to be customized for this specific application and some shapes cannot be achieved due to the need of accessibility for the milling tools. The cavity shape is determined by the optimization of the inertia on the bending axis[11] of the component. Some basic characteristics of the component featured in the current car design are presented in Table 3.1.

The component in analysis ideally represents the second evolution of the design of the RTWB bracket since it develops after a preliminary study representing an heavier (and "therefore"[12] stiffer) version. The reference stiffness of this early reference[13] is reported in Table 3.2. The importance of including the first design iteration becomes clear in the definition of advantages which can be calculated in terms of relative differences ratio. The efficiency of the component can be therefore calculated taking as a "zero" design reference the heavy concept component and comparing every design to it. The topic of accessing the design efficiency will be treated in the dedicated Section 4.1.

3.2.2. MATERIAL OF THE MACHINED COUNTERPART

The choice of titanium for the development of this component is partly dictated by the rules as stated in Section 3.1 and partly by the design requirements of the part. Titanium offers, as presented in the literature review[14], a high level of tensile properties that can be tuned by controlling either the alloy or the microstructure of the component. Among titanium alloys titanium grade 5 represents one of the best compromises between cost, performances and machinability. It is offered widely on the market and his supply is granted by a vast part of mechanic workshops. Even though better material are present in the market regarding the specific stiffness[15] such as the Ti6242[16] the choice between the competitive advantages on this component are not so limiting to imposing a choice in an other

[10] To prevent the leak of any air below the external surface it can be noted how onto the metallic component it has been implemented a metallic winglet that represents the ideal junction with the sealing coming from the rear brake duct.
[11] A theoretical axis that goes from the center of the plane in common with the upright to the center ball joint located at the other end of the component.
[12] As it will be more precisely presented later the relation between weight and stiffness represents the quality parameter (or figure of merit) through which the component has been optimized.
[13] Which has not been produce due to the need of optimizing weight over stiffness.
[14] cfr. Section 2.5.5.
[15] The ration between the elastic modulus and the density.
[16] Titanium 6242 is a special grade that has been developed for high temperature application but retains a higher modulus due to its composition.

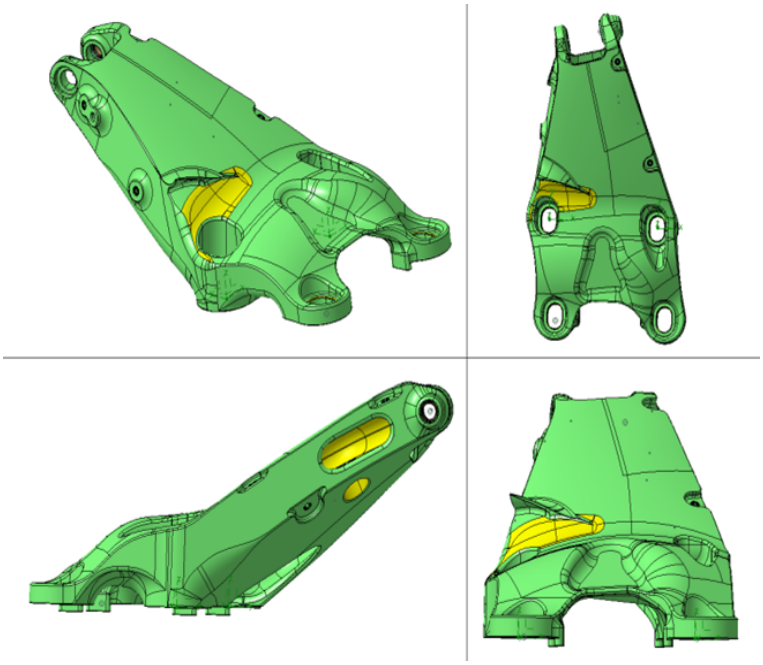

Figure 3.3: Geometry of the actual component: the shape is limited by the boundary conditions such as aerodynamics limits and clearances due to the presence of the rear rim structure but as well by the manufacturing limits represented by the need of accessibility for machining operations. The components features an overall length of 185 mm and an height of 150 mm from the lower to the upper attachments. An approximated scale on the component is shown in Fig.3.16 representing the design space with the applied maximum braking load.

direction. As briefly explained in Section 2.5.5, it is possible to heat treat the biphasal α and β titanium alloys (such as Ti6Al4V) to obtain an age hardening process given by the deposition of the β phase into the matrix of the alloy. Therefore two possible states of supply exist for Ti6Al4V: annealed and heat treated (age hardening). The heat treatment carries some inconveniences[17] such as longer lead time for supply and does not grant an increased stiffness since the precipitates ensure only a higher elastic limit but they have no influence on the elastic properties of the material. Since the nature of the component (which is stiffness limited - or designed with a target stiffness) the natural choice has been Ti6Al4V in the annealed state.

3.3. DESIGN CRITERIA

In the opening of the chapter it has been mentioned the load case that determine the efficiency of the RTWB bracket. In the following section, an extended presentation of those loads is reported and each contribution in the final analysis explained. The text is organized such to keep separated the functional loads (that determine the stiffness requirements) and the limiting loads (which are responsible for the strength requirements). The presented design criteria (or defining loads) are the basis through which the simulation process of optimization has been based. As already mentioned in Section 2.1, the chance to explore complex geometries with the aid of topology optimization has found a proper manufacturing method that requires no added cost or that faces no limits in the make of extremes

[17] The heat treatment for age hardening of Ti6Al4V requires a solubilization (that takes place at 900°C *circa*) process that is followed by water quench. Subsequently the alloy need to be heated to reach a precipitate density high enough to make it more resistant to dislocation movement and this second heating period takes place at 500°C *circa* for 8 hours. Due to a series of issues reported with this heat treatment at present there are few homologated suppliers that makes critical the choice of this version of the alloy.

topologies in additive manufacturing. In order to exploit the full potential of this novel manufacturing technology the process has been carried out as follows for both components:

- **Definition of design requirements:** in this phase the component functionalities are analyzed and the load applied by the vehicle dynamics and recorded in testing are determined.
- **Definition and analysis of a design space:** the maximum material allowed by the geometrical and functional constrains is added to the design space. The contact surfaces are kept as are in the actual component as well as the envelopes for mounting interferences and clearances for relative motion of other suspension components are considered.
- **Topology optimization:** the implementation of the determining loads is done on the design space. The allocation of the material is tuned to reduce the mass while targeting the required stiffness or other limiting constraints.
- **Geometrical reconstruction of the structure:** the result is extracted in the form of a meshed structure. The implications about the feasibility of a real geometries are considered at the step and the structure is reconstructed from the design space to reach a manufacturing CAD geometry.
- **Final FEM assessment and stress check:** finally the CAD geometry is validated by a traditional linear or non-linear FEM analysis.

A final target reduction in weight has been roughly estimated on the experience and engineering judgment of the author and the company supervisor[18] to be around 7-10%. Then the target weight for the optimization final result and geometrical reconstruction has been defined around 1050 and 1080 grams for the same target stiffness.

3.3.1. STIFFNESS REQUIREMENTS

As mentioned in the presentation of the chapter it is known that the RTWB bracket is a component that has to be designed with a target stiffness to camber variation. The camber angle is defined, for a wheeled vehicle, as the angle that is present between the vertical line passing through the center line of the vehicle and the line perpendicular to the wheel axis and passing through the center of the wheel itself. A graphical interpretation of this simple definition can be seen in Fig.3.4. The camber angle influences the car behavior heavily and has influence on the tire dynamics as well and all those interconnections are what make a car stiff in camber robust in performances over a range of different dynamic events.

The camber stiffness can be defined by the total amount force to be applied at the wheel contact patch to obtain an unit of camber angle increase. The definition for easiness is not reported hereby in SI units but with a custom parameter which is MN/°. Its inverse is the camber compliance which is evaluated in °/MN. Due to the usual stiffness of the system (as already seen to obtain 30° degree of camber increase it is necessary to apply a MN) and the relatively small displacement involved the stiffness load that determines the camber stiffness (or compliance) is a fictitious load of 1000N in the directions through which camber is most sensible.

[18] Ir. Marco Civinelli - Head of Mechanical Design Department

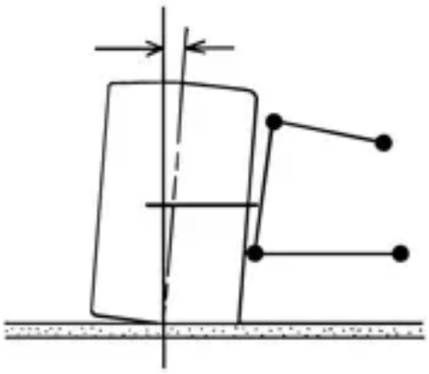

Figure 3.4: Definition of camber angle by the mean of a graphical scheme [21]: for a better picture the vertical centerline (or the Z-axis) has been translated in the proximity of the wheel center.

It is necessary before proceeding to make unambiguous definition of the car coordinates to properly refer to directions and orientations of loads and components. The car coordinate follow a logical determination and are coherent with the intent of the final product (the car itself). The origin is placed onto the longitudinal centerline at the height of the presumed center of gravity at the front of the chassis where the aerodynamic nose of the car is installed. The ***X-axis*** is defined against the natural forward movement of the machine and is directed horizontally (parallel to the ground) pointing at the rear wheels. The ***Y-axis*** starting from the common origin and being as well parallel to the ground points at the right end side of the vehicle. Automatically being a right-handed axis system the ***Z-axis*** would point perpendicularly to the ground with the positive direction against the ground location. An example of such a arbitrary definition is presented in the Fig.3.5.

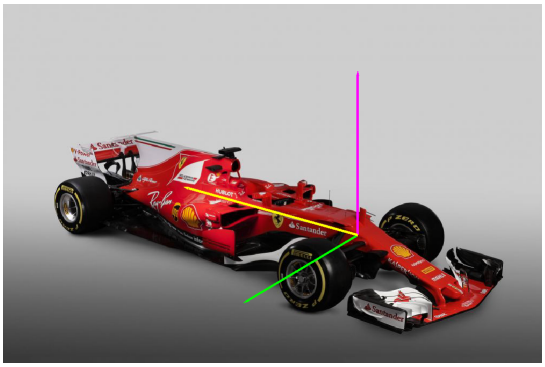

Figure 3.5: Definition of a arbitrary and unambiguous axis-system: the X-axis is presented in yellow, Y-axis in green and Z-axis in pink.

The direction of the load is for the stiffness analysis is the combination of X and Z. The applied load is therefore a load of a 1000 N in the X direction and 1000 N in the Z direction as resumed in Table 3.3.

Such definition of the camber load makes simple the definition of the camber stiffness as far as at the end of a simulation process the camber angle or the component deflection can be calculated.

Table 3.3: Definition of Stiffness load components referred to the reduced simulation and therefore related at the top attachment of the component.

RTWB Bracket Stiffness Load	
X-load	-243.3 N
Y-load	80 N
Z-load	983 N

3.3.2. STRENGTH REQUIREMENTS

Sideways to the driving stiffness case the definition of proper design criteria has to face the case of loads which are no critical for the component stiffness but for its strengths as well. Even though titanium is a high strength material[19], the need of designing a lightweight component makes the assessment of stress on the part itself critical. Furthermore, even if usually stiff driven designs are overdimensioned in respect of strength designed components peculiar load cases that act in different direction from the stiffness definition case might put the component at high stress levels. For the RTWB bracket the definition of the limiting stress cases has been developed based on the history of the component analyzed during the years. As specified in the previous sections despite the presence of the uniball at the top attachment point of the component that spans the loads over a continuous angle the limiting cases analyzed for the simulation have been reduced to two extreme conditions. First is the analysis of the load under the maximum cornering conditions. This is the load that defines the strength for the top wishbone suspension link as well. Due to load transfer and rolling condition the definition of this load is a mixture of forces applied at the ground point reported at the bracket position as resumed by Table 3.4 and in Fig. 3.16. The second case load for stress evaluation is the case of maximum braking. The reaction on the suspension top link from the braking torque that originates the inertia load of the chassis in respect of the unsprung mass is carried by the upright through the bracket in question. The axis of the load in this case is quite far from the one that defines the stiffness in camber of the component. The force components expressed global car coordinates are resumed as well in Table 3.4 for the reduced simulation and therefore are reported at the bracket top attachment point.

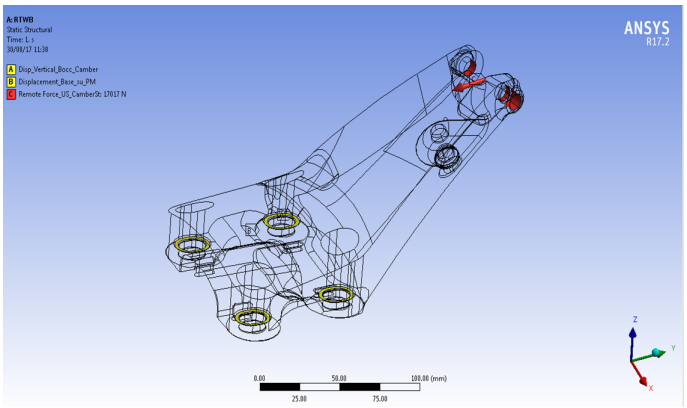

Figure 3.6: Max braking load for strength evaluation on the RTWB bracket as set up in the reduced version of the simulation.

[19] cfr. Section 2.5.5

Table 3.4: Definition of Strength loads: maximum cornering load and maximum braking load in the reduced simulation.

Max Cornering		Max Braking
X-load	-3970 N	-17600 N
Y-load -2040 N	15500 N	
Z-load	11100 N	15200 N

3.4. TOPOLOGY OPTIMIZATION

Having defined the design criteria the next step is the set up of the topology optimization routine. Since the results are highly dependent on the user definitions and applied constraints extreme care and validation has been taken both during the analysis and during its report as well. The topology optimization set up has been done for the stiffness case only but some stress limits could have been applied towards a more complete definition of the problem. The choice of excluding the stress constraints from the simulation has been made since it has been decided to put the maximum focus of the design effort in the search of an effective structure with the highest possible level of efficiency in terms of camber stiffness addressing any stress issue with local measures.

Two different analyses have been set up for the topology optimization problem to investigate which was the best way to achieve a high efficiency component but as well to have a simulation quick enough to be adapted to multiple iterations. The main differences between the two simulations is the presence or not of the outboard stiffness matrix which in representative of the stiffness contribution in camber given by the upright and by the rim.

The first simplified simulation, that has defined the baseline for both simulation, will be presented in detail since the fundamental constituents are shared by the two as well as any simulation parameter and choices. In this simulation the RTWB bracket has been fixed at the planar interface as it can be seen in Fig.3.16 as it is done during the homologation fatigue testing and the load is applied coherently with the load definition at the top attachment. These represents accurately enough the real usage of the component but giving away the need of modeling other components has run times[20] that has enabled the author to proceed with more than 3-4 simulations per day.

3.4.1. DEFINITION OF THE DESIGN SPACE

As already mentioned in the presentation of this section the definition of a proper design space is fundamental to properly assess the implication of a topology optimization [21]. To simply classify the various limitations usually encountered during the definition of a design space we might remember the followings:

- **Aerodynamic boundaries:** those are the indication of the wet surfaces that determine the car performance in terms of drag and lift. Since aero design is a driving factor over mechanical design and weight saving no compromise can be taken in respect of those limitations.
- **Mechanical interfaces:** the reference of other mechanical attachments limits the design space to have proper limits when encountering other mechanical components such as the upright or the RTWB suspension link in this case.

[20] Runtime is considered as the time lapse between the start of the first calculation step and the final converged results in the analysis.
[21] cfr. as presented in Section 2.1

- **Envelops of relative moving components:** being part of the suspension unsprung mass this components experiences relative motion of the suspension leverage system. This has to be considered and since the component is part of the regulation movement for the camber adjustment the relative positions have to be evaluated over the camber span angle.

The first limitation for the component is the the aerodynamic shape of the part. As it has been emphasized in the introduction, aerodynamics drive the most of the design of a modern F1 car [81] since the average speed of a GP[22] is usually above 150 km/h. In this case the aerodynamics boundaries are shown in the Fig.3.7.They represent the geometrical constraints coming from the CFD simulations that define the aerodynamic shape of the car. This is by far the most limiting condition since has an effect on the overall shape and on the two most influencing surfaces of the component which are the top and the bottom surface[23]. The limitation deriving from the envelopes of the RTWB and the upright are less evident and especially localized in the attachments regions. Especially the presence of a relative movement around the upper bolt joint limits locally the design space of this components. Having taken those considerations through the implementation of a new CAD geometry the starting point of the simulation was set. The design space can be seen in Fig. 3.8. In the simulation that drives the topology optimization the design space represents the volume of material in which the variation of material density is allowable. The variation of material density is representative of the effectiveness of the material in a particular location and can help in redefining the geometrical shape of the component. Since the component needs to be successfully implemented in the car assemblies some regions have to be excluded by this optimization routines and will be defined specifically in the next section.

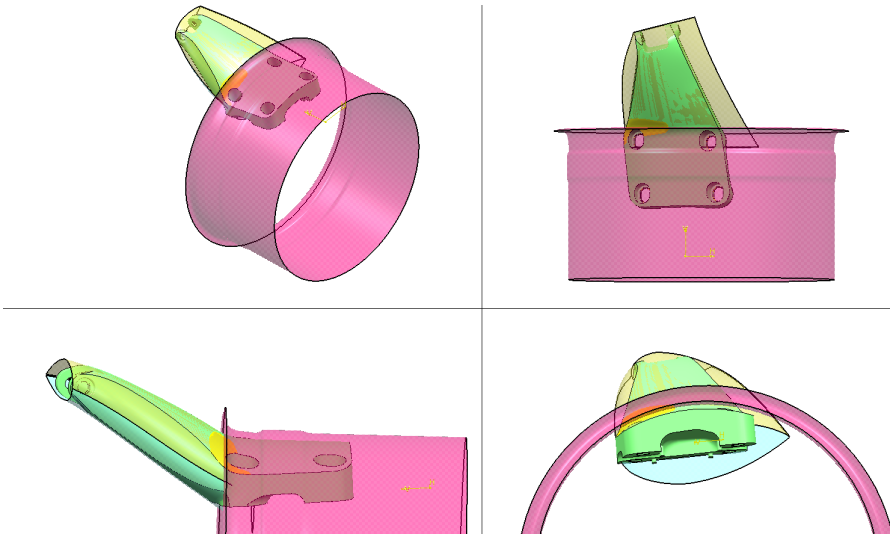

Figure 3.7: Aero design boundaries: those are usually derived from various iteration on CFD-calculation that searches for the best combination between drag and lift coefficient for a specified configuration.

EXCLUSION ZONES

As mentioned early, the need of having a feasible design makes necessary to fix some geometrical features in the process of running the optimization routines. First of all the mechanical interfaces

[22] Grand Prix.

[23] The top and bottom surfaces are responsible for the bending inertia of the component in a bigger share rather then the thicknesses of the two walls.

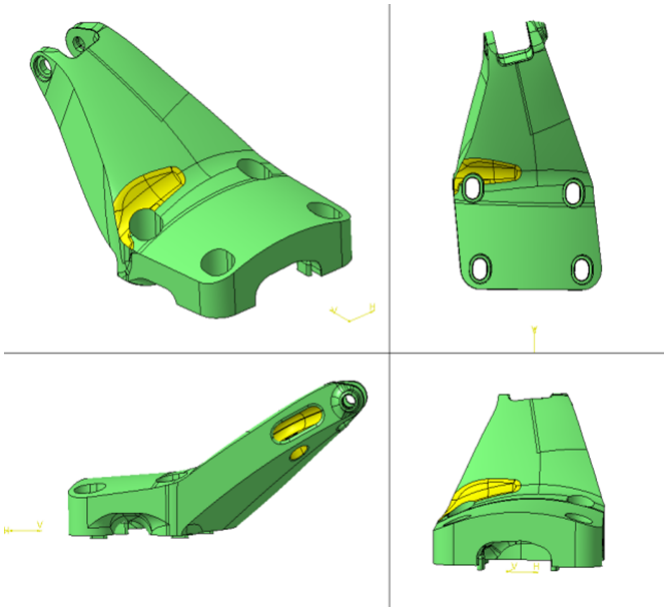

Figure 3.8: Design Space reproduced to exploit the full potential in camber stiffness of the component: the presence of mechanical interfaces and aerodynamic boundaries reflect in the basic geometrical splits of the design space.

have to be fixed. In the case of the RTWB bracket we have: the planar interface with the upright (1), the bushing for determining camber set up (2), the mechanical interface of the upper ball joint (3) and the fixture of the wheel tether which is a safety polymer reinforced fiber safety retainer that prevents the rear wheel to come loose in the event of an accident or an unsafe release of the car after pit-stop operations. The shape and installation of the tether is presented in Fig.3.9a while the exclusion zones are highlighted in Fig.3.9b.

3.4.2. DRIVING LOAD CASES

As already discussed the component has been design to match the existing camber stiffness and is therefore considered to be stiffness designed. In the first set up of the simulation process it has been tried to make a mixed formulation in the form of a multi-objective optimization function including to some extend the stress and strength limitations.

even though some successful run have been achieved the implementation of stress results in the calculation process through topology optimization has been always regarded as an unstable process. As any search for minimum algorithm the problem has to be stated in such a form that it can achieve convergence around a point that minimize the optimization function while keeping the variable into a limited existence field. Regarding a structural optimization problem this translates in the need of defining an optimization variable and one or more design constrain. Therefore, two approaches in order to implement the simulation can be pursued, as follows:

- **Minimum Compliance**: the optimized variable is the compliance of the structure and the algorithm would base its routine depending on the contribution in stiffness that each element would grant to the entire structure in the established load cases. To be allowable this formulation of the problem has to be completed by a constraint on the final mass. In this way it is

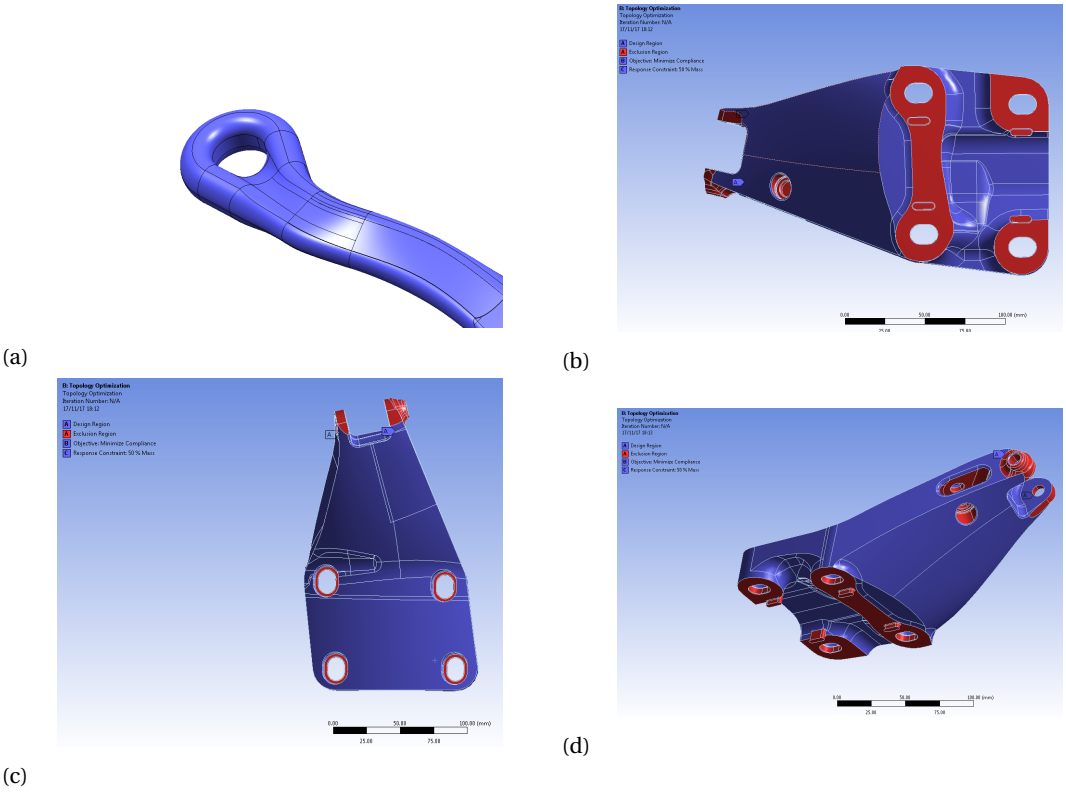

Figure 3.9: Images of the tether shape and of the exclusion zones as they have been adapted in the simulation carried out in ANSYS Mechanical - R18.2. The blue region represents the design space that the simulation will try to optimize. On the contrary, the red zone will have a density parameter of 1 and will therefore be retained as geometrical features to be preserved from the optimization simulation.

possible through the aid of a sensitivity analysis[24] for the system to prioritize certain elements with respect of others through the assignment of a higher density that describes the quality of the same element to contribute to the stiffness of the structure.

- **Minimum Mass:** similarly the problem could be approached from the other extreme. Since the actual camber compliance (the characteristic compliance of the part in analysis) is known for the machined counterpart this could set a lower limit for the acceptable compliance and the mass can be reduced as much as this condition is satisfied. Mixed approaches are valid as well in which the mass weight reduction variable is optimized against the minimization of compliance. Such approach might be useful for the initial stages of the simulation with the purpose of qualitatively assess the driving factors for the two components of the problem and has been used especially in the simulation of the rocker beam to stress the design towards a defined geometry.

[24] Sensitivity analysis, in common engineering practice, is referred to a linearization approach used to predict in the proximity of a function its near future value basing it on the simple derivative of the function in the previous known point. This is used to evaluate for instance the car performance: *e.g. the sensitivity of the car lap-time is 0.05 s per each kilogram added on is curb lower weight limit - which can be read as "adding or removing from the curb lower weight limit one kilogram this would influence the time on one lap of +0.05 s or -0.05 s respectively". The assumption since it is sensible only in the proximity of that weight limit is not valid for a 100 kg of difference.* More about sensitivity analysis in general can be found in [82].

DEFINITION OF MANUFACTURING LIMITS

In the definition of the problem it is possible to add a number of constraints to the simulation that can be regarded as simulative counterpart for manufacturing limits -*they can be representative of machining operations or represent the minimum thicknesses of a component.* In the course of the simulation the most used implementation has been the definition of a minimum member size. Since the end result can assign high level of density to very small regions of materials which are not representative of a feasible design (e.g. the presence of highly triangulated structures with characteristic section smaller than 1mm, presence of isolated material separated from the main body due to mesh inaccuracy or algorithmic issues) the easiest and most logic way to approach the issue is the assignment of a minimum member dimension in excess of usually 3-4 mm which is approximately the 2% of the characteristic length of the component. It has to be noted that this implementation reduces the presence of small structures but it does not prevents the existence local thicknesses smaller than the limit size.

3.4.3. TOPOLOGY OPTIMIZATION RESULTS

The set up of the reduced simulation has granted the chance to run the simulation itself on a number of different parameters to fully understand the model behavior. The final result is presented in Fig.3.10. From a first analysis it can be derived how the final optimized structure has many features in common with the starting geometry of the component. The presence of two main sections that connect lower and upper attachments are the result of a structure that experiences a bending load deformation since the material strives to fill the design space as far as possible from the neutral bending axis. Even though the original component presented a similar section the distribution between top and bottom section is rather different. Other dissimilarities are visible after a comprehensive analysis and among the most evident we can include:

- Lower opening and shape as it can be seen in Fig.3.11a.
- Lower attachment leg shape and structural concept (Fig.3.11c).
- Internal connection between upper and lower surfaces (Fig.3.11d).
- Upper attachment to the kinematic joint (again presented in Fig.3.11d at the left upper part of the image).

The most evident change among the mentioned is the presence of internal structures between the top and bottom surfaces of the component. This can be interpreted as the need of preventing excessive bending in the middle section where the structure stiffness is influenced by the rear lower attachment points. The presence of those rear attachments releases some of the bending load in this section. Since the structure is determined mainly by the two sections, the most of the bending is concentrated in this section. This is influenced by the presence of a geometrical variation that can be examined from Fig.3.7. The discontinuity between the two aerodynamic limits give rise to a sharp angle in lateral view that makes the structure weak in bending around this location. The possibility of adding internal structures that would not be implementable through conventional machining will prove part of the gain in the weight definition of the component redesign. The reconstruction of the component is presented in the next section.

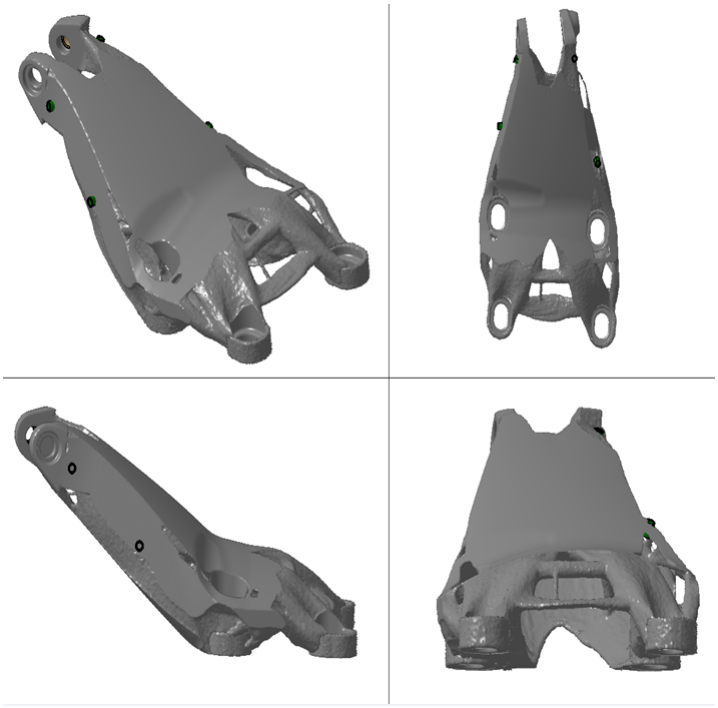

Figure 3.10: Topology optimization results: the presence of two thick external section demonstrate the bending nature of the stiffness load case. Furthermore, the presence of a frontal connection between the two outer legs of the component are a suggestion of needed stiffness between the attachment points.

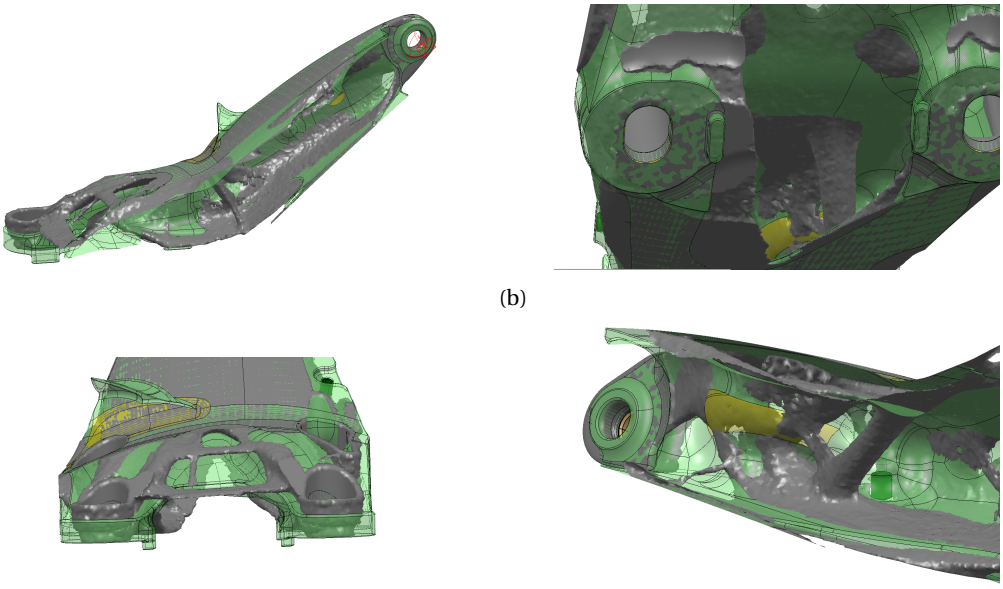

(a) (b)

(c) (d)

Figure 3.11: CAD comparison of the optimized structure and the actual components. The green transparent geometry represents the actual component while the gray is representative of the optimized structure: top and bottom section (Fig. 3.11a), lower opening (Fig. 3.11b), leg geometry for lower attachments (Fig. 3.11c) and internal structure presence (Fig. 3.11d).

3.5. GEOMETRY RECONSTRUCTION

The reconstruction of the component had to assess a series of challenges and choices. The main indication from topology optimization were evident as the need of designing new shape for the leg

attachments in the lower section or the need of reducing the material around the rear edge of the component, as well as the fundamental presence of internal connection to prevent bending in the middle section. Other aspect of the reconstruction were more debatable since their presence was either highly dependent on which simulation was used or on how the parameters for the simulation were set. As a first starting point an agreement was reached with the manufacturing team to keep the minimum wall thickness at 1.5mm. From here a distinction was made among the possibilities of implementing internal structures that would effectively prevent the bending of the component without being excessively exposed to high stresses in the case of limiting stress cases. The first iteration has

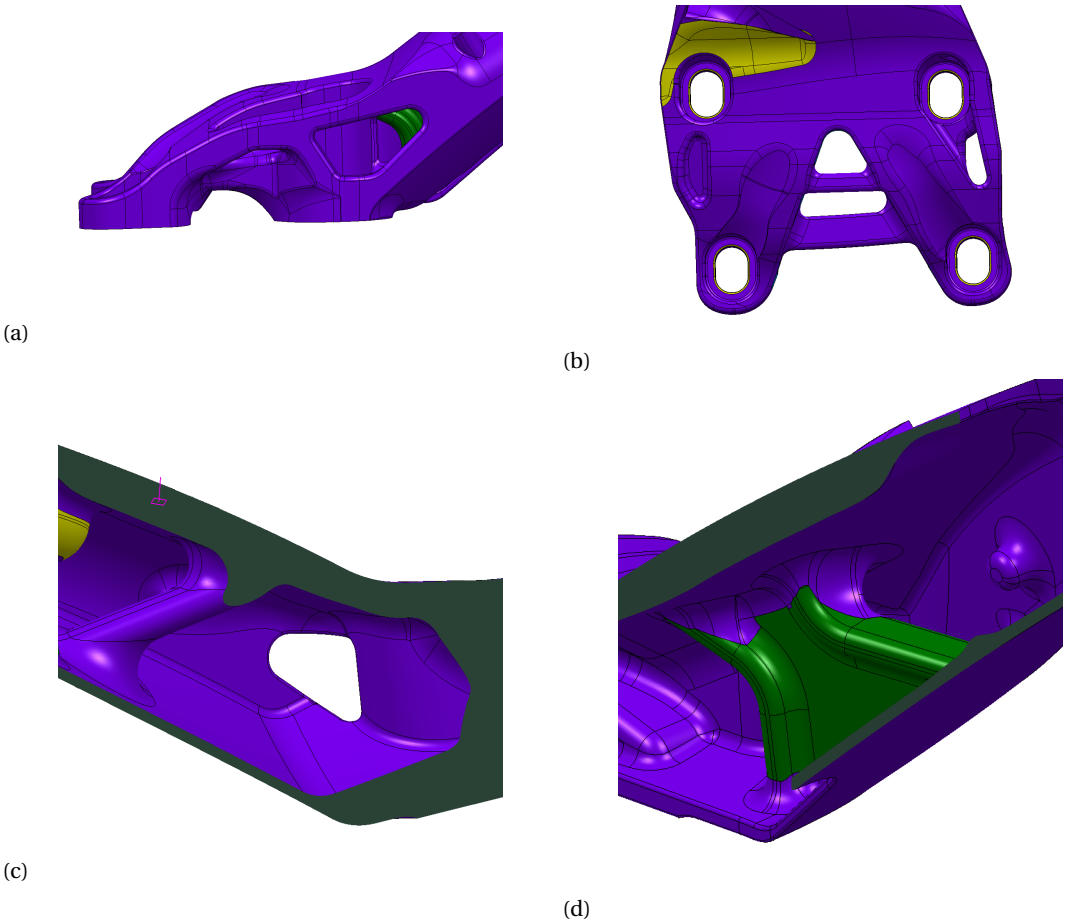

(a) (b) (c) (d)

Figure 3.12: Peculiar feature presented in the first design reconstruction: lower leg geometry, leg upper connection, internal nerve (highlighted in dark green) on the rear side and connection in the front section of the component. The presence, and subsequent implementation, of non-machinable geometries is an added value of the strict synergy between topology optimization and additive manufacturing.

regarded a modification of the original geometry on a number of different features:

- The leg geometries have been revised as it is reported by Fig.3.12a
- The lower opening features a new geometrical concept and each thickness has been reconsidered on the topology optimization result.
- Internal connection between upper and lower surfaces on the front side. The presence of this truss structure was evident among most of the simulation settings and therefore it has been implemented in the geometry. The final shape can be seen in Fig.3.12c.

Table 3.5: Main characteristics of the first design iteration as presented in Fig. 3.13.

Bracket for AM (first iteration)	
Weight	1054 g
Material	Ti6Al4V Annealed
Camber Compliance	34.8°/MN

- Second internal connection has been implemented to feature the stiffness between the upper and lower surfaces. The wanted effect is similar to the one that led to the introduction of sandwich designs of composite and aluminum plate able to withstand bending loads[25].

An overview of the first geometrical iteration is presented in Fig.3.13. The first iteration of the component did not reach the target stiffness. Its characteristic camber stiffness has been calculated in the first FEM stress assessment in which the geometry has been validated to be lower than the requested target and the overall component had a reduction in weight that was equal to the reduction in stiffness in term of efficiency. The FEM assessment will be presented with further details in Chapter 4. Basically the first iteration has the same efficiency of the original component at a lower weight level. The camber stiffness and weight are reported for comparison in Table 3.5.

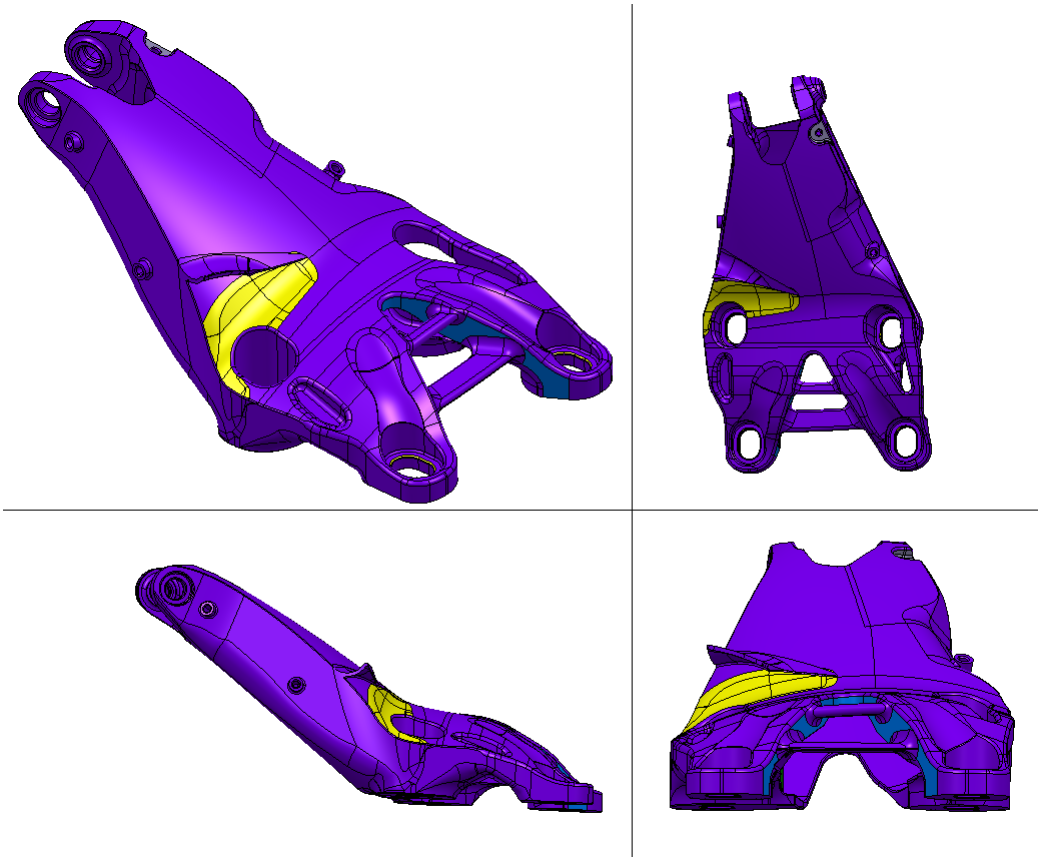

Figure 3.13: First CAD geometry of the topology optimized structure. The reconstruction procedure, developed in CATIA v5, has to face some compromises since the interface has not been optimized for the quick reconstruction on a meshed surface (as the one provided by the topology optimization). The need of parametrize the design into a number of finite operation rather than reconstructing the component on the optimized surface, is a current limitation of the designer's tools.

[25] The mechanical behavior of sandwich structures is well explained in every mechanical design book and refers to the mechanics of bending. For reference and examples cfr. [83]

Since a result that would not increase the efficiency of the component was not admissible to justify the project and since the room for improvement in the geometry was present the process of optimization based on the strain energy density approach has been carried out with linear FEM analysis[26]. The results of this process will be presented in Section 4.1 of Chapter 4, as mentioned earlier.

3.6. DESIGN FOR MANUFACTURING ASSESSMENT

During the first iteration the manufacturability of the component has not been taken into account with the aim of freezing the most efficient geometry and to cope with small manufacturing adjustments in the subsequent iteration. During the process of designing new geometries it became clear that the manufacturing limits had to be taken into account in the loop of the FEM assessment since the small geometries of the nerves, used to restore the proper printing angle in order to avoid the presence of internal supports, could potentially give rise to stress issues. The introduction of those elements will be seen in this section, even though the presence of such details was not present in the first geometry reconstruction, since they represent a common issue in the geometrical design of components for additive manufacturing. As described in the literature review[27], the printing angle has a decisive influence in the definition of a design process since it is its relative positioning the drives the presence of supporting structures.

In the case of interest the component printed in titanium has a printable limit of approximately 30° and the best print quality can be achieved with unsupported angles that are steeper than 45°. This means that every portion of the component, seen along the print direction, that has an angle between the feature and the printing plane lower than 30° needs to be supported by external structures. Supporting structures are usually minimal portion of material printed in the direction of the print such to allow the deposition of material at certain height with no need of the minimum angle requirement. Since they need to be removed their geometry usually presents a reduced section at the interface with the component in order for the support to fail in a controlled zone in the post working operations. Titanium supports are strong enough to require dedicated tooling for their removal and the manual operation, aside from being costly and time-consuming, requires extreme care in order to properly remove the unnecessary features while avoiding any scratch on the component surface.

For the RTWB bracket there has been the need of reducing supporting structures specially in the inner side of the component: the reduced access to this region would have made very complex any removal operation with a high chance of featuring scratches related to the isolation from the operator of its working area. A compromise has therefore been taken to avoid completely supporting structures in the inside of the component but to implement them in the outer surface. Few examples of those structures are reported in Fig.dfm where we can see the printing direction 3.14a and some of the details added to prevent excessive angled features (cfr. Fig.3.14a and Fig.3.14b).

The design process of the new geometry for the RTWB bracket has been presented and the rest of the chapter will analyze in a similar manner the performed activities that led to the full redesign of the

[26] During the linear analysis of a component through FEM simulation (not including topology optimization) it is a common practice to analyze the structure, apart in term of Von Mises stress and principal stresses also under the view of strain energy. The strain energy density is a scalar value that represents the coupling of the strain energy with the deformation gradient. It is an indication of regions that are contributing more making the structure compliant and therefore are under-dimensioned to provide the correct stiffness level. Ideally a structure should be all with the same strain energy density - *meaning all the material in the component is equally contributing to the end stiffness of the part.*

[27] cfr. Section 2.5.5

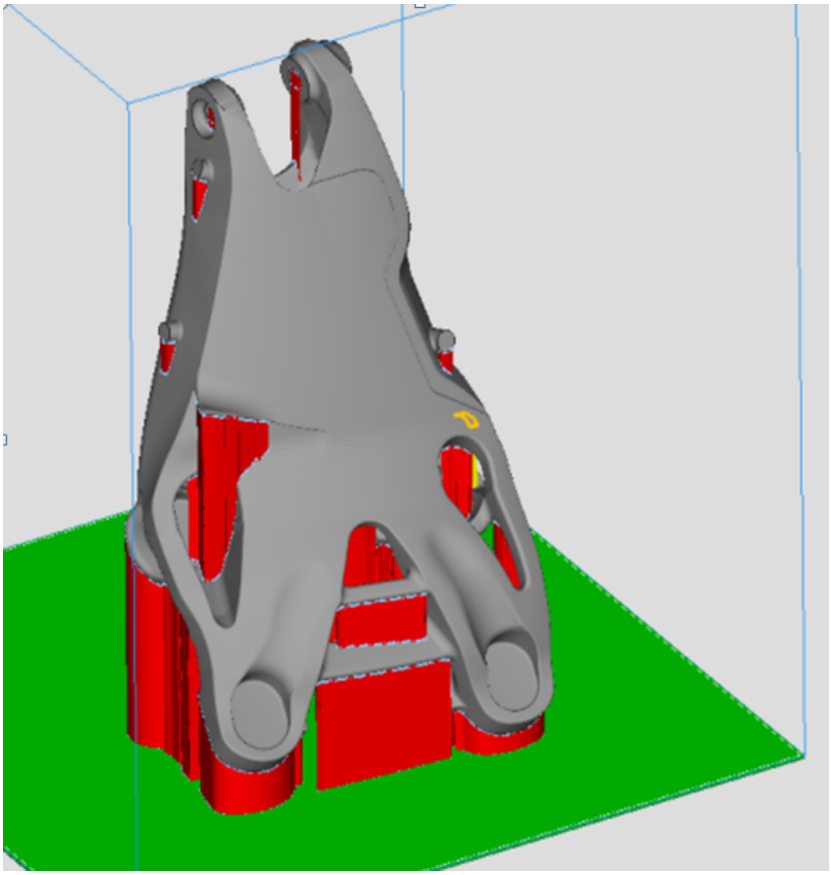

(a) Printing direction relatively to the printing plane: in red is highlighted the support structure

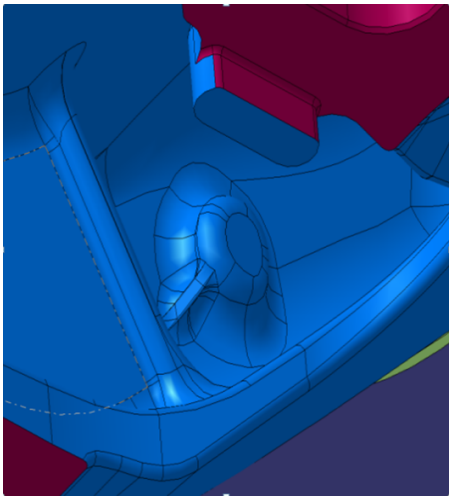

(b) Local detail added to the geometry to limit the impact of internal supports

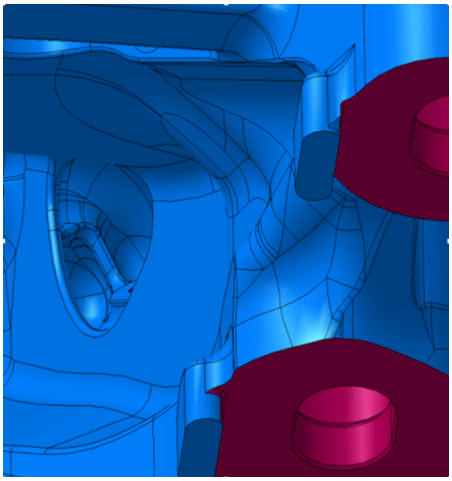

(c) Local detail added to the geometry to limit the impact of internal supports

Figure 3.14: Design assessment for manufacturing and reduction of supporting structures. The implementation of small nerves is strategical to obtain good surface finishing (minimizing the layering effect driven by the high angle between the feature and the printing direction) and remove the need of subsidiary supporting elements: their removal operation will negatively influence the surface finishing as well.

rocker beam.

3.7. DESIGN OPTIMIZATION OF THE ROCKER BEAM

As already seen for the RTWB bracket, the design process of the rocker beam has followed similar engineering phases and processes. Even though the process is similar, the need of introducing new materials (namely AlSi10Mg and Scalmalloy as well as Ti6Al4V) in the comparison required some specific attention in order to redefine the leading figures of merit for the material choice among the available options. After the analysis of the machined counterpart and a brief description of the material currently in use for this component the material comparison will be carried out and the decision of undertaking Scalmalloy as the design material will be explained. The chapter will finally present in the last sections similar to the previous one including: design criteria, topology optimization and geometrical reconstruction.

3.7.1. ANALYSIS OF THE MACHINED COUNTERPART

The rocker beam, as already described in the beginning of Chapter 3, is part of the suspension components that are located inside the bodywork of the car[28], and it is the component that houses the bearings for the suspension rockers, reaction arms and anti-roll bar link connections. Its second main function is to stiffness the gearbox carbon case that presents a less stiff section were the suspension components are installed because of geometrical reasons. From a geometrical point of view it can be describe as a medium length beam featuring along the middle section two bearing houses connected by an open section that features a cross sectional area resembling the one of a C-shaped beam. On both sides the component presents two short arms in which is located the anti-roll bar assembly with its subsidiary systems. On the two lateral extremities the faces are prepared to be connected to the gearbox by the mean of a steel spacer. The component as well has a series of ancillaries details (*verbi gratia*: the connection for electronics and hydraulics manifold by the mean of small M4 - M5 fasteners) and is limited in the geometrical shape by the presence of envelopes of the suspension inboard components. Due to the poor ductile properties of the material the fixtures to the gearbox housing are two M7 bolts that are connected not in a threaded section of the component [29] but with a dedicated housing with an inserted barrel nut. The machined counterpart for the project AMed component is presented in Fig. 3.15. It can be noted in how the presence of added material is needed to support the barrel nut housing featuring as well an anti-rotation device. Furthermore the need for machinability prevents the component to be made out of a hollow structure between the two bearing houses that could potentially better cope with the limiting stresses.

3.7.2. MATERIAL OF THE MACHINED COUNTERPART

As already presented the material of interest for the machining counterpart is an aluminum matrix composite. Specifically this material has been developed for F1 championship components. The commercial designation is AMC225 and exists in two available versions - XF and XE depending on the mean dimension of the strengthening particles. The base line material is a copper based aluminum

[28] The suspension component that are placed inside the gearbox external case are usually referred to as *inboard components* and this nomenclature will be used in the same extend in the present work. The inboard components such as torsion springs, lateral dampers and anti-roll bar assembly are considered as sprung mass. For antithesis the components that are out the bodywork are considered to be outboards components and are unsprung mass.

[29] It is not advisable to have structural thread in metal matrix composite due to their already mentioned poor ductile nature given by the present of reinforcement particle in the microstructure.

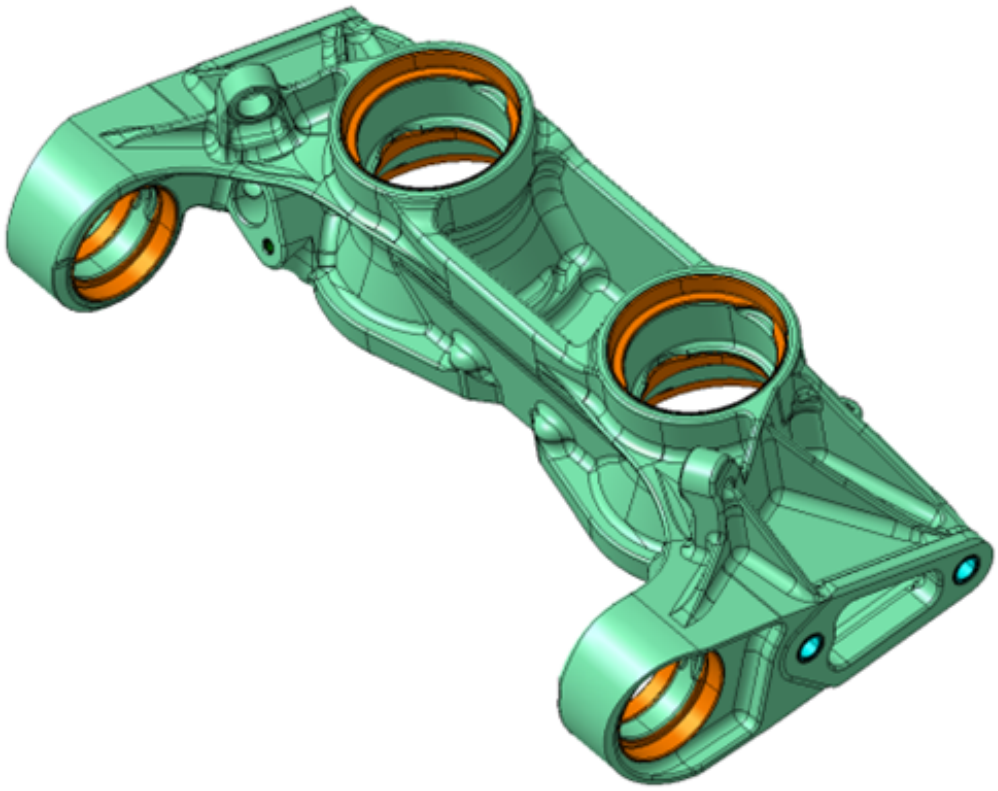

Figure 3.15: Actual machined component as it is present on the SF70H rear suspension assembly: the need for machining operations led to an open section profile of the component. The component features an overall length of 285 mm in its longest characteristic dimension. The height is of 85 mm with a third dimension of about 110 mm from the back to the anti-roll bar installation housing.

alloy (Al 2124) developed for high temperature operation that requires a high strength aluminum alloy. The baseline alloy for the development is the heat treatable Al 2024 which is one of the reference alloys for aerospace fatigue designed aluminum component. The main differences are in the content of poisoning elements in the mixture such as *Fe* and *Si*. *Fe* has a negative impact on aluminum microstructure since it features a very low solid solubility limit and a high solubility limit in the liquid phase. This prevents the existence of any effective way of separating the two elements in the molten phase but upon cooling *Fe* tends to precipitate in small incoherent intermetallic precipitates (with aluminum and other elements) making the final alloy brittle. Furthermore, the tendency of reducing the grain size is limiting high temperature performance since the grain boundary sliding provides a method for creep movement. Limiting *Si* and *Fe* the 2124 alloy features better high temperature properties and general tensile properties upon heat treatments (solubilization and artificial aging). The temperature properties are normed to be at 200°C for yield strength after 10 hour time of 310 MPa and after 100 hours of 140 MPa. The reduction of impurities is responsible for the increment of stress corrosion cracking performances as well that used to be a limiting aspect of 2xxx aluminum alloy series. The addition of ceramic particles dispersed in the alloy has two main effects: increasing the stiffness modulus as the material is now a composite material (the equivalent modulus can be approximated by the rule of mixing) up to values close to those of titanium alloys and secondly to increase the material tensile properties with particles that are stronger than the matrix. All the benefits in tensile properties

and modulus are counterbalanced by a poor ductility of the new material. The presence of spherical shaped reinforcing particles in the aluminum matrix are responsible for localizing the dislocation movement at the matrix interface. The increment of dislocation density at peculiar zones makes the material susceptible to fragile fracture. The particle of choice for the processing of this metal matrix composite is SiC[30]. The material properties of AMC225 will be addressed as the benchmark material for the material comparison presented in the following sections.

3.8. DESIGN CRITERIA

Similarly to the performed activities on the RTWB bracket the design criteria for the rocker beam are of two nature: the first is the stiffness contribution that the component has in respect of the contact patch of the tire responding certain loads and secondly it has to retain a sufficient reserve factor for extreme load cases (such as episodes of accidents or bump occasions). To determine the topology of the component a simplified approach has been taken to assess possible geometries. The load configurations on each bearing were assigned and the component constrained to the gearbox case. The loads and design criteria are explained in the next sections.

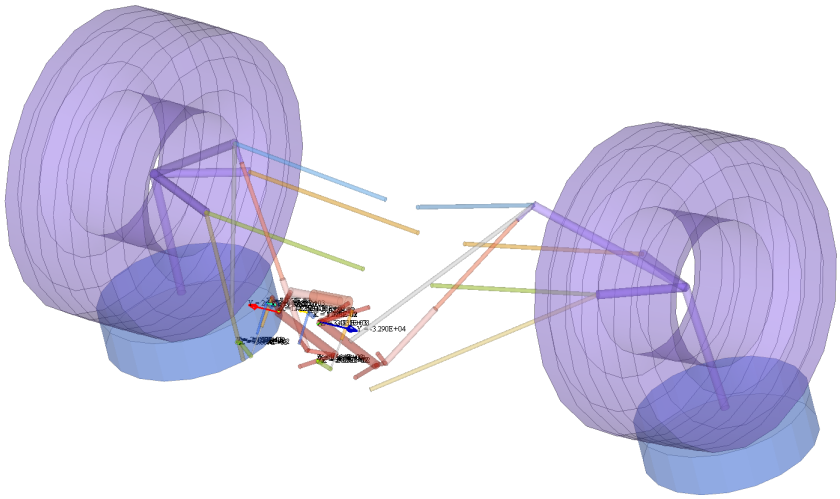

Figure 3.16: Multi-body model for load generation: this model is the generator of loads for all inboards component of the suspension. From the analysis of the contact patch forces it extracts the relative forces on the other components.

3.8.1. STIFFNESS REQUIREMENTS

The driving factors for stiffness requirements are determined by the displacement of the bearing housing. The bearings are the connection that allows relative motions between the rocker and the gearbox and any displacement in the rocker beam interface will result in a reduced stiffness chain downstream to the contact patch of the wheel. The rocker beam features eight bearings and to assess the influence of those on the car performance a sensitivity check has been done. The influence on the wheel position is given only by the displacement of the rocker bearing that is the lowest and biggest of the present bearings. The bearing stiffness has been set as the reference parameter to evaluate differ-

[30] SiC is a renown ceramic particle used also as a bulk ceramic material. More on the particle effect on the mechanical properties of aluminum can be found in [84]

ent rocker beam options. The implementation of a series of different geometries rising from various topology optimization routines will be explained in the rest of the chapter and an in-depth analysis will be carried out.

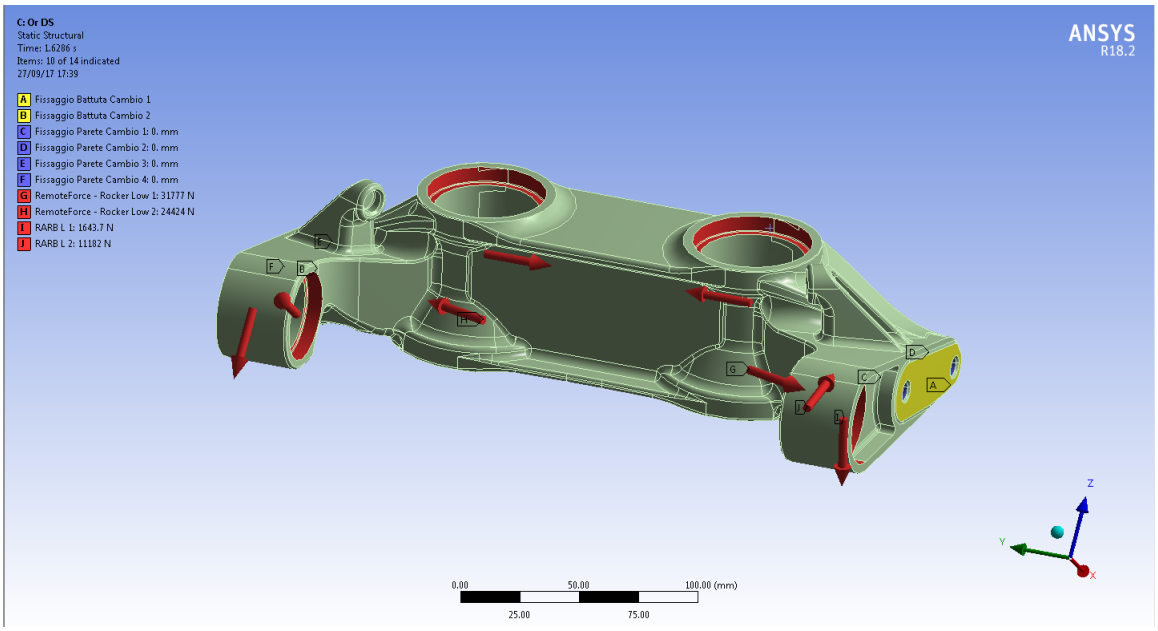

Figure 3.17: Design space with applied loads for the topology optimization of the rocker beam. A small scale bar shows the actual dimension of the component. The central section in khaki green represent the optimization region. The load applied on the red faces are responsible for the mechanical behavior of the rocker beam that has been constrained in axial displacement around the gearbox interfaces (highlighted in yellow).

3.8.2. STRENGTH REQUIREMENTS

The dimensioning load cases for strength were the events of two different bump episodes: the first limiting case for the inboard components is the case of a symmetric bump while the second is referred to as a roll bump scenario. the main differences involved are the forces direction that in the case of the roll bump are anti-symmetric since the load transfer is changing the reaction of the car weight on the suspension components. The load components are evaluated through a multi-body simulation that is prepared for anticipating the car behavior from simulations by the structural department and an image of it is presented in Fig.3.17. Each interface load is present as seen by the bearing so the effect on the rocker beam is its opposite reaction force. The two load cases for symmetric and roll bump are presented in Table 3.6, the components of the load are presented in global coordinates and are expressed in Newton (N). The loads on the reaction arm bearings are not reported since their direction does not change in the two mentioned scenarios and in both cases are around 6-8 kN only in the Y-axis direction[31]. Furthermore, since the component is wall-mounted inside the gearbox in a closed environment the temperature element has to be taken into account as well. The design temperature for components that are in the first proximity area of this component ranges from 100° to 145°C. The target temperature for the design of the rocker beam has been set 120°C that proved to be an accurate

[31] This specific behavior is explained by the nature of the reaction arm which is a device of the full-split rear suspension: splitting the different modes of the suspension such they can be reacted individually (having no roll and bump interconnection) makes the reaction arm reacting to a tensioning bar which is aligned in the Y-axis direction from which the load on the rocker beam that counteracts the other components is aligned on the same axis

value of what happen during a race event. The temperature has been used for the strength evaluation but during the topology optimization its contribution has been reduced in order to stabilize the simulation process[32].

[32] The compliance definition of a topology optimization process is not always well posed for a thermal varying process and can lead to solution instabilities. This behavior can be tracked back to the example of the simple bar installed between two fixed walls with a temperature increase. The maximum deflection of the beam does not depends on the cross section but only on the temperature difference. The absence of a linear relationship between the geometry and the deflection, contrary to what happens in the case of a force load that is connected directly to the displacement through the stiffness of the component which depends on the component geometry, constraints the process in finding a correct solution path.

Table 3.6: Symmetric bump case for strength and stiffness on the rocker beam optimization; all values are expressed in newton (N). Being originated by the multi-body model and not coming from a car measurement those values are considered as perfect inputs (no level of accuracy is associated with the simulation procedure).

	Rocker Bearing SX	Rocker Bearing DX	RARB SX	REARB DX
X	-3481	2125	1637	-1885
Y	-30900	28600	0	0
Z	-2530	1423	1306	-1323

Table 3.7: Roll bump case for strength and stiffness on the rocker beam optimization; all values are expressed in newton (N). Being originated by the multi-body model and not coming from a car measurement those values are considered as perfect inputs (no level of accuracy is associated with the simulation procedure).

	Rocker Bearing SX	Rocker Bearing DX	RARB SX	REARB DX
X	-13010	10030	10390	-17030
Y	-27750	23570	0	0
Z	-8710	6710	9870	-10255

3.9. MATERIAL CHOICE AND COMPARISON

As already mentioned in the previous section, the material choice for the suspension inboard components is not limited as much as for the outboard components. The materials taken into account for the rocker beam were a series of aluminum and titanium alloys that have been compared to the baseline material that is the AMC225. The materials of interest are, as mentioned earlier in the report, titanium Ti6Al4V, as for the RTWB bracket, aluminum AlSi10Mg and Scalmalloy. All the materials have been briefly presented in the literature review section[33] but in this section the analysis would focus on the specific properties able to maximize the component performance on the overall car performance.

3.9.1. FIGURES OF MERIT

To be able to define a specific performance parameter for the material choice there is the need of establishing a series of figures of merit to properly judge the combination of the material properties over the specific needs of the component in analysis. This has to be done a step ahead of the topology optimization and can be included as well in the topology optimization process itself. The quality of the component can be expressed in terms of weight and stiffness as already described in the design criteria. Furthermore, the presence of a thermal expansion effect between the gearbox case (designed in composite design with near zero CTE[34]) requires to evaluate also the strength and stiffness reduction with increasing temperature levels up to 120°C. The main tensile properties are related to the specific weight of each material as reported by Table 3.8.

A graphical interpretation of the result presented in Table 3.8 is reported in Fig.3.18. As it can be easily inferred the advantages of the AMC on the specific stiffness is evident. The two different options presented for the Scalmalloy and for the titanium Ti6Al4V represent the range that is present in the literature. The lower values are reported from homologated values that are granted by company specifications while the best results are evaluated on real characterization campaign that has been carried internally for both titanium and Scalmalloy. The measured differences are quite consistent and are representative of the uncertainty of the material characterization especially when related to novel materials and additive manufacturing technologies.

[33] Cfr. Section 2
[34] Coefficient of thermal expansion.

Table 3.8: Specific material properties of interest: Specific Yield Strength and Specific Modulus

	Specific Modulus [GPa*dm^3/kg]	Specific YS [MPa*dm^3/kg]	Specific Weight [kg/dm^3]	CTE [1/K]
AMC225	39.93	138.8	2.88	13 x 10-6
Ti6Al4V	24.83	186.23-230.24	4.43	9 x 10-6
AlSi10Mg	26.11	104.47	2.68	25 x 10-6
Scalmalloy	24.34-26.6	176.03-183.5	2.67	21 x 10-6

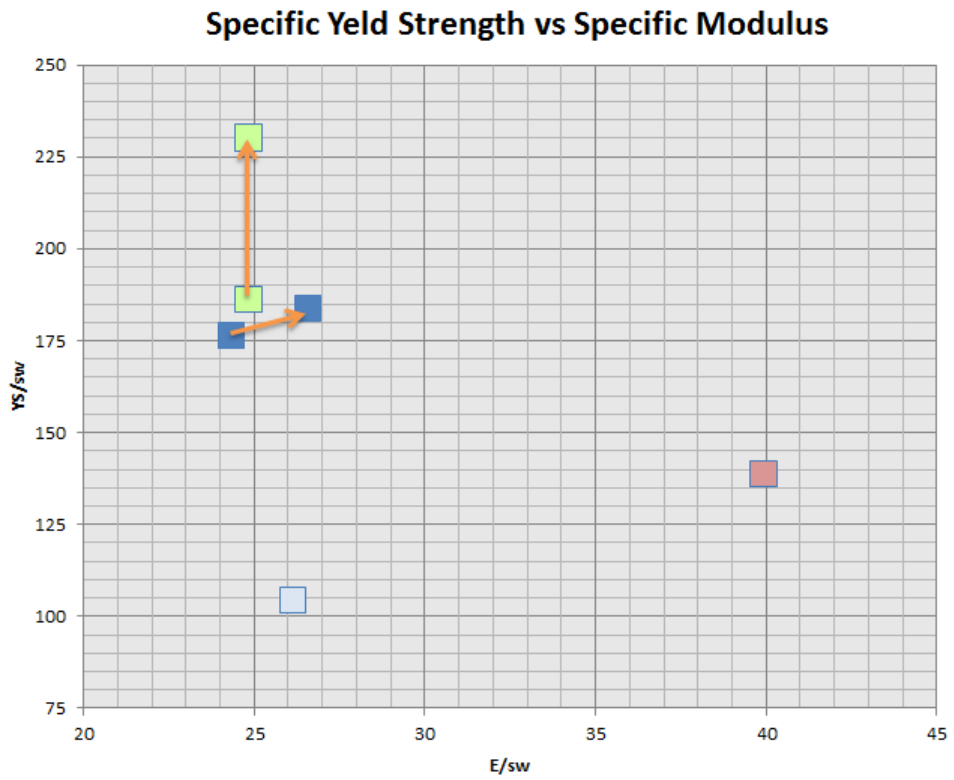

Figure 3.18: Graphic representation of the room temperature figures of merit for specific stiffness and strength for the selected materials: in red the AMC225, in light blue the AlSi10Mg, in blue the Scalmalloy and in green the Ti6Al4V. As it can be seen, the scatter in the properties of Scalmalloy and titanium is quite relevant: this is an indication of the uncertainty about the manufacturing process and its reflected on the mechanical properties. The specific stiffness of the AMC225 definitely overruns the other materials but all strength limited regions would benefit of titanium as a baseline material. The Scalmalloy is a compromise between the two with a specific strength not far from titanium values its implementation will be beneficial for all the density limited regions.

At high temperature the relative distance in terms of figure of merit is not completely changed. The reduction of performances in temperature for AlSi10Mg is the highest for the materials analyzed with a reduction of YS down to 79% of the original value at 150°C[35]. On the contrary the strength of AMC225 is reduced to 99% of the original value. The high temperature values are reported in Table 3.9 and graphically in Fig. 3.19.

A first evaluation would make the material selection for additive manufacturing to strive for titanium over AlSi10Mg and also over Scalmalloy. Since the temperature is less influencing the properties the opportunity of having a titanium component would also benefit for lesser stresses related to the lower expansion difference between the wall mounted rocker beam and the gearbox. Other considerations, necessary for a proper evaluation, are the fatigue performances of the alloy and the strategic

[35]All the high temperature properties are evaluated for a short hold at temperature (0.1hrs). The effect is greater in the reduction of properties if the temperature is considered to be kept for longer periods.

Table 3.9: Retained specific properties at 150°C for the selected materials

	Specific Modulus [GPa*dm^3/kg]	Specific YS [MPa*dm^3/kg]	Specific Weight [kg/dm^3]
AMC225	39.1	137.5	2.88
Ti6Al4V	23.7		4.43
AlSi10Mg	26.11	104.47	2.68
Scalmalloy	24.71	135.95	2.67

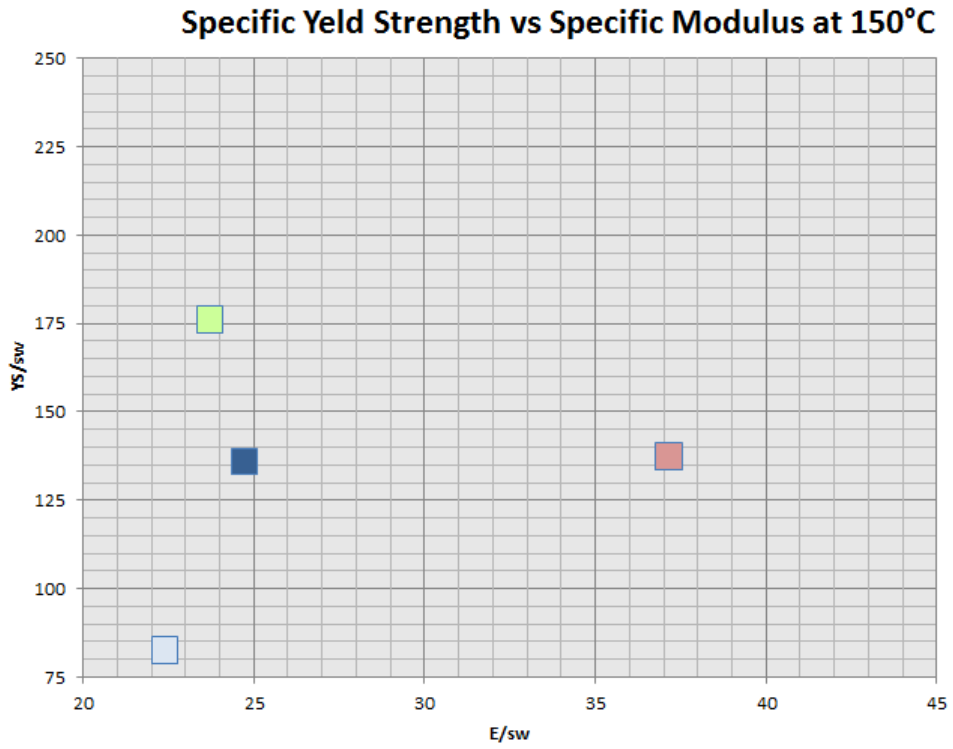

Figure 3.19: Graphic representation of the high temperature figures of merit for specific stiffness and strength for the selected materials: in red the AMC225, in light blue the AlSi10Mg, in blue the Scalmalloy and in green the Ti6Al4V. The almost temperature independent properties of the AMC225 are a reasonable rational for its implementation in the conventionally machined component: the development of additive manufacturing processes of composite material might brake the barrier of implementing its usage in combination with the novel manufacturing technique.

interest in developing a novel material processing technique that is already known for titanium but not for Scalmalloy. Furthermore, the influence on the final weight of areas in which a minimum material thickness is needed (bearing housings, threaded section, connecting areas to the anti-roll bar bearings) have a negative influence on the titanium version of the component. In fact, in those sections the only properties that matter are the pure densities rather than the specific properties. Those two reasons (density limited zones - strategic development of a quality process for Scalmalloy manufacturing and its metallurgical characterization) were the main drivers for the choice of Scalmalloy for the development of the rocker beam over titanium - AlSi10Mg was not reputed sufficient for the temperature level at which the component is operating.

3.10. TOPOLOGY OPTIMIZATION

Similarly to the actions performed on the RTWB bracket the topology optimization has been carried out for the rocker beam following the same logical steps: definition of a design space with the definition of exclusion zones, definition of driving load cases based on the design criteria and evaluation of manufacturing limits. The results of the process are presented with a series of different topologies that have been proposed varying basically on the attachment zones with the hypothesis of different methods to secure the component to the gearbox due to design choices reasons and to improve the overall weight saving on the component.

3.10.1. DEFINITION OF THE DESIGN SPACE

The design space definition followed the geometrical constraint of the component. The main limitation can be listed as follows:

- **Mechanical interfaces:** as mentioned in the previous chapter the rocker beam features ten bearing housings (4 dedicate to the anti-roll bar, 2 for the suspension rockers and 4 for the reaction arms) that are dimensioning the central section of the component.
- **Mounting operations:** the mounting operation of the rocker beam needs consideration and can limit the total height of the object. Since the mounting procedures is done with other components pre-installed the all assembling envelope must be considered.
- **Inboard envelopes:** the inboard components of the suspension have relative motions in respect of the rocker beam. This is related to the dynamical response of the suspension systems to the applied forces at the contact patch. The envelopes of those motions are limiting the shape especially in the region where the anti-roll bar is installed and are causing, as it will be described, a poorly designed geometrical region responsible for one of the highest stressed regions.

Having considered the limiting portion of space above described, the optimization routine started with a fullness of material both at the side at the rocker bearing as well as in the central section of the component. The presence of complete freedom in defining the geometry in this section should grant a better efficiency of the used material able to grant sufficient weight saving to justify the experiment of the novel technology. The design space showing the exclusion zones is presented in Fig. 3.20.

EXCLUSION ZONES

As presented in the previous section as mechanical interfaces the exclusion zones have been determined similarly to what has been done on the RTWB bracket. The implementation of fixings and bearing housing provided the basic zones to be kept. In further development of the component different areas has been frozen from optimization routine to force the simulation towards a defined geometry.

3.10.2. DRIVING LOAD CASES

In order to properly define the optimization result the driving factors for the optimization routine had to be adjusted from the first simulation. The objective of the simulation, since the stiffness load were as well the strength limiting load cases, has been set on the stiffness of the bearing housing of the

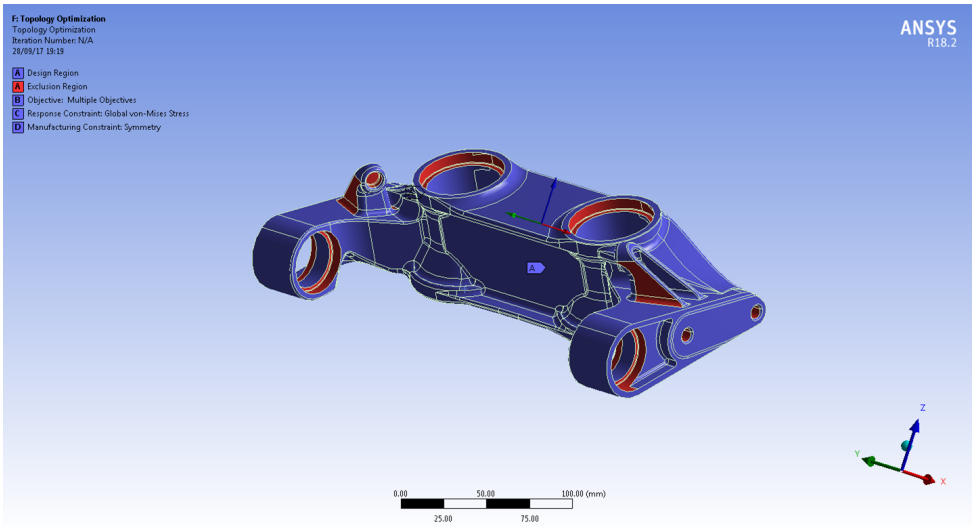

Figure 3.20: Reconstruction of the design space for the Rocker Beam: highlighted in red are the surfaces which are excluded from the optimization routine. The need of saving the end stops on both sides is made evident by the red color applied on the two small features that are housing this characteristic. The other exclusion areas are th bearing housing and the attachment points.

rocker which has a direct influence on the wheel stiffness in reaction to a contact patch load. The stiffness of the reaction arm bearing set has also being taken into account since the installation of the whole system requires a high grade of precision and operational misalignment are not admissible.

3.10.3. TOPOLOGY OPTIMIZATION RESULTS

The topology optimization results are the end result of a series of simulation on which the design space and simulation parameters have been adjusted, as already mentioned, to provide a solid and robust geometrical reconstruction that would represent a clear indication of a feasible designable structure, in Fig. 3.21 the main passages trough the simulation process are presented. The following steps are representative of the evolution of the simulation results:

- **1st set up [only roll bump case]:** the first set up was required to check the solution procedure but since there was no complete load case was implemented. The non feasible single loaded result can be seen in Fig. 3.21a.
- **2nd set up [complete load case]:** in the second step the full load case has been implemented and the first feasible geometry was reached. The weight of the objectives (mass, roll bump compliance, heave bump compliance) were set arbitrarily after a scan of their effect on the geometry (Fig. 3.21b).
- **3rd set up [modified design space]:** the definition of a reduced design space was implemented with the aim of forcing the simulation more clearly in the lower section of the component and to achieve this a second iteration has been done varying the ratio between the objectives weight (Fig. 3.21c).
- **4th set up [modified design space]:** as already presented this version implements a further iteration on a modified design space with more weight on compliance objectives rather than weight optimization, cfr. Fig. 3.21d.

- **5th set up [added torque stiffness]:** since the modified design space approach was not making the simulation converging on a precise result a torsion load was implemented at the contact patch level to simulate the braking condition adding an element to the simulation to force the result towards a better define geometry. This las simulation has been taken as the final result for the reconstruction after an optimization on the simulation parameters done in order to obtain the more sound geometry as presented in Fig. 3.21e.

From the final step after the described optimization of the objective function weights the end result used as reference for the geometrical reconstruction is presented in Fig. 3.22 and in Fig. 3.23 with a multi-view image showing the result from more than one perspective point.

3.11. GEOMETRY RECONSTRUCTION

The design reconstruction has been done in CATIA V5 R24 similarly as for the RTWB bracket. From a geometrical point of view the component now features two different connection between the bearings. A lower section connects the rocker bearings axially and a tie section on the top is the connection between the two upper bearings of the reaction arm. The trabecular structure is a triangulation of the two main sections and provides stiffness for load cases in which the applied force on the bearing is not purely axial. The lateral geometry features a direct connection of the upper bearing to the side of the component providing axial stiffness with loads that would tend to separate the two reaction arms (wheel rebound loads).

Apart from the geometrical description of the main differences with the current version different optional geometries have been developed at the concept stage: the evolution of the design required an evaluation on the fixing methods for the rocker beam. In the design space, for removing the need of barrel nuts, and allowing a proper optimization routine of the component geometry there has been an implementation of a threaded section for connecting the rocker beam to the gearbox housing. After few considerations on the operating life of the component, the presence of a thread on the component has been judged insufficient: the high number of mounting and de-mounting cycles would be critical to be addressed by a thread and helicoil combination. Wear resistance and free play on aluminum thread with stainless steel helicoil are unlikely to be sufficient during the number of assembling iterations. Therefore, in order to prevent the implementation of a barrel nut that requires an anti-rotation device and is likely to add a portion of material, it has been proposed to implement a solution featuring a screw-lock nut as a good compromise between availability and service life operations. A comparison has been carried out between the standard geometry (considered in both AMC and in Scalmalloy to compensate the material stiffness effect) the nut geometry optimized and other versions of the optimized component as obtained from the topology optimization. The comparison has been carried out at room temperature level in order to classify the component from the mechanical perspective and because the The different configurations are:

- **SF70H Version**: this is the baseline configuration and the target in stiffness for the redesign of the component.
- **SF70H in Scalmalloy**: this version has been done to check the influence of the material specific stiffness.

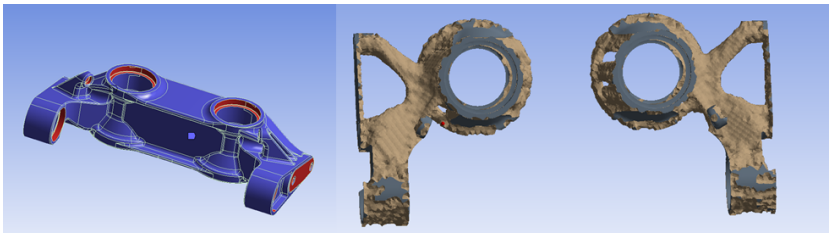

(a)

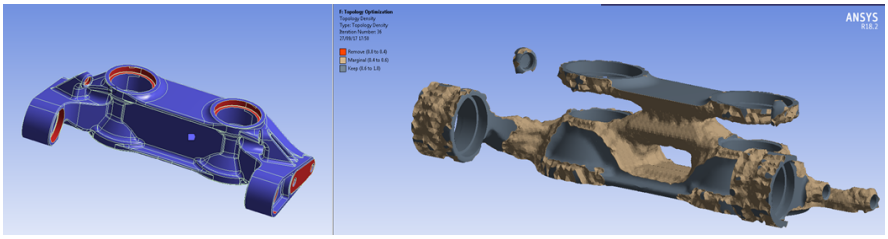

(b)

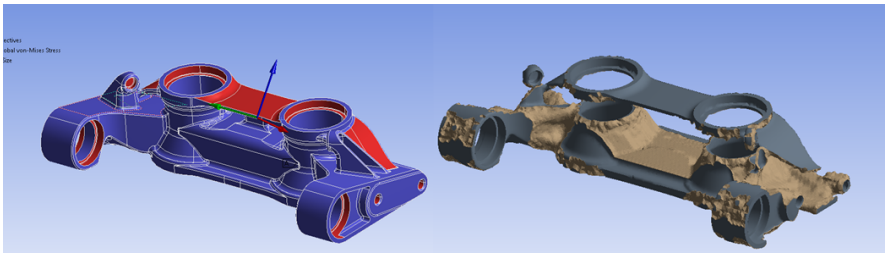

(c)

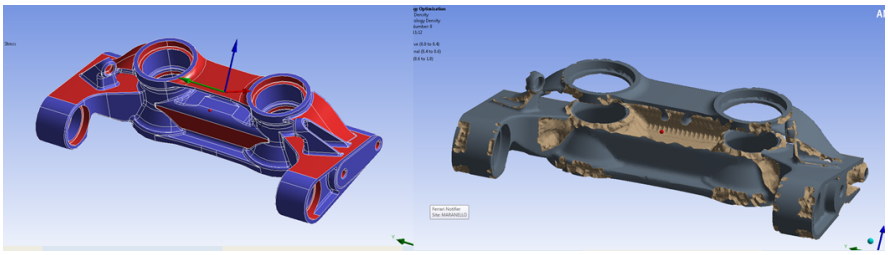

(d)

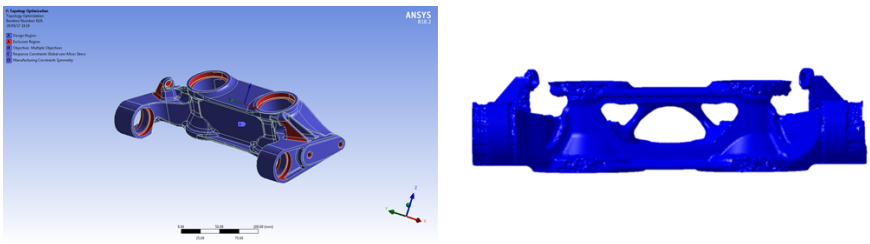

(e)

Figure 3.21: Evolution of rocker beam topology optimization results. The different configurations of the simulation has a strong influence on the final geometry. The need of calibrating the solution parameters in order to obtain a feasible geometry is the expression of the designer understanding of the structure behavior.

- **Optimized Nut Attachment**: the attachment to the gearbox has been implemented with a hexagonal screw-lock nut. This has also been the final design decision for the component.
- **Optimized Nut Attachment MK2**: this version is an optimization on the attachment area of the previous geometry. The section of the two attachments is in its final configuration featuring a section of material for axial continuity of the material. The geometry is presented in Figure 3.26.

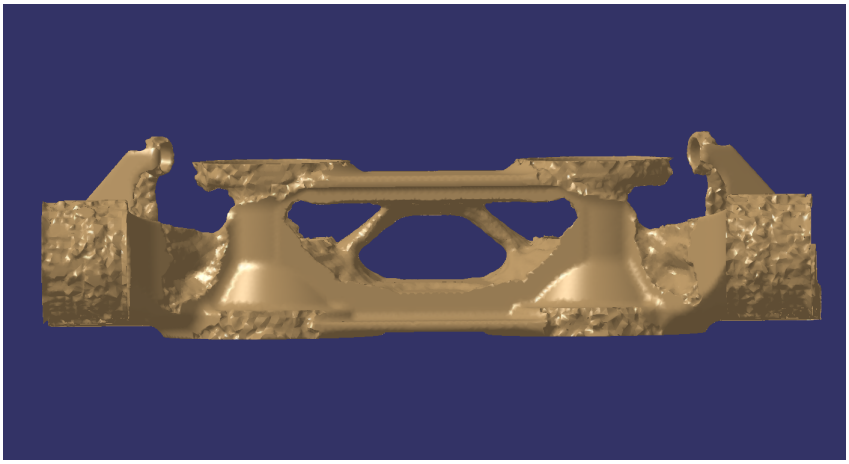

Figure 3.22: End result of the topology optimization for the rocker beam.

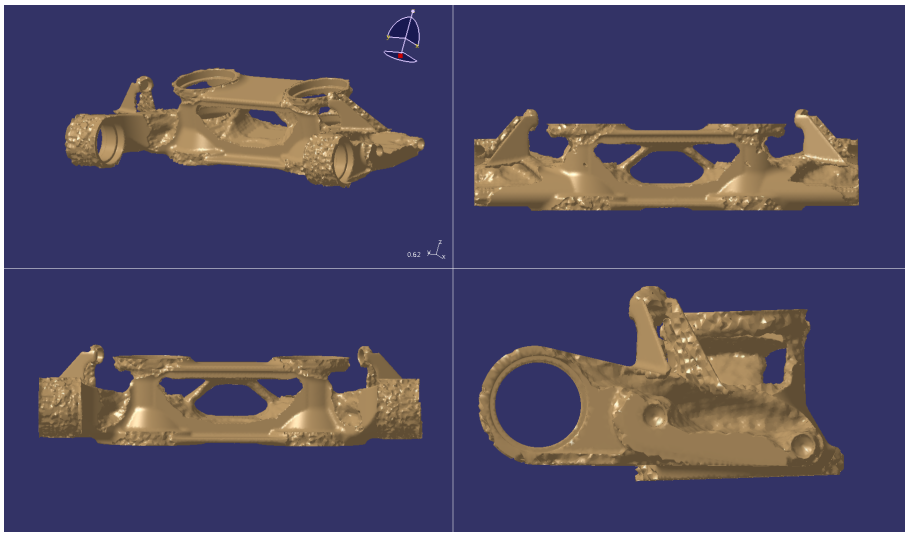

Figure 3.23: Multi-view image of the rocker beam optimization as presented in the last version of the topology optimization results

- **Optimized Barrel Nut**: the optimized version has been implemented with the presence of four attachments point for barrel nuts and anti-rotation features.
- **Optimized Threaded**: this is the starting point of the reconstruction from the topology optimization.
- **Optimized Threaded Light Version**: the optimized version has been reconstructed with a stronger drive towards weight reduction, even if some weight has been removed the specific stiffness of the component was decreased.

The room temperature comparison has been carried out, as specified, for two stiffness cases on both the rocker bearing and the reaction arm bearings. The deformation is considered in total deformation of the center of the bearing housing which would represent the loss of stiffness of the assembled system. The displacement are related to the weight of each reconstruction in order to take into account the effect of the different weight of the various solutions. The seven geometries characteristics are reported in Fig. 3.24 and 3.25.

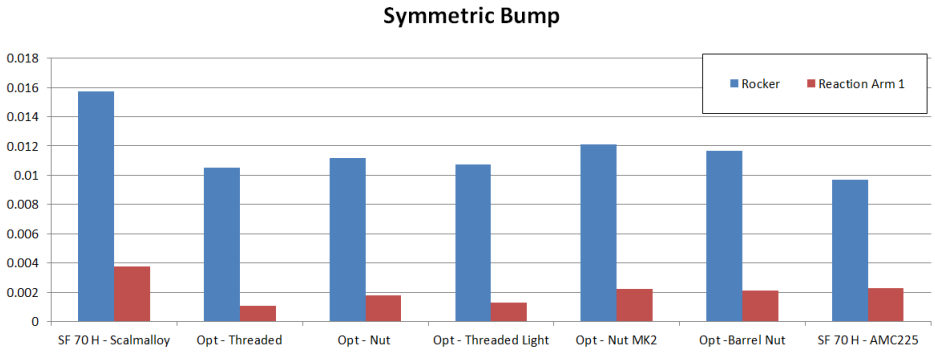

Figure 3.24: Design comparisons between different geometries: symmetric bump load case specific stiffness. Being a specific stiffness the parameter is expressed in displacement over weight (since the load is constant for all the configurations). The unit of the evaluation is mm/g. The blue bar represent the specific stiffness of each geometrical reconstruction at the rocker (lowest) bearing housing. The red series are the specific stiffnesses of the central bearing housing (lower rocker arm bearing). In both cases the influence of the material of choice is evident and the ability of closing the gap is representative of the potential that can be unlocked with proper topology optimization.

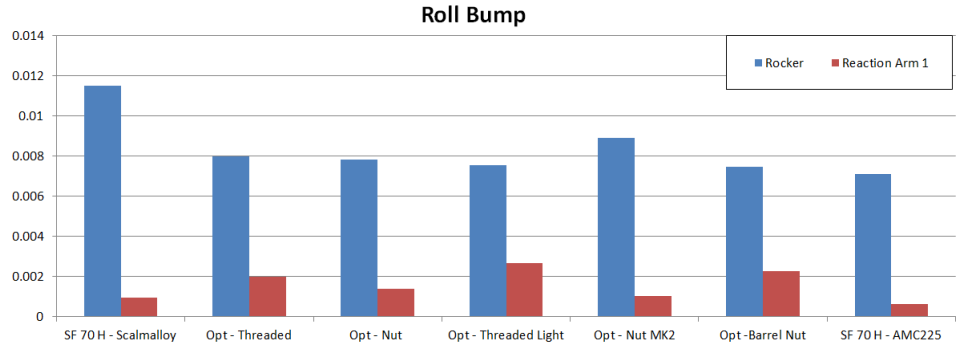

Figure 3.25: Design comparisons between different geometries: roll bump load case specific stiffness. The blue bar represent the specific stiffness of each geometrical reconstruction at the rocker (lowest) bearing housing. The red series are the specific stiffnesses of the central bearing housing (lower rocker arm bearing). As defined before, being a specific stiffness the parameter is expressed in displacement over weight (since the load is constant for all the configurations). The unit of the evaluation is mm/g.

The first comment on the results of the different designs is about the material effect: the advantage in stiffness given by the AMC over the Scalmalloy in terms of displacement is evident in its specific definition. Furthermore, it is clear how the behavior of the geometries is similar for the two load cases. Among the tested geometries the specific stiffness of the component in analysis has been recovered from the SF70H version in Scalmalloy: the implication is that the new component features a better mechanical and structural efficiency. The higher efficiency shows how even changing the material towards a less performing one, but unlocking the potentially free design makes the AM technologies able to cope with standard processes and overrun them in terms of structural behavior.

The final reconstruction of the component is presented in Fig. 3.26. The central section and the grooves removal will be subsequently modified in the final version during the final FEM assessment of the structure as it will be described in Chapter 4.

With the first reconstruction of the two geometries Chapter 3 reaches the end of the logical discussion on topology optimization. In Chapter 4, as already mentioned, the final assessment of the two structures will be presented and for both, the RTWB bracket and the rocker beam some revisions of the geometries will be presented and explained. The potential application of topology optimized struc-

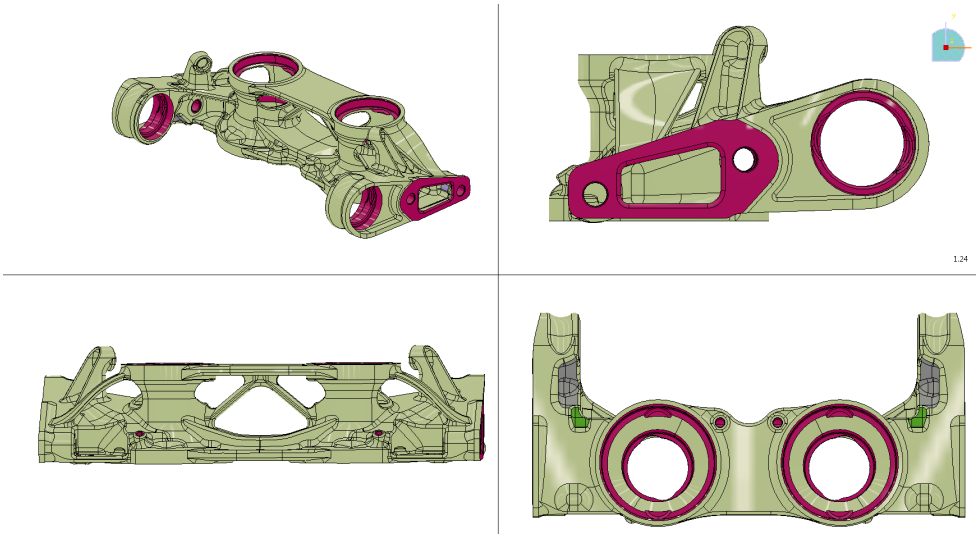

Figure 3.26: Final CAD geometry of the optimized rocker beam structure: the green color represents the semi-finished product while the dark red regions are those that will be finished by a machining post process as will be explained in details in Chapter 5.

tures in combination with additive manufacturing processes is considered an added value and the know how developed in this project has been seen as one of the foundations for future weight-saving strategies in the process of structural optimization of racing components.

4

FEM DESIGN ASSESSMENT

After the presentation of the design work in this brief Chapter the final FEM assessment will be presented. The initial geometries are set in linear and non-linear simulations in the most complete simulation regarding the component behavior and therefore the stress limitations of the new geometries are presented. The geometrical changes hereby presented represent the usual iteration work that the design of structural components requires. The set up of the simulations includes also the definitions of the material properties of interest. This is done *ex-ante* since the material testing from the component AM processes is at this stage of the process, not yet ready. Every decision on the fatigue limit or on safety factor and material properties is done on the basis of the company know how (in terms of metallurgy report and material characterizations) as well as on the literature study performed at the beginning of this report.

This chapter presents, more specifically, in the first section, following the layout already used in Chapter 3, the calculations for the RTWB bracket and in the final part the simulations done on the reconstructed geometry of the rocker beam. For the RTWB bracket a series of analyses is presented that led to a final geometry. The different iterations are presented not with the focus on the geometrical changes, but on the overall contribution in the definition of camber specific stiffness. Afterwards, the rocker beam analysis is presented. A complete outboard load cases simulation is implemented and together with the structural department the decision of redoing a topology optimization is presented. The final geometry is therefore reconstructed with a new central section that is implementing some of the additive manufacturing advantages in freedom of surface manufacturing. This last geometry has been stressed tested in the same simulation and approved for release.

4.1. DESIGN ITERATIONS AND STRESS COMPLIANCE OF THE RTWB BRACKET

As described in the brief introduction the first geometrical iteration has been simulated for stress. The first assessment features a linear analysis in which the limiting loads presented in Section 3.3.2 are applied to the bracket connected with the stiffness matrix representative of the upright and of the wheel

assembly. As seen in the previous Chapter, the geometrical reconstruction has a certain advantage on the original weight (around 11-12%) but the camber compliance level was increased to 34.8°/MN. The starting point of the iteration was to restore the original camber compliance (33.89°/MN). As well the design limit for stress was set taking into consideration the level of fatigue performance that a non-finished (*as-built*) titanium Ti6Al4V is able to grant. The fatigue considerations have been made onto the standard homologation procedure that will be described.

4.1.1. DESIGN FIGURE OF MERIT ASSESSMENT

The reconstruction of the geometry being presented in Chapter 3 has been improved through the definition of better section of the components. The reconstruction involved as well some other features as the leg geometries and upper attachment geometry. As well the machining of the component has been redesigned in order to represent the real geometrical nature of the process. The machined geometry represents a subsequent technological process after the component is printed in the form of a rough geometry in which the main surfaces are set to the final dimension but a surplus of metal is present in all areas that needed a reconstruction to meet the higher level of tolerances requested. Since the semi-finished product cannot be thought to be ideally corresponding with the CAD geometry, and therefore, since the CNC machining will be set by some best fit routine done by the machine to position the mechanical features on the base of some technological planes that will be removed from the initial material, it is not possible to grant perfect match in tangent continuity and there has been the need to properly represent this on the CAD geometry to make the calculation process more robust[1].

In the graph presented in Fig. 4.1 the main geometrical versions of the RTWB bracket are presented. The various iterations are valued by the camber stiffness and by the mass of the component. The first point in the graph is representative of the design component that has not been produced, representative of a graded level of compliance. As a reference point, the versions are referenced on this heavy version since the car component (N=2) has been referenced as well on this hypothetical geometry. As already mentioned, the second iteration (N=2) represents the car component installed on the rear suspension of the SF70H. The third version presented in the graph is the first reconstruction presented in Chapter 3. Iterations from 4 to 9 are representative of the development in camber compliance achieved through the stress and strength final FEM assessment.

It is worth to notice how the camber compliance has been minimized with a proper reconstruction of the upper and lower section of the component (as it will be clear with the definitive geometry). The limit in weight saving through the different versions of the component are a good indication of a process that has reach a proper optimization. In iteration six (N=6) an attempt has been done trying to remove some additional mass basing the modification on the strain energy density plot but the effect on the stiffness of the component is evident; such plot presenting the energy density plot on the component geometry is presented in Fig. 4.2, the areas in red are representative of the regions that are carrying more load rather than the nearby zones. Even though the strain energy density plot is a common tool for analyzing mechanical soundness of structures, being able to modify the geometry

[1] The presence of machined zones not tangent on the semi-finished product can lead to the presence of sharp edges around the component. Usually those resulting from this kind of machining operation are positive sharp edges (not under load) but it can happen that the presence of internal light-weighting pockets might give rise to negative sharp edges.

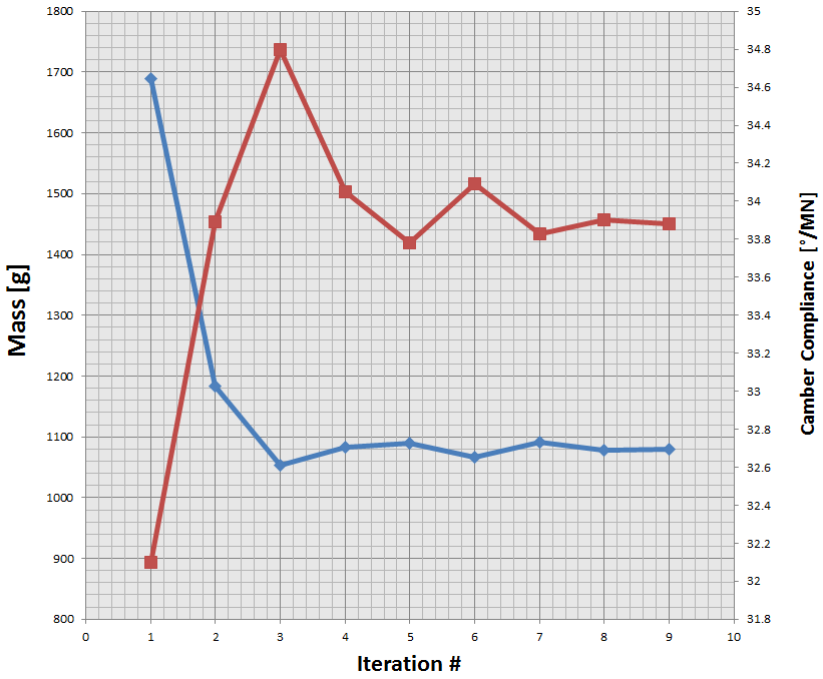

Figure 4.1: Mass and Camber Compliance plotted by the different geometries that have been tested: the iteration 0 represents the point of efficiency requested but at an high weight level (no car component has been produced with those characteristic. The iteration 1 is the actual car component featured on the SF70H.)

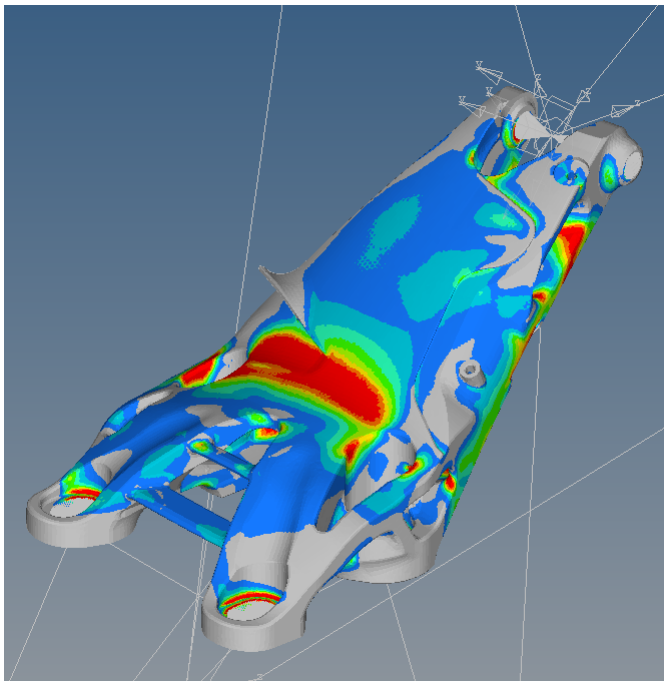

Figure 4.2: Strain energy density plot for RTWB bracket: the zones are varying from blue to red showing area which are participating more in the load-carrying capability of the component. The presence of a geometrical non linearity given by the aerodynamic limitations is representative of the bending behavior of the structure that tends to suffer in the section that features the change of orientation in respect of the neutral bending axis.

efficiently with this reference is an iterative process and there is no quantitative indication of material needs contrary to the indication of a topology optimization.

Other important modifications that were driven by strength factors are the internal supports be-

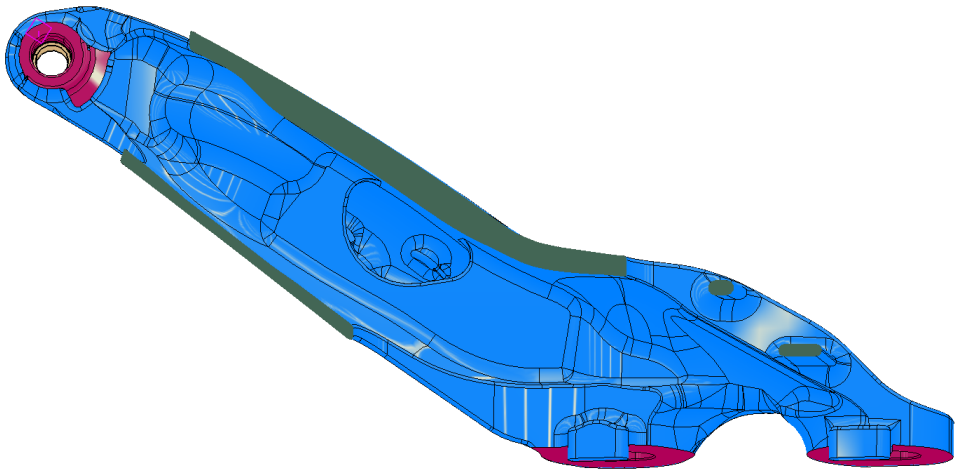

Figure 4.3: Final internal geometry of the RTWB bracket. The present section shows the optimized upper and lower section with thicknesses continuously varying over the component. the presence of the internal wall is also evident on the rear side of the component. The wall structure is open for accessibility and inspection operations.

tween the two inner faces of the component. Since it was clear the poor contribution of the nerve presented in Fig.3.12 during the strength cases (the out of axis load was making the nerve working into a bending condition) it has been substitute by a continuous thin section wall as presented with the final geometry in Fig.4.3 while the overall geometry is presented in Fig.4.4.

4.2. FINAL ASSESSMENT FOR STRESS ON THE RTWB BRACKET

The stress level for the final stress assessment on the bracket has been decided verifying the material properties against the fatigue life of the component. A season of races has historically determined a certain level of short cycle fatigue (maximum loads are present for approximately 45000 times). The fatigue properties of Ti6Al4V have been indicated in Fig. 4.5 and will be taken as a guideline to define the admissible stress on the component. The level therefore at which the fatigue life had to be calculated has been set at the value present for the as-built material at a number of cycles equal to 100000. One of the most stressed regions is located on the outer surface (indicatively on the red indication presented in Fig. 4.2). The choice of using the as-built properties is justified by the ignorance of the effect that a sandblasting or manual mirror finishing would have had on the component. Therefore the selected admissible fatigue strength has been set at 400 MPa.

The safety factor[2] for the present component is set by the internal management of the structural team at 1.5 on the yield stress. The yield strength is related for titanium alloy to what is prescribed by the normative of the alloy taken into consideration: even if the company internal characterization has shown better strength level the possibility to refer the parameters to commercial standards has the benefit of making the components ready to be purchased in case of shortage of availability from the internal production source. The standard of reference for Ti6Al4V produced via powder bed fusion technologies is the ASTM F2924-14. The yield strength of reference is set to 825 MPa and therefore the

[2]From here onwards the term safety factor would be used interchangeably with reserve factor, both will be indicated by the annotation RF.

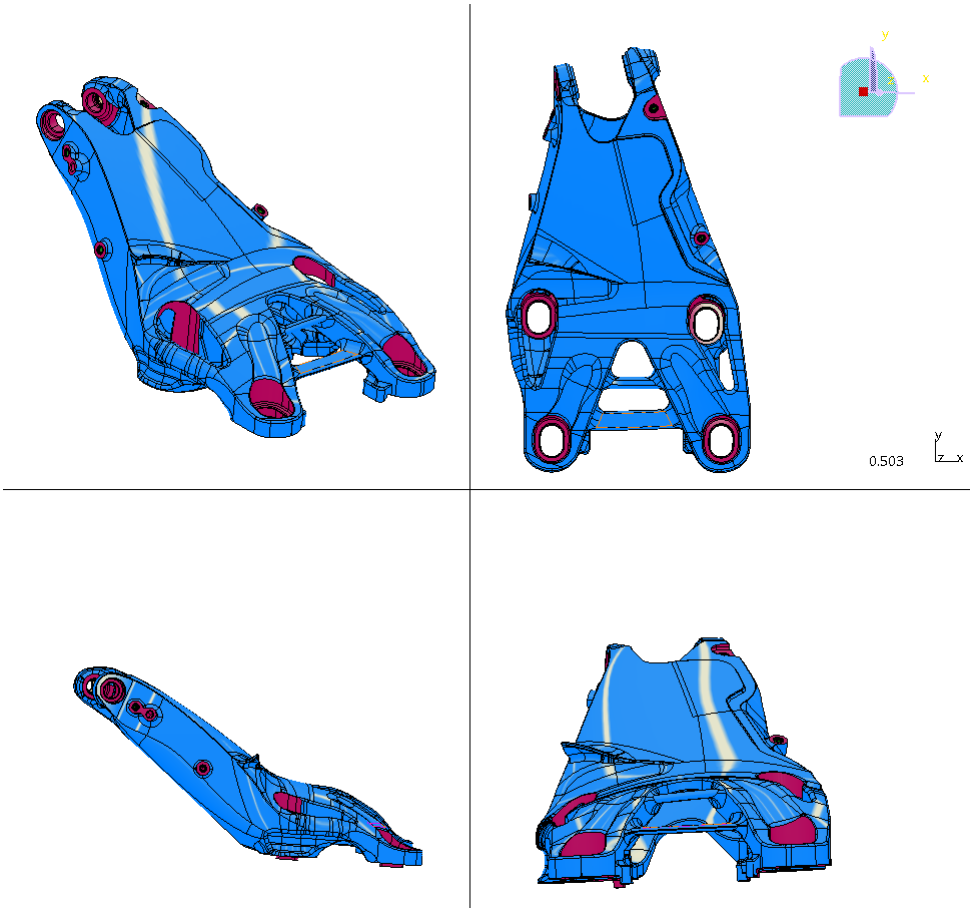

Figure 4.4: Final geometry of the RTWB bracket shown under four different prospectives: the evolution presented includes structural and functional changes as described. The blue surface is part of the semi-finished component while the dark red regions do represent the machined areas. To allow the machining operations to be successfully implemented the semi-finished geometry features extra material for a thickness of 1.5 mm.

admissible for a RF=1.5 is 550 MPa (nominal value).

The most stressed regions of the component are shown in Fig. 4.6. The final intent was to keep all the stresses lower than the fatigue strength as to be sure to pass any fatigue homologation test[3]. Due to attach geometries few point are actually rated at RF=1.6 and RF=1.7. Those point would be critical areas for fatigue testing and therefore it has bee decided to proceed with a full machining of those areas. Since the geometry required tolerances in the described region, most of the times the implication of added machining for fatigue life performances were minimal[4][5].

4.3. DESIGN ITERATION AND STRESS COMPLIANCE OF THE ROCKER BEAM

Similarly to the process of assessment of the RTWB bracket the rocker beam has been tested for stress compliance in collaboration with the structural department team. The simulation implemented for the component has been done with the reduced version of the gearbox geometry and with, as compliant members, the two suspension rockers. The simulation is considering for strength evaluation a

[3] This would implicate a RF higher than two on the whole component.

[4] An examples of such machining area is presented in the section presenting the internal geometry of the component: Fig. 4.3

[5] If the print quality provides sufficient results in term of porosity the machining process has the benefit to lower considerably the surface roughness from Ra>6 to typical levels for conventionally machined products complying with the standard ISO 2768-mk standard (Ra3.2).

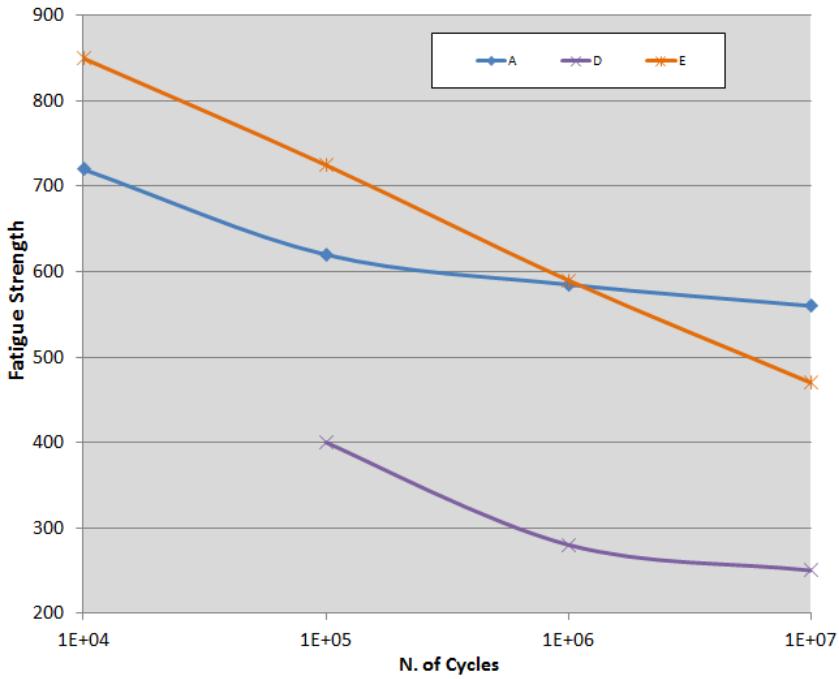

Figure 4.5: Fatigue properties for annealed titanium Ti6Al4V alloy from internal characterization champaign. A-series represents wrought product fatigue properties while D and E series DMLS produced with either *as-built* or machined finished. The fatigue performances are analyzed with rotating bending fatigue testing with an applied stress ratio R=-1. as it can be found the mechanical properties of additively manufactured specimens greatly depends on the surface finishing; Furthermore, the presence of internal defects does not make the E-series to show a clear fatigue limit as it is evident for wrought products.

series of outboard and inboard load cases that are the reference loads for both inboard and outboard components (from suspension links to the rockers themselves).

4.3.1. INITIAL ITERATION AND COMPLEXITY ASSESSMENT

The first geometrical reconstruction showed a poor compliance to stresses. The main reason for this is related to the oversimplified load case used for the first set up of the topology optimization. The central section, featuring a top shear tie design and a lower axial connection, was sufficient to provide the correct amount of stiffness but the trabecular structure was not able to sustain the variety of loads that are to be considered in the stress verification. The limitation of trabecular structures optimized in tension and compression but not able to compensate the stresses originated from bending load cases has been already explained in the section related to the internal geometry of the RTWB bracket. A second loop of topology optimization has been therefore implemented as it has been thought to be beneficial rather than reinforcing the originally compromised version.

4.4. SECOND LOOP OF TOPOLOGY OPTIMIZATION

The second loop of the topology optimization considered as the optimization region only the central section of the component since the side attachment zone was providing already good results on the stress assessment simulation. The optimization has been developed on the NUT MK2 geometry with proper allocation of extra material to allow the process to be successful. The applied load were this time all the inboard loads and the outer loads. The objective function has been set for mass reduction

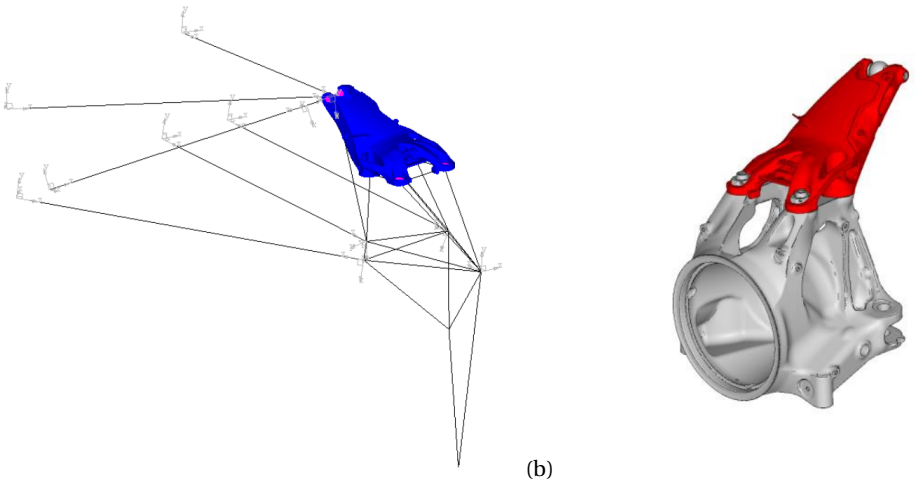

(a) (b)

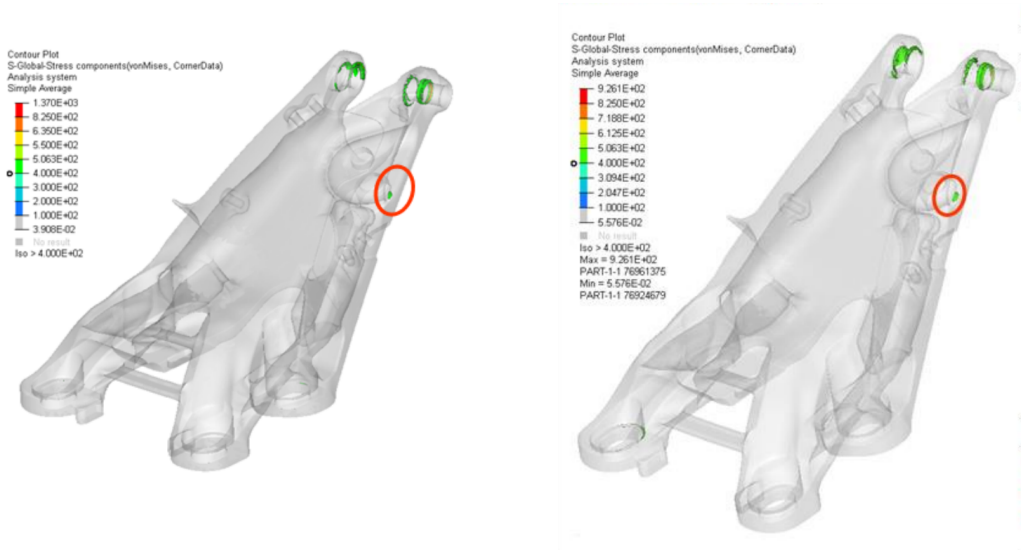

(c) (d)

Figure 4.6: Final results of the finite element analysis for the RTWB bracket: the simulation includes the presence of the upright in the non linear analysis and as well the presence of the reduced model of the suspension links to react the contact patch loads. The most stressed regions are reproposed in Fig.4.6c and in Fig.Fig.4.6d and originated from geometrical discontinuities due either the presence of the wheel tether or by the machining of its fixing.

with both strength and stiffness constrained. Due to the contact presence within the model setting constraints over the admissible stress was not possible and therefore the results has been based on the stiffness constrained simulation.

4.4.1. TOPOLOGY OPTIMIZATION RESULT

The optimization results for the stiffness geometry is shown in Fig. 4.7. As it can be noted the revision on the geometry is focused in the central section. As it could be easily understand the section moved towards a round feature connecting the bearings along the axial direction but also on the sides of the structure. A common indication is related to the presence of pockets in the sides of the bearing housings. Furthermore, it is interesting to note the presence of a pillar connecting axially the two

rocker bearings. the section in contact with the gearbox case does not present by differences but in the lower section some space for better defining the structure with *ad hoc* pockets can be seen.

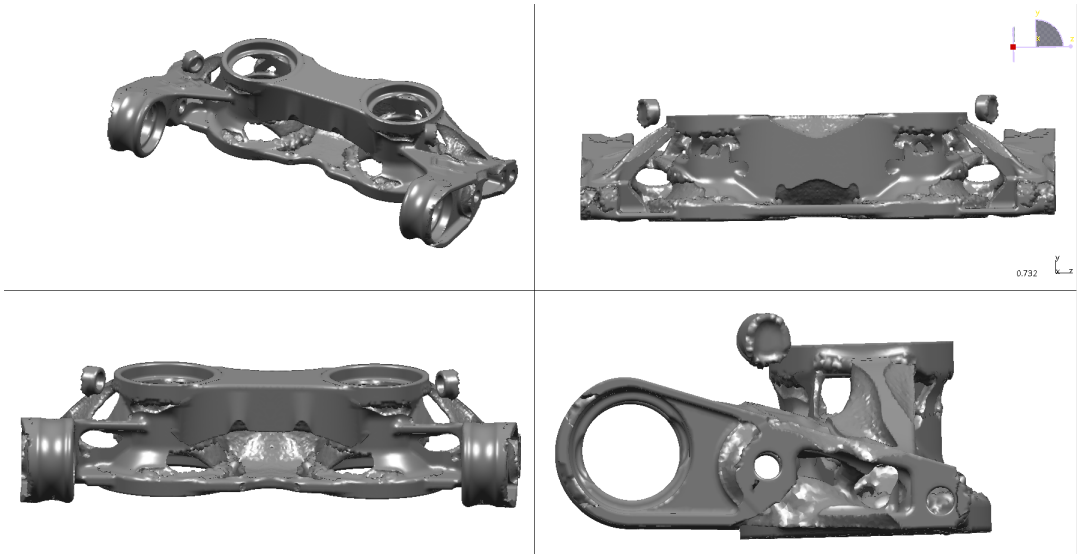

Figure 4.7: Second result of the topology optimization: the component has been revised especially in the central section due to the implemented level of complexity introduced in the simulation. As a result, the central section now features a shape that resembles a continuous round section with a frontal opening. The nature of this geometry would not be machinable (it can be considered a closed section from the machining) and therefore the implementation of an additive manufacturing process is needed.

4.4.2. GEOMETRY RECONSTRUCTION

The geometrical reconstruction has followed the same principles as in the two cases already presented. The main differences to the optimized geometries are based on the feasibility of the geometry and the possibility to be implemented on a real component. The attachments have been revised and the machining of the component has been implemented, as for the RTWB bracket, properly to expose the geometrical sharpness as explained in the aforementioned example. In Fig. 4.8 the geometry is presented and the changes can be noted. The overall weight of the component has passed from 1035 g to the final weight of 1077 g in respect of a initial weight for the SF70H component of 1144 g. The reduction in weight is going to be increased with the contribution of weight saving produced by the new attachment method and the substitution of barrel nuts with normal screw lock hexagonal nuts.

4.5. FINAL ASSESSMENT FOR STRESS ON THE RTWB BRACKET

The final assessment has been briefly explained in the previous section: it features the load that are limiting the outboards and inboards components. The definition of material properties has been done similarly to what described for the RTWB bracket. Since the component is subject to an high temperature of operations the tensile properties have to be validated for the target temperature level. As mentioned earlier, the target temperature for inboard components is set to 120°C. The Scalmalloy properties in temperature are therefore a good indication of the material figure of merit for this specific application and furthermore they will be the object of further experimental testing. The yield

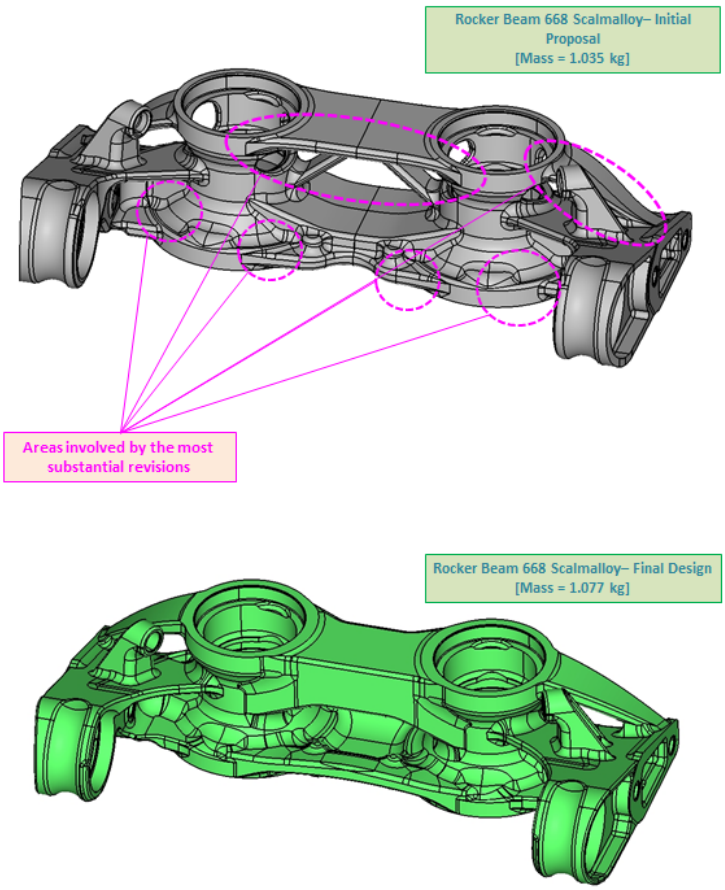

Figure 4.8: Final reconstruction of the rocker beam geometry basing the features on the second loop of the topology optimization. The main changes are highlighted: the central section geometry has been revised and the openings on the bearing side removed. As well, the reinforcement features on the side connecting the top bearing with the gearbox attachments did undergo some optimization.

strength of the material is reported in Fig.4.9[6] as a function of the testing temperature[7].

The linear interpolation between 100°C and 150°C sets the yield strength for a temperature of 120°C at 338 MPa that would therefore set the admissible stress level at 225 MPa. In this case, the room temperature fatigue properties are set by AP Works with a value of 300 MPa at 10 million cycles for a machined specimen at a stress ratio R=-1 (complete reversed fatigue). High temperature fatigue is not reported by the powder producer and since the component is not subject to fatigue loads for the dimensioning load cases the only stress check is done on the reduced high temperature yield strength.

4.5.1. STRESS SAFETY FACTORS AND PRINCIPAL STRESS ANALYSIS

The minimum and most stressed areas are presented in Fig. 4.10. As it can be seen the reserve factor is as low as 1.21 in certain areas next to the attachments and towards the machining for the nut placement. As well some areas which are limited by the envelopes of rotating parts show critical values of applied stress.

A further analysis is shown in Fig. 4.10d and has been used to study the mechanical behavior of the

[6] Elaborated from AP works data.
[7] The effect of aging at that temperature during the component's life is for now not taken into account.

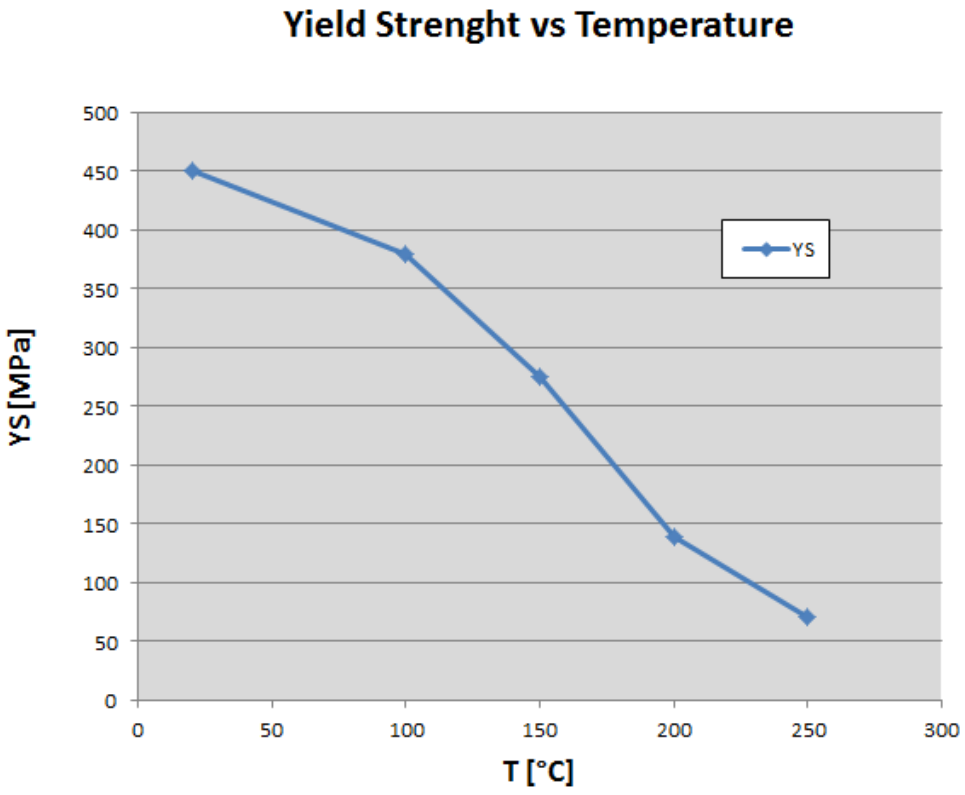

Figure 4.9: Scalmalloy properties in temperature. The yield strength is represented against the rising temperature. The data provided here are an elaboration of the powder producer specification. The non linear behavior make the material optimum range of operation between room temperature and 100°C.

areas with a reserve factor lower than 1.4. This figure is showing the principal stress of the component. The analysis of principal stresses is usually implemented to show the tendency of a structural region to be under compression or tension. The analysis, being capable of distinguish tension and compression areas, can be determined if a failure induced by fatigue cracking could occur or not. Since the opening *mode I* is the most common in crack growth mechanisms area below RF=1.5 are acceptable only if the maximum principal is negative (compressive principal stress). This analysis will be the base for the determination of the peening areas in the manufacturing process of the component as it will be described in the following Chapter.

4.6. FINAL ASSESSMENT OF WEIGHT SAVING RESULTS

At the end of the simulation processes the two components are able to withstand the load prescribed by the process and expected for their functionalities. The end result on the weight saving has shown similar results to what the expectations were. On the RTWB bracket the final weight saving has been of 116 g in respect of the original component. The weight saving of the rocker beam has to consider the new attachments as well and is featuring 70 g for the component itself and 30 g for barrel nut and anti-rotation device removal. Both weight reduction are included in the range of 7-10% reported in Chapter 3, and the results are resumed in Table 4.1.

With the final stress assessment of the two components the content of Chapter 4 is complete. The

Table 4.1: Car weight saving for the additive manufactured components.

Component Version	SF70H	AMed Components
RTWB bracket	1183 g	1067 g
Rocker beam	1144 g	1077 g
Component weight saving [%]	5.9%	9.8%
Total car weight saving [g]	67	232

two components have been modified and optimized to sustain the same load prescribed by the requirements for racing components. In Chapter 5 the components will be analyzed in their production process and how the different materials have been used to achieve the most suitable components for the prescribed application.

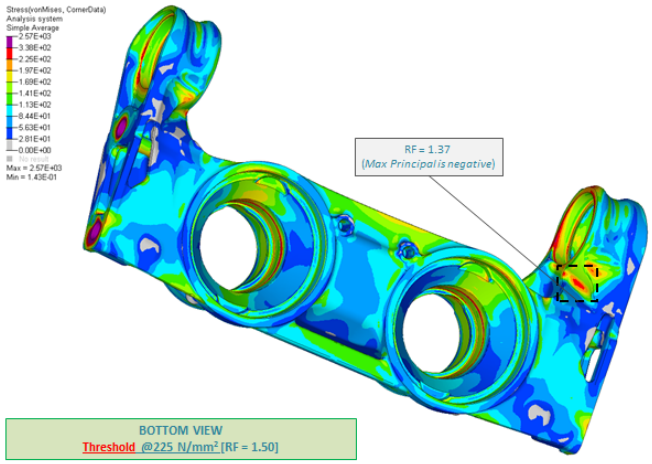

(a)

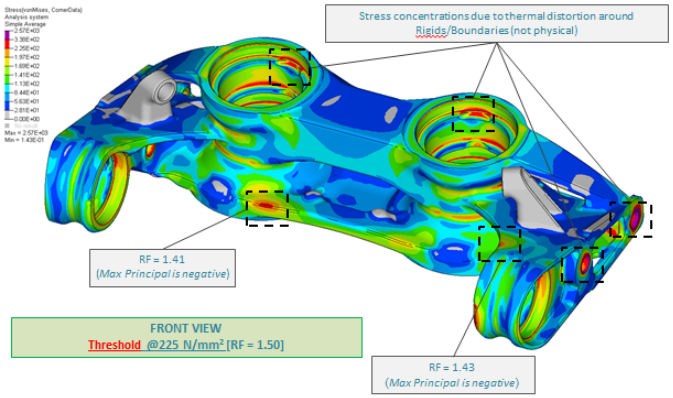

(b)

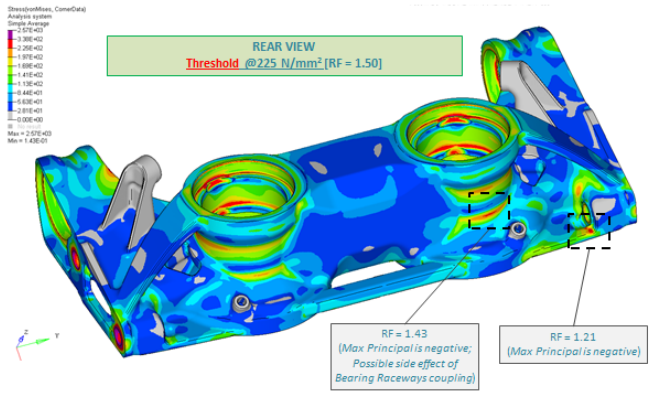

(c)

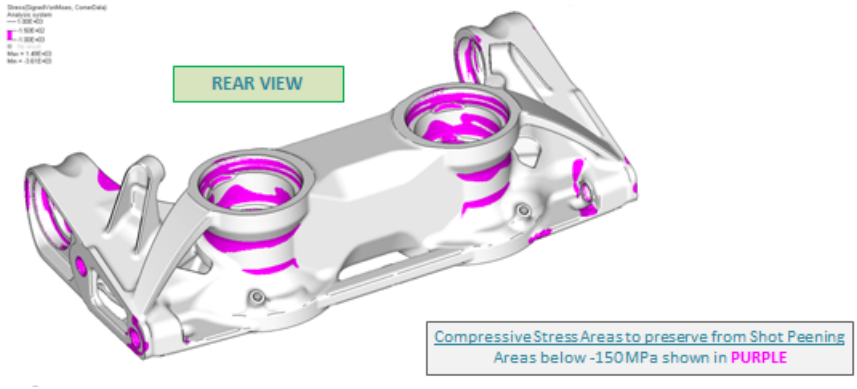

(d)

Figure 4.10: Final results of the finite element analysis on the Rocker Beam. In the first three figures final stress envelope is shown. The last figure (Fig.4.10d) is representative of principal stress analysis done to deliberate regions with a RF lower than 1.5.

5

MANUFACTURING OF SUSPENSION COMPONENTS THROUGH ADDITIVE MANUFACTURING TECHNIQUES

In the present Chapter the manufacturing processes for producing will be presented. In view of the material differences and as well machine differences two independent production processes will be shown. The production approach for AMed components has been seen in some parts of Chapter 2 but can be resumed as follows:

- **Raw production**: the production of a semi-finished product is the part of the process in which the advantages of additive manufacturing techniques can be exploited. This is substituting the process conventionally represented by casting or by forging and has the benefits explained earlier in this report.
- **Heat treatment**: for any metal component produced with AM techniques there is the need of proceeding with a stress relief heat treatment. This heat treatment is used to remove internal stresses and it can (but not always) be around the recrystallization temperature to achieve the formation of new grains in the structure. For some alloys there might be the need of completing an aging process to achieve the precipitation of second phases to strengthen the alloy.
- **Support removal**: after the heat treatment there is the need before proceeding with final machining to remove the extra structures used by the machine (but user defined) to support the undercut geometries that might be present in the component, as presented for RTWB bracket in Chapter 3. The process can be fully manual for aluminum alloys with low strength or aided with mechanical and electro-mechanical tools. It is of fundamental importance that the support removal process has the smallest possible impact on the surface quality of the product (ideally zero).

- **Final machining**: due to mechanical interfaces there is a need to process with a material removal from the raw semi-finished product: tolerance fittings and linear dimensions are fundamental in the operating life of the component and as well the highest surface finishing can be obtained only with conventional CNC machining. From the semi-finished product the presence of extra material has to be provided for the proper removal of material and the machine, after some basic operations (definition of planes or axes), through a best fitting process proceeds with the final removal of the extra material.

- **(Optional) Hot isostatic pressing**: as presented in Section 2.5.3 this optional process requires the component to face a pressure environment at elevated temperature to compact the micropores that might be present. An analysis on this aspect of the process will be presented further in the discussion related to the internal porosity of the rocker beam component. As stated in the aforementioned section the presence of some defects can be solved while other inclusions or gas containing porosity will not benefit from this treatment.

- **(Optional) Surface finishing**: surface finishing might be required by the fatigue life requirements of the component or because the presence of excessive surface defects is not acceptable. Within the scope of the project different techniques have been implemented such as manual mirror finishing, sandblasting and shot peening[1].

In Fig. 5.1 the described process is presented in the form of a flow chart. It is worth to mention that the surface finishing and the HIP procedure location in the process flow is not fixed. The optimal option would be to do the treatments on the semi-finished product, avoiding the need of custom tools for protection of the machined zones, but special needs in the process can modify the ideal order of the manufacturing process[2].

After this brief introduction, following the previous chapters structure, the two processes for the manufacturing of the components will be presented while reporting the design information of concern and peculiar aspects and differences of the two application with the intent of understanding the material influence on the manufacturing process. As anticipated, the first section presents the production process of the RTWB bracket in titanium while the second half of the Chapter is focusing on the rocker beam production process.

5.1. DMLS MANUFACTURING OF THE RTWB BRACKET

The manufacturing of the RTWB bracket has been done at the Ferrari facilities in Maranello thanks to the possibility of developing the component completely internally. The process definition has been based on previous know-how and experience in 3D printing but with the need of establishing a robust method of production, in order to minimize the production constraints and being able to homologate

[1] The shortage of time did not grant the chance of a proper investigation on the effect of each treatment on the mechanical properties apart from a qualitative point of view. Furthermore, the need of customized processes for additive manufacturing is still present as of today and the applicability of novel techniques (*verbi gratia* - laser shot peening) in combination with aM might be one of the future need to achieve proper industrial implementation of this new manufacturing process.

[2] A quality assessment might be the reason for moving the treatment to the end of the process as presented in Fig. 5.1. Furthermore the quality assessment might better be positioned in an intermediate position before machining processes but this is depending on the type of control that is required (*e.g.*: the first article inspection might be done after print but all other components might undergo only a final qualitative assessment).

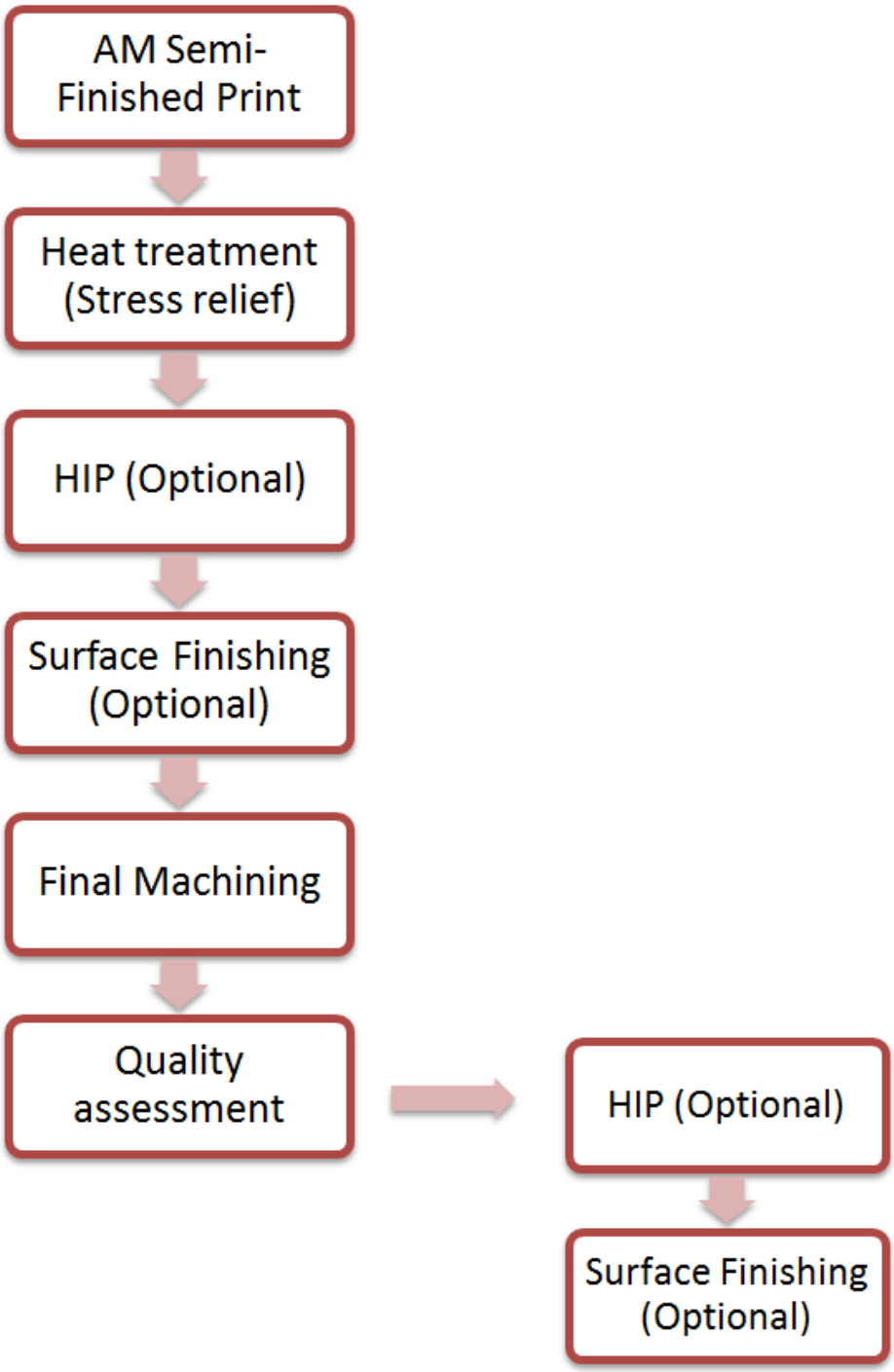

Figure 5.1: Flow chart showing a possible manufacturing cycle for a additively manufactured component featuring a final quality assessment that make optional treatments to be done after a quality evaluation of the print component.

the process to become a feasible option to conventional machining of wrought product for structural suspension components.

5.1.1. DEFINITION OF PROCESSES FOR TITANIUM DMLS PRINTING

The production process is following the main process described in Section 5.1. The need of having a reduced lead time and the material properties that were granted both by the normative and by the internal characterization made the decision of not having an HIP process clear; still the temperature at which the stress relief is done is higher than the average nucleation temperature and therefore the material will undergo a certain degree of recrystallization: this is needed since the high residual stress level would not grant sufficient mechanical properties. At the moment of the design release of the components the possibility of specific surface treatment was limited. The first batch of production was featuring two left components in order to produce a spare component for fatigue testing. On those components the choice was to proceed with two internally available surface treatments to solve the materials low quality external roughness. The production process is presented in Fig.5.2. For the final testing on the 329-test bench the decision has been taken not to mirror finish the component anymore since the sandblasting procedure has been judged to be able to provide a better uniformity of the finishing[3].

5.1.2. SURFACE FINISHING

As mentioned earlier, two different levels of surface finishing were selected for the first production batch of the left components produced in order to be tested in a fatigue cycling test. The two different finishing processes were selected because of their limited complexity and internal availability. The first component was prepared after support removal with a manual mirror finishing obtained by removing the top layer of the semi-finished product with the aid of superfine sandpaper and water (>2000 grit). On the contrary an automated process was selected for the finishing of the second component: sandblasting. As resumed in the literature review, sandblasting is an industrial finishing technique that removes and homogenizes the surface of a (metallic) component by the interaction with small particles (sand particles) used as projectiles. A limit of the technique is to suffer from shadow effect of some peculiar geometries. The surface roughness reduction can be therefore achieved only in the areas of the component that “see” directly the particles flow (the surface roughness remained unaltered in most of the internal section). The result of a visual inspection of the components revealed that both of the processes are unable to guarantee uniform and high quality on the surface roughness of the component[4]. The final choice, due to the indication of high dependency of the operator effect on the final mirror finished version, was to keep the production of the last two components for the assembly fatigue testing with the sandblasting procedure only.

5.1.3. MACHINING PROCESS AND QUALITY ASSESSMENT

The machining areas that have been selecting for material removal can be identified by the dark red color presented in Fig.4.4 in Chapter 4. The machining operative principle has been already presented in the first section of the introduction to the present Chapter. The first area to be machined is the lower attachment zone that defines the first planar reference. Then, the lower attachments are placed to refer all the other features to those references in order to establish a proper functional distance

[3] Since the mirror finishing is a manual process the operator dependent result was evident in the analysis of the component as reported in Section 5.1.2.

[4] It has to be noted that the mirror finishing process has followed the sandblasting which has been done on both components.

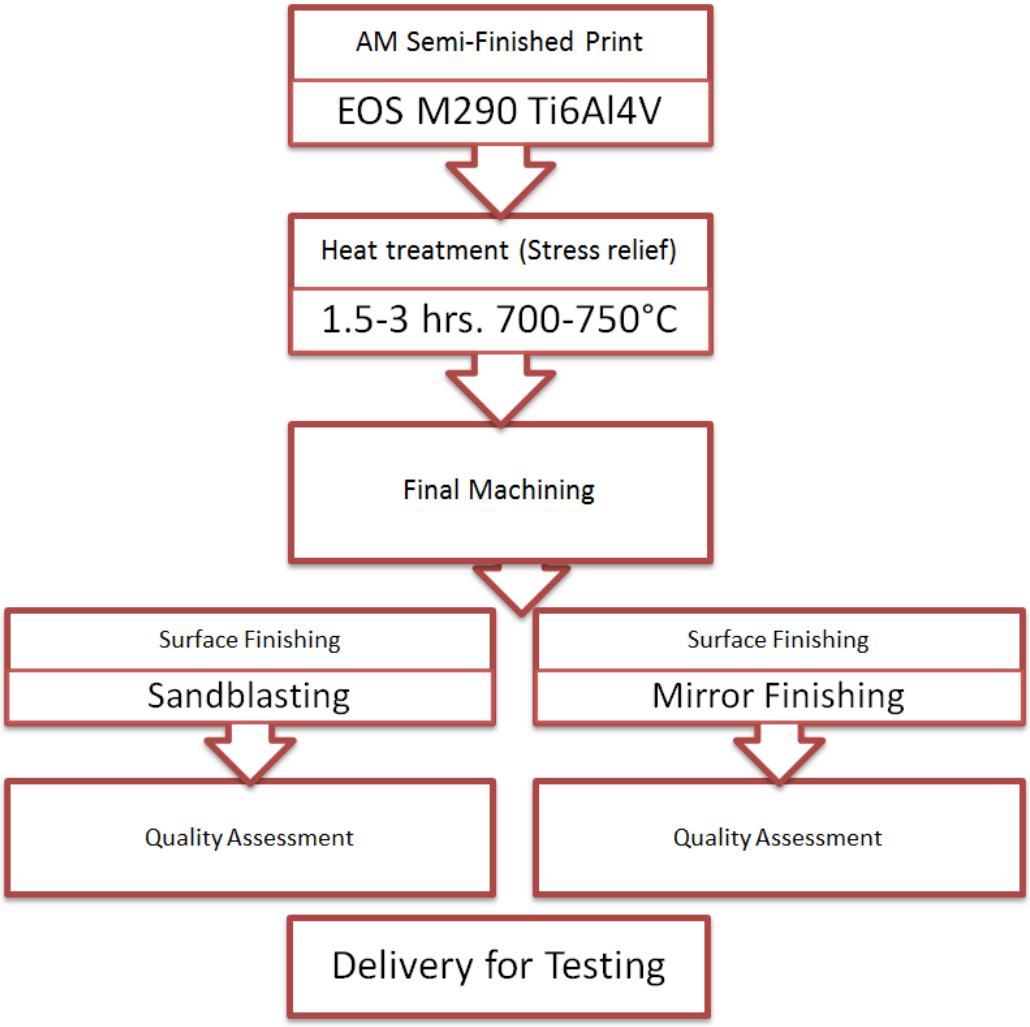

Figure 5.2: Flow chart showing the production process of the RTWB bracket in Ti6Al4V.

between the various mechanical interfaces.

The quality assessment on the component did require two types of testing. The most important has been the dimensional accuracy and location of the machined zones. The control has been done with a standard Zeiss coordinate measuring machined on the basis of the engineering drawing. The mechanical tensile testing of specimen from the same printout represented the second part of the quality assessment. Since the machine tolerances and processes have been established during the time of use and they are part of the company know-how it was judged sufficient to assess the quality of the product under those two testing procedures.

5.2. MANUFACTURING OF THE ROCKER BEAM IN SCALMALLOY

The manufacturing process of the rocker beam due to strategical reason has been outsourced to one of the company suppliers. The definition of agreement on the various processes required careful consideration since it represented the first component made in this alloy that was not purely a material specimen but a real component. In the following section the process is described, with particular fo-

cus at the quality management of the component. The need of having a robust process of acceptance and a proper evaluation of the process quality itself led to a series of adaptations in defining the quality assessment that will be presented within the presentation of the quality results.

5.2.1. DEFINITION OF MANUFACTURING PROCESSES

As specified earlier, since the manufacturing process has never been used internally for producing structural components, the choice has been on proceeding in agreement with the supplier with a standard implementation of the print following the powder supplier indication. Therefore the process would require a heat treatment for precipitation hardening and stress relief of the metal. The treating temperature is set by the material specification to be at 325°C. At this temperature, as already seen for titanium, the material would face some nucleation process that is going to induce a reduction of the residual stresses by lowering the dislocation density with new grain nucleation. After the treatment, since the quality of the surface was unknown[5], a shot peening process was prescribed. After the shot peening, the final machining takes place and is followed by the installation of the bearing bushings (a strong interference fit). Due to the severity of the installation a further machining is needed to set the correct tolerances for the subsequent bearing installation. The production process is graphically represented in Fig. 5.3.

5.2.2. MATERIAL ASSESSMENT AND DEVELOPMENT OF A QUALITY PROCESS FOR SCALMALLOY PRODUCED COMPONENTS

Simultaneously with the definition of the manufacturing process it was evident that both material and the component needed to be assessed though a quality assessment. Particularly the material properties were to be tested at room temperature and at high temperature. Furthermore, the strategical advantage of developing a robust production and quality process lies in the possibility to freeze the manufacturing processes concerning hatch spacing, input energy, scan speed, layer thickness and a long series of machine parameters to ensure the future production would retain quality levels high.

Therefore, to fully characterize the material a series of destructive and non destructive testing approach has been defined. The strategy of control operated in two different directions: first to functionally classify the material a series of mechanical testing campaign at room temperature and at high temperature (150°C) has been set up; secondly, to classify the quality of the print set up a series of controls were prescribed such as a micrography density measurements and the analysis of defects as well as a micro-hardness measurement. For the component itself the quality process was approached to guarantee both the dimensional accuracy on the semi-finished product and the controlled presence of defects in the product [6].

Final agreement with the supplier was found in applying a FAI[7] able to quantify the quality of the process and to have reliable data on both the material and the component itself. The FAI layout has regarded the following aspect:

- **Process Characterization**: in order to access the process quality the implementation of two

[5] The reported quality by the powder supplier (AP Works) for Ra values is at a level of Ra10.
[6] A list of the most common defects has been presented in the literature review section: gas induced porosity, process induced porosity and lack of fusion.
[7] First Article Inspection.

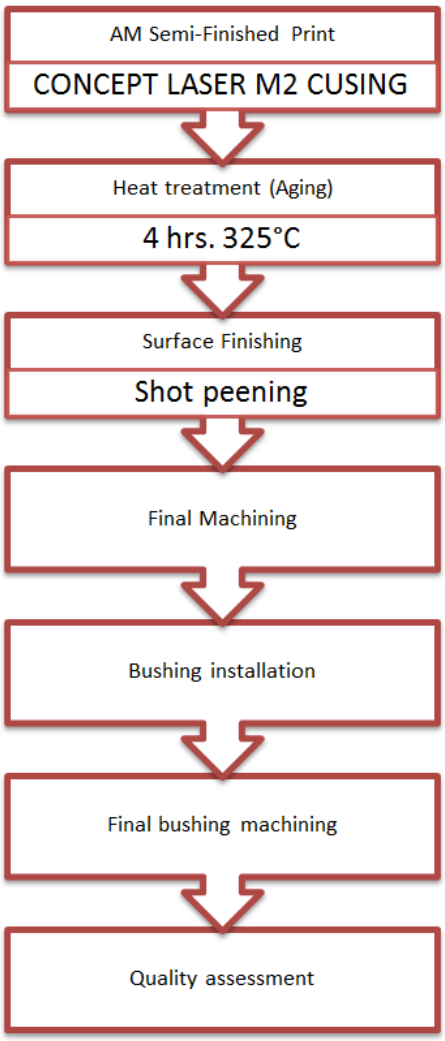

Figure 5.3: Flow chart showing the production process of the rocker beam in Scalmalloy.

kinds of measurements was prescribed. The first is a porosity level assessment done by the analysis of micrography images. This has to be done on the broken specimens from the tensile testing. As well in this testing procedure the characterization of the porosity defects has to be assessed. The maximum defect for each specimen has to be reported and measured. To prove the effectiveness of the heat treatment (precipitation hardening) a micro-hardening test has to be provided. All present tests were to be performed on the same print of the rocker beam component (in the same machine job).

- **Mechanical behavior of Scalmalloy**: a dedicated job to access mechanical properties for Scalmalloy has been defined. The production of six specimens is prescribed with six back up specimens in case of unsatisfactory or debatable testing results. The specimen for tensile testing are round specimens of characteristic slimness ratio of 1D to 6D for the reduced section with D=6mm following the prescriptions of the ASTM normative E8M[85]. A taper is prescribed to promote localization of plasticity in the mid section (strain-gauged). The taper is described on the measure of two small cylindrical sections of the reduced section of the specimen. The reduction required, which is based on the quality assessment of other high strength aluminum

alloys that might show poor elongation, is of 0.02 mm in respect of the measured sections. The orientation of the specimen has to be Z, XY and XYZ following the definition of ASTM F2921. Following the mentioned specification, the plane of printing is described by the X and Y axes. The Z-direction is referred at the printing direction intended as the direction on which subsequent layers are deposited.

- **Component quality**: for each produced components there is the request to provide after the print and the heat treatment a CTScan measurement with a 3D scan of the external surfaces as well. The CTScan (Tomography) is prescribed to find internal pores and defects on the structure while the external 3D laser scan is done to assess the dimensional accuracy of the print: the detection limit for the tomography is reputed to be around 0.2 mm for round defects. For each print there is the need to mechanically test the tensile properties by the mean of three cylindrical tensile specimen as the ones described earlier with orientation in Z, XY and XYZ. The component is prescribed to be tested by liquid penetrant inspection to access surface defects (linear indication of cracks or excessive superficial porosity); this test has to be performed before any machining operation. Finally the component has to be tested for residual stresses with XRD techniques[8].

The quality process is reported graphically by the scheme presented in Fig. 5.4. The definition of a FAI in the acceptance of outsourced components is useful for a number of reasons: it allows the receiving organization to benchmark the quality of the process; it enables the supply of multiple components with fewer total tests for each production batch; reduces the possibility of producing rejectable parts if the quality process is carried out on the first component of the batch. The intent of the present FAI is the chance of blocking a novel process once it has been successfully characterized and keep the machine settings constant for the production of any other component in Scalmalloy. The characterization of the temperature behavior of the alloy will be as well the basis for a proper material characterization. The natural future request would be a fatigue characterization of the material.

Establishing the quality of the process required integration of the know-how of the company combined with the process know-how of the supplier and based on the results of the first data of the prescribed test some modifications where needed in order to properly set up a robust controlling method. Furthermore, the absence of any established acceptability criterion (no specific normative exists nowadays on this particular process and therefore is treated as a special process) led to the definition of an internal specification for additive manufacturing in Scalmalloy. As well, as will be presented in the presentation of the quality results for the rocker beam, the presence of certain defects in some of the tests has required supplemental assessment on the quality process to enable the positive outcome of the project.

The definition of the quality process for the Scalmalloy component ends the arguments presented in Chapter 5. The various results in terms of tensile performances, defectivity and the rest of the required testing are presented in Chapter 6.

[8]Due to the peculiarities of the process (3D printing, shot peening and high interference fittings) the residual stresses expected are high and they need careful consideration to access the process feasibility on the finalized component.

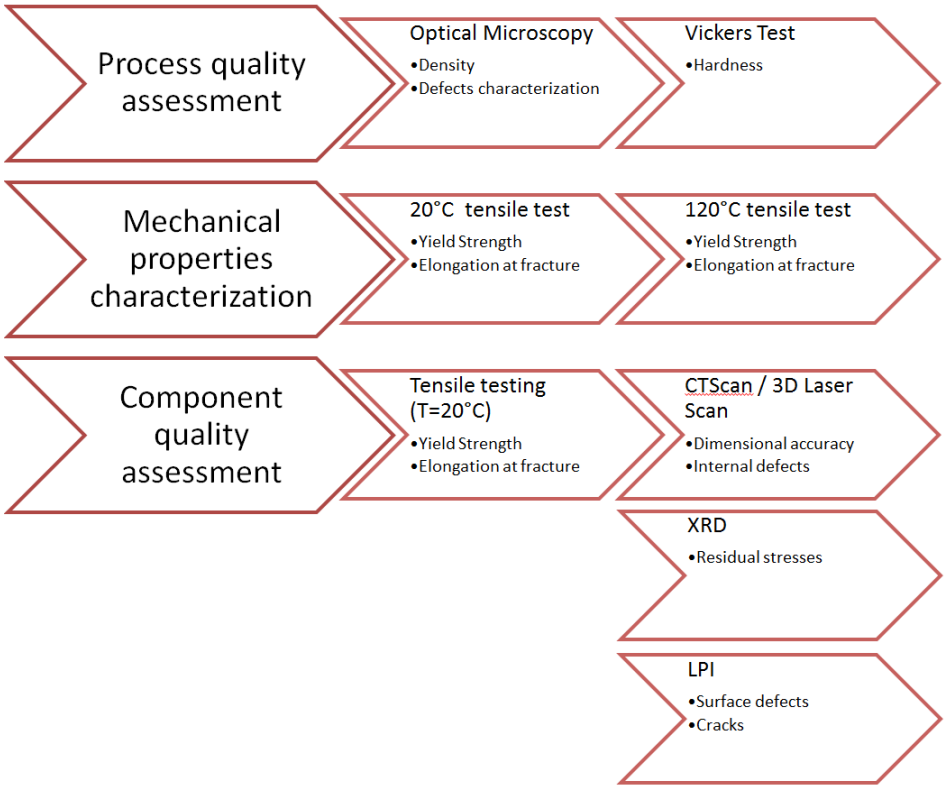

Figure 5.4: Flow chart presenting the different parts of the quality process for the incoming Scalmalloy component. This control represent the implementation of the FAI for this specific process.

6

RESULTS OF FINAL COMPONENT TESTING AND QUALITY ASSESSMENT

Starting from the processes described in Chapter 5 regarding the production of the two components, in the present chapter the results from the quality assessment and mechanical and structural characterization will be presented. The discussion is developed following the usual reporting scheme used for the previous sections. The outline is split in two: the first section deals with the material characterization in static testing and in quality assessment while the second half reports the fatigue testing results for the two components.

6.1. TITANIUM TESTING RESULTS

The company know-how in treating titanium alloys is strongly developed due to the high merit of specific properties that titanium has regarding the requirements of metal racing components. Therefore, as prescribed in Chapter 5, the number of tests for quality assessment has been reduced to the minimum possible in order to achieve the correctness of the process while reducing the lead time for the component and the added costs of extra controls. The results are presented in the form of mechanical testing and the machining dimensional quality of the RTWB bracket.

6.1.1. TI6AL4V - TENSILE TESTING

The metallurgical testing history of titanium alloys is well established for Ti6Al4V in the case of both wrought products and additively manufactured components. The tensile specimen properties measured in the present project originate from cylindrical specimens printed alongside the Z-direction (coherently with the ASTM specification this is considered to be the printing layering direction). The characterization and machining has been performed internally. The tensile properties are reflecting the amount of established data on this material-machine-processing parameters combination. The ASTM 4999A norm is prescribing the minimum values for elongation, tensile strength and yield stress

limit for the mentioned alloy. Specifically the average values of the tested specimens are: UTS and YS respectively at 1050 and 1020 MPa. The elongation at break registered is 13% with a Young modulus averaging 107 GPa. The fracture surfaces show the indication of typical ductile fracture with slip plane oriented approximately at 45° with respect to the applied load direction.

6.1.2. QUALITY ASSESSMENT - DIMENSIONAL ACCURACY

The quality assessment for the RTWB bracket is represented by the functional measurements of the machined features: to grant the perfect ability of the component to be assembled in the rear suspension assembly the machining tolerances have to be within the specified limits. Since the machining settings are able to reproduce true positions disregarding the surface tolerances derived from the additive manufacturing processes the functionality of the component is granted even if there is no perfect match between the semi-finished surfaces and the CAD ideal geometry.The machining indications are reported for the tolerated holes in the form of a report done during the Zeiss 3D measurement control procedure. A representative image of one of the typical measurements is reported in Fig.6.1. The reported measure shows a tolerance of +/-0.001 mm and represents a high level of coherence with the engineering drawing. Similarly, the majority of the component tolerances were respected and the component was considered ready for fatigue testing without any further machining required.

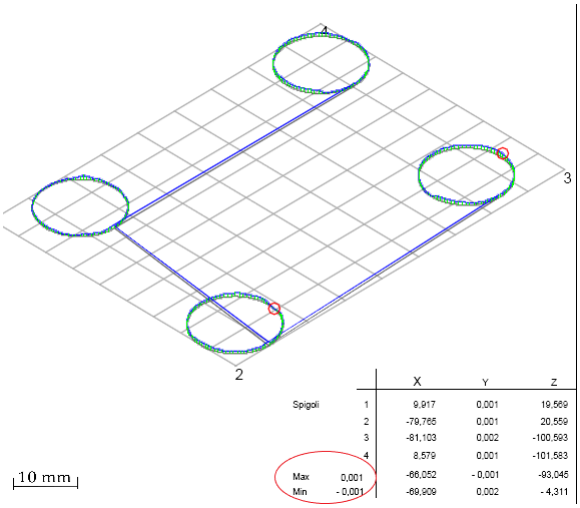

Figure 6.1: Planarity check report on the lower attachments plane of the RTWB bracket. The plane is partially visible in Fig.4.3. The planarity check reports a maximum deviation of+/- 0.001 mm, perfectly matching the designer requests. For the measurement the machine takes four reference points on the surface of the four attachments: in the engineering drawing it has been prescribed to machine the plane in analysis in one single operation; this process is able to grant small oscillations in the planarity between the four features and therefore can ensure a perfect fit on the upright geometry.

6.2. SCALMALLOY TESTING RESULTS

The testing required for homologating a component produced in a novel material is much more extended than the process required for the RTWB bracket produced in DMLS titanium. The results are presented following the prescribed logical sequence presented in Chapter 5 for the quality assessment: the first section regards the basic mechanical properties of the material; secondly the process quality is addressed in a dedicated section; finally the component quality is analyzed in the last section of this first half of this chapter. Due to the limited time between the bench test and the reception of the

component the XRD testing for assessing the residual stresses has been aborted.

6.2.1. MECHANICAL TESTING - TENSILE TESTING AND HARDNESS MEASUREMENTS

As mentioned in the description of the manufacturing processes, the mechanical testing of the produced metal required three different stages of testing: the tensile testing at room temperature, the tensile test at high temperature (150°C) and the hardness test. The tests are presented in the mentioned order starting from the results of the tensile testing at room temperature.

TENSILE TESTING - ROOM TEMPERATURE RESULTS

The tensile specimens machining and testing has been carried out at a certified outsourced laboratory since the testing task was part of the job definition of the external supplier[1].

The specimens were requested to be machined in the prescribed geometry with a tapered reduction of the central section. Due to some misunderstandings between the supplier and the laboratory the final geometry did not comply with the geometrical constraints given and this resulted in the failure localized out of the gauge lengthfor half of the specimens (3 out of 6). In Fig.6.2 the fractured specimens are presented. The direction of the specimens has been described earlier in Chapter 5 but is here reported for better understanding of the results; of the six specimen two have been printed in the XY direction (laying on the building platform), two in the Z direction (printing vertical axis) and the last remaining in the XYZ direction and therefore with a 45° angle between the printing direction and the specimen axis. Generally speaking, additive manufacturing of metal alloys gives rise, depending on the technology involved, to some anisotropy of the material properties: due to the thermal history the components are usually less ductile and less strong alongside the Z-axis because of microstructure banding phenomenon.

The banding phenomenon is related to the layering process through which an AMed component is built up. Since the energy application is consequently applied onto a single growing direction the in plane (related to the printing plane) section of the material are exhibiting a uniform structure originated by each layering section while the material analyzed alongside the Z-axis (the printing direction) is usually characterized red by subsequent remelting (or partial remelting) of the applied powder material. Due to this specific behavior in some occasions, for specific combination of material and cooling rate some element can segregate during the solidification process and therefore origine a banded microstructure. Furtermore the banding can be combined with the layering effect in AM produced component reducing the properties of the material considerably along the Z-axis. Especially in DED-AM techniques the banding phenomenon is present and is considered to be the cause of the poor elongation and strength in this specific orientation.

This effect has been observed by a variety of materials and processing techniques and implemented as well in the AMS specification regarding minimum strength level for titanium alloys [2]. Aside from this, the other characterizing direction is the XYZ direction which carries usually a strong layering behavior, intrinsically related to the production techniques, although the presence of machining operations removes any trace of this in the final version of the specimen[3].

[1] The laboratory used for tensile testing and for the CTScan tomography is Tec-Eurolab. Their references can be found on the website reported in [86].

[2] The specification recalled here is the AMS4999A; crf. [78]

[3] A proper fatigue characterization campaign would be the logical conclusion to understand the phenomenon of layering and

A first comment related to the presentation of the broken specimens regards the fracture surface. The resolved stress to cause ductile failure in tensile testing suggests the presence of 45° angle between the two halves of each specimen and the tensile load direction. This is originated by the simple tensile failure criterion with the determination of the Schmid parameter for the slip angle of the slipping planes. If the fracture behavior does not involve ductile slipping of the central section but the influence of other phenomena is driving the fracture, the corresponding surfaces might present different orientations.

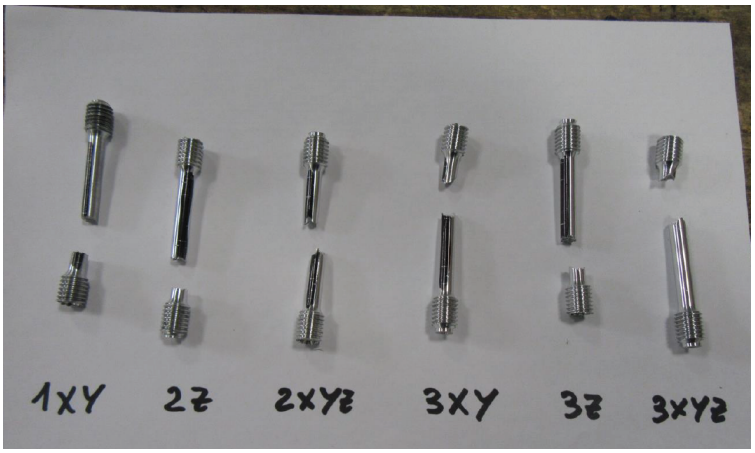

Figure 6.2: First batch of Scalmalloy tensile specimens after room temperature tensile testing. The fracture surfaces are not in line with the gauge length sections. This problem can be tracked back to the poor ductility of the material in combination with the loose tolerances on the geometry of the specimens not made with agreement to the specifications.

Of the presented specimens, 3 out of 6 specimens clearly show a fracture plane lying around the prescribed slip plane direction. On the other three the indication is unclear and therefore there is the need of investigating whether or not the influence of a excessively defective structure was involved in the fracture propagation.

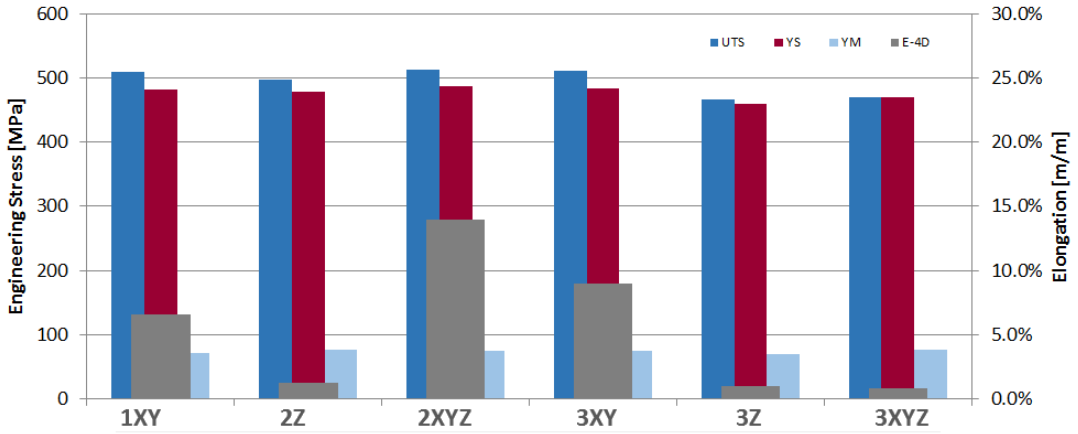

Figure 6.3: Tensile results of the first batch of specimens. The naming style for the specimen has been kept as from Fig.6.2

The tensile properties of the six specimens have been reported in Fig. 6.3. The results are showing an average YS of 477 MPa (max 488 MPa, min 459 MPa) and UTS of 494 MPa (max 513 MPa, min 466

surface behavior with respect of the different *as-built* surfaces finishing related to the printing direction and as well to address the influence of certain technological treatments on the material (for both thermal treatments - *hipping* - and surface finishing - *laser and shot peening*) fatigue properties.

MPa) if all specimens are considered. The respective average elongation at break for the specimens is 5.4% (max 14%, min 0.8%) and the average registered Young modulus is 73 GPa. If only the broken specimens with a correct fracture (inside the gague length) are considered (1-XY, 3-XYZ and 4-XY), the YS and UTS achieve 485 MPa and 511 MPa respectively. The elongation shows a consistent improvement averaging on those three specimen 9.8% with a standard deviation that varies from 4.9% for the six specimens to 3.0 %. It is worth to mention that, for what is indicated in the specification for tensile testing of metallic material [4], the results coming from specimens broken out of the gauge lengthof the reduced section should not be considered[5].

The second batch of testing specimens was part of the work performed in the definition of the high temperature properties. Those specimens have been built in the same directions as previously indicated and they represent a second testing of tensile properties at room temperature. To avoid issues with the reduced ductility of the specimens the required tolerances were required on this specimens with explicit agreement between the supplier and the laboratory on the author's request. The broken specimens are reported in Fig.6.4 while the results are presented in Fig.6.5.

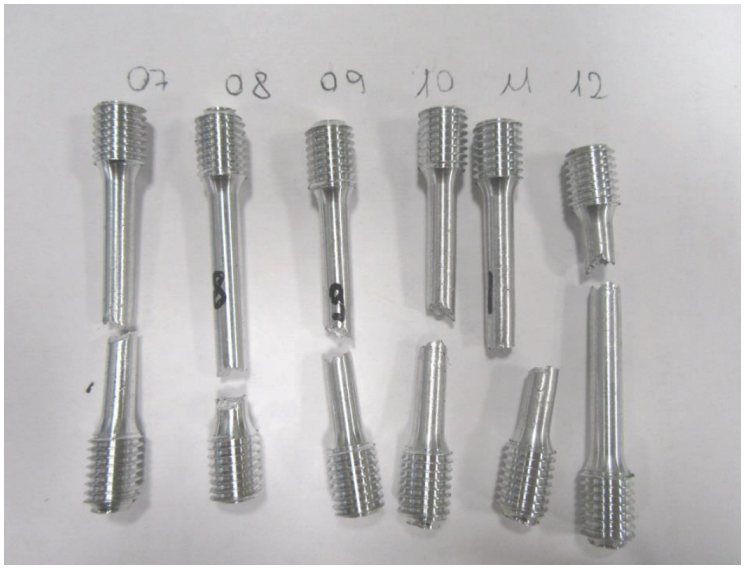

Figure 6.4: Second batch of Scalmalloy tensile specimens after room temperature tensile test. The fracture surfaces of 5 out of 6 specimens are in line with the gauge lengthsection. Still the elongation registered did not meet the level that should be achieved as reported in the powder producer specification.

At first sight the quality of the machining is clearly superior to the previous batch, a positive indication that more refined tooling was used in the definition of final dimensions on the six specimens. The fracture surfaces presented by the six specimens do not give an unambiguous indication of the style of fracture of the material: at a closer visual inspection the fracture surfaces seem to not be showing a clear slip plane. The presence of small imperfections is evident at a naked eye but microscopy imaging would be needed to properly assess the fracture plane appearance. In 5 out of 6 cases the specimen has been broken in the central gauge section. One of the Z-aligned specimens of the batch did not meet the requirements of necking inside the controlled section. All other specimens at a visual inspection do show an inclined slip plane that is an indication of the ductile phenomenon leading to

[4] cfr. ASTM E8M.

[5] This is related to the fact that the measurements from the machine linear actuators does not represents precisely the real axial deformation of the specimen.

the fracture occurrence. The results show values which are similar to the reported characteristics for the first production batch. Here all results are evaluated together since only one of them broke out of the measuring section. The average YS is at 480 MPa (max 492 MPa, min 468 MPa in Z) and 506 MPa for the UTS (max 512 MPa, min 500 MPa). The average elongation sets at 2.9% showing a consistent reduction with respect of the previous measurements and the Young modulus reaches an average value of 82.3 GPa with an increase of almost 9 GPa[6]. Between the two batches the standard deviation in the results of stress level passed (evaluated both times on the whole six specimens) from 19 and 10 MPa, respectively for UTS and for YS, to 4.8 and 8.8 MPa showing an improved measuring probably granted by the better tolerances ensured on those components.

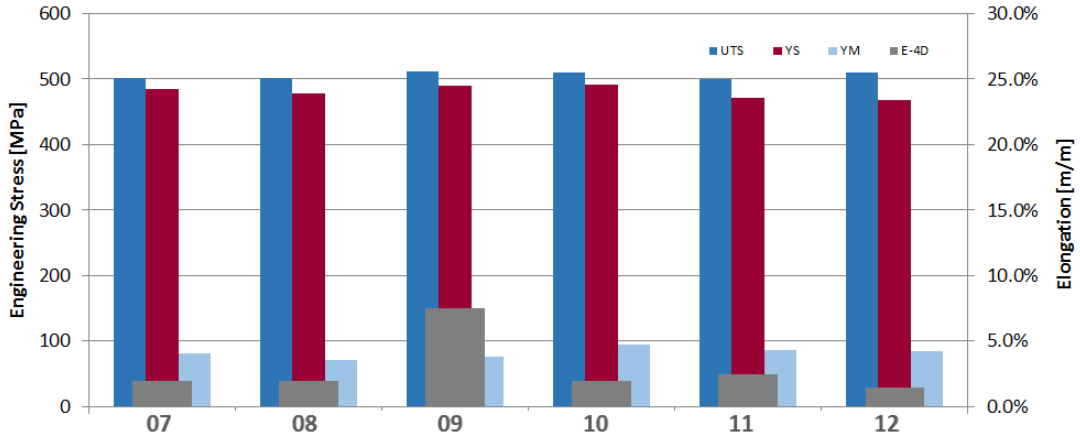

Figure 6.5: Tensile results of the second batch of specimens produced for high temperature testing. The results are shown in the same order as taken from the picture representing the broken samples. The average YS is registered at 480 MPa while the UTS reports an average of 506 MPa.

TENSILE TESTING - HIGH TEMPERATURE RESULTS

In the aforementioned process of characterizing the material properties at elevated temperatures, a high temperature tensile testing of specimens from a dedicated job[7] was prescribed in accordance with ASTM E21-09 [87] with the supplier. As for the previous testing procedure a total of six specimen has been produced with the presented directional orientations with respect to the printing axis (XY, Z and XYZ). Afterwards, the specimens have been tested at a temperature of 150°C. The recorded results will be compared with results from internal references and as well will be verified against the powder manufacturer specification which is the official reference for the material properties.

As for the second batch of specimen dedicated to room temperature testing the tensile specimens were checked for tolerances in order to have a machined central section reduced by 0.02mm with respect of the nominal diameter measured at the reduced section extremities near the fillets leading to the clamping heads. Further discussion on the proper specimen preparation and measuring techniques for poorly ductile materials is presented in Chapter 7. The broken specimens are shown in Fig. 6.6. The fracture surfaces are located in the measured and gauge section. Three of them are located near the indication made for the installation of the measuring device (indicated in the picture as spec-

[6]This apparently higher result has to be the object of further investigation since the raw data of the testing were not available for the analysis.

[7]In the industrial practice it is common to refer different orders as job; in this specific case the dedicated job refers to the implementation of a dedicated print for the specimens to be tested at high temperature.

imens 01 - 02 - 06). An interaction between the indentation needed for the installation of the gauge and the presence of defects in the region has to be investigated. The elongation of those specimens (as reported in Fig.6.7) is not suggesting any influence and a visual inspection of the surfaces is needed.

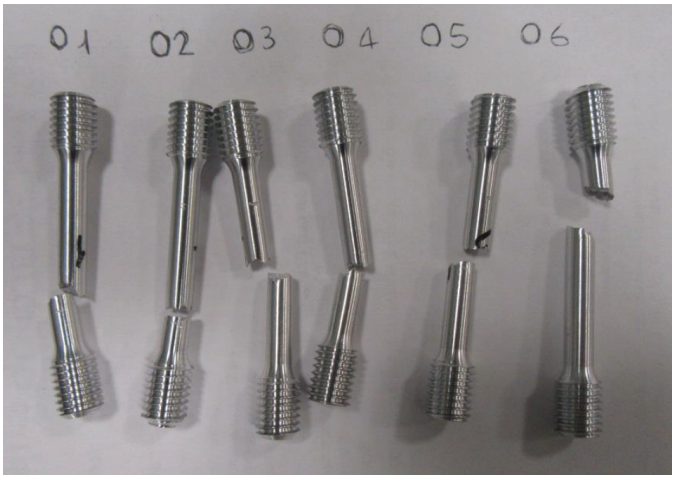

Figure 6.6: Second batch of Scalmalloy tensile specimens produced for high temperature testing. The fracture surfaces are in line with the gauge lengthsection. The superior machining and the enhanced plastic behavior at high temperature made the measure more stable. Still one specimen has shown a brittle behavior (3-z).

For the high temperature tested samples the average YS is 344 MPa while the UTS reaches a value of 367 MPa. The maximum values for YS and UTS are 351 MPa and 377 MPa respectively while the minima were registered at 335 and 357 MPa respectively. The increment of elongation due to the higher temperature level has shown an average E-4D of 8.6% with a maximum value of 16% (3-xy specimen) and a lowest of 1% (3-z specimen). The standard deviation of the measurements, representing the variance in the registered values, is 4.8%. The Young modulus averages a value of 61 GPa with a reduction of *circa* 17% on the first room temperature measurements average[8].

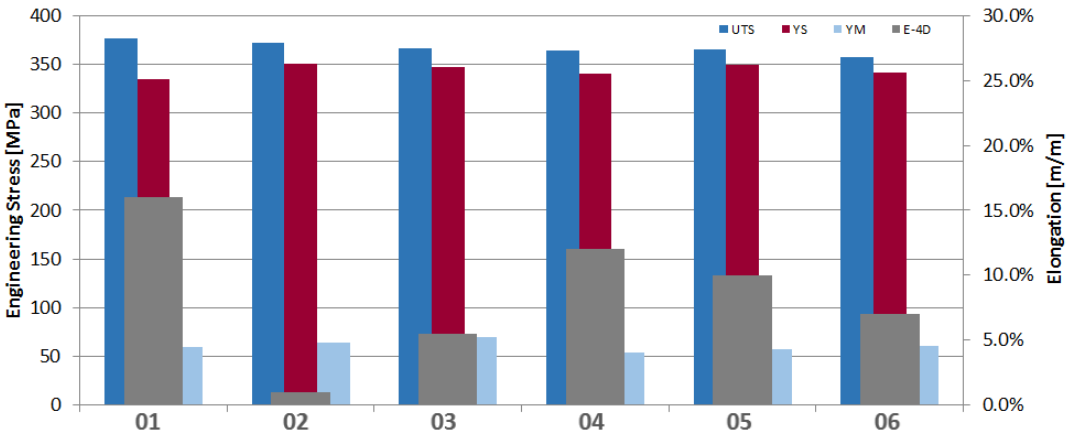

Figure 6.7: Tensile results of the second part of the batch of specimens tested at high temperature. The results are shown in the same order as taken from the picture representing the broken samples.

The obtained values for stress levels (YS and UTS) are superior to the ones described in Fig.4.9. The presented tensile properties will be compared in Chapter 7 with other sources and references

[8]The comparison has been done with the first measuring batch since the values of 83 GPa presented as the second average is not in strong agreement with literature and other sources.

Table 6.1: Hardness test results coming from a 2x2x2 [cm] cube from the same print of the component.

Hardness Vickers
163 H_V
161 H_V
162 H_V

to properly a if the provided material and process is targeting the powder specifications and other benchmarking results.

HARDNESS TEST

Three hardness tests were performed on a dedicated cubic specimen. The usefulness of the hardness test is to check if the heat treatment has given rise to precipitation hardening effect and might be a quick and cost-effective method to assess the process and heat treatment ability to achieve sufficient strength level. As one of the other hardening measurements[9], the Vickers hardness test involves the presence of an indenter that with an applied load will leave an indentation on the metal specimen. The conversion from the size of the trace and the hardness values is simply computed by measuring, with the aid of optical microscopy, the average of the two diagonal lengths. The Vickers formula is based on the angle of the indenter and has to reconstruct the penetration depth to achieve a relation between the applied force and the indentation area. Generally the formula reads as follows:

$$H_V = \frac{2Fsin(136/2)}{d^2} \tag{6.1}$$

and therefore it approximates to:

$$H_V = \frac{1.854F}{d^2} \tag{6.2}$$

with intending F the load axially applied to the indentator, with d the diagonal of the indentation as measured by optical microscopy and reporting the result in Vickers points (H_V) The tested sample results are reported in Table 6.1. The average value is of H_V=162.

The results of the hardness test conclude the section of mechanical testing results. In the next section the process quality will be addressed by means of density evaluations and micrography analysis.

6.2.2. PROCESS QUALITY ASSESSMENT - OPTICAL MICROSCOPY: DEFECTS CHARACTERIZATION AND DENSITY MEASUREMENTS.

In order to establish the quality level of the process of additive manufacturing, in agreement with the supplier a series of tests have been conducted: the density was identified by the use of optical microscopy analysis. Also the defects characterization was developed in the same context. The biggest defects have been recorded for the five sampling areas taken on the section of the six specimen heads.

DENSITY OF SCALMALLOY AND DEFECTS

The density has been measured, as mentioned earlier, in five positions for each of the tensile test specimen head sections considered. The results are summarized in Table 6.2. The results are the six measurements taken with the standard deviation of the five measurements inside each specimen. The highest value has been registered at 99.8% for both Z and XYZ specimens.

[9] *E.g.:* Rockwell or Brinnell tests.

Table 6.2: Density for the printed specimen calculated by optical microscopy. For each of the six section five measurements were taken: the reported results are the average with the standard deviation of the five measurements within a section.

Specimen	Density [%]	StdDev [%]
1-xy	98.8	1.66
2-z	99.7	0.13
3-xyz	99.8	0.06
4-xy	99.5	0.24
5-z	99.8	0.13
6-xyz	98.4	2.06

In Fig.6.8 a graphical interpretation of the tabular results presented in Table 6.2 is given. The lowest average density was found in the second XYZ oriented specimen. The lower material density reveals a higher density of defects present in the analyzed specimen. The kinds of defects detected by the optical microscopy are mainly two: gas induced porosity and process induced porosity as they can be detected in the reported images.

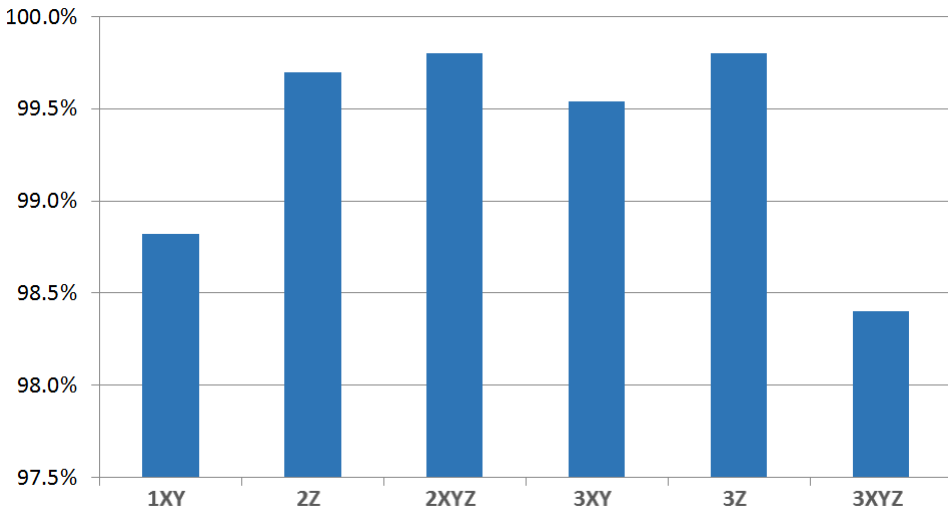

Figure 6.8: Density against specimens orientation. As it can be seen there is no clear relation between these two characteristics. The average density as it will be further explained in Chapter 7 is showing some low values that are rating below 99.5%. The defect level responsible for the low density seems to be related with the lack of fusion during the laser scan of the powder.

In Fig.6.9 six micrography sections are reported with Scalmalloy specimen heads cut along the specimen axis. The presented images are originated by the analysis of the first XY oriented specimen, by the XYZ (Fig.6.9c and Fig.6.9d) and Z (Fig.6.9e and Fig.6.9f) oriented specimens. The average density of the XY specimen was computed to be 98.8% and therefore the level of defects present is rather high for this specific orientation. More specifically we can see in Fig.6.9a a typical example of horizontal lack of fusion, a process induce defect specific of additive manufacturing. In the subsequent image presented in Fig.6.9c the same kind of defects are oriented by an angle of about 45° indicating, possibly, the presence of the same defects. Since the horizontal lack of fusion is present in the XY plane a section along the XYZ would presednt indeed an inclined defect at around 45°. This is somewhat reflected as well in the Z-axis specimen in which the defects seem to be relatively long but very limited in height. The biggest characteristic dimension of those lack of fusion aligned in the horizontal (printing plane) XY plane is in the range of 0.5-0.7 mm. The dimension of the average gas induced porosity is

around 0.1mm or 0.2 mm: an example of such defect can be seen in the mid-ground of Fig.6.9b. The presence of the horizontal lack of fusion is evident analyzing the corresponding defects on the differently oriented sample: the long defects in Z (Fig.6.9e and Fig.6.9f) show a very small height and the same defects are oriented approximately on a 45° direction in the XYZ samples (Fig.6.9c and Fig.6.9d). More analysis on the defects present in those microscopic analysis is presented in Chapter 7.

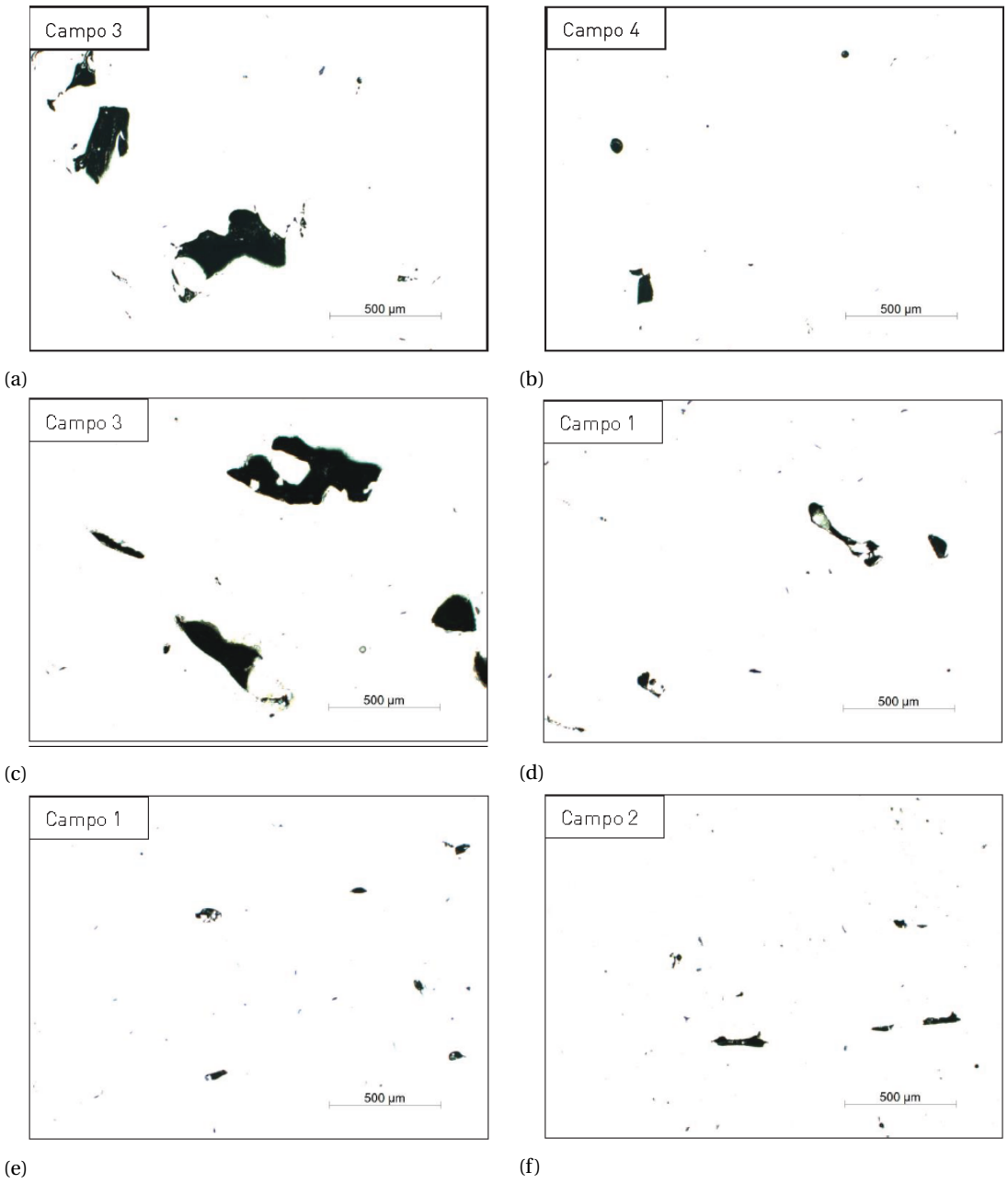

Figure 6.9: Microscopy comparison between Scalmalloy tensile specimen sections produced by laser cusing: the direction of the first two images show an XY specimen (Fig.6.9a and Fig.6.9b); Fig.6.9c and Fig.6.9d are relative to an XYZ specimen while the final images (Fig.6.9e and Fig.6.9f) are relative to a specimen printed in the Z direction. Since the specimens have not been etched the black color represent the material porosity.

6.2.3. COMPONENT QUALITY ASSESSMENT - NDT: TOMOGRAPHY, LPI AND 3D LASER SCAN

Having assessed the product quality with defect level and density by means of optical microscopy analysis, it is important to check the defects present in the component itself with the aid of non destructive techniques (NDT). On the semi-finished product three controlling techniques were required in agreement with the supplier as stated in Chapter 5: CT Scan tomography, 3D laser scan and Liquid Penetrant Inspection (LPI). The most relevant results indicative of the component quality are resumed in the present section.

CT SCAN AND 3D LASER SCAN RESULTS

The 3D laser scan gives an indication of the differences between the semi-finished product and the ideal CAD geometry. In the analysis multiple surfaces are analyzed and a distribution curve is elaborated by the software which gives an indication of the offset present between the CAD geometries and the measured points. The comparison reported in Fig.6.10a an in Fig.6.10b show the actual differences between the real component and the ideal CAD geometry. Two comparison sections are reported in Fig.6.11. As it is clear from the indicated images, the difference can range from some cents of mm to few tenths of a mm but some surfaces are offset by almost 1 mm.

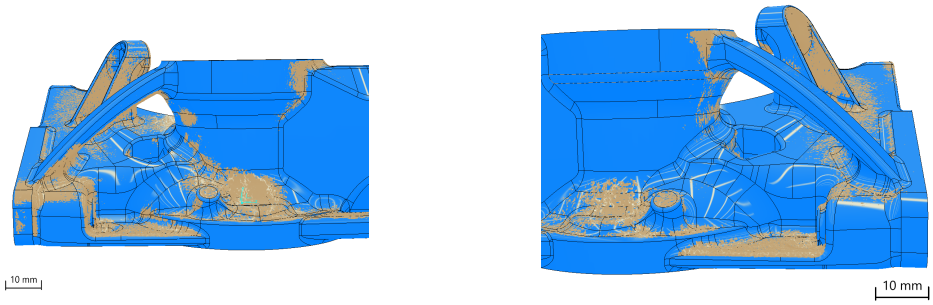

(a) (b)

Figure 6.10: CAD comparison between the ideal semi-finished product and the 3D scan laser results: generic outer surface of the component. In blue the ideal CAD geometry is reported while in light brown the 3D laser scan results are compared. A general tendency of material lacking in specific orientation can be noted but most of the times this shift did not influenced the resisting sections.

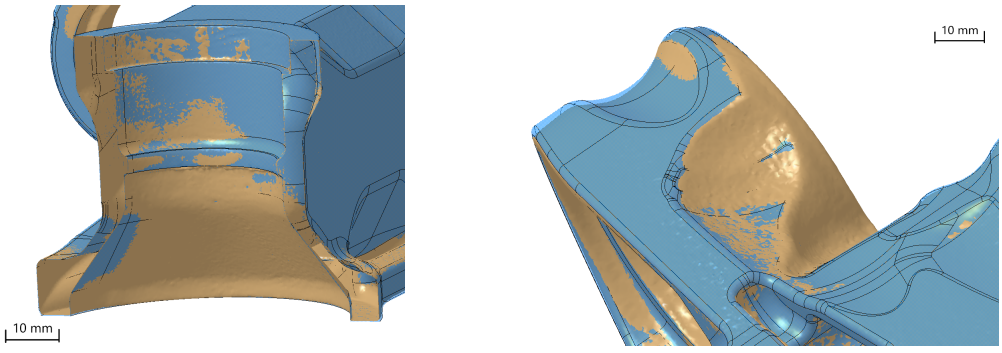

(a) (b)

Figure 6.11: CAD comparison between the ideal semi-finished product and the 3D scan laser results (in transparent blue the CAD geometry while in light brown the results from the 3D scan): section of the bearing housings. Some drift in the accuracy is present and might be related to a certain affinity of the process to deform the component with respect of the printing direction.

In order to address numerically the differences in terms of dimensional accuracy of the component the cumulative curve and the statistical distribution of the measures are reported in Fig.6.12. The maximum values are in the order of 1 mm of negative offset and around 0.65 mm for surfaces measured in excess of the ideal CAD geometry. The tendency of showing zones where material is lacking requires consideration on the strength limited section as presented by the FEM analysis.

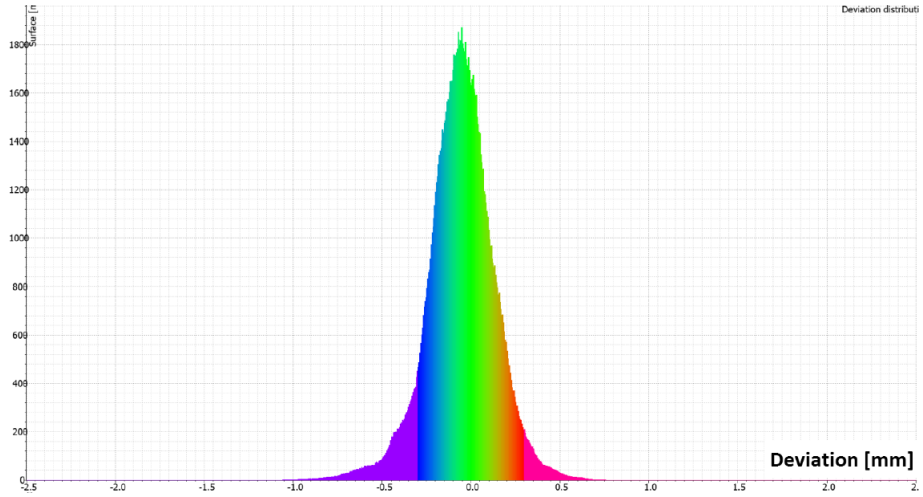

(a)

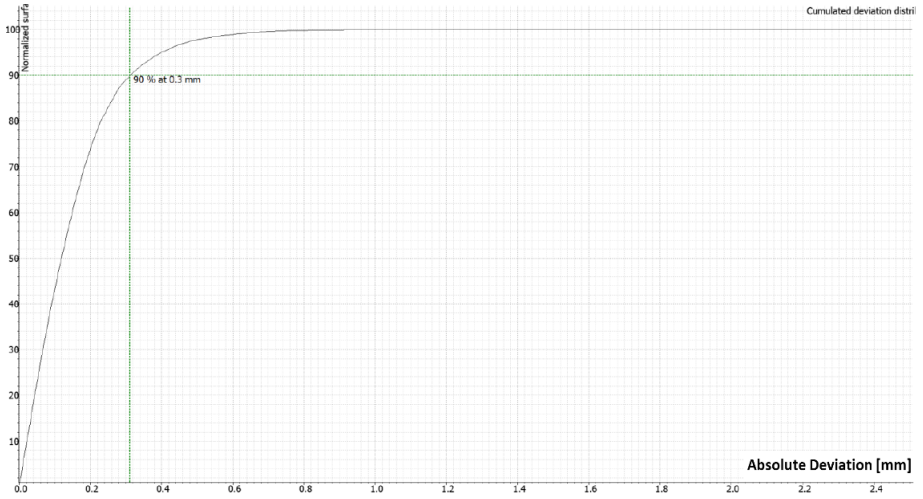

(b)

Figure 6.12: Distribution of offset measures between CAD geometry (Fig.6.12a) and their cumulated curve (Fig.6.12b): 90% of the measured points are within +/- 0.3 mm (the X-axis is showing here the absolute deviation). In Fig.6.12a the number of measured surfaces on the Y axis is plotted against the relative deviation from the ideal CAD geometry. As specified, it is clear that exists a tendency toward a negative offset from the CAD surfaces of the real geometry. Furthermore, the maximum values are around 1 mm for negative measurements and of 0.65 for positive measurements.

After the 3D laser scan the component was subjected to CTScan tomography: with this NDT technique is possible to access the internal material of the structure and analyze the presence of defects such as big porosities or lack-of-fusion defects. All defects where analyzed in two section to understand the aspect ratio of each of them; the five more consistent defects are reported in Table 6.3. The most concerning defect is the one reported as #4. The characteristic dimensions are about 1x0.7 mm^2. The presence of such defects was the reason to reconsider the quality process of acceptability in order to properly control the defects in the different areas of an AMed component.

Table 6.3: Five biggest defects detected by the tomography analysis: the reported dimensions represent the major axes of each defect on two perpendicular sections (longitudinal and transverse)

Defect	L1 [mm]	L2 [mm]
1	0.43	0.58
2	0.36	0.83
3	0.55	0.62
4	1.02	0.66
5	0.42	0.63

LIQUID PENETRANT INSPECTION

As an intermediate step in the qualification process of the component the control of LPI was a logical step in the process of volumetric defect controls (CTScan and 3D laser scan). The process requires the implementation of a specific fluid on the component that is afterwards removed with various techniques. The removal of the excessive dye penetrant fluid[10] is not removing the fluid from the surface cavities and pores. By analyzing the component under ultra-violet light the fluorescence of the fluid results evident and therefore pores, cavities and cracks are highlighted. The results from the first DPI analysis are presented in Fig.6.13. In Fig.6.13a the general geometry is presented while in Fig.6.13b the presence of a linear indication can be seen in the bottom of the bearing housing.

The same situation is shown in Fig.6.13c regarding the other bearing housing. A similar indication was already present in the 3D laser scan analysis as documents Fig.6.13d. The region of interest presents 2 mm of exceeding material for machining reasons as illustrated in the process definition in Chapter 5. By visual inspection the defect was already evident as reported by the two pictures in Fig.6.13e and in Fig.6.13f. The geometrical discontinuity of the defect is not clearly visible with LPI and an investigation with X-ray technique would be required to specifically address the dimension of the crack/absence of material.

[10] The technique is sometimes called dye penetrant inspection -*DPI*.

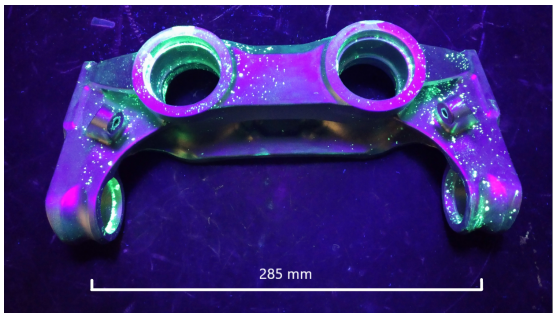

(a)

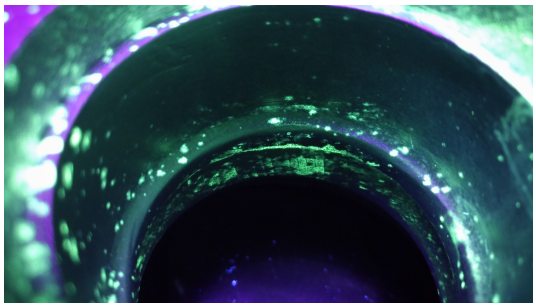

(b)

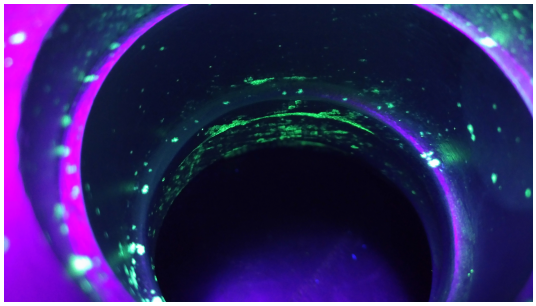

(c)

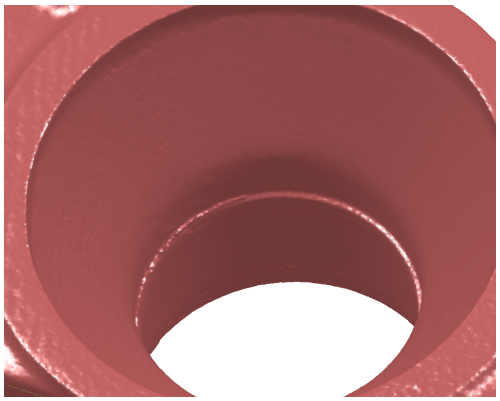

(d)

(e)

(f)

Figure 6.13: Results from the first liquid penetrant inspection: the defective zone was present and even evident from the laser scan (Fig.6.13d). In Fig.6.13a the whole geometry of the component is visible. In the last two images the defect is presented as it can be seen by a visual inspection (Fig.6.13e and Fig.6.13f). The colours in the images representing the LPI testing reflect wether or not the dye penetrant fluid remained after the removal procedure showing a clear flourescence (light green spots). On the contrary clean surfaces remain of the reflected ultra-violet light (resulting in the violet-blue color in the presented images.)

Still, even if the machining should be able to remove the presence of a linear indication the decision taken was to reassess this issue after the first machining process and after the re-machining of the bushing once they have been interference fit on the rocker beam. On the LPI analysis are visible also some open pores that were not corrected with the shot peening procedure.

6.2.4. ADDITIONAL TESTING RESULTS - LPI AND X-RAYS

The need of re-establishing a quality process led to the definition of a more intensive testing procedure in order to address and analyze the problems emerged during the first part of NDT. As a result, in agreement with the supplier, two extra LPI tests were decided and as well an X-ray inspection was set up internally at the Ferrari foundry in Maranello. The results of this second set of testing are presented in the present section.

LIQUID PENETRANT INSPECTION

As mentioned, two extra levels of liquid penetrant inspection were required respectively after machining and after the bushing installation and re-machining. The results of the second LPI analysis are shown in Fig.6.14: the matte surfaces represent the machining areas. At a first look on the general surface of the back of the component (as presented by Fig.6.14b) some open pores are evident as a result of the rough surface finish. On Fig.6.14a the top of the right bearing housing is presented and the machining seems to have solved the linear indication even if it has exposed some pores that are now open; still their dimension seems to be relatively small. Similarly, some exposed pores are present in the machined surfaces in Fig.6.14d. The lower section of the bearing housing presented in Fig.6.14e is showing what seems to be a linear crack initiation but the low quality of the picture does not permit a proper evaluation. The final LPI indication might solve the issue but some concerns are still open on this specific defect: the detection of a crack will be assessed with the X-ray imaging technique.

X-RAYS FOR DEFECT ALLOCATION AND CHARACTERIZATION

As a part of the novel quality process definition there has been the need of establishing a robust and unambiguous method to define the defect level through the introduction of an analysis based on X-ray technology. The X-ray procedure is the established method for grading the quality of aluminum castings and has been seen by the author in agreement with the quality department as a robust benchmark in the characterization of defects since the perceived quality of CTScan images was regarded as insufficient. The images were obtained through X-ray imaging for industrial analysis (as for analyzing aluminum castings) and the beam power was set to 140 kV at 4 mA for an exposure time of 90 seconds (for the rocker beam). As well the tensile specimens were tested to achieve the defective structure that was responsible of the poor ductile behavior.

On the rocker beam image reported in Fig.6.16 it was not possible to track back the defects that were recorded with the tomography. Due to the limited testing time there was the chance of having only a frontal X-ray slab of the component. Still, a good portion of the component is shown at the correct density to assess any defect of considerable size since the defect detection limit with this NDT technique is around 0.1-0.2 mm. Further X-ray imaging is prescribed after the fatigue testing procedure.

As for the rocker beam, also the image of the specimens in the digital format is not able to clearly

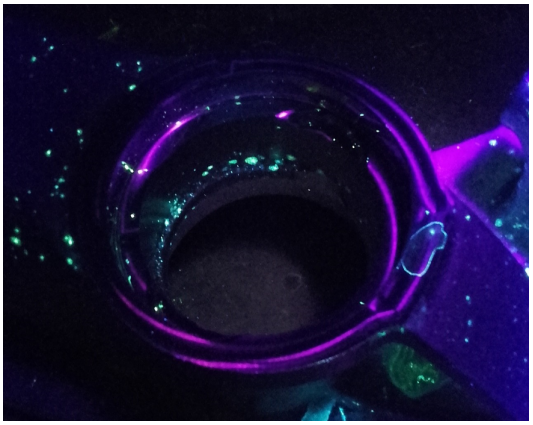

(a)

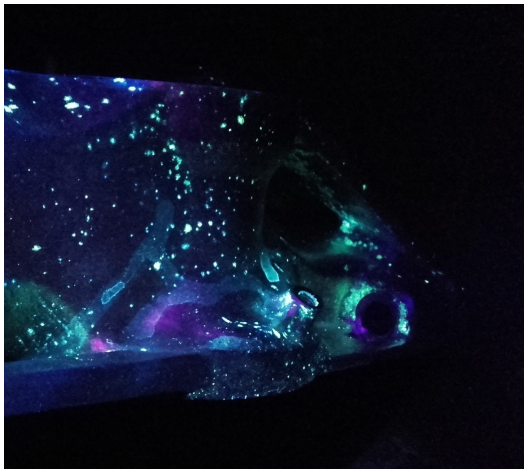

(b)

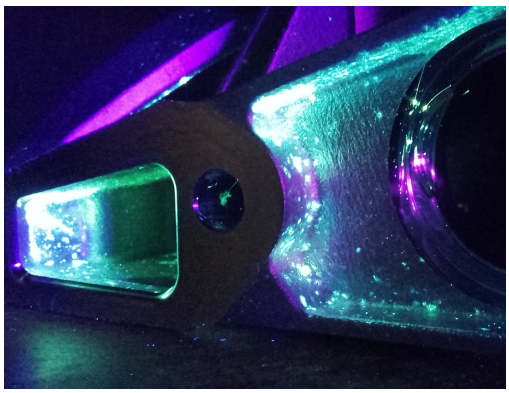

(c)

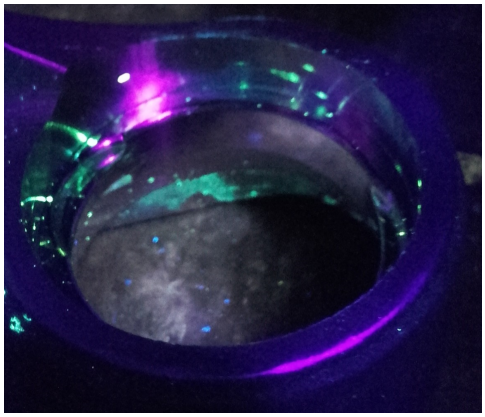

(d)

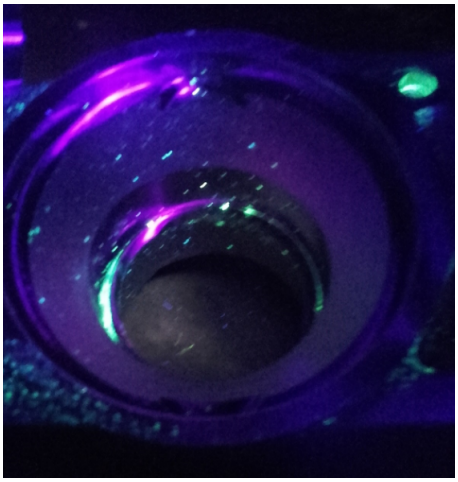

(e)

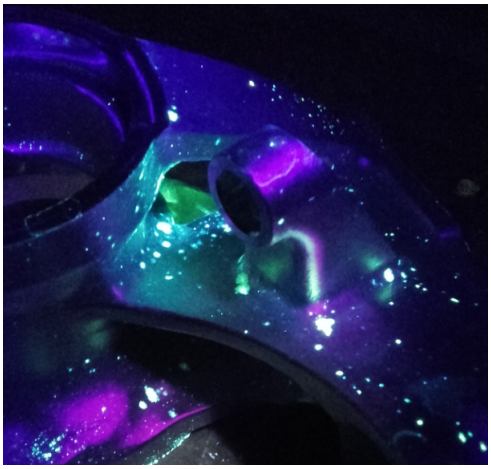

(f)

Figure 6.14: Results from the first of the two extra liquid penetrant inspections: the defective zones previously presented seem to be without any linear indication on the machining surface. The comparison can be made by the two images presented in Fig.6.13b and in Fig.6.13c with Fig.6.14a and Fig.6.14e. The linear indication presented by Fig.6.14e might be related not to a crack but to the stick of some fluorescent liquid on the machined surface: the defect will be analyzed with X-ray imaging to solve the concerns. In Fig.6.14c it can be seen how the machining of a porous material can expose some of the porosities that are present in the component. The effect and presence of those defects should be analyzed in the acceptability of the component.

show the level of defects detected: the X-ray slab shows generally porous specimens. A part from diffused porosity (of regular circular shape with a diameter around 0.2mm) the vast majority of the XY

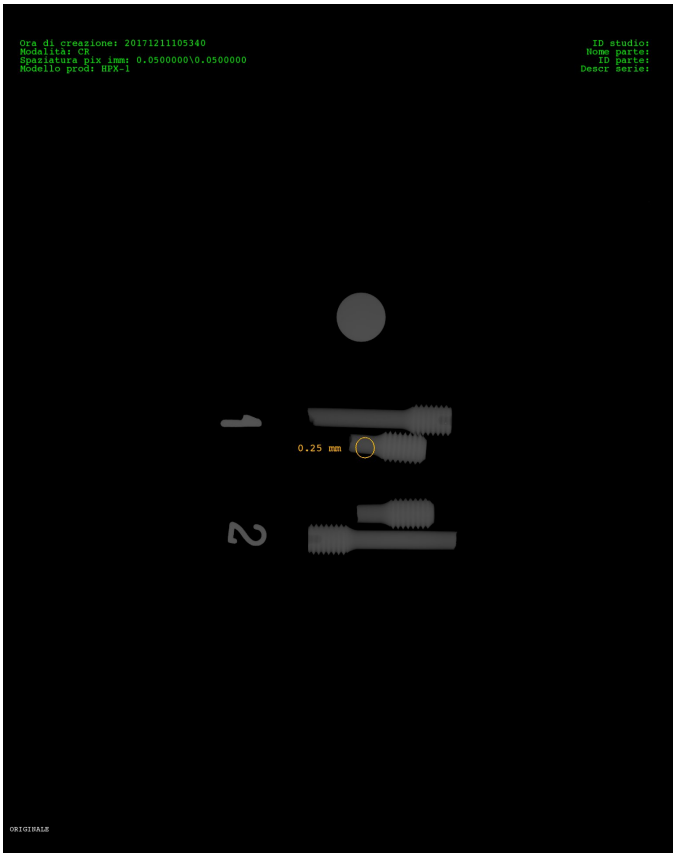

Figure 6.15: X-Ray imaging for two broken tensile specimens. The specimens analyzed are both from the second batch (respectively in XY-direction and in Z-direction): the quality of the picture is not high enough to show the interesting defects; the X-ray slab was showing defects oriented alongside the printing direction (horizontal lack of fusion) that have been characterized by the use of a specific software application. The small yellow circle reports one of the measured defects having a characteristic shape of 0.25 mm. The tested specimen are the 1XY and 2Z from the first batch of room temperature tensile testing.

specimen shows long defects approximately aligned with the specimen axis. The same defects are present on the Z specimen but their section is very limited in height: the characteristic dimension shows what is usually called (as specified in the micrography analysis) a diffusive presence of horizontal lack of fusion.

6.3. FATIGUE BENCH TESTING - RTWB BRACKET

As part of the homologation process for the implementation of new manufacturing technologies into engineering practice for the design of structural components, the need of a full component fatigue testing was considered still fundamental in proving the technological functionality of additive manufacturing. From a strategic point of view, since the machine counterpart has been similarly tested, such testing set up was requiring low effort and therefore has been granted to properly assess the mechanical properties of the produced alloy. The original testing procedure was developed to be representative of only one loading condition -*maximum cornering*- and represented the starting point for the definition of the other load cases. Since the braking conditions were regarded as well as the most stressing FEM-simulated load case a second set up has been developed in order to test this condition as well. In the next section the testing procedure and results are briefly reported.

Figure 6.16: X-ray image of the rocker beam: the reduced digital quality does not give proper relevance to the revealed defects: their magnitude appear to be reduced with respect of the defects detected by the CTScan tomography. With the aid of the dedicated software is possible to reach identification of defects in the order of 0.1-0.2 mm. Two indicated defects are representative of the porosity level found in the structure.

6.3.1. FATIGUE TESTING CYCLE

As mentioned in the introduction of the present section, the fatigue testing has been set up in order to simulate on the test bench the two most limiting load cases prescribed for the RTWB bracket: the maximum cornering condition and the maximum braking condition. The second case is reported in Fig.6.17: the bracket mounted on a dummy upright simulating the real load condition and direction. The load application is done through a steel ball joint which is either in direct contact with the linear machine with an hertzian contact (maximum cornering load) or with a tooling-rod replicating the assembly of the ball joint on the car RTWB (maximum braking condition). To prevent the rod coming loose from the steel ball joint the prescribed assembly features a small threated detail tighten up with the aid of some Loctite.

The test itself is composed of two parts: the first half of the testing procedure represents the homologation of the component; the second (optional) part of testing is a second proof for the real evaluation of the fatigue properties of the component and it is aimed to see if increasing considerably the level of load, while remaining at the limit of the design limit, the component would fail. To optimize the mounting sequence the test is organized as presented in Fig.6.18. The homologation regards the first four load applications on the component, namely: two fatigue cycles for both load configuration (at 85% of the design load) for 45000 cycles (one season average equivalent) and two strength checks of 10 cycles at 100% of the design load. After the homologation test, and the requalification of the

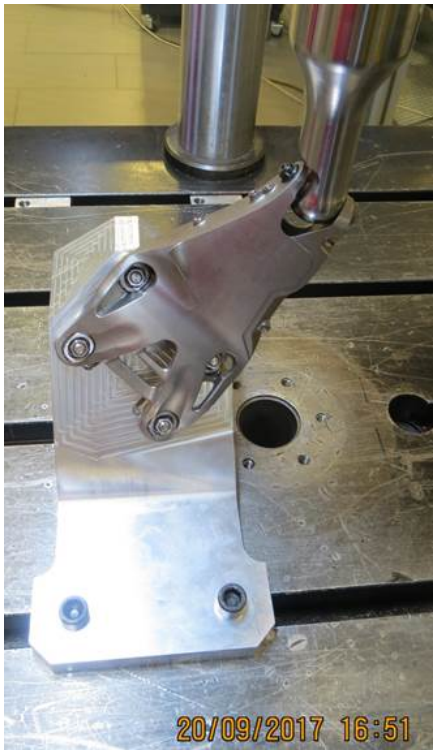

Figure 6.17: Installed set up for maximum braking condition tests: the component has to be positioned along the force axis coming from the simulation results and for doing so the related tooling is presented in its final assembly. The component is tested for both braking and cornering load cases.

component, the cycle prescribes a second cycle of fatigue evaluation in order to assess how close to the nominal fatigue properties the component can withstand. This second cycle (as represented in the last two bars on the graph presented in Fig.6.18) is made up of two load applications: the first is a strength check at 150% of the design load while the second is a fatigue cycle at 100% of the design load.

Both components, with different surface finishings, were set to undergo this cycle and no differences were found in the component conditions at the end of the tests. As well the mechanical test shown the same stiffness of the component as compared to the current version - *the machined counterpart* - which represents one more degree of agreement between the design work on the camber stiffness and the actual stiffness of the real component.

6.3.2. REQUALIFICATION OF THE BRACKET DURING AND AFTER TESTING

A requalification procedure is fundamental to establish if the fatigue load application has been positively passed in order to move in the testing procedure to the subsequent load cases. For the specific case of the bracket two different testing procedures were requested: first an LPI inspection in order to assess the presence of superifical cracks. Secondly, in order to assess the presence of local yield the component was prescribed to undertake a dimensional check on the attachment geometrical features (a coordinate check was considered too time consuming for establishing the relative position of mechanical features). Each of those two tests have been requested after every load application in order to detect at which stage of the testing routine the component would have failed.

As a result of the testing and requalification of the two brackets both have passed the homologa-

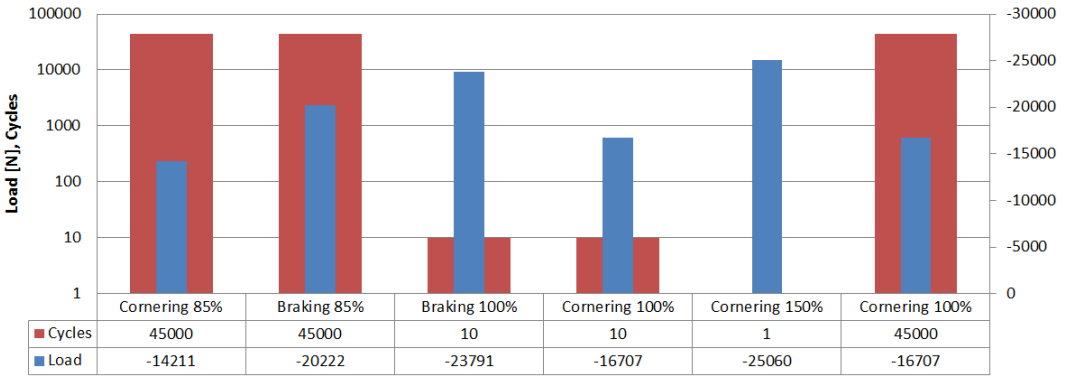

	Cornering 85%	Braking 85%	Braking 100%	Cornering 100%	Cornering 150%	Cornering 100%
Cycles	45000	45000	10	10	1	45000
Load	-14211	-20222	-23791	-16707	-25060	-16707

Figure 6.18: Graph presenting the set up fatigue cycle. On the bottom table are reported the number of cycles and the relative load for each step on the fatigue process indicated in newton. The first four load applications are representative of the homologating procedure while the last two strength and fatigue proof are extra load steps for proving the limit of the mechanical properties of the component.

tion requested and the project was successful. Regarding the second part of the testing, as well both components passed the requalification procedure and are considered to be ready for further testing. The possibility of running the test internally within the company facilities and the component being produced completely with the company know how represents the readiness of the whole process to be applied at structural component of the car as it will be further discussed in the following chapters.

6.4. FINAL FATIGUE TESTING OF AMED SUSPENSION COMPONENTS

In order to assess the rocker beam component fatigue properties it was not possible to set up a single component bench test: because of geometrical reasons and different functionalities of the component - *such as the ten bearing housings* - the only way to properly stress the component is a simulation bench with the whole rear mounted suspension. For such test the market benchmark equipment is represented by the MTS-329 multiaxial road simulator bench. The test is carried out with the external gearbox mounted with the whole inboard and outboard suspension component but without the aerodynamics fairings. The test is considered the top level technology for testing suspension system without the presence of the chassis[11].

6.4.1. MTS - 329 - MULTIAXIAL SPINDLE-COUPLED ROAD SIMULATOR TEST BENCH FOR SUSPENSION SYSTEMS

In the present section the testing set up will be briefly described in order to properly present the origin of applied loads on the produced components. An example of the machine used in the testing is presented in Fig.6.19: half of the installation is presented and the housing for the spindle (the wheel hub) is clearly visible. Being a six-degree of freedom system it can apply different forces and torques. The system is hydraulically operated by six actuators through controlling units and is aimed to reproduce the load application that a suspension system is designed to carry. The load capabilities represent the following cases: vertical forces (bump and rebound), lateral forces (coming from the cornering

[11] For such tests the *apparatus* needed is a bench able to sustain the car weight and to apply the loads directly at the tires contact patch. The machine able to carry similar test is the 7-post testing rig. An example about a 7-post rig for a Chevy Racing car is presented in [88].

forces) and longitudinal forces (acceleration). Furthermore, the system can provide braking and driving torque for the full representation of loads. The presented system is able to provide as well all presented forces at the variation of the steering angle (specifically for front suspension).

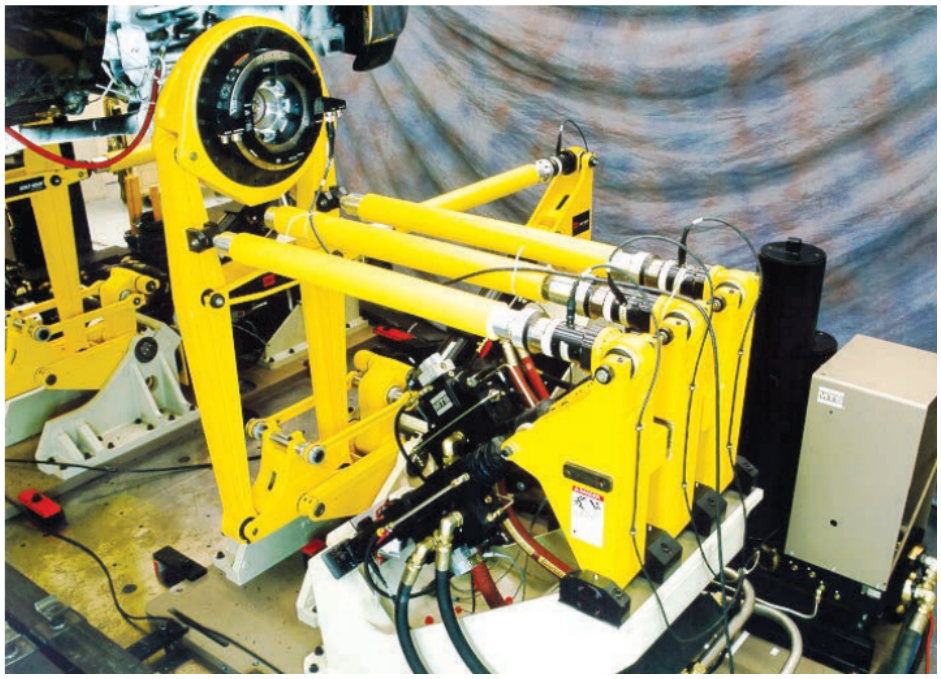

Figure 6.19: MTS 329 Road Simulator Bench element: the forces are reproduced through the direct connection of the machinery with the spindle [22] of each car corner. The chance of applying the three different forces and two torque loads with varying steering angle make the test bench a 6-dof testing machine. In the testing of the rear suspension the steering angle is kept constant since the rear end does not contribute in the steering of the car.

6.4.2. TEST SPECIFICATION - LOAD CASES OF 2000 KM

The test set up was meant not only to test the rocker beam produced in Scalmalloy but as well to test the RTWB bracket couple (*left* + *right*) specifically produced for car testing. As mentioned in the present section title, the test is representative for a significant number of kilometers run with similar loads to the ones the car experiences in the racing environment. The set up for the test, once the gearbox has been bolted on a dummy chassis and all sensors have been connected, is carried on with a lap simulation.

Since the car features a number of sensor for estimating the contact patch loads applied by the dynamic forces of the vehicle, the reconstruction of an ideal lap is a relatively straightforward process. Once the representative lap has been selected, the same cycle load is applied for the equivalent of 2000 km[12] which is a representative number of loads before a usually deep maintenance cycle is performed.

6.4.3. TEST RESULTS AND REQUALIFICATION OF THE COMPONENTS

For the requalification of the component a strategy similar to the one described for the RTWB bracket fatigue testing has been set up: for the brackets themselves the two procedures were identical to the ones reported in the previous section. For the rocker beam an LPI control was set to specifically ad-

[12] For reference an F1 Grand Prix lasts on average 300 km.

dress the issues presented in during the quality assessment of the component presented in the first section of the present Chapter. For the rocker beam since there where no attachment points apart from the fixings on the gearbox case, no dimensional control was prescribed.

Both components at the end of the testing procedure were tested by LPI method and successfully passed the test with no evidence of cracking present or surface defects originated by the applied cyclic loads. With this final assessment on the fatigue properties the present results chapter ends; the commenting section on the achieved results will be presented in Chapter 7.

7

DISCUSSION

Starting from the results presented in Chapter 6, the topic of the present chapter will be a technical comment on the preformed work and how the results have met or not the requirements set during the design process.

The present discussion section is divided into three parts: the first regards the mechanical behavior of the titanium alloy more specifically as implement on the RTWB bracket; secondly the focus would point on the results of the testing campaign done on the Scalmalloy, the process will be revised and comments made on the issues that have been faced with a metallurgical analysis on the development of the Scalmalloy concept and on its strengthening mechanisms; finally for the Scalmalloy (but with the aim of not being limited only to this material) a proposal towards the definition of a (*internal*) standard for the acceptability of defects in the microstructure is presented taking technical inspiration from the current norms and from what are nowadays the established testing methods for aluminum and magnesium castings.

7.1. TITANIUM MECHANICAL BEHAVIOR AND TECHNOLOGICAL ASSESSMENT

The discussion about the mechanical properties and functional analysis of the titanium produced component is reduced to the essential since all testing performed on the material was successful and was over the specification requirements for this specific application. The discussion will follow in the subsequent section within two different subsections: first the mechanical behavior is presented and secondly the functional assessment of the component is reported.

7.1.1. MECHANICAL BEHAVIOR

For the mechanical behavior of the component, since the material is largely used in the engine components, it has been judged as sufficient only the three tensile specimens coming directly from the print of each component. The direction alongside which the specimen are aligned is the Z-direction.

The tested samples were all in line with the specification showing elongation results well in excess of the ASTM 4999A. Since no metallography check has been performed it is not possible to address the material defect level. Due to the robust know-how all components printed in titanium (the first batch of left component and the second batch of testing component *left and right*) were considered successfully mechanically characterized by the analyzed specimens and by the historical database of mechanical properties on this combination of *alloy+process* .

7.1.2. FUNCTIONAL ANALYSIS - FINISHING AND ACCURACY

The functional assessment for the RTWB bracket comprehends three different controls and commenting sections: the surface finishing assessment deriving from the two possible options tried for the component; secondly the influence of the supporting structure will be analyzed and finally the dimensional accuracy of the machining is reported.

SURFACE FINISHING

Regarding the surface finishing of the component, as presented in Chapter 3 and Chapter 5, two different treatments were prescribed: a manual mirror finishing and a sandblasting procedure that has followed the support removal operation. Both finishing techniques, as further clarified in the subsequent section, were not able to achieve the complete removal of the presence of supporting structures. For future purposes, therefore, it might be necessary to investigate and characterize the benefits of alternative finishing techniques. Among the most promising techniques we can mention abrasive flow machining,[1] the tribological isotropic superfinishing process (ISF) and as well as chemical super finishing in which the mechanical abrasive forces are aided by the presence of a chemically aggressive environment.

INFLUENCE OF SUPPORTING STRUCTURES

The functional presence of supporting structures is fundamental for the correct achievement of an high quality level of the external printed surfaces. The interest in dimensioning and developing the best printing strategy is an essential part of the design for manufacturing assessment: since the supporting structures are needed for features characterized by angle smaller than 45° *circa* they already present a rough and irregular external skin given by the layering effect. In the bracket a continuous improvement approach has been used for the dimensioning and orientation of the supports. The presence of supporting structures left visible traces as reported also for the rocker beam component and the surface finishing of both sandblasting and mirror finishing were not able eliminate the presence of surface defects. From this, it is advisable that some custom finishing process is researched and applied to titanium components to solve the issue in the future for fatigue designed components. An increase in the fatigue strength measured after a proper surface finishing treatment would grant the possibility of exploiting further the weight saving opportunities given by the AM process. Furthermore, it will remove the need of having machined zone for fatigue reason as presented in Chapter 4 for the component in analysis.

[1] Already presented in the literature review section.

DIMENSIONAL ACCURACY

Even if considerably more precise than the rocker beam, still, some dimensional issues have been encountered in the manufacturing process of the bracket as well. The origin of distortion of long components or of small features during the printing process is inevitable due to the thermal gradient in the structure that originates from the low thermal conductivity of titanium when compared, for instance, with aluminum. In facts, the thermal conductivity of TI6Al4V is around 7 W/mK at room temperature while values for Scalmalloy are reported at 23°C to reach 100 W/mK. As the same time, the CTE of titanium is one third that of aluminum which counteracts the thermal distortion but not enough to make them acceptable.

Any thermal gradient in the structure impose a deformation on the geometry which the material counteracts with an internal stress state: the deformation being caused by the thermal gradient is proportional to the heat addition from the energy source (the laser beam), invasively proportional to the thermal conductivity (a hypothetical material with infinite thermal conductivity would not experience any thermal gradient). Furthermore, the deformation is directly proportional to the CTE of the material (a higher CTE would deform more the material under a constant thermal gradient). From the internal deformation an internal stress would rise accordingly with Hooke's law. A stiff material will suffer from imposed deformation while a less stiff material would develop lower internal stress levels. The consequence for additive manufacturing is the deviation from the ideal CAD geometry especially present in the case of structure that are not really stiff and therefore compliant with the imposed deformation.

The biggest error in the components, printed out during the duration of the project, was the location of the small functional cylinders prepared to host functional connection of aerodynamic extensions on the component itself, as in the installation presented in Fig.3.2 presented in Chapter 3. To achieve the functionality the machining procedures rely onto true positioning of the holes in respect to the given reference features. Since the small cylindrical pad containing the threaded section was offset, the material left between the thread and the external side of the pad was less than the designed one. Even if for the present project this was not a critical connection the aspect of thermal deviation needs to be properly addressed in the design process especially for non-stiff (highly compliant) component's regions that can experience substantial deformations in the production process.

7.2. SCALMALLOY MECHANICAL BEHAVIOR AND TECHNOLOGICAL ASSESSMENT

The following section will revise the results presented in the previous chapter in the perspective of understanding the current value of the additive manufacturing process, in order to establish the best further implementation of the technology for the development of the car performances. The scheme followed in commenting the results repeats the quality process with a step-by-step approach: in the first section the mechanical properties are analyzed in comparison with other literature and databases; in the second, the process quality is addressed with specific focus on the defect location and morphology; lastly the component quality will be addressed: the surface finishing, the dimensional accuracy and

all other functional related measurable characteristics will be analyzed.

7.2.1. MECHANICAL BEHAVIOR

The mechanical properties investigated during the tensile testing campaign were the basic elasto-plastic properties of metals: the yield strength, the ultimate strength, the elongation at break and the Young's modulus. The results of the first batch presented in Chapter 6 are hereby compared to the results of three other sources that will be used as benchmark for rating the material properties. The first comparison would be the database given by the supplier through which the homologation was done in agreement with the powder producer (this series is reported in light red color with the label of ZARE-OMOL). Secondly, the second benchmark properties are originated by an internal characterization campaign done with a different additive process (DMLS instead of SLM - or Laser Cusing[2]): the DMLS produced series is represented in the light blue color with the label MEC-Ges . The third reference is the powder producer specifications: this represents the formal agreement between the company and the supplier on the minimum quality of the purchased material and is reported in the attached images with a gray bar with no accuracy since it represents a pure value.

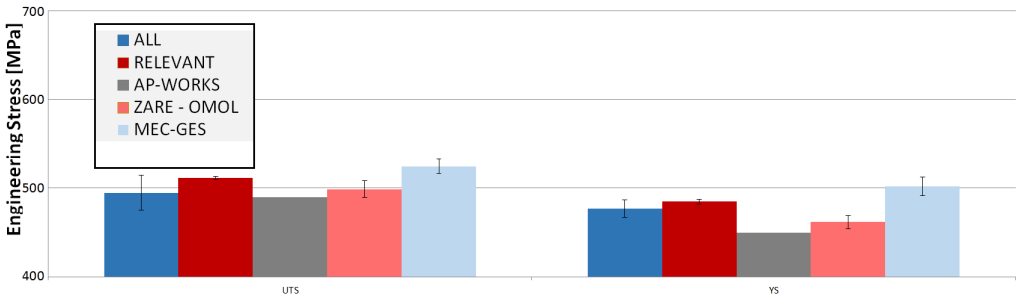

Figure 7.1: Mechanical comparison of UTS and YS for four different databases of Scalmalloy produced specimens. The comparison regards two different productive processes: even if the metallurgical processes differ both are meeting the powder producer specifications (reported in gray, labelled as AP-Works). The best properties registered are the ones of DMLS specimen internally produced (light blue bars, labelled as MEC-GES), still all production averages are in excess of the prescribed strength values. The low accuracy for the SLM (Laser Cusing) produced specimens (blue bars, label ALL) can be related with the poor machining of the first testing batch which has shown poor measurements and in part to the defect level of the Scalmalloy produced by the Laser-Cusing technology.

The comparison of mechanical properties starts with the comparison of the strength levels: in Fig.7.1 the average results of the different sources are compared. The specimens tested in the present project are reported in two different columns: the "ALL" series represents all specimens tested while the series "RELEVANT" excludes the specimens in which necking occurred out of the central gauge section of the specimens themselves. As it can be noted, the best properties are the ones related to the internal characterization with a DMLS process involved. Still, all tested series are well above the minimum required of strength (gray bar series). The standard deviation on the measured samples is in line with what has been seen for the other benchmarking databases and reflects the typical scatter of results between the printing direction samples and the stronger in plane specimens.

Regarding the elongation of the different material sources, the differences are quite relevant as

[2]The Laser Cusing commercial name is the same technological process of SLM. This denomination refers to the machines of ConceptLaser a GE spin-off company.

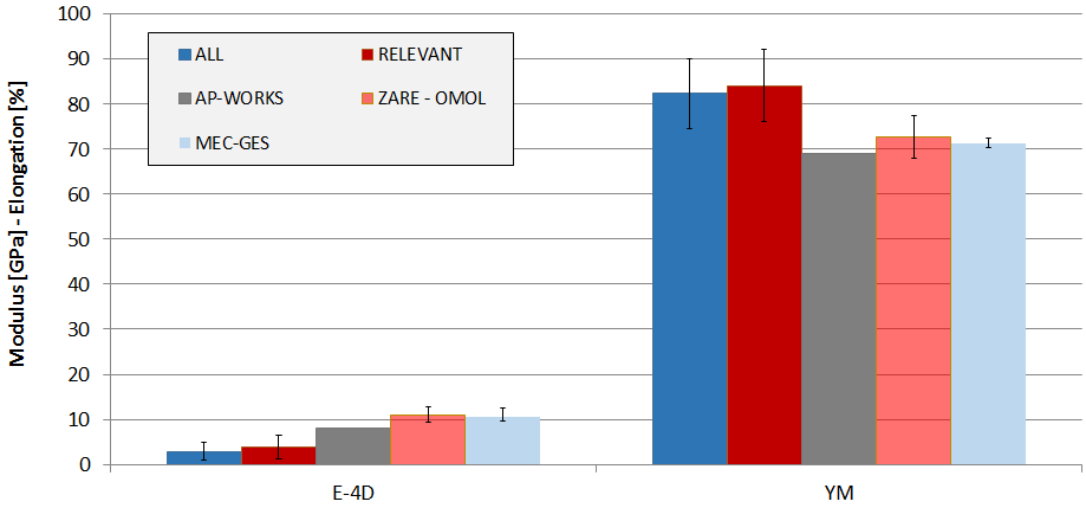

Figure 7.2: Comparison of Young's modulus and elongation at fracture between four different production batches. The reduced elongation of the first series is compromised by the presence of the specimens broken out of the gauge section as presented in Section 6.2.1. Again the DMLS results are the highest for the elongation properties while the YM measurements are in line between all the different sources. The difference in elongation between the tested sample and the homologation batch of the supplier is the indication of a quality issue in the performance of the production process.

presented by Fig.7.2: elongation results are directly linked to the ductility properties of the printed material. If the average of the first batch is taken under consideration the level of elongation does not meet the specification. As well the average of the second batch is not sufficient to grant the 8% of minimum elongation in the Z-direction as specified by the powder manufacturer. All other sources are process compliant and show average elongation well in excess of the tested material: therefore it is assumed, and will be later shown, that the defect levels of the tested material is most probably the cause for the poor elongation results.

Since the tensile testing has failed in presenting specimens broken in the central reduced section a further improvement in the gauging strategy can be made, in agreement with the ASTM normative: the measurement can be implemented at the start of the fillets connecting the reduced section with the specimen heads; if such a measure would not be good enough in estimating and preventing wrong measurements also the option of non contact measurements techniques could be investigated.

For the Young's modulus all tested materials are in excess of the powder specification and therefore meet the criterion: the material tested in Chapter 6 shows among the best Young's modulus of the different sources. The Young's modulus shows only the properties that are linked to the general chemical composition of the specimen but it does not explicitly express any merit on the defect levels (apart in case of serious porosity which has not been found in the analyzed material since the accuracy of the measurements is not high, cfr. the error bar). Since the Young's modulus is directly linked to the density but its accuracy is considerably low it is not possible for the present specimens to account for this.

High temperature properties are compared as well in this section (graphically represented by Fig.7.3 and by Fig.7.4). The benchmarking for the latter is reduced at the available high temperature databases which are namely the internal characterization (light blue bar) and the actual powder manufacturer specification. The results for high temperature strength are specifically reported in Fig.7.3: both materials are showing stress levels in excess of the prescribed properties and therefore the specification

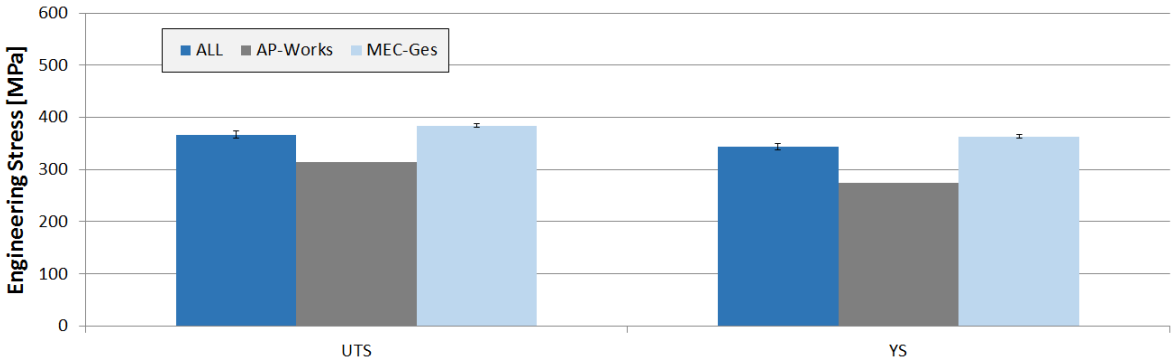

Figure 7.3: Mechanical comparison of UTS and YS for two different databases of Scalmalloy produced specimen recorded during high temperature tensile testing. The comparison regards two productive processes as earlier mentioned. Even if DMLS and SLM (or Laser Cusing) differ in the solidification process both batches are meeting the powder producer specifications reported in the gray bar labelled AP-Works. The MEC-Ges results are from an internal characterization campaign (DMLS produced specimens) while the ALL series are the results presented in Section 6.2.1.

is met. As well the standard deviation is similar between the two batches (but might be influenced by the reduced number of data). The good results in temperature characterization are making the design choices presented in Chapter 3 and 4 reasonable and rather on the conservative side of the problem with effective reserve factors probably exceeding the prescribed RF=1.5. The decrease of material strength at high temperature is determined by a series of factors: because of the higher thermal energy the dislocation movement is enhanced. Furthermore, the higher temperature favorites the diffusion of solute elements around dislocations increasing the plastic behavior of a material. On the contrary, the Young's modulus is negatively affected: for aluminum alloys the relationship between temperature and the Young's modulus is linear from room temperature to about 300°C [89]. The effect is mainly related to the easiness of stretching metal atomic bonds[3]: the energy barrier for moving atoms from their natural position in the crystalline form is reduced because their interaction is less strong.

In Fig.7.4 elongation and Young's modulus of the material are compared for the only two references available: the tested specimens and the characterization done during the DMLS internal campaign. The differences in the Young's modulus are limited and in favor of the DMLS produced specimens. A significantly bigger difference is present in the analysis of the elongation values: the average elongation of the Laser-Cusing samples is barely meeting the minimum 8% reference of the specification at room temperature (while for the aforementioned reasons the plastic, and therefore ductile behavior, shall be enhanced at higher temperature levels). The low elongation is even more concerning due to the significant difference with the DMLS produced samples which are all above 30% of elongation at break. The poor ductility at high temperature can be mainly explained by the occurrence of a brittle rupture in the elongation of the SLM-produced specimens (specimen 02 as reported by Fig.6.7). Such brittle behavior in the Z-direction reveals the presence of defects that did not grant the mentioned specimen to properly plastically deform before rupture.

As seen in the present section the properties of the material of interest do not completely comply with the required specification: the most probable reason for the mentioned issue is the presence of

[3]As presented with a numerical approach in [90] where the whole viscoelastic model of an aluminum material has been developed with dynamic and static Young's modulus.

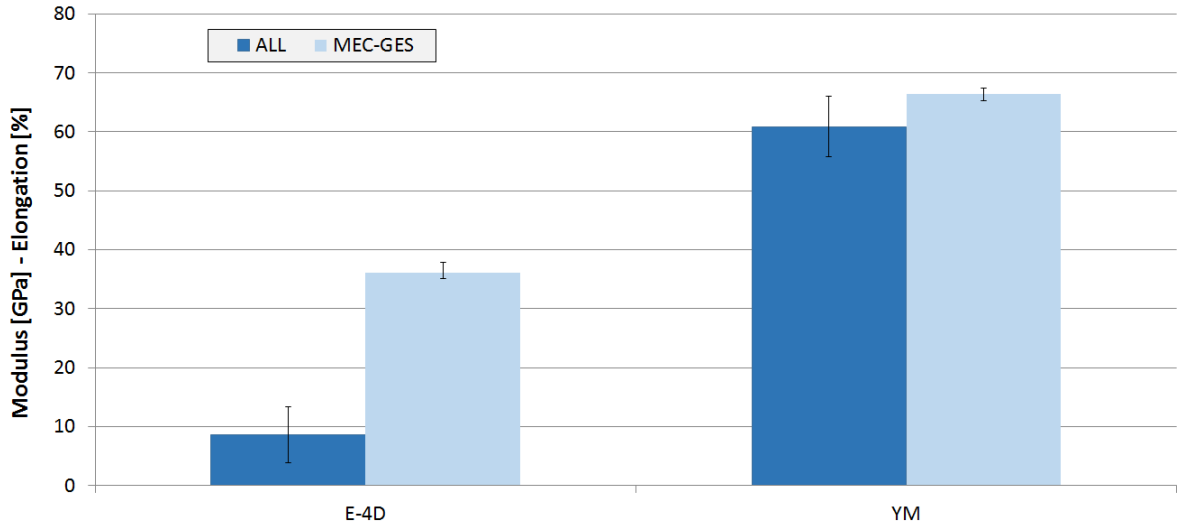

Figure 7.4: Comparison of Young's modulus and elongation at fracture between different production batches when tested at high temperature level (150°C). The reduced elongation of the first series is compromised by the presence of the specimens broken out of the gauge section. Still the huge difference between the two production processes is representative of two different defect levels of the tested materials: whether the material can be accepted or not needs to be addressed in the quality management of the component in analysis.

localized defects mainly process induced such as lack of fusion and extended porosity (shown and described in Chapter 6, cfr. Fig.6.16 for the X-ray results and as well the micrography presented in Fig.6.9).

7.2.2. MICROSTRUCTURAL EVOLUTION OF SLM PRODUCED SCALMALLOY AND COMPARISON WITH WROUGHT ALLOYS

To properly address the metallurgical effects that led to the analyzed tensile properties of Scalmalloy produced specimens the present section presents the microstructural evolution of SLM produced Scalmalloy and the comparison with reference wrought alloys. The peculiarities of the process will be explained such to show the mechanisms that synergize in the definition of the mechanical properties of the selected alloy.

In the first part the process that led to the engineering of Scalmalloy is presented, with the historical background, first as a wrought product and in the second place its implementation for additive manufacturing techniques; secondly, the microstructure evolution of the alloy is presented during the SLM manufacturing process and the subsequent heat treatment: a comparison with conventional age hardenable alloys is presented in order to show the main differences in the microstructure that are responsible of the mechanical response of the material to the applied stresses.

METALLURGICAL DEVELOPMENT OF SCALMALLOY

As mentioned in the literature review section, Scalmalloy is a high strength aluminum alloy derived from the 5XXX aluminum series. Those alloy feature in the composition Mg as the primary solution element and are considered not to be age hardenable since the absence of high Si content prevents the formation of strong precipitates. The main mechanism through which those alloys achieve high strength levels is due to the cold working that while increasing the admissible stress diminishes the

elongation at break by using part of the available plasticity to work harden the material.

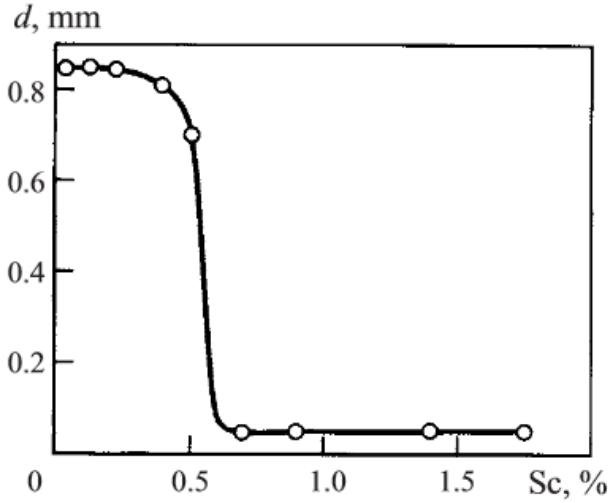

Figure 7.5: Relation of the grain refinement effect of Scandium for aluminum alloys. As soon as the eutectic composition is reached the presence at high temperature of Al_3Sc-precipitate favors the nucleation of grains in opposition to the usual epitaxial growth found in the normal cast process where the solidification process is driven mainly by the partially melt grains that act as solidification points.

In the development of AlMgSc alloys (such as RUS1570 or ALCOA C557) the focus of the Sc addition was to implement a grain refiner in the mixture to promote small grain sizes to be able to plastically deform more the alloy (therefore achieving higher tensile properties). The basic procedure for production of AlMgSc alloys has been for decades the cold rolling process. Through high level of deformation the cold work material could achieve sufficient tensile properties to be usefully implemented in the aircraft industries. This effect is usually combined with the non-recrystallized structures that can be obtained through hot rolling as well due to the high resistance to recrystallization that Sc addition features. In this context, the precipitation hardening of the Al_3Sc-precipitate is relatively small.

The mechanism that promotes grain refinement is the nucleation of equiaxed grains in proximity of the Al_3Sc precipitate from the melt. Since the precipitates are stable at high temperature, and tend solidify before the aluminum matrix (because of the hyper eutectic composition), during the cast process (of an aluminum alloy containing hyper-eutectic composition) they remain in solid phase, and therefore, the melt liquid tends to solidify with a high concentration of nucleation spots (at the precipitate locations). The substitution of dendritic grains with equiaxed microstructure with much smaller equiaxed grains is one reason for the strength as explained in [24]. The resulting effect on the grain size of Sc addition is reported in Fig.7.5. The refinement is immediate since the nucleation of the solid grains changes abruptly after the eutectic composition. The grain size immediately matches the dedritic parameter and even smaller grain are present. The mechanism of this nucleation process is made possible by the crystallographic properties of the Al_3Sc-precipitate; this particular microstructural constituent features usually nano-dimensions and it is evenly distributed in the material. Furthermore, the unique correspondence in terms of lattice dimensions and crystal orientation make this precipitate highly capable of being the nucleus of a new grain. The crystal structure of the carbide is the simple cubic Ll_2.

Since 2006, a new concept for the addition of Sc has been proposed as reported in [25] . The rev-

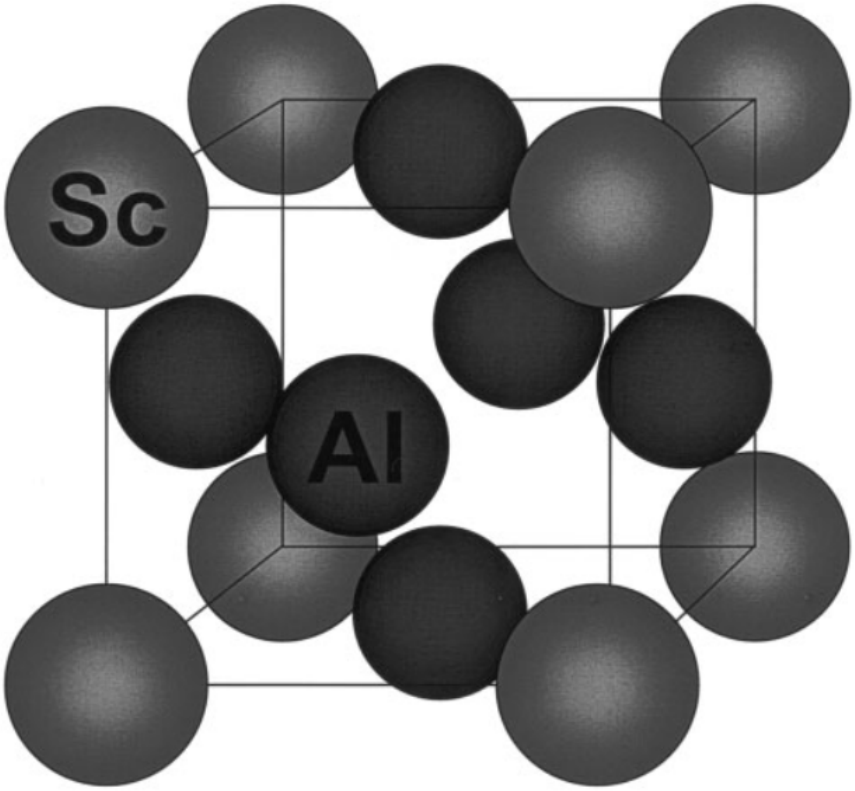

Figure 7.6: Atomic arrangement of Al_3Sc-precipitate as described in [23]. The close geometrical relationship with the aluminum *fcc*-structure makes this precipitate the ideal location for nucleation from the melt. Note that even if at a first glimpse this structure might be seen as *fcc* as well in terms of crystallographic terminology is a simple cubic arrangement.

olutionary idea has been not to use Sc addition only as a grain refinemer but to implement addition of Sc as high as 1% in combination with some Zr. The combined effect of these alloying elements is to promote the formation of a highly coherent and high temperature stable precipitates with the approximated formula $Al_3(Sc_{1-x}; Zr_x)$. This precipitate originates from the solid solution of Zr in the Al_3Sc-precipitate that substitute Sc in the structure. The effect of Zirconium moves the disintegration of aluminum grains during solidification from a Sc-content of 0.55% down to 0.18% (as reported in [24]). The technological limit of solving in solid solution and successfully quench aluminum with more than 1% of dissolved Sc has been recently removed by the industrial implementation of melt spinning procedure which can grant extreme cooling rate while forcing the solution of Sc and aluminum in thanks to the applied forces over its solubility limit.

To better understand the precipitation process the phase diagram of Al and Sc is reported in Fig.7.8. The eutectic temperature is 655°C which is comparable to the fusion of aluminum (660°C) as reported in [24]. Furthermore, the second effect of combined Sc and Zr addition to aluminum alloys is the high anti-recrystallization. Scandium is considered to be the most effective anti-recrystallization addition of aluminum alloys and can postpone the recrystallization temperature up to 600°C[4].

Before the SLM processed reached industrial application for Scalmalloy, the production of spec-

[4]This temperature is considerably close to the melting temperature of the alloy. Usually, the reference temperature for recrystallization is 0.5 of the melting temperature (T_m) in kelvin. Here the ratio between recrystallization temperature (T_R) and T_m in kelvin is much closer to 1.

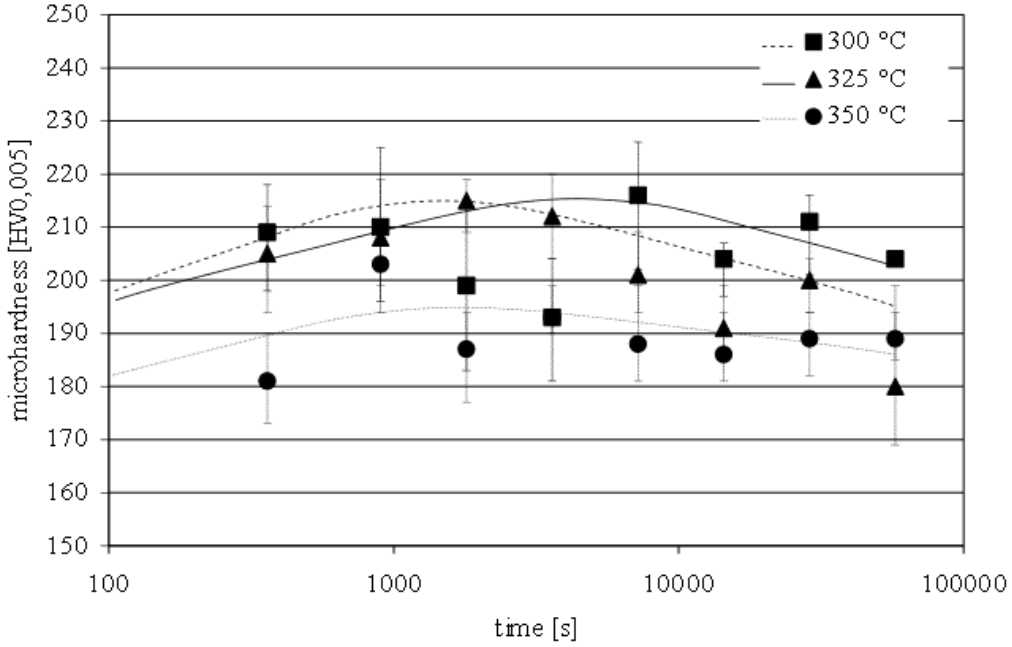

Figure 7.7: Series of results of micro-hardness tests for different combinations of hold time and temperatures for Scalmalloy precipitation hardening (three temperature levels: 300°C, 325°C and 350°C; for timing ranging from 30 minutes to 16 hours). The combined effect of time and temperature is evident by the different stages at which the peak in microhardness is found. An higher temperature level the peak hardness is reached in shorter times and the over-aging process starts. Due to precipitate coarsening the hardness level decreases of the artificial hardening process is endured over the prescribed time.

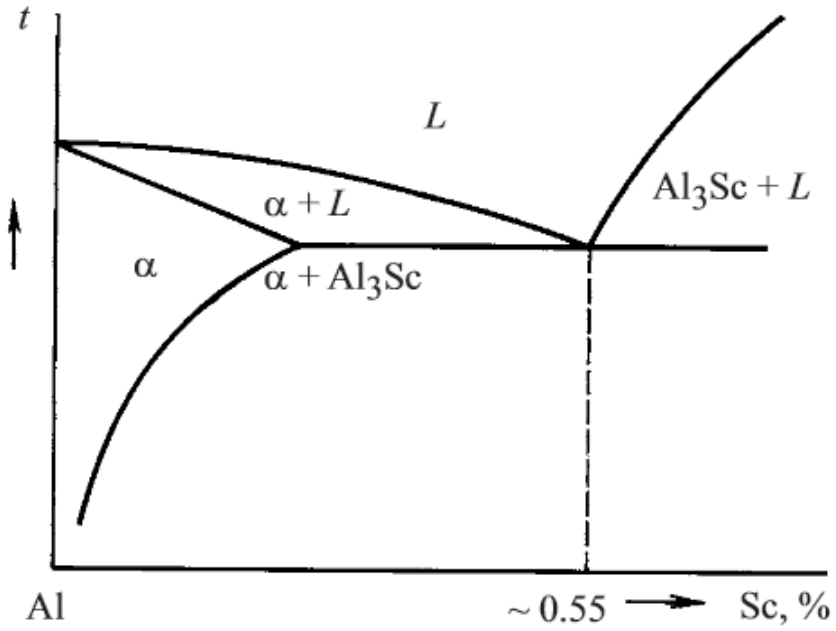

Figure 7.8: Aluminum Scandium phase diagram. The solubility is limited (0.55% wt.) with an eutectic temperature of 655°C which is considerably close to the aluminum fusion temperature (660°C). Over the saturation the equilibrium diagram prescribes the presence of Al_3Sc precipitate phase. The diagram has been adapted from [24].

imens for scientific purposes was implemented through the compaction of melt spinned flakes with spark plasma sintering. During these preliminary studies on the alloy composition the parameters of the best aging process have been developed [25]. The resulting microstructure needs to cope with the

precipitation of the $Al_3(Sc_{1-x}; Zr_x)$-precipitate without provoking unwanted precipitation processes or coarsening of the $Al_3(Sc_{1-x}; Zr_x)$-precipitate that would lose its strengthening ability if a loss of coherence takes place. For an evaluation of the best temperature range at which the heat treatment should be implemented a series of micro-hardness tests have been done in [25] and are reported in Fig.7.7.

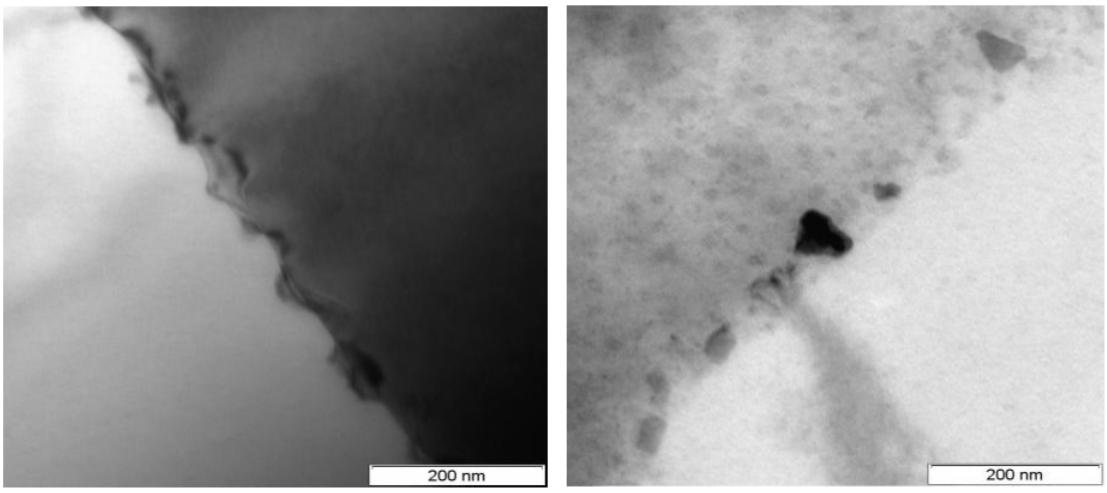

(a) (b)

Figure 7.9: Microstructure TEM images of Scalmalloy produced ribbons as presented in [25]. In Fig.7.9a the grain boundary of two grains is presented after the spinning cast process; the darker shadows are the effect of residual stresses present mainly in the proximity of the grain boundary. In Fig.7.9b the same microstructure is presented after heat treatment at 300°C for 2 hours. The presence of small distributed precipitate is evident (smaller darker gray areas). Their characteristic dimension is around 10 to 20 nm.

As it can be understood by the interpretation of the graph represented in Fig.7.7, the peak of micro-hardness is reached at two different combinations of temperature and hold time. As expected an higher temperature shows a faster increase to the hardness peak value (in the order of 215 H_V for 30 minutes of aging at 325°C). The highest registered value is around 220 H_V after aging at 300°C for 2 hours. After the hardening peak the tensile properties tend to decrease due to the coarsening of the precipitate. Since the present heat treatment has been done on very thin specimens (micro-hardness test) the absolute values of hardness might be over-estimated.

The precipitation event of the $Al_3(Sc_{1-x}; Zr_x)$-precipitate is evident in the TEM images reported in Fig.7.9. In the first Fig.7.9a the microstructure is presented after the solidification process. The grain boundary is evident in the mid-field of the picture while the shadows present in both images are indication of residual stresses. In Fig.7.9b two grain sections and their boundary are presented after the precipitation process. The characteristic dimension of the precipitates is around 10 to 20 nm. Their dimension is limited to prevent loss of coherence which can be described by the relation with the Burger's vector of the aluminum matrix (this quantify the dimension at which the presence of a boundary is more energetically favorable rather than further straining the matrix for comply with the lattice parameter mismatch):

$$d_{cr} = \frac{b}{\delta} \tag{7.1}$$

where the critical diameter is describe as the ratio between the Burger's vector (b) and the lattice

mismatch δ. This relationship is established on the hypothesis that the critical size is reached when, while considering the whole diameter of the particle, the misfit matches the Burger's vector for the aluminum matrix [23]. The results of the present approximation gives a critical size of approximately 21 nm.

Having seen the peculiarities in the development of Al-Mg-Sc-Zr alloys in the next section the microstructural evolution for SLM produced Scalmalloy will be presented.

MICROSTRUCTURAL EVOLUTION OF SLM PRODUCED SCALMALLOY IN COMPARISON WITH CONVENTIONAL WROUGHT PRODUCT AGE HARDENABLE ALLOYS

The thermal history of SLM processed alloys has been briefly introduced in the literature review section (cfr. with Fig.2.3 and Fig.2.30). In the present section the description of the specific thermal history of the material is presented to highlight the differences in the process with reference precipitation hardenable aluminum alloys produced with wrought product techniques. To compare the two manufacturing processes each of them is presented in its main production steps with the relation to the influences that each of those has on the microstructure of the material.

As already mentioned in the course of Chapter 5, material produced by AM follows a series of treatment from the print to the stress relief procedure. Firstly the microstructure undergoes full melt in the SLM process.

All the deposited powder reaches fusion and afterwards faces solidification. The most important parameter for this first production process is the interaction between the molten pool and the energy source. The energy per unit volume in PBF processes is referred in literature as E_V. The definition of E_V depends on the characteristics of the process:

$$E_V = \frac{P_L}{v_S \cdot t_L \cdot d} \tag{7.2}$$

Therefore the specific volumetric energy (expressed in J/mm^3) is proportional to the laser power (P_L) while it is inversely proportional to the scan speed (v_S), to the layer thickness (t_L) and to the hatch spacing (d)[5].

The relationship between the input specific energy and the density is usually regarded as the first approximation for establishing the processing parameters in the definition of the machine set up for a specific material. For Scalmalloy the processing window has been defined, as reported by [26], for density in excess of 99%, between E_V=75 [J/mm^3] to E_V=225 [J/mm^3]. The relation between the processing parameters and the density is represented by Fig.7.10 for different hatch spacings. The higher the energy the lower the defect level and therefore the density rises at cost of scanning time that requires a longer production process since the deposition rate diminishes[6]. In the following sections a correlation between defects and processing specific energy will be better explained.

An interesting feature of Scalmalloy is the relative low anisotropy level in the tensile properties with respect to other SLM processed materials (AlSi10Mg for instance), as it is reported in Chapter 6.

[5] The hatch spacing is the space between two parallel laser scan lines. It's influence is related to the thermal conduction of the alloy: a highly conductive alloy will feature more space between scans since the effective horizontal dimension of the molten pool is likely to be bigger; on the contrary, for titanium for example, the molten pool tends to be reduced and the hatch spacing is usually reduced to obtain proper solidification.

[6] The bottleneck is given by the presence of a limitation of the laser power to maintain a small focus. Furthermore, the scan speed cannot increase too much either due to the possible loss in processing precision.

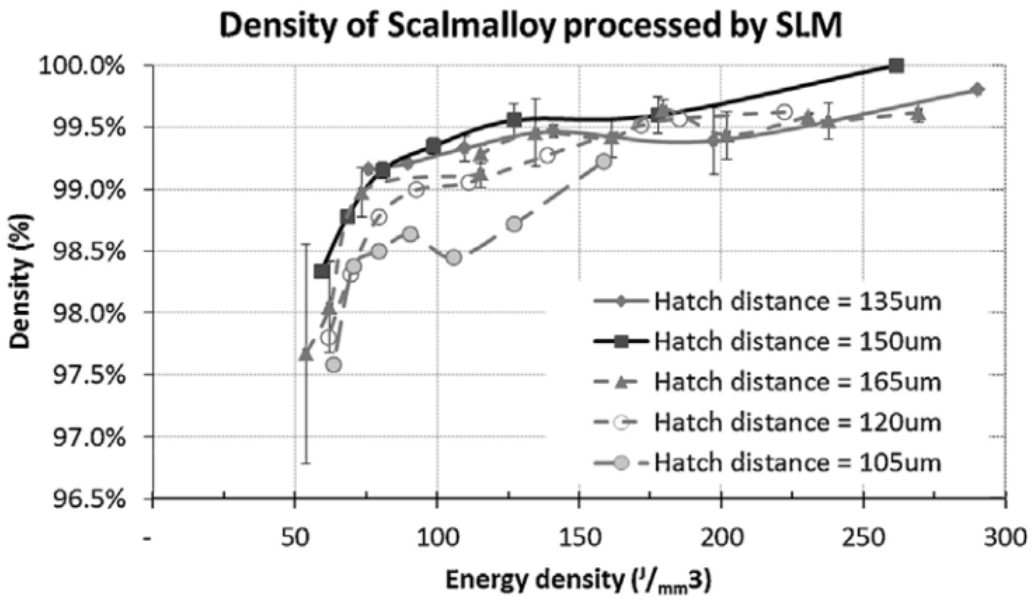

Figure 7.10: Relationship between the specific energy and the density of SLM produced Scalmalloy for different hatch spacings. The trend between the energy and the density is present as higher energy level can grant better solidification of the powder material. It is also clear that due to the high thermal conductivity of Scalmalloy better densification can be reached with bigger hatch spacings (up to 150 μm). Taken from [26].

From Fig.6.3 and Fig.6.5 there is no evidence of a weak Z-produced specimen. This can be tracked back to the microstructural evolution presented in the previous subsection: the peculiarity of Al_3Sc-precipitate to act as nucleation for the solidification process. This removes the columnar grain formation along the printing direction that is the reason for weak tensile strength of AM materials on the Z-direction (banding phenomenon). This is true up to point, in fact the microstructure of as-processed Scalmalloy presents two different grain structures as in can be noted from Fig.7.11. The image obtained and presented by Spierings in [26] shows two interesting structures in the as built Scalmalloy: the presence of small equiaxed grains where the nucleation of grains in the solidification process in fast enough to prevent epitaxial growth; secondly, an other scan-pass microstructure can be seen in which the grains are much bigger and elongated as expected in a directional solidification process.

These two microstructures exists for several reasons even if their full scientific explanation is still unclear. The two mechanism in challenge for the solidification process are influenced by the scan sequence and by the remelting of layers (observed melt lines indicate a thickness for each pass of around 100 μm in the mentioned study while for the presented etched image of DMLS produced Scalmalloy, crf. Fig.7.13c, the average dimension is around 60-80 μm. This indicates the remelt of two to three layers of material for each scan pass). If that happens and the cooling rate is slow enough it might happen that solidification is directional with columnar grains (CG-region; coarse grain zone with average dimension reaching 13 μm); on the contrary if there is no time for effective segregation and grain solidification the equiaxed grain mechanism prevail (FG-region; fine grain zone with average dimension from 0.6 to 1.1 μm).

Furthermore, the effect of precipitates is crucial in the solidification phase. Since during gas atomization the cooling rate is fast enough to suppress any precipitation (indeed gas atomized powders

are considered to be precipitate-free) there is the need of precipitating the Al_3Sc-precipitates during the SLM process. This is not usually happening for all the scan pass since the cooling rate are considerably fast in SLM procedure (contrary to EBM for instance) as they can reach rates between 10^3-10^8 Ks^{-1} according to simulation results [91]. Based on the latest sentence, the ratio between the two phases seems to be controlled by the E_V as well as by the build platform pre-heating [92] but as well is controlled by the atomization process of the powder as reported in some unpubblished work of Eric Jagle[7]: there is a relationship between the remelting and intrinsic heat treatment and intermidiate precipitates with the percentage of FG and CG regions and the presence of those precipitates seems to be related with the powder atomization process. There is therefore some contradiction in the explanation of the mechanism for the transition from the two different microstructures that would need further investigations but is clear that is related to the precipitation of the Al_3Sc phase and with its presence or segregation during the solidification process.

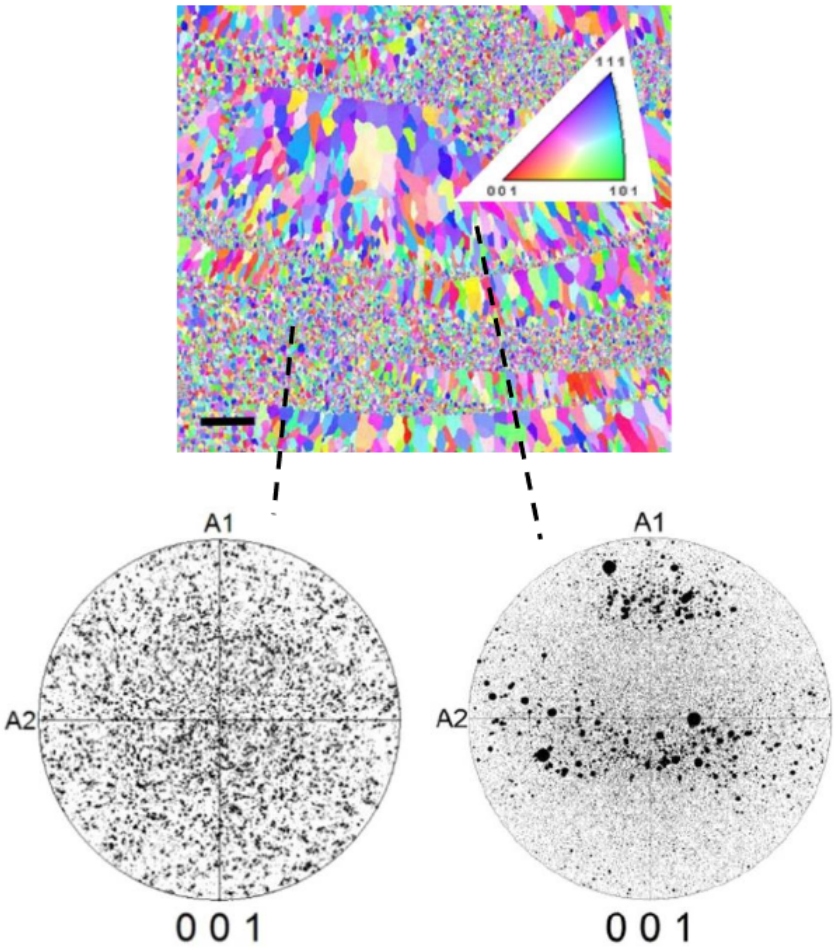

Figure 7.11: Coarse grain region and fine grain region and their relative pole figures. As it can be understood from the pole figures the preferential orientation for the CG zone is the printing direction (001). On the contrary the small grain region does not show any preferential orientation for the grains. This is due to the solidification process that nucleates from the Al_3Sc-precipitate and is responsible for the limited anisotropy in the mechanical properties in the printing direction when compared to the print platform plane specimens. Adapted from [26].

[7] For further informations refer to darealloys.com

After the printing process the as-built material undergoes a heat treatment in order to achieve two different objectives: first the precipitation of the remaining of the dissolved Sc in the aluminum matrix (the original composition is slightly hyper eutectic but due to the complex thermal history some Sc and Zr can be trapped in the Al matrix) and secondly to partially remove some of the internal stresses that have accumulated due to the thermal gradient in the structure. The prescribed heat treatment for Scalmalloy hardening is an artificial aging at 325°C for 4 hours, parameters well in agreement with the hardening results presented in [25] and in line with the presented results of hardening taken from [93] in Fig.7.12. The precipitation of Al_3Sc from solid solution increases the hardness considerably in mentioned study the end results are higher than in the analyzed material (as reported in Chapter 6 the average hardness measured was 162 H_V).

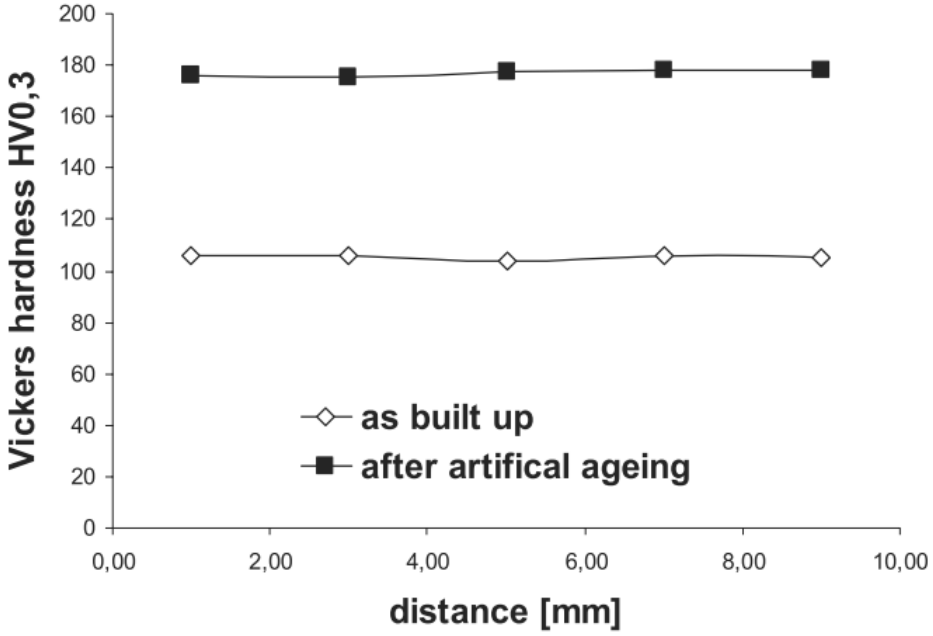

Figure 7.12: Artificial hardening effect on DMLS produced Scalmalloy from gas atomized powder. The increase in the hardness is the proof that the hardening process already described in [25] is sound. The possibility given by AM in respect of traditional sintering techniques is evident. Still some differences are present between conventionally produced Al-Sc alloys and Scalmalloy in the fact that for the first the mechanism of hardening is not responsible for the majority of the strength increase (which is related to the nonrecrystallized structure) while for Scalmalloy the age hardening is mainly responsible for the higher tensile strength.

The special thermal history of AMed materials defines new standards for the strengthening methods and strategies for developing novel alloys. In particular the possibility of having very high cooling rate with the implementation of gas atomized powders allows the chance of having Scalmalloy material with still solid solution between Sc (and Zr) in the aluminum matrix. For comparison we can briefly analyze the thermal history of a common Al2024 which is the base material for the AMC225 presented in the previous section that has been substituted by Scalmalloy.

Al2024 is a copper alloyed aluminum alloys which represented the baseline material for aircraft structures for decades: the possibilities for hardening are granted by the presence of excessive copper in solid solution that upon quenching remains in metastable solution with the aluminum matrix. The stable phase in the phase diagram is the θ-phase with the approximate formula $CuAl_3$. The grain size will be determined after rolling of the slab and eventual forgings. Once the geometry is ready for

heat treatment (the machining is usually done with the alloy in the naturally aged conditions T4) the material undergoes an annealing process which is prescribed at 488-499°C in order to avoid partial melt in zones in which the local composition might have a low melting eutectic point, while optimizing the solubilization: if the equilibrium phase is in a multiphase domain of the phase-space some of the alloying elements will not succesfully precipitate. It is important to maximize the quantity of solute in the mixture to maximize the effect of the hardening. If some copper, for instance, precipitate prematurely the final hardening would be less effective. The hold time, since the alloy is well above its recrystallization temperature T_R, needs to be properly selected since will determine the final grain size.

After annealing and water quenching to "freeze" the solid solution composition as well as the grain size, the alloy needs to undergo a precipitation process; before this stage it is considered to be in the solution heat treated state (T3). For parallelism all those processes[8] take place in AM materials during the printing phase and the grain size is much more related to the interaction between the specific energy and the material behavior rather than on a specific annealing procedure. To prevent premature aging and recrystallization the artificial aging of Al 2024 takes place at 185 to 196°C for 11-13 hours. The alloy composition needs to take into account for the chance of other precipitation phenomena happening: this is the reason why the Fe %wt. is controlled; the Fe presence is responsible for side precipitation effects that take out copper from the solid solution[9]. Here a second difference can be found with AMed Scalmalloy: the heat treatment procedure usually leads to considerable size in the precipitate of copper reinforced aluminum. Due to the tendency of natural aging the microstructural constituents (and specially the precipitate), do need to reach a degree of stability. Since the strengthening effect is given by precipitate density and not by their dimensions[10] is clear how having small and dense precipitate as found in the Scalmalloy is a positive in the definition of mechanical properties.

With this brief comparison the metallurgical phenomena that are driving Scalmalloy behavior is finished and some more specific remarks will be address to the process quality and especially to the presence of lack of fusion defects that in the author's perspective were responsible for the diminished ductility found.

7.2.3. PROCESS QUALITY

Since the material behavior has shown unsatisfactory results with elongation in defect of what the specification prescribed, it is worth to analyze the process quality assessment already presented in Chapter 6 to highlight the possible differences responsible for the poor ductility. In the present section two different tests will be analyzed: firstly, the micrography results are compared with metallography analysis of other aluminum alloys in order to assess the different porosity levels; in the second half the density levels will be briefly checked with the data from other sources.

In Fig.7.13 three images are presented showing different microstructures to be compared with the microscopy sections analyzed in Chapter 6: they represent DMLS produced aluminum alloys (Scalmalloy and AlSi10Mg) taken from the internal characterization campaign. In Fig.7.13b a Scalmalloy

[8] The phenomenon of rapid cooling found in AM metals is often referred to as quench-in.

[9] Note that 1%wt. in Fe eliminates any hardening in Al 2024 by adsorbing Cu into a incoherent precipitate that dislocations are easily capable of climbing.

[10] It is to note that the strengthening effect is probably in the two different regimes: the dislocation will cut through small precipitate in the AMed Scalmalloy while they would need bowing mechanism to pass the copper precipitates.

(a)

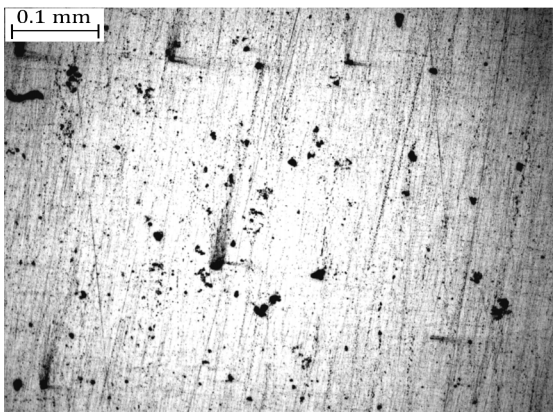

(b)

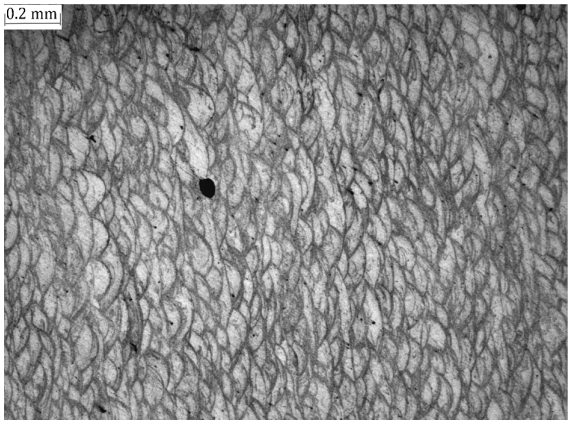

(c)

Figure 7.13: Comparison of different batches of Scalmalloy and AlSi10Mg produced by DMLS additive manufacturing: in the first (Fig.7.13a) a section of AlSi10Mg DMLS-produced specimen is presented, the porosity level reflects small .

DMLS produced specimen section is presented, the defects level is lower than the SLM counterpart and porosities present can be described as gas induced porosity due to their quite regular circular shape. Similarly in Fig.7.13c an etched section of Scalmalloy is presented from a specimen cut along the Z-direction (axis of the specimen parallel to the printing direction). The presence of a layered microstructure is made clear by the etching of the used acid[11]. The present porosity shows a dimension of *circa* 0.1mm and can be described as well as a gas induced porosity. For a comparison, an other aluminum alloy, also printed with DMLS technique, is presented in Fig.7.13a. This sample has been cut alongside the Z-axis and is representative of the melt banding phenomenon typical of the AM processes. The latter image presents a compact structure with some dispersed gas porosity defects of the order of 0.05-0.1mm.

To compare the density level with historical database of eighty results, all of them obtained by the same process (SLM), and measured by micrography technique Fig.7.14 is reported. The measurement

[11] As standard for aluminum alloys the used acid was a solution containing H_3PO_4.

is taken by substracting the dark areas from the total area of the measurement and to compute their ratio on a 100% scale. As it can be seen the average level and most of the samples are in excess of 99.5% of dense region over voids. Few measurements are below that threshold and only one reaches a density level lower than 99%. These number can be compared with the average density reported by the six measurements done in the present project and reported in Fig.6.8 in Chaper 6. Two out of six measurements are below the 99.5% density threshold and in both cases the specimen was showing a density level below 99%. This indicates a lower value than what could have been expected by the process history and might be an indication of increased defect levels. The source of defects is related not by the level of gas induced porosity, which density seems to be similar to other microscopy analysis but by the excessive presence of fusion defects most probably cause by a wrong interaction between the input energy and the molten pool.

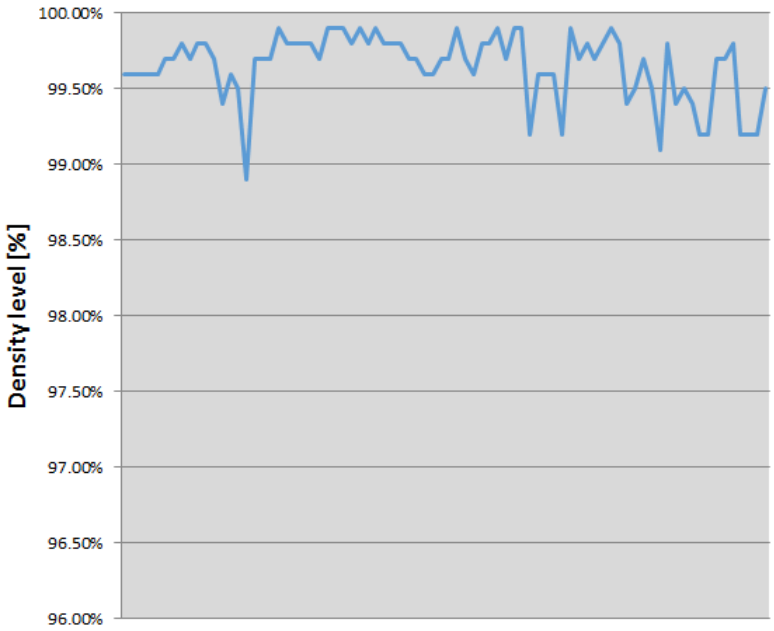

Figure 7.14: Flowing in the density characteristic for different micrography for eighty tests on the historical database for SLM produced Scalmalloy specimens. On the vertical axis the density level is reported while the horizontal axis reports the various measurements from 1 to 80. Only one measurement was found to be lower than 99% with most of the results ranging over 99.5%. When this historical database of density results is compared to the actual level found in the analyzed specimens it is clear that the production of the component sits at the lowest range of the registered densities.

As it is evident for the presented images and comments on the density levels, that are not fully-comprehensive but still representative of what the benchmark production is like, the lack of fusion is a peculiar defect of the SLM-produced Scalmalloy tested in the context of the production and characterization of the rocker beam. The current issue can be related most probably to process input parameters, or parameters combination out of the prescribed ranges or not properly set. More specifically, the scan speed or the balance between the scan speed and the laser power is regarded as the source of the problem since it is related to the fusion process that takes place during SLM produced components and is mainly driven by the energy interaction between the molten pool and the energy source. An interesting study on the process parameters shows how defect level is related to the E_V levels as presented in Fig.7.15 through the modification of the hatch spacing and the scan speed. The biggest influence is seen in the hatch spacing while the scan speed has a lower effect. This is a sugges-

tion towards the improvement of the defect level that might be researched in future characterization of Scalmalloy components.

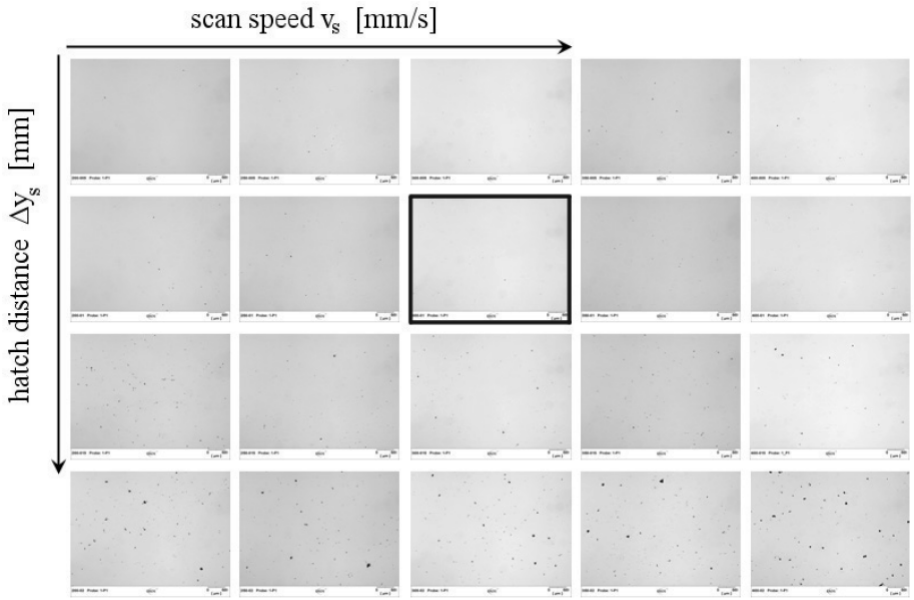

Figure 7.15: Microstructure defect level in SLM pruced as reported in [93]. The two parameters analyzed at constant laser power are the scan speed and the hatch spacing: the highest influence of the latter might suggest to optimize it in the future production of Scalmalloy components.

7.2.4. COMPONENT QUALITY AND FUNCTIONAL ANALYSIS

The last section regarding Scalmalloy quality analysis regards the component quality and the functional analysis again of the component itself. The tests regarding the component quality have been reported in the last section of Chapter 6 as they contain different tests: the CTScan and the 3D laser scan; the three levels of LPI inspections; the dimensional analysis (not presented in the aforementioned chapter since it was not relevant to the "process related" quality of the component but it needs to be considered for functional analysis of the part); the X-ray slabs processed after the first round of quality assessment.

To better present the component finishing and aspect Fig.7.16 is reported: the lower section of the component can be seen in order to access the level of finishing achieved through the shot peening process. The roughness level was quite satisfactory due to the mentioned surface finishing process while still some open porosities are present even on surfaces well exposed to the process[12]. This open porosity can still be acceptable, if inevitable, but a reconsideration of the deposition rate (and especially on the hatch spacing) might influence the external quality and might be a further optimization on the printing process needed to successfully implement the analyzed manufacturing technique. At the top of Fig.7.16, top right red circle, another characteristic defect is present: near the tip radius of the rear strut connecting the two rocker bearings some surface defects can be clearly seen. They are most probably originated by a poor supporting structure removal. Those indications might not be seem to alarm the designer at a first sight but their presence is for sure detrimental to the component mechanical performances especially regarding fatigue performances. Furthermore, the uncontrolled

[12] Cfr. for reference Fig.6.14 reported in Chapter 6.

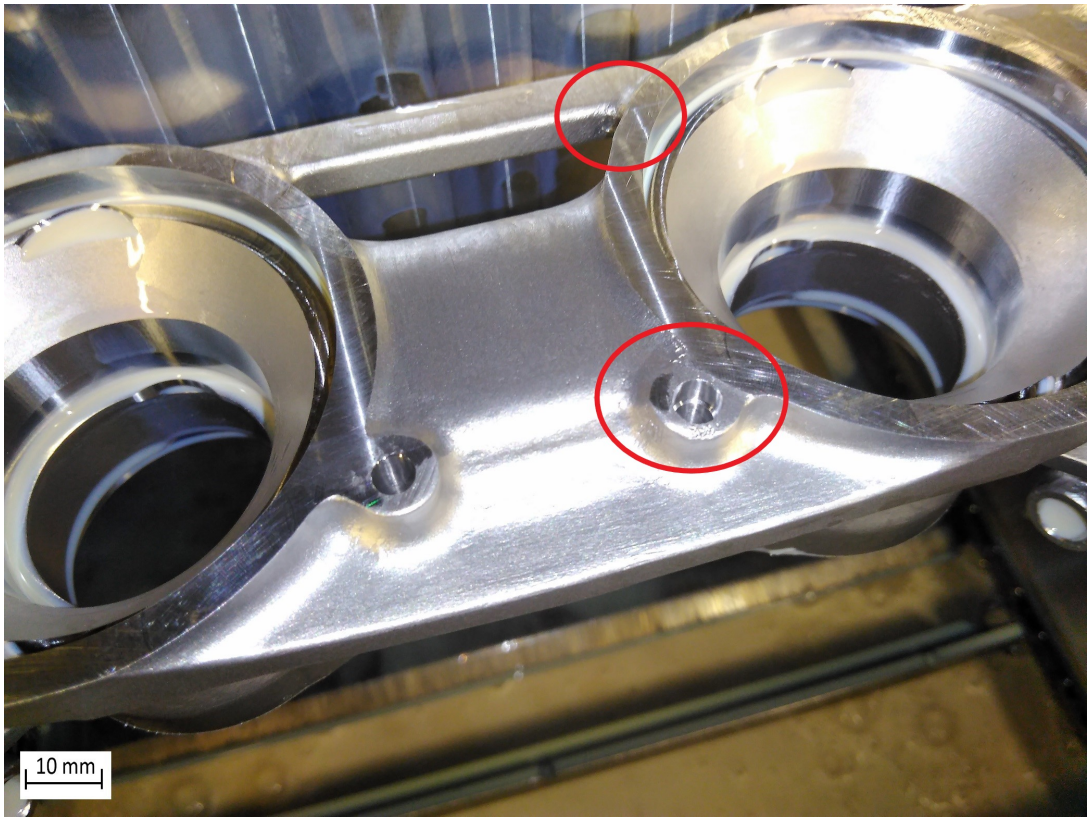

Figure 7.16: Lower section of the component as presented after the machining of the semi-finished product: the roughness and porosity is partly solved by the shot peening process. Some defects are visible at the intersection between the rear strut geometry and the bearing housing: the presence of localized support his exposing the surface to the removal operation of which indications are visible at the top right end of the image (top red circle). The defect present in the lower red circle is presented in Fig.7.17

presence of such structures is to be regarded as an issue if their removal is done unproperly by the operator: a small scratch in a highly stressed zone with poor surface roughness is likely to fail earlier than expected under repetitive load applications.

Another surface defect is presented in Fig.7.17. The mentioned picture represents in detail one of the connecting threaded section already present in Fig.7.16. In this example a sum of errors adds up with some poor design choices: the limited difference in height between the bearing zone and the threaded section planes is probably too small to be perfectly matched by AM. The poor geometrical precision of the component (90% at +/- 0.3mm from the CAD geometry is reputed to be insufficient) combined with layering effect and a poorly designed sharp edge (at the hole contour) made the local error to sum up: combining this with the choice of the machinist to remove manually the sharp edge with an inconstant and irregular chamfer has made the final aspect of the geometry to be particularly poor. Still being this region over-designed the result has been taken as acceptable for bench testing. In the perspective of improving the quality of the end results it could be suggested to revise the machining of the area to completely re-define the lower plane: the extra costs and machine time will repay with a proper finishing or the connection area and the height difference between the two planes could be easily achieved.

Regarding the LPI indication the second round of control was considered to be sufficiently passed for the test once the linear indication presented in Fig.6.14e was double checked in the X-ray slab and

Figure 7.17: Detail of the rocker beam in which the presence of surface defects is evident: geometrical inaccuracy and layering effect are responsible for the poor finishing. To solve such problems (that might be related to the presence of supporting structures) a more integrated design for manufacturing approach could have been applied. As well it might have opted for a complete machining of this lower section since the added cost of a similar operation would not have influenced the overall price of the component significantly but the final result would have been a considerable improvement.

was concluded that no crack or linear defect was present at the interface between the steel bushing and the rocker beam semi-finished product. Similarly, volumetric defects were considered to be acceptable since the indication of the CTScan were not found in the first test with the X-rays. This might be due to poor interpretation of one of the two tests but since there was the chance of personally check the X-ray while not the same was true for the CTScan, the X-ray measurements where considered the leading indication of real defects. More specifically on volumetric defects and their acceptability, the next section will present a possible starting proposal for the quality assessment of such AMed products since the current standard is not granting satisfying results for both supplier and receiver.

7.3. TOWARDS THE DEFINITION OF A QUALITY ACCEPTABILITY LEVEL

As specified in the introduction to the present chapter, during the microscopic and macroscopic analysis of the Scalmalloy component it was clear that there was not a specific idea about the possible real life defect level of a component and how to address specifically the issue of acceptability of such components. The presence of different defects originating from both the process and from process parameters are, as explained earlier, unavoidable. To technically address the problem, the implementation of a robust quality process was decided: the component specification needs to feature a defect level acceptability in order to decide if technologically the component with defects would be able to carry positively the prescribed load cases with considerably high level of safety.

The discussion will be developed in two different sections: in the first half the zone approach is presented in order to show how the stress acceptability and therefore a reduction in the reserve factor can be done; secondly the acceptability level of the defects will be presented for a range of defects representative of the quality of Scalmalloy produced components.

7.3.1. DEFECTS ACCEPTABILITY - INCREASE IN THE REAL STRESS

Starting with the assumption that all AMed products present some surface and volumetric defects there is the need, in the industrial practice, to properly address their influence on the structural behavior of mechanical components. Nowadays, as mentioned earlier, a standardized method is not well defined even if some normative committees are developing the proper specifications. When the problem is related to a specific novel material the chance to obtain formal guidelines and agreement is consistently lower and therefore it became clear, in the course of the present project, that the development of a specific and relevant internal standard for defect acceptability was needed to regulate the future flow of AMed components through the quality process.

Defects in structures are inevitable and their general effect is to create localized stress risers that would critically reduce the effective reserve factor of the structure itself. From this very basic assumption it can be clearly understood that the relationship between the acceptability of defects and the RF is inevitable. The proposed approach is a zone-based acceptability set of criteria: each AMed component would be ideally divided into different zones based on the relative reserve factor and for each zone a proper acceptability criterion will be applied; the present approach has the advantage of not discarding components with defects in non critical areas but as well to reduce the increased stress in a controlled way. An example on the mentioned proposed zone-based criterion effect is presented in Fig.7.18. This graphical representation reports the acceptable increase in effective stress over the admissible stress for different RF applied on the YS criterion for the tested component in Scalmalloy.

The present proposal features the distinction of the component in four different areas, each of them described by an average RF and by an approximated area on the component in order to be easily determined by the quality operator. The first area represents the safety critical areas with RF between 1.2 and 1.5, while all other areas are scaled from 1.5 to 2.5 (mechanically critical areas), 2.5-4 for mechanically stress regions and finally for overdesigned areas where the RF is higher than 4. For each area different stress increases are acceptable since their risk of failure is, as well, different: this translates to the different offsets in the graph presented in Fig.7.18 between the nominal admissible stresses and the effective admissible stress.

For each zone different defect size and defect distribution must be accepted in order to the trend shown in the reported example: the presented number, though representative of the implementation of the specification, have been set arbitrary since it is the definition of the defect dimension that would grant the proposed values. The idea is to tune the specification itself, not on the real stress increase level (which would be critical to be analyzed) but on benchmarking the internal production to the pass the specification with components that have been previously successfully used on the car. Once the specification is tuned it will represent the quality standard for acceptability for externally supplied components.

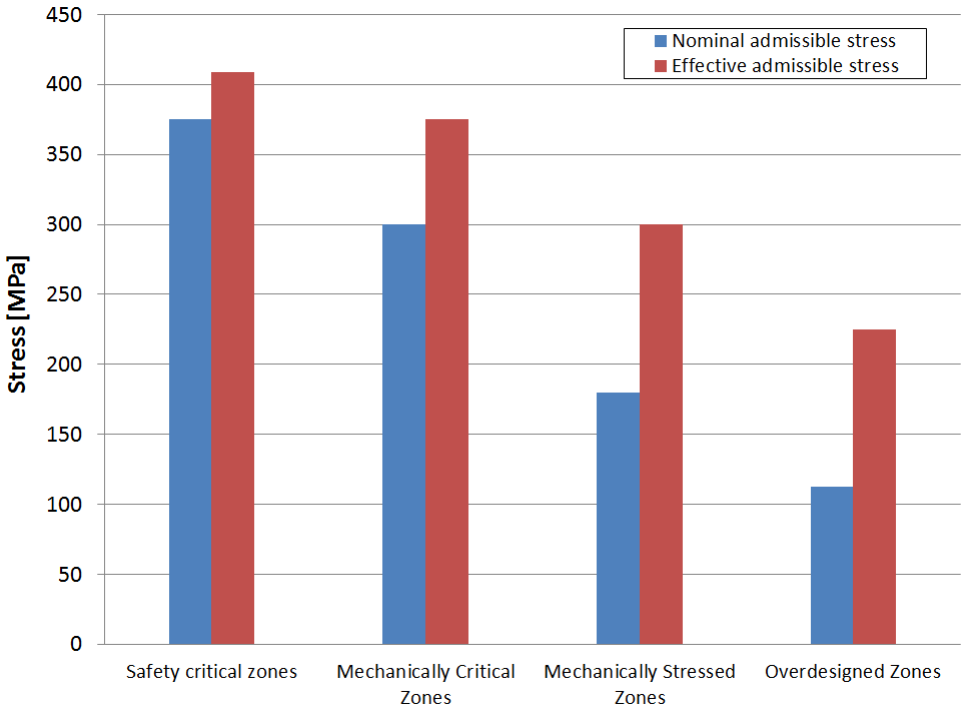

Figure 7.18: Graphical qualitative interpretation of the controlled stress increase on the area based quality acceptability proposal: the blue bars are the nominal stress while the red bars show the real accepted stress increase due to presence of different level of defects. Since the relative criticality of each zone is different the acceptance of an increased stress level changes *per* each zone.

7.3.2. QUALITY ACCEPTABILITY PROPOSAL - THE EXAMPLE OF CASTINGS

The proposal for an acceptability criterion zone based is not a completely new concept even if its application to AMed components does not have a clear literature background. The logical context for the development of the proposal is the characterization done in aluminum cast components. The main literature and industrial references can be found in the ASTM specification for aluminum and magnesium castings reported in the E155 normative and the relative AMS 2175. The present norms combined with reference X-ray images reported in the specification, do assign to cast components a grade (usually from A to C or D) depending on the quality and presence of a multitude of different defects or characteristics. The underlying idea is to relate every grade to the different level of tensile properties that can be effectively found due to the presence of defects and discontinuities.

Two graphical representations are presented in Fig.7.19a and in Fig.7.19b in order to address the aforementioned concept: the grade level corresponds to the presence of different defects and different defects distribution in the cast. As it can be clearly seen, the degradation on the specimens tensile properties corresponds to the lower quality level of the component. Furthermore, it is interesting to note that the influence of degraded cast is much more evident on the elongation at break rather than on the yield point. This behavior can be tracked back to the nature of the tensile testing from which the results are originated: the presence of a defect is unlikely to reduce consistently the area that is resisting the load application (and therefore the offset of detection of plastic behavior at a macroscale). Still due to the localized higher stresses in the presence of a defect the plasticity is much more localized rather than in a defect free specimen and therefore the event of fracture originates from the region

already plastically deformed in the surroundings of the defect.

Having based the discussion on the parallelism with casting, the proposal elaborated from the present projects regards defects that are typical for the AM processes and are recognized in the corresponding literature and as well on those detected in the quality assessment of the rocker beam component. The defects included in the proposal are therefore divided into two categories[13]: surface defects and volumetric defects.

Among surface defects the control procedure would require the check of four different defects: the surface roughness, the check of open porosity, the occurrence of metal balling formation and the surface defects related to post processing parameters. For each zone the acceptability criterion has to be tuned in a characterization of the internally produced aluminum components.Volumetric defects will be treated similarly: the control would require to assess for each zone defects of three different types. The controlled volumetric defects on which the control procedure would be implemented are going to be: gas porosity, horizontal lack of fusion and vertical lack of fusion. As for the surface defects, they will be tuned on the current capability of obtaining defect free components from the internal manufacturing. The controlling procedure would be set for surface defects with the aid of visual inspection and roughness measurements while for the volumetric defects the only reference point, at a first step, would be the X-ray analysis, which is considered to be the best NDT currently available to address this kinds of defects. At a later stage this could be substituted by CTScan tomography or 3D X-ray analysis when those methods will be judged to be sufficiently correct in the defect estimation accuracy.

This last section concludes the comments in the constitutive work of the present project and represents the end of Chapter 7. In Chapter 8 the conclusions of the present project will to be briefly presented discussing the current *state-of-art* of AM for the motorsport industry and what are the logical future steps in the development of this manufacturing technology.

[13] For the easiness of the first approach the *"beta"* version of the proposal would present only single and countable defects. It may happen to encounter non countable defects such as micro-porosity or sponge defects (mainly present in castings but some similar defects were described for AMed components) but for a first application of a novel standard the proposal is not taking those into consideration. The approach is still reasonable since the global defect level is usually originated from process parameters or deviations from the correct and *state-of-art* procedures and limiting the dimension of single and countable defects is likely to reduce the presence of other defects as well.

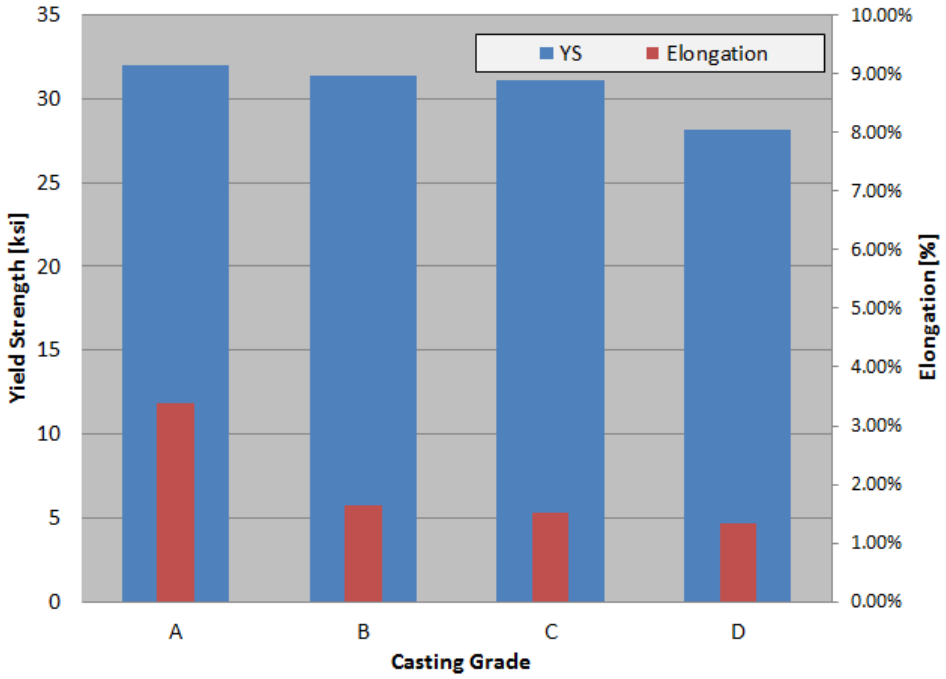

(a)

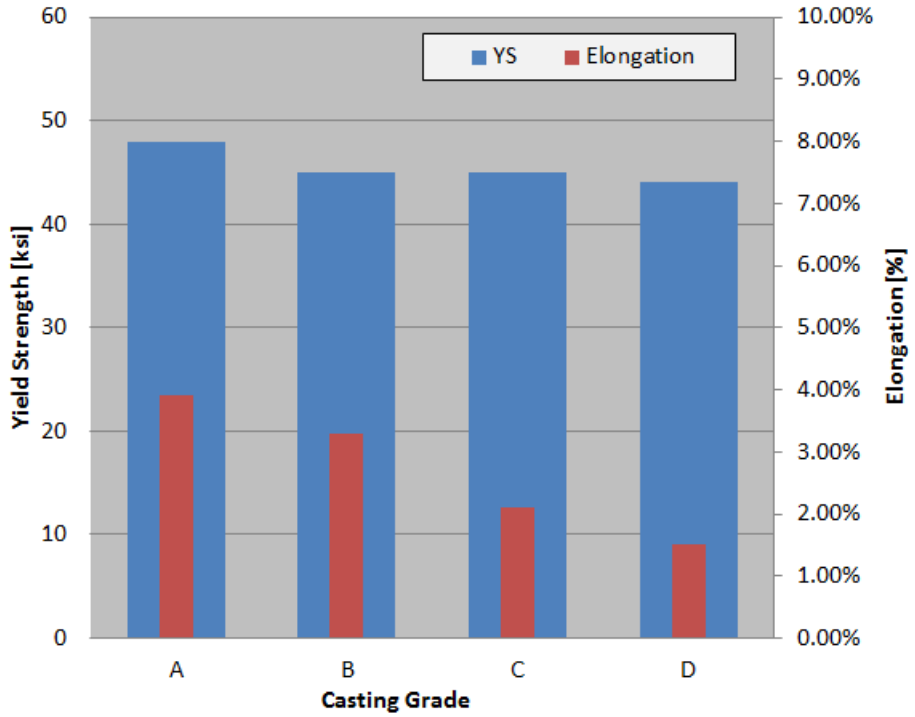

(b)

Figure 7.19: Graphical representation of diminishing properties as a function of casting grades elaborated from different literature sources: the first example (Fig.7.19a) represents an industrial cast while Fig.7.19b is representative of aerospace alloys. The grades from A to D refer to the MIL-STD-2175 casting quality standards. Graphical results are relaborated from [27]. The quality of the cast has a primary effect on the elongation properties of the material, an effect which is similar between cast products and additively manufactured components. In fact, the presence of lack of fusion defects in SLM specimens reduced considerably the elongation while not compromising the strength level.

8

CONCLUSIONS AND FURTHER INVESTIGATIONS NEEDED

As presented in the thesis introduction this brief chapter presents a final comment on the AM technology and *state-of-art* for the motorsport industry. These final comments are presented in two sections: the first half presents the current level achieved during the project for the manufacturing of structural components with AM technologies; the second part presents a series of future needed investigations suggested and the current missing information for a successful chain of knowledge in the industrial practice.

8.1. DMLS AND AM FOR STRUCTURAL COMPONENT DESIGN

It can be concluded from the experimental testing, design studies and fatigue bench testing that AM is a mature technology capable of granting weight reduction of structural components, due to the ability of overcome manufacturing limits, by 7-10%, even in the case of highly optimized structures. The machine diversity and material availability is likely to grow in the short future since the processing capabilities of laser bed fusion processes have shown to meet high industrial standards.

Some materials (Ti6Al4V) have shown full achievement in the mechanical properties and high level of accuracy in the definition of surface tolerances, mainly due to the know how on the processing parameters (knowledge on the DMLS process) and the full functionality of the component is achieved thanks to top class machining finishing techniques. Other materials tested (Scalmalloy) were not fully compliant with the specification standards. As specified in the extensive discussion reported in Chapter 7, the excessive presence of process induced porosity (in the form of horizontal lack of fusion) reduced the average elongation properties; still all other tensile parameters were in line or above the industrial standard which means that the microstructure is sufficiently strengthened by the precipitation heat treatment process and the almost absence of anisotropy on the tensile strength of the components (as reported by the directional results presented in Fig.6.3 and Fig.6.5) is the proof of a microstructure that presents almost no banding. The process induced defects could be corrected with

the implementation of tuned processing parameters and a defect characterization campaign. Especially the balance in the energy with the melting pool has to be correctly tuned to avoid lack of fusion defects and therefore a loop of control on the scan speed and laser power is suggested for the SLM process.

The quality process established for the Scalmalloy component was sufficient to grant good control on the defects of the part and as well it was able to detect the mechanical properties of interest to properly assess the real state of the process and of the component. Still the lack of a properly described acceptability criterion was considered critical in the flow between supplier and OEM.

The industrial know how and engineering practice in the motorsport industry is not reputed to be as mature as the technological process: the need of better understanding of the manufacturing process and to properly re-engineer the design process re-benchmarking it on the process specific limitations and boundary conditions is still in the developing phase. The aid of good engineering practices and specific software applications (such as quick surface reconstruction tools or *in-the-loop* topology optimization) is suggested to achieve higher quality in the end products. Furthermore, a closer interaction between the manufacturing and the design team could have granted higher overall quality of the supporting strategy for the components printing procedure.

8.2. FURTHER INVESTIGATIONS IN THE FIELD OF STRUCTURAL DESIGN FOR AM

From the missing information and lack of knowledge encountered in the various phases of the present project the main research directives, accordingly with the author's view in agreement with the company supervisor, suggested for the future success of the analyzed manufacturing technology, are among others:

- **The need of a robust material database for novel material**: as described in the design process and during the simulation procedure (Chapter 3 and Chapter 4) the absence of a robust material properties database for AM materials and the absence of a standardized determination of the minimum mechanical properties is a critical barrier to the large scale use of this manufacturing technology. The proper development of a standardized characterization (including proper and severe thermal and fatigue characterization) would lower the skeptical attitude of designers with respect to additive manufacturing.
- **The need of specific surface finishing techniques for AMed products**: the absence of dedicated surface finishing techniques for additive manufacturing materials has been faced as a second critical point in the definition of the manufacturing processes for components in need of sustained repetitive fatigue loads. The surface finishing and the presence of a layering effect is currently seen as one of the principal limitations for fatigue components and the development of custom processes together with a proper fatigue properties characterization would unlock further potential in the weight saving on structural components.
- **The need of standardizing the quality processes**: the absence of a standardized quality process makes the work-flow between supplier and OEM quite complex and the definition of singular standards on specific agreements for each component represent a further barrier in the

applicability of the technology. Since the maturity of the processing technique, a standardized guidelines on how to develop material specific acceptability parameters is crucial to the industrial scale up of the process. A basic strategy proposal, limited in the intent for the Scalmalloy produced component, has been presented in Chapter 7. From this proposal the connection of the technology to established processes (casting quality assessment) is made clear and could be taken as a first inspiration for the development of general acceptability guidelines for AMed structural components. In a further future on site defect evaluation through the implementation of live control with ultrasound techniques (*Phased Array*) can be seen as a future breakthrough in the control strategy of defect evaluation at the very early stages of production.

BIBLIOGRAPHY

[1] D. E. Cooper, M. Stanford, K. A. Kibble, and G. J. Gibbons, *Additive manufacturing for product improvement at red bull technology,* Materials & Design **41**, 226 (2012).

[2] H. Bikas, J. Stavridis, P. Stavropoulos, and G. Chryssolouris, *A design framework to replace conventional manufacturing processes with additive manufacturing for structural components: A formula student case study,* Procedia CIRP **57**, 710 (2016).

[3] A. Spierings, G. Levy, L. Labhart, and K. Wegener, *Production of functional parts using slm – opportunities and limitations,* in *Innovative Developments in Virtual and Physical Prototyping*, edited by P. Bártolo, A. de Lemos, A. Tojeira, A. Pereira, A. Mateus, A. Mendes, C. dos Santos, D. Freitas, H. Bártolo, H. Almeida, I. dos Reis, J. Dias, M. Domingos, N. Alves, R. Pereira, T. Patrício, and T. Ferreira (CRC Press, 2011) pp. 785–790.

[4] S. Curran, P. Chambon, R. Lind, L. Love, R. Wagner, S. Whitted, D. Smith, B. Post, R. Graves, C. Blue, J. Green, and M. Keller, *Big area additive manufacturing and hardware-in-the-loop for rapid vehicle powertrain prototyping: A case study on the development of a 3-d-printed shelby cobra,* (SAE International400 Commonwealth Drive, Warrendale, PA, United States, 2016).

[5] L. Esposito, *Topological optimization strategies in multi-physics problems,* Università degli studi di Napoli, PhD Thesis (2013).

[6] M. P. Bendsøe and N. Kikuchi, *Generating optimal topologies in structural design using a homogenization method,* Computer Methods in Applied Mechanics and Engineering **71**, 197 (1988).

[7] *3d design & engineering software - dassault systemes,* `https://www.3ds.com/` (2017), (Accessed on 10/18/2017).

[8] *Disciplines,* `https://www.3ds.com/products-services/catia/disciplines/engineering/tag/120-10029/`, (Accessed on 10/18/2017).

[9] *Additive manufacturing of titanium alloys,* `https://ewi.org/eto/wp-content/uploads/2014/10/06A-Froes-AM-South-Africa.pdf`, (Accessed on 12/04/2017).

[10] W. J. Sames, F. A. List, S. Pannala, R. R. Dehoff, and S. S. Babu, *The metallurgy and processing science of metal additive manufacturing,* International Materials Reviews **61**, 315 (2016).

[11] H. J. Niu and I. T. H. Chang, *Selective laser sintering of gas atomized m2 high speed steel powder,* Journal of Materials Science **35**, 31 (2000).

[12] M. Shellabear and O. Nyrhila, *Dmls - development history and state of the art,* .

[13] L. M. Sochalski-Kolbus, E. A. Payzant, P. A. Cornwell, T. R. Watkins, S. S. Babu, R. R. Dehoff, M. Lorenz, O. Ovchinnikova, and C. Duty, *Comparison of residual stresses in inconel 718 simple parts made by electron beam melting and direct laser metal sintering,* Metallurgical and Materials Transactions A **46**, 1419 (2015).

[14] A. E. Patterson, S. L. Messimer, and P. A. Farrington, *Overhanging features and the slm/dmls residual stresses problem: Review and future research need,* Technologies **5** (2017).

[15] W. E. Frazier, *Metal additive manufacturing: A review,* Journal of Materials Engineering and Performance **23**, 1917 (2014).

[16] B. Dutta and F. H. Froes, *Titanium Powder Metallurgy* (Elsevier, 2015) pp. 447–468.

[17] E. A. Jägle, Z. Sheng, L. Wu, L. Lu, J. Risse, A. Weisheit, and D. Raabe, *Precipitation reactions in age-hardenable alloys during laser additive manufacturing,* JOM **68**, 943 (2016).

[18] V. Azar, B. Hashemi, and M. Rezaee Yazdi, *The effect of shot peening on fatigue and corrosion behavior of 316l stainless steel in ringer's solution,* Surface and Coatings Technology **204**, 3546 (2010).

[19] B. Vrancken, L. Thijs, J.-P. Kruth, and J. van Humbeeck, *Heat treatment of ti6al4v produced by selective laser melting: Microstructure and mechanical properties,* Journal of Alloys and Compounds **541**, 177 (2012).

[20] R. Pederson, R. Gaddam, and M.-L. Antti, *Microstructure and mechanical behavior of cast ti-6al-4v with addition of boron,* Open Engineering **2**, 112 (2012).

[21] *How to calculate a camber angle to design an atv - updated 2017,* `https://www.quora.com/How-do-I-calculate-a-camber-angle-to-design-an-ATV`, (Accessed on 11/15/2017).

[22] MTS, *Model 329 multiaxial spindle-coupled road simulators,the ultimate testing solution for the most demanding road simulation challenges,* `https://www.mts.com/cs/groups/public/documents/library/cm3_002014.pdf`, (Accessed on 11/04/2017).

[23] J. Røyset and N. Ryum, *Scandium in aluminium alloys,* International Materials Reviews **50**, 19 (2005).

[24] V. V. Zakharov, *Effect of scandium on the structure and properties of aluminum alloys,* Metal Science and Heat Treatment **45**, 246 (2003).

[25] F. Palm, R. Leuschner, T. Schubert, and B. Kieback, *Scalmalloy ® = A Unique High Strength AlMgSc Type Material Concept Processed by Innovative Technologies for Aerospace Applications,* PM2010 Wolrd Congress - PM Aluminum and Magnesium 2 , 0 (2010).

[26] A. B. Spierings, K. Dawson, M. Voegtlin, F. Palm, and P. J. Uggowitzer, *Microstructure and mechanical properties of as-processed scandium-modified aluminium using selective laser melting,* CIRP Annals - Manufacturing Technology **65**, 213 (2016).

[27] M. Ozelton, S. Mocarski, and P. Porter, *Durability and damage tolerance of aluminum castings,* Wright Laboratory, Northrop Corporation Aircraft Division (1991).

[28] *Eos datasheet alsi10mg aluminum alloy,* http://gpiprototype.com/images/PDF/EOS_Aluminium_AlSi10Mg_en.pdf (), (Accessed on 11/01/2017).

[29] K. Schmidtke, F. Palm, A. Hawkins, and C. Emmelmann, *Process and mechanical properties: Applicability of a scandium modified al-alloy for laser additive manufacturing,* Physics Procedia **12**, 369 (2011).

[30] B. P. Conner, G. P. Manogharan, A. N. Martof, L. M. Rodomsky, C. M. Rodomsky, D. C. Jordan, and J. W. Limperos, *Making sense of 3-d printing: Creating a map of additive manufacturing products and services,* Additive Manufacturing **1-4**, 64 (2014).

[31] M. R. D. Bourell, D.I. Leu, *Roadmap for additive manufacturing,* University of Texas at Austin (2009).

[32] H. Bikas, P. Stavropoulos, and G. Chryssolouris, *Additive manufacturing methods and modelling approaches: A critical review,* The International Journal of Advanced Manufacturing Technology **83**, 389 (2016).

[33] *Eos offers enhanced procedures for quality control in additive manufacturing,* http://www.pm-review.com/eos-offers-enhanced-procedures-for-quality-control-in-additive-manufacturing/ (), (Accessed on 12/04/2017).

[34] *Fia, 2017 formula one technical regulations,* https://www.fia.com/regulation/category/110 (2017), (Accessed on 12/04/2017).

[35] Xuanping Wang, Shichong Li, Youzhi Fu, Hang Gao, *Finishing of additively manufactured metal parts by abrasive flow machining,* Solid Freeform Fabrication 2016 Solid Freeform Fabrication 2016 (2016).

[36] *Fsaeonline.com,* http://fsaeonline.com/, (Accessed on 12/04/2017).

[37] G. Ericlson, M. Heath, D. Woods, B.and Dolan, E. Henderson, and J. Sears, *Design and manufacture of titanium formula sae uprights using laser-powder-deposition,* Proceedings of the 2004 SAE Motorsports Engineering Conference and Exhibition (2004).

[38] L. T. Farias, A. Schommer, B. Z. Haselein, P. Soliman, and L. C. de Oliveira, *Design of a brake caliper using topology optimization integrated with direct metal laser sintering,* (SAE International400 Commonwealth Drive, Warrendale, PA, United States, 2015).

[39] *Deloitte university press presents: 3d opportunity in the automotive industry – additive manufacturing hits the road | machine design,* http://www.machinedesign.com/3d-printing/deloitte-university-press-presents-3d-opportunity-automotive-industry-additive-manufactu, (Accessed on 12/04/2017).

[40] *Ford f-150 flaunts aluminum's allure; honda pitches a fit,* https://www.boston.com/cars/news-and-reviews/2014/02/03/ford-f-150-flaunts-aluminums-allure-honda-pitches-a-fit (2017), (Accessed on 12/04/2017).

[41] *Range rover aluminum body is 420kg lighter than steel predecessor -*, http://altairenlighten.com/news/new-range-rover-aluminum-body-is-420kg-lighter-than-steel-pre/ (2017), (Accessed on 12/04/2017).

[42] *Agreement reached on cutting co2 emissions from cars further in 2020*, https://ec.europa.eu/clima/news/articles/news_2013062501_en (), (Accessed on 12/04/2017).

[43] W. Cramer, A. Bondeau, F. I. Woodward, I. C. Prentice, R. A. Betts, V. Brovkin, P. M. Cox, V. Fisher, J. A. Foley, A. D. Friend, C. Kucharik, M. R. Lomas, N. Ramankutty, S. Sitch, B. Smith, A. White, and C. Young-Molling, *Global response of terrestrial ecosystem structure and function to co 2 and climate change: Results from six dynamic global vegetation models*, Global Change Biology **7**, 357 (2001).

[44] H. Schleifenbaum, A. Diatlov, C. Hinke, J. Bültmann, and H. Voswinckel, *Direct photonic production: Towards high speed additive manufacturing of individualized goods*, Production Engineering **5**, 359 (2011).

[45] *Stereolithography sla 3d printing | additive manufacturing at materialise*, http://www.materialise.com/en/manufacturing/3d-printing-technology/stereolithography, (Accessed on 10/16/2017).

[46] M. P. Bendsøe and O. Sigmund, *Topology optimization: Theory, methods and applications / M.P. Bendsøe, O. Sigmund* (Springer, Berlin and London, 2003).

[47] *Site map*, http://www.catiadesign.org/_doc/v5r14/catpdfqsrug_C2/qsrug.pdf, (Accessed on 10/18/2017).

[48] P. Ciraud, *Verfahren und vorrichtung zur herstellung beliebiger gegenstaende aus beliebigem schmelzbarem material method and device for making any belongings from any fusible material*, (1973), de Patent App. DE19,722,263,777.

[49] D. Gu, *Laser additive manufacturing of high-performance materials* (Springer, Berlin, 2015).

[50] M. Qian, F. H. Froes, and S. Abkowitz, *Titanium powder metallurgy: Science, technology and applications / Ma Qian, Francis H. (Sam) Froes ; contributors, Stanley Abkowitz [and sixty-four others]* (Butterworth-Heinemann, Waltham, Massachusetts and Oxford, England, 2015).

[51] A. Simchi, *Direct laser sintering of metal powders: Mechanism, kinetics and microstructural features*, Materials Science and Engineering: A **428**, 148 (2006).

[52] C. Hull, *Method and apparatus for production of three-dimensional objects by stereolithography*, (1996), uS Patent 5,554,336.

[53] O. Nyrhila and S. Syrjala, *Manufacture of dimensionally precise pieces by sintering*, (1991), uS Patent 5,061,439.

[54] *Eos metal materials for additive manufacturing*, https://www.eos.info/material-m (2017), (Accessed on 12/04/2017).

[55] M. Larsson, *Arrangement and method for producing a three-dimensional product,* (2010), us Patent 7,713,454.

[56] S. Biamino, A. Penna, U. Ackelid, S. Sabbadini, O. Tassa, P. Fino, M. Pavese, P. Gennaro, and C. Badini, *Electron beam melting of ti–48al–2cr–2nb alloy: Microstructure and mechanical properties investigation,* Intermetallics **19**, 776 (2011).

[57] *Dmls vs slm 3d printing for metal manufacturing | element materials technology,* https://www.element.com/nucleus/2016/06/29/dmls-vs-slm-3d-printing-for-metal-manufacturing, (Accessed on 12/04/2017).

[58] *Eos datasheet nickelalloy in718,* http://ip-saas-eos-cms.s3.amazonaws.com/public/4528b4a1bf688496/ff974161c2057e6df56db5b67f0f5595/EOS_NickelAlloy_IN718_en.pdf (), (Accessed on 10/17/2017).

[59] *Titanium powders,* http://www.readingalloys.com/products/titanium-powders (), (Accessed on 12/04/2017).

[60] A. F. H. Kaplan and J. Powell, *Spatter in laser welding,* Journal of Laser Applications **23**, 032005 (2011).

[61] R. Li, J. Liu, Y. Shi, L. Wang, and W. Jiang, *Balling behavior of stainless steel and nickel powder during selective laser melting process,* The International Journal of Advanced Manufacturing Technology **59**, 1025 (2012).

[62] *Arcam ebm system - ti6al4v titanium alloy,* http://www.arcam.com/wp-content/uploads/Arcam-Ti6Al4V-Titanium-Alloy.pdf, (Accessed on 10/19/2017).

[63] M. J. Donachie, *Titanium: A Technical Guide, 2nd Edition* (ASM International, 2000).

[64] *Eos datasheet titanium ti64,* https://cdn2.scrvt.com/eos/fe8d0271508e1e03/d6e4d305e880/EOS_Titanium_Ti64_en.pdf, (Accessed on 10/17/2017).

[65] M. E. Fine, *Precipitation hardening of aluminum alloys,* Metallurgical Transactions A **6**, 625 (1975).

[66] *Titanium ti-6al-4v (grade 5), sta bar,* http://www.matweb.com/search/DataSheet.aspx?MatGUID=f87a4a1c92d34da2b1ecde4e4dec7a73 (), (Accessed on 10/18/2017).

[67] J. E. Hatch, *Aluminium: Properties and physical metallurgy / prepared by engineers, scientists, and metallurgists of the Aluminum Association, Incorporated ; edited by John E. Hatch* (American Society for Metals, Metals Park, Ohio, 1984).

[68] B. R. Sridhar, K. Ramachandra, and K. A. Padmanabhan, *Effect of shot peening on the fatigue and fracture behaviour of two titanium alloys,* Journal of Materials Science **31**, 5953 (1996).

[69] T. Honda, M. Ramulu, and A. S. Kobayashi, *Effect of shot peening on fatigue crack growth in 7075-t7351,* Journal of ASTM International **2**, 12569 (2005).

[70] R. Nalla, I. Altenberger, U. Noster, G. Liu, B. Scholtes, and R. Ritchie, *On the influence of mechanical surface treatments? deep rolling and laser shock peening?on the fatigue behavior of ti?6al?4v at ambient and elevated temperatures,* Materials Science and Engineering: A **355**, 216 (2003).

[71] L. Slătineanu, t. Potârniche, M. Coteata, I. Besliu, L. Gherman, and F. Negoescu, *Surface roughness at aluminium parts sand blasting,* Proceedings in Manufacturing Systems (2011).

[72] *Ap works datasheet scalmalloy,* http://www.apworks.de/en/wp-content/uploads/sites/2/2015/07/20170626_SCALMALLOY_REV0010.pdf (), (Accessed on 11/01/2017).

[73] *Additive manufacturing of aluminum components with minimal distortion 2011,* https://www.ilt.fraunhofer.de/content/dam/ilt/en/documents/product_and_services/laser_material_processing/HO_Additive_Manufacturing_of_Aluminum_Components_with_minimal_Distortion_2011.pdf, (Accessed on 11/01/2017).

[74] N. Read, W. Wang, K. Essa, and M. M. Attallah, *Selective laser melting of alsi10mg alloy: Process optimisation and mechanical properties development,* Materials & Design **65**, 417 (2015).

[75] *Aluminium alloys - aluminium 5083 properties, fabrication and applications, supplier data by aalco,* https://www.azom.com/article.aspx?ArticleID=2804, (Accessed on 11/08/2017).

[76] T. DebRoy, ed., *Trends in welding research: Proceedings of the 9th International Conference on Trends in Welding Research ; June 4 - 8, 2012, Hilton Chicago/Indian Lakes Resort, Chicago, Illinois, USA* (ASM International, Materials Park, Ohio, 2013).

[77] M. Ashraf Imam and F. H. S. Froes, *Low cost titanium and developing applications,* JOM **62**, 17 (2010).

[78] A. A. M. Specification, *Titanium alloy direct deposited products - 6al - 4v - annealed,* (2016).

[79] J. Sieniawski, W. Ziaja, K. Kubiak, and M. Motyk, *Microstructure and mechanical properties of high strength two-phase titanium alloys,* in *Titanium alloys - advances in properties control*, edited by J. Sieniawski and W. Ziaja (InTech, Rijeka, Croatia, 2014).

[80] *2017 f1 cars 20mph quicker through fastest corners than last year - f1 - autosport,* https://www.autosport.com/f1/news/132057/2017-cars-20mph-quicker-in-f1-fastest-corners (), (Accessed on 11/14/2017).

[81] *Ferrari reveals groundbreaking 2017 f1 car, but can they topple mercedes and red bull? // f1 news // james allen on f1 – the official james allen website on f1,* https://www.jamesallenonf1.com/2017/02/ferrari-unveils-its-sf70h-2017-f1-car-but-can-the-scuderia-topple-mercedes-and-red-bull/ (Accessed on 11/16/2017).

[82] *Sensitivity analysis - an overview | sciencedirect topics,* http://www.sciencedirect.com/topics/medicine-and-dentistry/sensitivity-analysis, (Accessed on 11/21/2017).

[83] A. Petras, *Design of sandwich structures,* https://www.repository.cam.ac.uk/bitstream/handle/1810/236995/design?sequence=1 (1998, Cambridge University Engineering Department), (Accessed on 11/21/2017).

[84] M. Song, *Effects of volume fraction of sic particles on mechanical properties of sic/al composites,* Transactions of Nonferrous Metals Society of China **19**, 1400 (2009).

[85] E28 Committee, *Test methods for tension testing of metallic materials,* (2009).

[86] *Centro analisi materiali, tomografia industriale, ct inspection, tec - eurolab,* https://www.tec-eurolab.com/, (Accessed on 12/07/2017).

[87] E21-09 Committee, *Standard test methods for elevated temperature tension testing of metallic materials,* (2009).

[88] *7-post testing | kaz technologies,* http://www.kaztechnologies.com/engineering/7-post-testing-and-test-development/, (Accessed on 12/09/2017).

[89] P. M. Sutton, *The variation of the elastic constants of crystalline aluminum with temperature between 63°k and 773°k,* Physical Review **91**, 816 (1953).

[90] J. Rojas Gregorio and D. Crespo, *Modeling of the effect of temperature, frequency, and phase transformations on the viscoelastic properties of aa 7075-t6 and aa 2024-t3 aluminum alloys,* Metallurgical and Materials Transactions A **43** (2012).

[91] R. Li, M. Wang, T. Yuan, B. Song, C. Chen, K. Zhou, and P. Cao, *Selective laser melting of a novel Sc and Zr modified Al-6.2 Mg alloy: Processing, microstructure, and properties,* Powder Technology **319**, 117 (2017).

[92] K. V. Yang, Y. Shi, F. Palm, X. Wu, and P. Rometsch, *Columnar to equiaxed transition in Al-Mg(-Sc)-Zr alloys produced by selective laser melting,* Scripta Materialia **145**, 113 (2018).

[93] K. Schmidtke, F. Palm, A. Hawkins, and C. Emmelmann, *Process and mechanical properties: Applicability of a scandium modified Al-alloy for laser additive manufacturing,* Physics Procedia **12**, 369 (2011).